ANL-7800

ANL-7800

LMFBR NUCLEAR SAFETY PROGRAM ANNUAL REPORT

July 1, 1969, to June 30, 1970

U of C-AUA-USAEC

ARGONNE NATIONAL LABORATORY, ARGONNE, ILLINOIS

The facilities of Argonne National Laboratory are owned by the United States Government. Under the terms of a contract (W-31-109-Eng-38) between the U. S. Atomic Energy Commission, Argonne Universities Association and The University of Chicago, the University employs the staff and operates the Laboratory in accordance with policies and programs formulated, approved and reviewed by the Association.

MEMBERS OF ARGONNE UNIVERSITIES ASSOCIATION

The University of Arizona
Carnegie-Mellon University
Case Western Reserve University
The University of Chicago
University of Cincinnati
Illinois Institute of Technology
University of Illinois
Indiana University
Iowa State University
The University of Iowa
Kansas State University
The University of Kansas
Loyola University
Marquette University
Michigan State University
The University of Michigan
University of Minnesota
University of Missouri
Northwestern University
University of Notre Dame
The Ohio State University
Ohio University
The Pennsylvania State University
Purdue University
Saint Louis University
Southern Illinois University
The University of Texas at Austin
Washington University
Wayne State University
The University of Wisconsin

NOTICE

This report was prepared as an account of work sponsored by the United States Government. Neither the United States nor the United States Atomic Energy Commission, nor any of their employees, nor any of their contractors, subcontractors, or their employees, makes any warranty, express or implied, or assumes any legal liability or responsibility for the accuracy, completeness or usefulness of any information, apparatus, product or process disclosed, or represents that its use would not infringe privately-owned rights.

Printed in the United States of America
Available from
National Technical Information Service
U.S. Department of Commerce
5285 Port Royal Road
Springfield, Virginia 22151
Price: Printed Copy $6.00; Microfiche $0.95

ANL-7800
Reactor Technology

ARGONNE NATIONAL LABORATORY
9700 South Cass Avenue
Argonne, Illinois 60439

LMFBR NUCLEAR SAFETY PROGRAM
ANNUAL REPORT

July 1, 1969, to June 30, 1970

W. R. Simmons, Director
J. F. Marchaterre, Associate Director

Reactor Analysis and Safety Division

with contributions by

Argonne Center for Environmental Studies
Chemical Engineering Division
Engineering and Technology Division

July 1971

TABLE OF CONTENTS

Page

I. INTRODUCTION. 25

Single-assembly Accidents 27
Whole-core Accidents. 30
Containment and Energy Release. 32
Postaccident Heat Removal 33

II. SAFETY R&D HIGHLIGHTS 34

Accident Analysis and Safety Evaluation 34
Reactor Control and Stability 34
Coolant Dynamics. 35
Core Structural Safety. 36
Fuel Element Failure Propagation. 36
Fuel Dynamics Studies in TREAT. 37
Materials Behavior and Energy Transfer. 37
Fast Reactor Safety Test Facility Study 38
Fuel-Coolant Interactions 39
Postaccident Heat Removal 40
1000-MWe Safety Studies 40
Reactor System and Containment Structural Dynamic Response. 41
Thermal-plume Dispersion Studies. 41
Plant Dynamics and Control Analysis 41

Nuclear Safety Research and Development--LMFBR Safety

III. ACCIDENT ANALYSIS AND SAFETY EVALUATION 42

Overall scope. 42

Code for Initiating Accident. 43

Scope. 43
Summary. 43
Incorporation of a slug-ejection coolant-voiding model into the SAS1A code. 43
Upgrading functions of the SAS1A code. 46
Creation of the first version of SAS2A with multiple-channel capability 46
Incorporation of spatially dependent (two-dimensional) kinetics into the SAS1B code package 47
Creation of SAS1B code 47
Future program 47

Analysis of Fuel Behavior 48

Scope. 48
Summary. 48
The revision of the fuel deformation module in SAS1A . 49

TABLE OF CONTENTS

	Page
Analysis of Disassembly Accident, including Computer-code Development and Sensitivity Studies	52
Scope	52
Summary	53
VENUS code development	53
Equation of state	54
Time-step requirements and pressure oscillations	57
Application to mild excursions	62
References	65
IV. REACTOR CONTROL AND STABILITY	67
Overall scope	67
Reactor Stability and Stability Design Criteria for Spatially Dependent Systems	67
Scope	67
Summary	67
Spatial stability analysis with linear model	68
Spatial stability analysis with nonlinear model	68
Future program	69
Transfer-function Techniques to Measure Large Fast Reactor Stability	69
Scope	69
Summary	69
Source-detector spatial effects	70
Computer programs for solution of spatially dependent systems	70
Analysis of spatial transfer function of typical 1000-MWe LMFBR systems	70
Future program	72
References	72
V. COOLANT DYNAMICS	73
Sodium Superheat	73
Future program	80
Sodium Expulsion and Reentry	80
Future program	83

TABLE OF CONTENTS

Page

Liquid-Vapor Dynamics 84

Critical flow, void fraction, and two-phase pressure drop 84
Sonic velocity and pressure-wave propagation 92
Techniques for flow-regime and gas detection 94
Sodium bubble growth and collapse 97

Sodium Simulations 100
Mathematical Models of Voiding and Reentry 106
References 110

VI. CORE STRUCTURAL SAFETY 113

Overall scope 113
Summary 113

Dynamic Plasticity Analysis of Circular Shells 113
Hexagonal-shell Analysis 119
Future Program 119
References 120

VII. FUEL ELEMENT FAILURE PROPAGATION 121

Overall scope 121

Out-of-pile Studies 122

Scope 122
Gas-jet impingement experiments in heated channel . . . 122
Rapid-gas-release experiments with 19-pin unheated test section 126
Pressure distribution in the coolant plenum during coolant expulsion 134
Design and fabrication of a small sodium test loop . . . 141
Design and fabrication of a 19-pin heated test section for use in water 146
Design and fabrication of a 91-pin test section 146
Design of externally heated test sections for study of gas-jet impingement in sodium 147
Testing of heaters for simulation of fuel pins in sodium 147
Design of transient flow simulation loop 147

In-pile Studies 149

Scope 149
Design description of FEFPL 150

Heat exchanger 154
Sodium pump 158

TABLE OF CONTENTS

Page

Design description of FEFP test train. 160

Design requirements 161
Test-train description. 162

FEFPL instrumentation. 164

Sensors 166
Protection system 172
Control system. 174
Data acquisition. 177

FEFPL-ETR interface study. 178
Plans for initial test sequence. 182

Purpose 184
Planning bases. 184
FEFPL experiments 184
Schedule. 185
Loop usage. 187
Test-assembly design. 188
Postexperiment examination. 192

Analytical Studies. 194

Scope. 194
Test fuel-pin performance and neutron-filter requirements 197
ATSR experiment description and results. 203
Preliminary FEFPL dynamic model. 214
In-pile experiment safety studies. 217

Basis for loop design and safety of FEFP experiments 218
Safety requirements for instrumentation and scram systems 224

Model development. 229

References. 229

VIII. FUEL DYNAMICS STUDIES IN TREAT. 231

Overall scope. 231

Transient In-pile Tests with Oxide Fuel 231

Scope. 231
Summary. 232
Checkout Tests E1 and E2 on Mark-II-loop experiments on oxide-fuel movement during a power excursion. . . . 232

TABLE OF CONTENTS

Page

Test E1. 233
Test E2. 235

First two Mark-II-loop tests (H1 and H2) on mixed-oxide transient fuel-element failure threshold with axial heat transport by flowing sodium. 242

Test H1. 243
Test H2. 244

First Mark-II-loop test (E3) on fuel-movement failure of irradiated oxide pin during a power excursion. . . 247
Future program. 248

Experimental Support 249

Scope 249
Summary 250
Shipping-cask procurement documentation 250
Revision of Mark-II-loop quality-control package into new QAM format. 251
Review of Mark-II-loop fabrication costs. 252
Safety aspects of the elevated-temperature behavior of DC-200 silicone cooling oil used with the Mark-II loop 252
Thermal-neutron filter for Mark-II-loop experiments . . 254
Suppression of sodium-slug impacts in the Mark-II loop. 255
Stress analysis of Mark-II loop with dump tank. 255
Prooftests of B1, B2, and B3 loops for use in Tests H1, E3, and L1. 258
Pressure transducers for Mark-II loops. 259
Adaptation of accessories for minimal cave usage of Mark-II loops with irradiated mixed oxide. 261
Future program. 261

Analytical Support 262

Scope 262
Summary 262
Evaluation of SAS1A modeling of loop Checkout Tests E1 and E2 262
Evaluation of SAS1A modeling of first mixed-oxide-pin loop experiment with single pin in simulated FFTF cell (Test H1). 263
Analysis of impacts inside Mark-II sodium loops under assumed limiting-case hazards conditions. 264
Analysis of radiation effects on superheating of liquid sodium. 265
Demonstration of basic capability for automated handling of hodoscope data. 265
Future program. 266

TABLE OF CONTENTS

Page

Hot Laboratory Examinations. 266

Scope 266
Summary 267
Postmortem inspection of pin from Checkout Test E1. . . 267
Nondestructive test of unirradiated PFR mixed-oxide pins. 267
Nondestructive test of PFR mixed-oxide pins irradiated to 5% burnup in DFR 267
Examination of the 3%-burnup "lead" pin from the first unencapsulated oxide assembly run in EBR-II 268
Postmortem inspection of sample from Checkout Test E2 . 272
Future program. 272

References 272

IX. MATERIALS BEHAVIOR AND ENERGY TRANSFER 276

Overall scope 276

Theoretical Extrapolation of Measured Physical Properties to Very High Temperatures. 276

Scope 276
Summary 277
Correlation of experimental data obtained from high-temperature physical-property studies with corresponding states theory and other pertinent theories; development of useful equations of state for reactor materials 277
Future program. 279

High-temperature Physical-property Studies 279

Scope 279
Summary 280
Experiments to determine enthalpies and heat capacities of molten UO_2 280
Experimental determination of enthalpies and heat capacities of solid $(U_{0.8}Pu_{0.2})O_2$ 282
Determination of total pressure over molten UO_2 using transpiration method. 282
Construction and testing of speed-of-sound apparatus. . 284
Speed-of-sound measurements in molten sodium to 1800°K. 284
Construction of apparatus for matrix-isolation spectroscopy. 285
Future program. 285

Segregation of Pu in Fast Reactor Fuels under a Thermal Gradient 285

TABLE OF CONTENTS

Page

Scope. 285
Summary. 286
Study of segregation of Pu in mixed-oxide and carbide fuel materials under an impressed thermal gradient . . 286
Future program 288

References. 288

X. FAST REACTOR SAFETY TEST FACILITY STUDY 289

Overall scope. 289

Programmatic Definition and Justification 289

Scope. 289
Summary. 290
Preliminary draft of report "Vol. I: Program," to RDT, DRL, PRO, and industry for review and comment. 290
Comments on Vol. 1 draft; revision of draft to take account of comments. 291
Delineation of LMFBR accidents to identify potential accidents, accident sequences, approaches, and uncertainties. 291

Single-assembly accident. 292
Whole-core loss-of-flow accidents 298
Whole-core power-excursion accidents. 301
Related safety issues 305

Future program 305

Facility Definition and Utilization 307

Scope. 307
Summary. 307
Evaluation of capability of existing and firmly planned facilities, including reasonable modifications 307

TREAT description 308
TREAT accommodations. 308
TREAT energetic capabilities. 308
TREAT operating limitations and availability. . . . 311
SEFOR description 311
SEFOR accommodations. 312
SEFOR energetic capabilities. 312
SEFOR operating limitations and availability. . . . 314
PBF description 314
PBF accommodations. 315
PBF energetic capabilities. 315
PBF operating limitations and availability. 317

TABLE OF CONTENTS

Page

ETR description 318
ETR accommodations. 318
ETR energetic capabilities. 318
ETR operating limitations and availability. 319

Future program 319

References. 319

XI. FUEL-COOLANT INTERACTIONS 321

In-pile Tests 321

Pressure and work energy (S series). 321

Description of piston autoclave 321
Summary of experimental results 323

Test S2. 323
Test S3. 326
Test S4. 328
Test S5. 332

Discussion of work energy 337

Impact of sodium on molten UO_2 (I series). 338

Laboratory Experiments. 340

Fragmentation of molten UO_2 upon contact with sodium . . 340
Fragmentation experiments with materials having different thermal properties 344

Experimental procedure and data analysis. 345
Results and discussion. 345

Simulation experiments of coolant entrapment in molten fuel. 349

Experimental procedure and measurements 349
Results and discussion. 350

Model Development 358

Rate-limited model of interaction of molten fuel and coolant. 358

Formulation of the model. 359

TABLE OF CONTENTS

Page

Compressible liquid; acoustic formulation . . 362
Incompressible liquid; inertial formulation . 362

Preliminary calculations 362

Fuel failure analysis 369

References 371

XII. POSTACCIDENT HEAT REMOVAL. 373

Engineering Analyses 375

Thermal conduction from and stability of individual fuel-debris pieces in sodium. 377
Natural convection from porous piles of fuel debris in sodium 377
Change in effective thermal conductivity due to nonfuel material in the debris. 378
Heat conduction from porous beds of fuel pieces in sodium. 379
Heating in a blocked subassembly. 380
Heat transfer from pools of fuel debris 380
Meltthrough of uncoded thin semisupported steel plates by molten fuel debris 383
Penetration by molten fuel debris of sacrificial barrier material such as concrete or depleted UO_2 . . 383
Meltthrough of metal plates or trays in sodium. 384
Fission-product-decay heating 385

Experiments on Interactions of Fuel and Materials of Construction 386

Future program. 386

References 387

XIII. 1000-MWe SAFETY STUDY CONTRACT MANAGEMENT, TECHNICAL REVIEW, AND EVALUATION 388

Overall scope 388

Management and Technical Review of Subcontractors' Studies . 389

Scope 389
Summary 389
Preparation and negotiation of technical scopes of work with subcontractors 390
Management and review of Babcock & Wilcox 1000-MWe LMFBR Accident Analysis and Safety System Design Study 390

TABLE OF CONTENTS

Page

Management and review of Westinghouse 1000-MWe Loop-type LMFBR Safety, Dynamics, and Primary-system Study 391
Management and review of General Electric 1000-MWe LMFBR Probabilistic Plant Safety Analysis Study 391
Management and review of Atomics International 1000-MWe LMFBR Emergency Shutdown System Study 392
Future program. 392

Technical Evaluation of Subcontractors' Formal Study Reports 392

Scope 392
Summary 393
Evaluation of safety aspects of 1000-MWe LMFBR Follow-on Studies; preparation of draft final evaluation report 393
Evaluation of phase reports on Babcock & Wilcox 1000-MWe LMFBR Accident Analysis and Safety System Design Study 393
Future program. 394

References 394

XIV. 1000-MWe SAFETY STUDY SUBCONTRACTS 395

Overall scope 395

The Babcock & Wilcox Co. Subcontract 396

Scope 396
Summary 396
Program Definition Phase: Preparation of Work Plan . . 396
Phase I: Malfunction and Safety Problem Survey 397
Adjunct study to determine effect of metal swelling on models and parametric ranges used in accident analysis. 397
Phase II: Accident Analysis and Selection of Safety Systems 397
Phase IV: Research and Development Delineation 397
Future program. 397

Westinghouse Electric Corp. Subcontract. 398

Scope 398
Summary 399
Reference-design modification for oxide core. 399
Program Definition Phase: Preparation of Work Plan . . 399
Phase I: Preparation for Accident Analysis and Safety System Development, and Related Work in Concurrent Dynamics and Loop Studies 399
Future program. 399

General Electric Co. Subcontract 400

TABLE OF CONTENTS

Page

Scope. 400
Program Definition Phase: Preparation of Work Plan. . . 401
Future program 401

Atomics International Subcontract 401

Scope. 401
Program Definition Phase: Preparation of Work Plan. . . 402
Future program 402

Reference 403

Engineered Safety Features--Safety Features Technology--R&D

XV. REACTOR SYSTEM AND CONTAINMENT STRUCTURAL DYNAMIC RESPONSE. . 404

System Geometries and Excursion Magnitudes and Durations. . . 410
Automatic Rezoning of Code to Extend Excursion Treatment into Sodium-momentum Domain 412
Code Transformation 412
Comparison of Codes with Existing Experiments 415
Heat Transfer in Postburst Accident Analysis. 420
Analysis of an Accident 421
The Heat-transfer Problem 422
Analysis of the Heat-transfer Problem 424
References. 425

Nuclear Safety Research and Development--Effluent Control--Environmental Studies

XVI. THERMAL-PLUME DISPERSION STUDIES. 426

Scope. 426

Numerical Modeling. 426
State-of-the-Art Reports. 429

Physical scale modeling. 429
Experimental field work. 432
Analytical modeling. 432

Mass-and-Energy Balance of the Great Lakes. 434
References. 436

Component Development--LMFBR--Instrumentation and Control

XVII. PLANT DYNAMICS AND CONTROL ANALYSIS 437

Scope. 437
Summary. 437

TABLE OF CONTENTS

	Page
Review and Monitoring of 1000-MWe LMFBR Follow-on Studies	437
Compilation of Information on Component Dynamics	437
Development and Simulation of Complete-plant Model	437
Reactor	438
Intermediate heat exchanger	438
Reheater	438
Steam generator	438
Coolant pipelines	439
Turbine, generator, condenser, and feedwater heaters	440
Control systems	440
Multiple loops	440
Future program	441
References	442
Systems and Plant Development--LMFBR--Plant and Design	
XVIII. 1000-MWe PLANT STUDY CONTRACT MANAGEMENT, TECHNICAL REVIEW AND EVALUATION	443
Overall scope	443
Management and Technical Review of Subcontractors' Studies	444
Scope	444
Summary	444
Preparation and negotiation of technical scopes of work with subcontractors	445
Future program	445
Technical Evaluation of Subcontractors' Formal Study Reports	445
Scope	445
Summary	446
Evaluations of 1000-MWe Follow-on Studies	446
Plant design and safety	448
Plant temperature study	450
Engineering analysis	454
Economics	456
Research and development	458
Overall	460
Future program	460
References	460

LIST OF FIGURES

No.	Title	Page
1.	ANL Safety Program	27
2.	Effect of Pressure-temperature History on Incipient-boiling Superheat	76
3.	Variation of Incipient-boiling Wall Superheat with Either Increasing or Decreasing Heat Flux	78
4.	Superheat Requirements for Various LMFBR Operating Conditions	79
5.	Effect of Incipient-boiling Superheat on the Nominal Void Fraction in the Two-phase Region during Expulsion	81
6.	Effect of Incipient Bulk Liquid Superheat ΔT_ℓ on the Transient Sodium-column Displacement	82
7.	Variation of Initial Pressure Rise in Liquid with Incipient Superheat	83
8.	Variation of "Sodium-hammer" Pressure Pulses following Vapor Collapse with Liquid Subcooling	84
9.	Sodium Flashing Facility	85
10.	Comparison between Measured Sodium Liquid Volume Fraction and the Lockhart-Martinelli Correlation	86
11.	Comparison of Measured Wall Temperatures and Saturation Temperatures Converted from Simultaneous Pressure Measurements	87
12.	Illustration of Incipient Superheat and Pressure Generation Followed by Steady Flashing in Forced-convection Sodium Flow	87
13.	Typical Pressure Profiles for Flashing Sodium, and Comparison with Calculated Values	90
14.	Measured Critical Flowrate of Sodium and Comparison with Several Models	90
15.	Comparison of the Critical Parameters for Different Downstream Geometries	91
16.	Comparison between Predicted and Measured Pressure Wave Propagation Velocities in Bubbly and Stratified Steam-Water Mixtures	94
17.	Comparison between Predicted and Measured Pressure-wave Propagation Velocities in Air-Water Mixtures	95

LIST OF FIGURES

No.	Title	Page
18.	Comparison of Analytically Predicted and Experimental Data for Pressure-propagation Velocity in Two-phase Flow Regimes	96
19.	Propagation Velocity in a Homogeneous Two-phase Sodium-Argon System at 1200°F and 14.7 psia as a Function of Mass or Volume Fraction.	96
20.	The Growth Behavior of a Sodium Vapor Bubble in Highly Superheated Sodium at Atmospheric Pressure	98
21.	Pressure of the Vapor P in a Collapsing Sodium Bubble as a Function of Its Dimensionless Radius R/R_o for a Range of Subcoolings ΔT_s and Initial Radii R_o	98
22.	Pressure Distribution in the Liquid for a Typical Case . . .	99
23.	Single-channel Expulsion Event Illustrating Rapid Bubble Growth, Slug Ejection, and Two-phase Flashing for Methyl Alcohol at 122°F, Depressurized to 0.4 psia.	104
24.	Voided Channel Height vs Expulsion Time, Illustrating Effect of Liquid Wall Film.	107
25.	Vapor Pressure within Bubble vs Expulsion Time, Illustrating Effect of Wall Film on Pressure History.	108
26.	Voided Channel Height vs Expulsion Time, Illustrating Effect of Heat Capacity of Fuel Pin on the Rate of Expulsion. . . .	108
27.	Vapor Pressure vs Expulsion Time, Illustrating Effect of Heat Capacity of Fuel Pin on Pressure History within Vapor Bubble	109
28.	Voided Channel Height vs Time for Slug Expulsion of Freon-113 at Constant Plenum Pressure.	110
29.	Circular Cylindrical Shell Loaded by an Axially Varying Pressure	115
30.	Load Shape $\Phi(Z)$ and Pulse Shape $\Psi(t)$	116
31.	Maximum Plastic Deformation as a Function of Ψ_{max} and Φ_e for Various Pulse Shapes	117
32.	Maximum Plastic Deformation as a Function of L and L_e for Various Load Shapes.	117
33.	Load Shape Family $\Phi_\gamma(Z)$.	118

LIST OF FIGURES

No.	Title	Page
34.	Spray Pattern and Interface between Gas Jet and Coolant. . . .	125
35.	Heat-transfer Coefficient at Point of Gas-jet Impingement. . .	125
36.	Test with 0.025-in. Orifice, 20-ft/sec Coolant Velocity, and 750-psi Gas Pressure	126
37.	19-pin Test Section Mounted Vertically in Forced-circulation Water Loop	129
38.	Water Test Loop.	130
39.	Typical Transient for Test with Coolant Velocity of ∿30 fps, Plenum Pressure of 900 psia, and a Slot of 1/16 x 1/8 in. . .	130
40.	Sequence of Bubble Expansion at Various Time Intervals for Typical Transient.	131
41.	Interface Displacements for Test Conditions: 900-psi Gas-plenum Pressure, 30-ft/sec Coolant Velocity, and 1/16 x 1/8-in. Slot	132
42.	Description of the Coordinate System	136
43.	Velocity and Acceleration Distributions in the Inlet Section during Coolant Expulsion Due to Rapid Fission-gas Release at the Center of 19-pin Fuel Assembly.	140
44.	Axisymmetric Two-dimensional Pressure Distribution in the Plenum at z = 0.	140
45.	Comparison of the Spatially Averaged Pressure with the One-dimensional Pressure Distribution.	141
46.	Small Sodium Test Loop	142
47.	Transient Flow Simulation Loop	148
48.	FEFP Loop within ETR	151
49.	System Diagram for Fuel-element Failure-propagation Loop . . .	153
50.	Heat Exchanger	155
51.	Annular Linear-induction Pump.	159
52.	FEFP Test Train.	163
53.	Instrumentation System	165

LIST OF FIGURES

No.	Title	Page
54.	Loop and Test-train Sensors	167
55.	Typical Element-centered FEFPL Test Sections	191
56.	Typical Channel-centered FEFPL Test Sections	191
57.	29-element Multiple-assembly FEFPL Test Section	192
58.	Multiple-assembly FEFPL Test Sections	193
59.	In-core Test-train and Loop Cross Section	197
60.	Analytical Model of FEFP Test	198
61.	Energy Dependence of Neutron Flux	198
62.	Heat Generation and Enrichment	202
63.	Effect of Quantity of Steel in Test Section	202
64.	Effect of Neutron-filter Mean Radius	203
65.	Heat Generation vs Enrichment for a 19-fuel-element Assembly in a Thermal Reactor with 10^{14} n/cm^2-sec Incident on the Neutron Filter	203
66.	Fission Distribution Among 16 Energy Groups for 19-fuel-element Bundle	204
67.	Effect of Filter Thickness on Power Density	204
68.	Power Gradient on the Diameter of Fuel	205
69.	Fission Distribution Inside Fuel Elements	205
70.	ATSR Experiment Cross Section	205
71.	Location of Foil Inside Typical Test Fuel Element	206
72.	ATSR Loading	207
73.	Neutron Radiograph of B_6Si Neutron Filter	208
74.	Typical Etched Fission-particle Tracks in Lexan	211
75.	Optical Density vs Number of Tracks	211
76.	Power Generation Across Fuel-element 1A	212
77.	Power Generation Across Fuel-element 2B	212

LIST OF FIGURES

No.	Title	Page
78.	Power Generation Across Fuel-element 3C.	213
79.	Power Generation Across Fuel-element 4C.	213
80.	Heat Exchanger	215
81.	FEFPL - ALIP Performance Curves.	216
82.	MFCI vs Chemical Explosion; P-V Plot	221
83.	MFCI vs Chemical Explosion Work Is Given As a Function of the Final Pressure of Expansion.	221
84.	Energy-release Time Histories Based on ANL Rate-limited Model.	222
85.	Transient Data from Checkout-1 Oxide Meltdown Experiment in the Mark-II TREAT Sodium Loop.	234
86.	Artist's Rendering of The Posttest Neutron Radiographs of the E1 Test Pin, Showing Extensive Movement of Molten Fuel Inside the Unfailed Cladding during the Transient	237
87.	Instrument Data from Checkout-2 Mark II Loop Experiment. . .	238
88.	View of E2 Test Section after Being Cut Open during Post-transient Inspection	240
89.	Orientation of Test Pins for E2 Test Section	241
90.	Transient Data for the Fuel-failure-threshold Test H1. . . .	243
91.	Comparison of Calculated and Experimental Transient Outlet Coolant Temperatures from Test H1.	244
92.	Transient Data for the Fuel Failure Threshold Test H2. . . .	246
93.	Transient Data from Irradiated-oxide-fuel Test E3.	249
94.	Configuration of the Revised Shipping Cask	251
95.	Cross Section of Shipping-cask Package	251
96.	Fretting Scratches under Spacer Wire in Fuel Region of Pin 012 from Subassembly X040.	269
97.	Transverse Section 5/8 in. from Top of Fuel Column in Pin 012	270
98.	Enthalpy of UO_2.	281

LIST OF FIGURES

No.	Title	Page
99.	Accident Sequences and Key Uncertainties for Single-assembly Accidents	294
100.	Axial Coolant Temperature Profiles in FFTF Hot-channel Subassembly after Sudden Reduction to 10% Flow	295
101.	Percentage of Fuel Molten vs Time after Complete Vapor Blanketing of FFTF Hot-channel Subassembly	296
102.	Accident Sequences and Key Uncertainties for Whole-core Loss-of-flow Accidents	299
103.	Peak Cladding Node Temperature vs Time for FFTF Flow-coastdown Transient	300
104.	Power and Reactivity vs Time for FFTF Hypothetical Flow-coastdown Transient	300
105.	Power and Reactivity vs Time for 1000-MWe Target-plant Hypothetical Flow-coastdown Transient	301
106.	Accident Sequences and Key Uncertainties for Whole-core Power-excursion Accidents	303
107.	Peak Fuel Node Temperature and Fraction Melted vs Time for FFTF Hypothetical $1/sec Reactivity-insertion Transient	304
108.	Piston Autoclave for High-energy Meltdown Experiments and Measurement of Transient Pressure and Sodium Expulsion	322
109.	Top View of 9-rod Fuel Cluster for Fuel-meltdown Studies in Sodium	322
110.	Motion, Pressure, and Reactor Power during Third Transient of Test S2	325
111.	Portion of Ruptured Fuel Rod Showing Failure	326
112.	Linear Motion, Pressure Response, and Sodium Temperature for Test S3	327
113.	Residue of Fuel and Dummy Rods from Test S3	329
114.	UO_2 Residue from Test S3 in Form of Hollow Cylinders	330
115.	Section of Fuel Rod Welded to Dummy Rod by Melting of the Cladding	331
116.	Linear-motion and Pressure-pulse Data from Test S4	332

LIST OF FIGURES

No.	Title	Page
117.	Pressure-response Output from Test S5 with Evacuated Fuel Pins	334
118.	Residue from Test S5 with Evacuated Fuel Pins	336
119.	In-pile Autoclave for Tests of Sodium Impacting on Molten UO_2	339
120.	Apparatus for Pouring Inductively Melted UO_2 into Liquid Sodium	341
121.	Size Distribution of UO_2 Particles Resulting from Interaction of Molten UO_2 with Sodium	343
122.	Effect of Entrance Velocity on Fragmentation of Molten Tin Quenched in 22°C Water	346
123.	Effect of Water Subcooling on Fragmentation of Molten Tin Quenched in Water	346
124.	Particle-size Distribution of Tin Fragmented in Water	348
125.	Percent Frequency vs Log Diameter for Tin Fragmented in Water	349
126.	Events after 1 ml of Room-temperature Water Was Injected Just under Surface of 600°C Molten Tin at Various Times from Start of Injection	355
127.	Events after 3 ml of Room-temperature Water Were Injected into Molten Sodium Chloride at 900°C	357
128.	Dynamic Relations of Volume Change of the Heat Coolant with Constraints by the Surrounding Liquid	363
129.	Effect of Heating Rates on Pressure Generation; Acoustic Constraints	365
130.	Voiding Histories in an FFTF Subassembly	368
131.	Yield Strength of 304ss and Gas Pressure in Active Section of Fuel Pin	371
132.	Calculated Maximum Thickness or Diameter of a Slab, Cylinder, or Sphere for No Fuel Boiling, where T_s = 900°C, T_b = 3179°C, and k = 0.005 cal/sec-cm-°C	378
133.	Heat Transfer from Blocked Subassembly to Adjacent Subassemblies	381

LIST OF FIGURES

No.	Title	Page
134.	Pool Radius for Depleted-UO_2 Barrier.	384
135.	Pool Radius for Concrete Barrier.	385
136.	Deformations of Lagrangian Grids at Various Times after Start of a Power Excursion in a "Pancake" Core Configuration. . . .	406
137.	Pressure Profiles Along Vertical Centerline of Core at Various Times	408
138.	Pressure Profiles Along Horizontal Axis of Core at Various Times	408
139.	Variation of Pressure at a Typical Mesh Zone Underneath the Plug.	409
140.	Total Force Acting on the Rotating Plug as a Function of Time	409
141.	Pressures (z) at Points on x-y Plot as Drawn by PLOT-3D Fortran Subroutine.	410
142.	Reactor Configuration with Two Vessels is Typical of Arrangement for Which REXCO-H Code Can Be Used to Study Sequence of Failures and Effects of Loads Imposed on System Components. .	411
143.	How Presence or Absence of Inner Vessel That Ruptures during Excursion Affects Total Force Imposed on Shield Plug.	411
144.	Example of Deformed Lagrangian Grid for Containment Study . .	414
145.	Eulerian Particle Distribution Corresponding to Deformed Lagrangian Grid Shown in Fig. 144	414
146.	Power-generation Cost vs Reactor Outlet Temperature	452

LIST OF TABLES

No.	Title	Page
I.	Illustration of Vapor Growth Rate Simulation	103
II.	Test-Train Sensors	168
III.	FEFPL Loop Containment Sensors	171
IV.	FEFPL Sensors External to the ETR	173
V.	Summary of FEFPL Reference Experiments	186
VI.	FFTF Fuel-element Design and Operating Conditions	190
VII.	Postexperiment Examination of FEFP Loop	194
VIII.	Postexperiment Examination of FEFP Test Train	195
IX.	Power Density in Assemblies Containing 7, 19, and 37 UO_2 Fuel Elements; 35-mil Cadmium Filter	200
X.	Power Gradients in Fuel Elements	201
XI.	Fast-fuel Irradiations in ATSR	209
XII.	Experimental Conversion Efficiencies of Thermal Energy to Work	220
XIII.	Estimated Work Energies	222
XIV.	FEFPL Design Capabilities	224
XV.	Experimental Backup to First Twelve Experiments	225
XVI.	Time Estimates L/C Event Sequence	227
XVII.	Time Estimates for Reactor Scram	228
XVIII.	Summary of General Accident Categories	293
XIX.	Uncertainties and Their Priorities for Single-assembly Accidents	297
XX.	Uncertainties and Their Priorities for Whole-core Loss-of-flow Accidents	302
XXI.	Uncertainties and Their Priorities for Related Safety Issues	306
XXII.	Uncertainties and Their Priorities for Whole-core Power-excursion Accidents	306

LIST OF TABLES

No.	Title	Page
XXIII.	Experimental Conditions and Results from Piston-autoclave Tests S2, S3, S4, and S5.	324
XXIV.	Experimental Conditions for Dropping of UO_2 into Sodium . . .	341
XXV.	Results of Experiments on Dropping Molten UO_2 into Sodium . .	342
XXVI.	Molten Material-Water Explosions in Water-injection Tests . .	351
XXVII.	Calculational Results for Acoustic Constraint	366
XXVIII.	Hydraulic Modeling of Thermal Plumes.	431
XXIX.	Effects of Utility Discharges on the Great Lakes--Present and Projected	435
XXX.	Summary of Plant Characteristics Reported	451

I. INTRODUCTION

The progress of safety activities at Argonne during FY-70 is described in this annual report. The material is presented by areas of phenomenology being investigated or by general technical areas of work. This introduction shows the relation of these research efforts to potential reactor accidents of interest and serves to put in perspective the ANL safety program as it relates to the development needs of the liquid metal fast breeder reactor (LMFBR).

The Liquid Metal Fast Breeder Reactor Program Plan (Volume I) lists safety as the first of the four major technical requirements for initial commercial feasibility of LMFBRs. It states that the goals of the safety plan are:

(a) To enable the designer to demonstrate that the probability of any major accident is very small and that minor accidents and mishaps cannot escalate into a major occurrence.

(b) To demonstrate that the containment design and site selection will be adequate to protect public health and safety.

The LMFBR Safety Program at Argonne is concerned with both of these goals. The program is guided by the projected information needs of the LMFBR designers and operators. These needs are developed from analysis of possible malfunctions of specific designs, experience in the design of early fast reactors, close touch with current safety problems by operation of EBR-II and by frequent communication with those engaged in reactor design and development, and by participation in safety development work for near-term AEC reactors.

The LMFBR activities at Argonne reported in this annual report are:

1) Accident Analysis and Safety Evaluation

2) Reactor Control and Stability

3) Coolant Dynamics

4) Core Structural Safety

5) Fuel Element Failure Propagation

6) Fuel Dynamics Studies in TREAT

7) Materials Behavior and Energy Transfer

8) Fast Reactor Safety Test Facility Study

9) Fuel-Coolant Interactions

10) Postaccident Heat Removal

11) 1000-MWe Safety Studies

12) Reactor System and Containment Structural Dynamic Response

13) Thermal-plume Dispersion Studies

14) Plant Dynamics and Control Analysis

15) 1000-MWe Plant Study Evaluation

Figure 1 shows schematically these LMFBR safety activities. The needs for safety research stem from the considerations of accidents. In fiscal-year 1970, the Laboratory conducted an extensive review of possible accidents, possible approaches to cope with these accidents, uncertainties associated with each approach, and design-related safety issues. This effort focused first on safety issues of importance to near-term reactors (FFTF and demonstration plants) and will be extended to safety issues peculiar to the larger target plants. The results of this accident delineation effort are reported under the Fast Reactor Safety Test Facility Study.

ANL programs address five major categories of LMFBR safety problems as described by the accident delineation study: single-assembly accidents, whole-core loss-of-flow accidents, whole-core power excursions, containment and energy release, and postaccident heat removal.

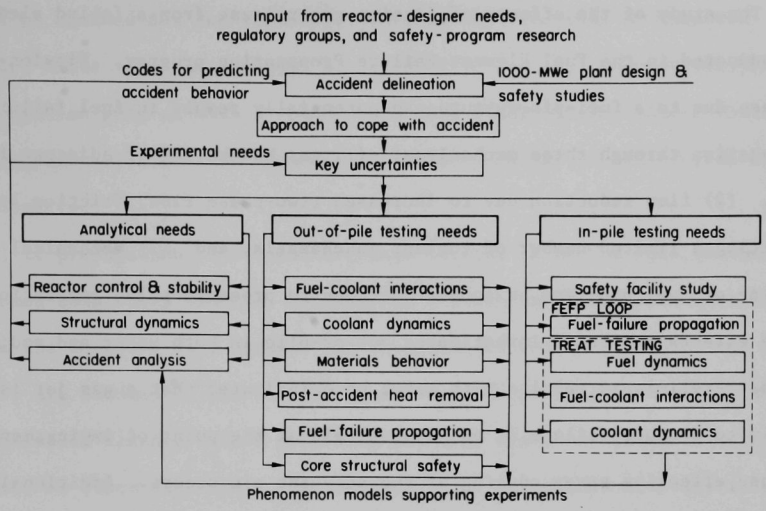

Fig. 1. ANL Safety Program

Single-assembly Accidents

Conceivably, local perturbations such as coolant blockage or random fuel-pin failure could lead to propagation of damage within a fuel assembly. An understanding of these potential propagation processes is needed so that reactor and fuel-assembly design parameters can be chosen to assure that damage is minimized and localized. The key uncertainties associated with single-assembly accidents include:

1) Effects of fission-gas release on failure of a single pin
2) Behavior of failed fuel
3) Behavior of small blockages
4) Effects of release of small amounts of molten fuel
5) Sodium expulsion and reentry
6) Work-energy release from molten-fuel coolant interactions
7) Ability of the duct to contain this energy release and to resist meltthrough

The study of the effects of fission-gas release from a failed element is conducted in the Fuel Element Failure Propagation program. Fission-gas release due to a fuel-pin rupture can potentially result in fuel failure propagation through three mechanisms: (1) gas blanketing of adjacent fuel pins, (2) flow reduction due to increased (two-phase flow) friction losses affecting a limited number of coolant subchannels, and (3) mechanical loading of fuel pins and hexagonal duct due to pressure-pulse generation. These effects are being investigated out-of-pile in both water and sodium loops. Preliminary results with water have indicated that a gas jet is not likely to produce failure in an adjacent pin at the point of impingement because effective spray cooling of the adjacent pin occurs. Additional tests and analysis of other potential modes of propagation by gas release are continuing. In-pile tests to study the behavior of fuel after failure are being planned in the Fuel Element Failure Propagation program.

The behavior of small blockages, large enough to cause localized boiling, will be studied out-of-pile in the Coolant Dynamics program. The purpose of this program is to determine whether localized boiling is stable; i.e., that the boiling will not lead to flow stoppage or other adverse conditions within the assembly. If small blockages lead to stable localized boiling, then the probable effect of a blockage in the heated zone is localized fuel-pin failure and melting with the ultimate release of small amounts of molten fuel. Tests in TREAT in the Fuel Dynamics activity are planned to investigate this effect and to determine if this is a potential mechanism for propagation, and, if it is, whether it is a rapid or slow, row-by-row process. These tests will be conducted with a few over-enriched pellets or a fuel blockage installed within a seven-pin cluster in the Mark-II Loop. Using a flat power burst in TREAT, a molten fuel release

will be created and the tendency toward propagation will be observed. Later, tests of a similar type are planned in the Fuel Element Failure Propagation program with a sodium loop in a steady-state reactor where propagation effects that might develop over a longer period of time can be observed.

If propagation of a local blockage occurs, or if the fuel assembly becomes completely blocked, boiling and general expulsion of the coolant from the assembly will occur. The phenomena of sodium expulsion and reentry are studied in the Coolant Dynamics program using both metallic and nonmetallic fluids. These phenomena are also important in whole-core accidents, as discussed later. In addition, work under this activity in bubble growth and collapse has indicated that pressure sensors might be used as detection systems in the event of fuel-assembly voiding. Considerable progress has been made in the understanding of sodium expulsion, and some early models describing the process are available. In the case of sodium reentry, the problems are more complex and a series of in-pile simulation tests are being planned.

If reactor scram does not occur after full fuel-assembly voiding, then fuel melting and a fuel-coolant interaction upon reentry might occur. The mechanisms of fuel-coolant interactions and the related work-energy release are being studied in the Fuel-Coolant Interactions program. In this program, tests in the laboratory and TREAT are underway to assess the effects of fuel-coolant interactions in reactor accident situations. Results of early tests conducted in TREAT have indicated low conversions of thermal to mechanical energy. Further tests and supporting laboratory experiments are planned.

Propagation of failure to adjacent ducts depends on the amount and character of energy release, and on the capability of the ducts to contain it. Analytical studies to establish the structural capability of assembly ducts are carried out under the Core Structural Safety activity. Experiments are being planned in the Reactor System and Containment Structural Dynamic Response activity to verify analytical results and to demonstrate duct capabilities. In-pile experiments to investigate the ability of assembly ducts to resist meltthrough are planned. Early experiments under the limiting conditions of the Mark-II loop and the TREAT reactor will be conducted in the Fuel Dynamics activity. These tests will be extended under the Fuel Element Failure Propagation program when the FEFP loop becomes available.

Whole-core Accidents

Coolant-pump failures, hypothetical pipe-rupture events, and reactivity insertions are important sources of potential whole-core accidents. The sequence of events following such initiating occurrences must be understood so the consequences of hypothetical, unprotected accidents can be established to test the adequacy of containment and consequence-limiting safety features.

Key uncertainties amenable to experimentation include: conditions for boiling initiation, failure thresholds, coherence of failure of elements, coolant expulsion and reentry, and fuel movement. Boiling initiation and coolant expulsion and reentry are studied out-of-pile in the Coolant Dynamics activity. TREAT experiments in the Fuel Dynamics activity are directed at establishing failure thresholds, the motion of molten fuel during simulated loss-of-flow accidents, fuel motion and interactions with coolant leading to coolant voiding, and possibly some

information on the coherence of failure of elements. A series of TREAT tests in the Fuel-Coolant Interactions activity will simulate expulsion and reentry and the following course of events. The end product of the experimental studies of the behavior of coolant and molten fuel are data and models that can be used to predict reactivity changes during loss-of-flow and reactivity accidents.

Analytical models of the above processes are incorporated into safety codes in the Accident Analysis and Safety Evaluation activity. This activity covers the two broad areas of whole-core accident initiation and core disassembly analysis. The computed yield of a disassembly accident can be influenced strongly by the character of the preceding initiating events. For this reason, Argonne's SAS code efforts have been focused on development of realistic models of these events, including: neutron kinetics and heat transfer, coolant voiding through expulsion by fission-product gases and by boiling, fuel-rod failure, fuel dynamics, coolant reentry, fuel-coolant interactions, and associated reactivity feedback effects. The adequacy of proposed analytical models for the various processes is tested by comparison with related experiments.

The analysis of low probability disassembly accidents typically used as a basis to test containment is done with the VENUS code. VENUS represents a significant improvement over previous disassembly codes. It employs more correct hydrodynamics, in that the equation of continuity is satisfied during the core expansion process: not included in prior disassembly codes. Density variations in core materials are computed explicitly, permitting a density-dependent equation of state to be used. The net effect is a capability to account for the influence of pressures generated by local compression of core materials, as well as the customary

material vapor pressures. Typically, this gives increased pressures at a given energy density, more rapid core expansion, and reduced total energy yield.

Material properties and equations of state for core materials at the high temperatures and pressures of interest in accident analysis are essential input data for all accident analyses. In general, these data are not known with adequate accuracy. Experimental measurements and theoretical estimations of such information are done in the Materials Behavior and Energy Release activity.

Containment and Energy Release

One result of hypothetical whole-core accidents is a rapid generation of thermal energy. Containment design requirements depend on the prediction of the extent to which this thermal energy can be converted into mechanical work and the capability of core and plant structures to contain safely this work-energy release. The Fuel-Coolant Interactions activity investigates the conversion of thermal to work energy that results from contact of molten core materials with coolant and the character of these events.

Codes to analyze the structural response of the reactor vessel, vessel internals, and appurtenances are developed in the Reactor System and Containment Structural Dynamic Response activity. the REXCO-H code treats the response of reactor components hydrodynamically and includes a representation of the reactor vessel by membrane stresses. An automatic rezoning technique to permit accurate computation for large expansions and low pressures has been incorporated into the code. Further work to treat the response of geometrically complex in-vessel structures is underway.

The input to REXCO is the output data from VENUS, which is obtained directly from the preceding accident-analysis studies. Thus, the computed

pressure-volume characteristic of the reactor excursion is used rather than the equivalent of a chemical explosion, as frequently is used for such work. A program of testing REXCO code predictions against the results of scale-model explosion tests is underway. Results to date show good agreement for intensity and time of arrival of pressure pulses at various points in the system.

Results obtained in these activities will have an important effect on LMFBR design features, including the reactor vessel, the vessel cover, the cover restraint, the head cavity, and the secondary containment.

Postaccident Heat Removal

This safety category concerns the long-term containment of core debris resulting from hypothetical disruptive accidents. Key uncertainties include: the behavior of molten core material in sodium and the interactions of core debris with structure. The former problem is studied in the Fuel-Coolant Interactions activity, while the latter is part of the Postaccident Heat Removal activity. Overall analyses of the problem are carried out in the Postaccident Heat Removal activity. Results from these efforts will have an important bearing on the design of heat-removal and debris-containment systems and on the design of a lower cavity of an LMFBR.

II. SAFETY R&D HIGHLIGHTS--FY 1970

Accident Analysis and Safety Evaluation. The basic programming for the multiple-channel accident-analysis code SAS2A was completed. Creation of the multiple-slug sodium-voiding module represents a major technical advancement. This model includes fission-product-gas escape as a possible sodium-voiding-initiation mechanism. Its treatment of dryout of sodium films provides a solid technical base for the fuel-collapse model that is being developed. If the course of the accident leads toward rapid reactivity addition and disassembly, SAS2A will switch to the VENUS reactor-disassembly analysis code.

The VENUS code was made available. It employs a two-dimensional hydrodynamics analysis of reactor displacements that lead to shutdown of the nuclear burst. This major improvement greatly increases the credibility of disassembly analysis, while often reducing computed yield. It also makes much better use of equation-of-state information.

A totally new computer routine was defined to compute the mechanical stresses in irradiated fuel that could lead to clad rupture. It will replace the old DEFORM routine (in SAS1A and SAS2A) which was appropriate primarily for unirradiated fuel. This new capability should extend to irradiated fuel an analytical ability that, with the old DEFORM routine, has been shown to work very well for unirradiated fuel in analysis of TREAT transients.

Reactor Control and Stability. Progress was made on the initial development of (1) stability analysis methods and stability design criteria for spatially dependent reactor systems, and (2) spatial transfer-function techniques for determining the dynamic characteristics of reactor systems. The stability techniques investigated included: Lyapunov's method, the

comparison-function method, and the maximum principle. Necessary extensions and improvements were made to enhance practical application of these methods to realistic LMFBR systems. The development of methods to obtain spatially dependent transfer functions for realistic LMFBR systems and the study of the source-detector spatial effects were completed. The quasi-linearization technique was applied to the spatially dependent reactor systems. The analysis of the spatial transfer function for a typical LMFBR system was initiated. This work was terminated at the end of the reporting period as program emphasis shifted to investigation of the more immediate problems of core protection systems for the FFTF, demonstration plants, and 1000-MWe LMFBRs. Two topical reports were issued on the work completed prior to termination.

Coolant Dynamics. Preliminary experimental data pertaining to incipient superheat and expulsion were obtained with sodium and nonmetallic fluids. These data verified the pressure-temperature history model for predicting inception of boiling and the slug model concept for calculating voiding rates as related to single-subassembly and whole-core accidents. New data and models of void fraction, two-phase frictional pressure drop, and critical flow of forced-convection sodium were obtained so that stability analysis of the boiling process associated with single-subassembly accidents can be carried out. Experimental and analytical work indicate that the acoustical properties of two-phase mixtures can be used in detecting minute quantities of gas that might be entrained in the reactor coolant. In addition, theoretical work in bubble growth and collapse has shown that pressure sensors might be used as detection systems in the event of fuel-assembly voiding.

Core Structural Safety. It was found that the effect of pulse shape on the maximum plastic distortion of core internal structures can be characterized by the impulse and an effective pressure. Both parameters are defined in terms of simple integrals of the pressure-time history, and so are easy to measure experimentally. It also was found that spatial variation of the pressure can be characterized by an effective load distribution parameter, also defined in terms of simple integrals. Investigation of the dynamic plastic deformation of hexagonal fuel cans was initiated.

Fuel Element Failure Propagation. Out-of-pile experiments examined the reduction in cooling capability on adjacent elements resulting from the release of fission gas from a failed fuel element. Gas-jet impingement scoping tests with water in a single rectangular heated channel indicated a spray-cooling effect, which, if present in the pin geometry and with sodium as a coolant, would prevent failure of an adjacent pin at the point of impingement. Tests in sodium were initiated to examine the spray-cooling effect and the effect of the flow transients produced by the released gas.

Rapid gas release in an unheated 19-pin bundle was studied with water and a plexiglass system allowing motion pictures to be taken. Gas was released from a 63-mil hole and a 62 x 125-mil slot (plenum pressure of 500 and 1000 psia). Preliminary examination of the data indicates that the transients are short enough (100 msec) that overheating of pins did not occur. The plexiglass system was not damaged by the tests. A more detailed analysis relating the results to reactor conditions was initiated.

A small sodium test loop was constructed. Also, the design and fabrication of a 19-pin heated test section for water tests and a 91-pin test section for freon tests were initiated.

The preliminary design of an in-pile loop in ETR with the capability of testing a multipin (19) bundle of fuel pins in a sodium environment was completed. The design is a packaged-loop concept making use of an ALIP pump, a sodium-to-water-to-gas heat exchanger, and a bayonet test section with countercurrent sodium flow (i.e., sodium flows down an outside annulus and returns up the center test zone). A safety study for the loop and a study of the interfaces with reactor operation were conducted. A set of reference experiments characteristic of the types of tests to be performed in the loop was established to provide a basis for a review of the loop design and to act as an initial step in establishing a joint ANL-HEDL plan for tests in support of FFTF.

Fuel Dynamics Studies in TREAT. Transient testing of LMFBR oxide-fuel samples under flowing sodium conditions that simulate reactor flow channels began in TREAT using the new Mark-II loops. Data on transient failure thresholds and mechanisms were compared against code predictions to guide development of analysis techniques. Extensive oxide fragmentation and postfailure dispersal were found. Early experimental data on the conversion of thermal energy to work done by transient sodium vaporization (two tests on failure of single unirradiated pins and one test on failure of three irradiated pins) showed conversion efficiencies that are orders of magnitude lower than calculated in the thermodynamic limiting-case model for a fuel-coolant interaction.

Materials Behavior and Energy Transfer. High-temperature physical-property data (such as heat capacity, enthalpy, compressibility, vapor pressure, and speed of sound) were provided for materials used in LMFBRs. Properties were chosen for study on the basis of their importance in fast reactor safety analysis--ranging from steady-state and mild transients to

core-meltdown situations. Enthalpy values of UO_2 were measured to 3475°K, thus extending previously available data by over 200°K; excellent agreement was found in the region of overlap with other workers at lower temperatures. The apparatus used for the UO_2 calorimetric studies was modified for use with mixed-oxide fuel materials. An analytical effort, which is coupled with the experimental program, is investigating a wide range of theoretical and semiempirical techniques for extending the utility of the data to temperatures that now are inaccessible experimentally.

Fast Reactor Safety Test Facility Study. In a delineation of LMFBR accidents, potential sources of LMFBR accidents were listed and the likely effects of initiating events were considered in detail. The effects were grouped to form a concise list of general accident categories, and general accidents were reviewed in specific terms, first for FFTF, then for a representative demonstration plant, and finally for a representative 1000-MWe target plant. Calculations with the SAS1A code were made to substantiate the considerations of accident sequences. Work continues to define the in-pile program required to resolve the uncertainties identified by the accident-delineation study.

Studies were made to assess the capabilities to carry out the LMFBR safety program in existing and firmly planned reactor facilities. Capabilities of TREAT, SEFOR, PBF, and ETR, in terms of accommodations, energetic capabilities, operating limitations, and availability were defined in detail. The principal capabilities of TREAT are the large burst energy and the ability to maintain a high steady power for a short time; considerable additional time at power can be obtained if a fast-neutron converter region is installed in the core. SEFOR has a limited capability for both transient and steady-state experiments. Modifications to the SEFOR reactor would be

required to achieve representative steady-state power in experimental pins; even then it is uncertain whether more than 19-element clusters could be employed in safety experiments. PBF, like TREAT, can provide a powerful transient burst. Unlike TREAT, PBF has significant steady-state operating capability, although it does not appear that representative steady-state power can be supplied to fuel-element clusters for more than a short time. ETR has steady-state capability adequate for generating representative operating power in fuel-element clusters. FFTF, EBR-II, and GETR are also being studied. Future work is concentrating on matching experimental needs and facility capabilities so as to complete recommendations for the optimum application of test-reactor facilities to the LMFBR Safety Program.

Fuel-Coolant Interactions. Power-excursion meltdown tests were performed in TREAT on fuel bundles containing five fuel pins and four dummy pins in a sodium-filled piston-loaded autoclave. Incoherent pin failures and pressure pulses occurred with thermal-to-mechanical energy conversion ratios of the order of 10^{-4}. Removal of the helium bond gas (1 atm) in the fuel pins increased the energy conversion ratio to the order of 10^{-3}. In laboratory experiments on the fragmentation of molten UO_2 upon contact with sodium, dropping gram quantities of molten UO_2 into sodium produced extensive fragmentation of the UO_2 with a mass-mean particle diameter of about 250 microns. A rate-limited model of molten fuel-coolant interactions was developed. This model calculates pressure-time histories from the dispersal of molten UO_2 into sodium under either an acoustic or an inertial constraint. The UO_2 thermal resistance is included in the model; UO_2 particle size or heat-transfer surface area (as a function of time), any film thermal resistance or cut-off, and the compliance of a preexisting noncondensable gas volume can be included as parameters. The computer-code representation of this model is available.

Postaccident Heat Removal. Models and equations were developed for fission-product-decay heat transfer from fuel debris in various configurations (individual pieces in sodium, porous piles in sodium, settled beds of particles in sodium, pools of molten fuel on grid plates, support plates, vessel heads, or concrete or ceramic materials, and fuel in blocked subassemblies). These equations enable the calculation of heat-removal rates from the fuel debris in various configurations. This, in turn, enables prediction of thermally stable configurations, meltthrough or penetration rates of structural members, and the conditions under which the fuel debris can be contained in the reactor vessel and, failing this, the secondary containment vessel.

1000-MWe Safety Studies. The Babcock & Wilcox Co. Analysis and Safety System (A^2S^2) Design Study was continued under ANL management, based on the reference commercial-plant design developed by B&W during its earlier 1000-MWe LMFBR Follow-on Study. A survey of possible malfunctions and safety problems was completed, and a preliminary selection was made of candidate safety systems for design later in the program. An adjunct study was initiated to determine the effects that radiation-induced metal swelling (a phenomenon not accommodated in B&W's reference core design) could have on the results of the safety study.

Subcontracts were negotiated with General Electric Co. for a probabilistic safety analysis study, with Westinghouse Advanced Reactors Division for a combined study of safety, primary-system design, and dynamics analysis and control, and with Atomics International for an emergency reactivity shutdown system study; the development of work plans by the subcontractors was begun. However, this entire program was terminated by AEC in October 1970 for budgetary reasons.

Reactor System and Containment Structural Dynamic Response. To extend the usefulness of the REXCO code system to longer times (for the response of primary-system components to excursions originating at the core), rezoning techniques were developed and incorporated into the program. Parametric studies on the FFTF primary system were performed.

Transformation from the Lagrangian to a Eulerian coordinate system was developed to treat excessive mixing in the primary system during the later stages of the excursion, and to estimate the inventory of sodium spillage into the secondary containment.

Comparison of the excursion codes being developed with existing experiments was initiated with satisfying results. The intent was to prove the validity of these codes and their eventual application to the design and safety analysis of LMFBR plants.

The overall codes were made operational. Study of the importance of inserting heat transfer into the codes was initiated. Consideration was given to adapting these codes to molten-core excursions.

Thermal-plume Dispersion Studies. Study began of the thermal effects produced by the discharge of waste heat into the Great Lakes. An early result was a state-of-the-art report on physical scale modeling of thermal plumes. Similar reports are also being prepared on experimental field data and analytical modeling. Numerical solutions of fundamental equations for thermal-plume dispersion are being developed.

Plant Dynamics and Control Analysis. Study began of the control systems proposed for the LMFBR plant designs in the Demonstration and 1000-MWe plant design studies. The 1000-MWe LMFBR designs were reviewed and the work scopes of the follow-on dynamics simulation studies were formulated. Information on individual-component dynamics was compiled and a simplified plant model was prepared for simulation on a hybrid computer.

Nuclear Safety Research and Development--LMFBR Safety

III. ACCIDENT ANALYSIS AND SAFETY EVALUATION*

(G. J. Fischer)

Overall scope. Analytical studies are conducted that lead to understanding and resolution of the principal safety problems of the liquid-metal-cooled fast breeder reactor. Emphasis is on support for near-term reactor plants.

Computer codes and routines are being developed to reduce uncertainties of safety analyses. These contribute to the LMFBR licensing process because of greater credibility of results, which often have smaller yields through reduction of pessimism in models, while increasing public confidence and protection. Plant-availability improvement and plant-design-compromise reductions are related benefits.

Studies are made to: (1) improve understanding of plant concepts for safety, while testing new methods, (2) make sensitivity and parametric surveys to evaluate basic data, models, and design concepts, (3) analyze potential and completed safety experiments to check analytical methods and to aid in experiment design.

This activity cooperates closely with the Coolant Dynamics, Fuel-Coolant Interactions, Reactor System and Containment Structural Dynamic Response, and Materials Behavior and Energy transfer work. Fuels modeling is performed in cooperation with the Oxide Fuel Studies at the Laboratory. Cooperative work also is accomplished with the study of stainless steel swelling in the Core Materials Applications study at the Laboratory. The SAS1B code will employ a two-dimensional kinetics routine being developed in the General Fast Reactor Physics work at the Laboratory.

---

*For references for this chapter, see p. 65.

Code for Initiating Accident

(F. E. Dunn)

Scope. Computer codes are being developed for understanding core-related safety in the liquid-metal-cooled fast breeder reactor. The emphasis in code development is on simplicity, meaningfulness of mathematical models, pertinence of new information to be gained, reduction of computer time costs, and usefulness and availability of the codes to users. Case studies are performed to evaluate safety aspects of fast breeder designs, to test the effectiveness of code developments, and to define the safety problem areas that most need new code development. Sensitivity studies are performed to evaluate the significance of data uncertainties.

Summary. SAS1A was used extensively at Westinghouse and at Argonne for FFTF safety analysis. The computational scheme used for the two-phase voiding calculations was improved to reduce computing time by about a factor of three. A slug-ejection coolant-voiding routing was created to provide an even more economical alternative to the two-phase-flow voiding routine, as well as to provide a voiding model that is more appropriate for some types of accidents. The characteristics of the new codes, SAS1B and SAS2A, and the priorities for their creation, were carefully defined. The development of the new codes started with the creation of a multiple-channel capability.

Incorporation of a slug-ejection coolant-voiding model into the SAS1A code. A refined slug-ejection coolant model was created in collaboration with the Coolant Dynamics program. A preliminary version of a slug-ejection routine was coded and incorporated into SAS1A for testing.

The new slug model is a modified version of the voiding model developed earlier.[1*] One of the main modifications in the new model is the direct coupling with the fuel-pin heat-transfer calculations in SAS1A. Another modification is the provision for initial coolant flow when boiling starts, permitting the treatment of flow-coastdown accidents, as well as the flow-blockage accidents considered by coastdown accidents, as well as the flow-blockage accidents considered by Cronenberg.[1]

The new slug-ejection routine starts from steady-state conditions and calculates the coolant temperature profile, mass flowrate, and pressure profile, as functions of time. A vapor bubble forms at the first axial node where the coolant temperature exceeds the saturation temperature plus a user-specified amount of superheat.

After a vapor bubble is formed, it is assumed to fill the whole cross section of the coolant channel except for a liquid film on the cladding. The routine simultaneously solves the energy, momentum, and continuity equations for the vapor temperature and the motion of the liquid-vapor interfaces and the liquid slugs. Saturation conditions are assumed for the vapor.

In addition to heat flow from the cladding and structure to the vapor, the routine considers the heat flow through the liquid-vapor interfaces at the ends of the vapor regions. In the initial stages of boiling, the vaporization from the liquid-vapor interfaces is the main source of the vapor that drives the expansion of the voided region.

A liquid film of user-supplied thickness is left on the cladding and structure as voiding occurs. Then the rate of vaporization or condensation on the films at an axial position determines the rate of change of

the film thicknesses at that point. Film dryout at a point is predicted when the film thickness becomes less than a user-specified value. After film dryout at a point, there is no further heat transfer at that point from the cladding or structure to the vapor until the surface is rewetted by a reentering liquid slug.

After boiling starts, coolant-temperature calculations in the liquid slugs continue. Also, the saturation-temperature profile is recalculated as the coolant pressure changes. These coolant-temperature calculations in the liquid slugs provide an indication of whether a single-vapor-slug voiding model is appropriate for the case being considered. The liquid temperature calculations indicate whether a second vapor bubble might form within a liquid slug, or whether a liquid-vapor interface might break up into a two-phase flow pattern due to superheating of the liquid.

Some preliminary tests have been made using the slug ejection routine for a flow-coastdown accident in an FFTF-type of core. A superheat of 70°C was assumed before boiling started. The results indicate that a single-vapor-bubble-type model is not adequate for this case. After a vapor bubble had formed at the top of the core, and it had only partly voided the core, the coolant temperature exceeded 70°C of superheat at points closer to the center of the core in the lower liquid slug. This indicates the need for either a multiple-bubble slug-ejection model or a two-phase flow model.

Work has started on a new multiple-bubble slug-ejection routine to treat cases where a single-vapor-bubble model is not adequate. The new routine will use a single vapor bubble when boiling starts; but as the voiding progresses, an additional vapor bubble will be started at any point in the coolant liquid where the temperature exceeds the superheat

criterion. The new multiple-bubble routine should have a considerably greater range of applicability than a single-bubble routine.

Upgrading functions of the SAS1A code. Based on the experience gained in extensive use of SAS1A during the year, modifications were made to the code to reduce the computation time and to allow greater flexibility for the user.

The numerical procedures used in the two-phase-flow coolant-voiding routine were improved to provide greater numerical stability and to allow the use of longer time steps. The use of longer time steps reduces the computation time for a problem. Another modification to the coolant routine was to include heat flow from the coolant to the structure in the coolant-temperature calculations. One new option in the coolant routine is to allow the user to specify an arbitrary variation of coolant mass flowrate with time until boiling starts.

A new capability was added for automatically producing computer plots of the SAS1A results.

Creation of the first version of SAS2A with multiple-channel capability. A preliminary multiple-channel version of the present SAS1A code was produced to serve as the initial version of the SAS2A code. The multiple-channel capability provides an explicit treatment of spatial variations across a reactor and the effects of the spatial variations on accident behavior.

Because of the modular structure of the SAS1A code, it was possible to produce a multiple-channel version by using a multiple-channel driver routine to link the computational modules from the single-channel version. The new slug-ejection coolant routine was used in the multiple-channel code, since the slug-ejection routine was written to be compatible with

a multiple-channel treatment. The two-phase-flow coolant-voiding routine is the only major SAS1A computational module that is not immediately usable in a multiple-channel treatment. A modified version of the two-phase-flow routine will probably be added to SAS2A in the future.

Incorporation of spatially dependent (two-dimensional) kinetics into the SAS1B code package. The use of two-dimensional space-dependent kinetics in SAS1B was planned. The coupling between the spatially dependent kinetics routines and the heat-transfer, coolant-dynamics, and fuel-motion routines was specified.

Creation of SAS1B code. The main features of the second-generation accident-analysis code SAS1B were determined. New capabilities will be included in the areas of spatially dependent kinetics, the accident behavior of fuels, coolant voiding, and two-dimensional hydrodynamics with new equations of state for the disassembly accident.

Future program. The first version of the second-generation accident-analysis code, SAS1B, will be developed. Also, an upgraded version of SAS1A, called SAS2A will be produced to provide a rapid means for testing new capabilities intended for SAS1B, and to make the new capabilities quickly available to users. Both codes will account for spatial behavior and noncoherence of accident behavior by explicitly calculating events at a number of positions (channels) in the core simultaneously. These new codes will also contain explicit treatments of the whole primary-coolant loop. SAS1B will use space-dependent (two-dimensional r-z geometry) kinetics, new routines for treating the accident behavior of fuels (see "Analysis of Fuel Behavior," p. 48), and new routines for the analysis of disassembly accidents (see "Analysis of Disassembly Accident, including Computer-Code Development and Sensitivity Studies.") Future

developments on coolant voiding will include a treatment of fission-gas release from failed fuel pins, a fuel-coolant interaction routine, and improvement of the multiple-bubble slug-ejection coolant-boiling routine and the two-phase-flow coolant-boiling routine.

Analysis of Fuel Behavior

(A. Watanabe and A. M. Judd)

Scope. Simple mathematical models are being developed to represent the behavior of LMFBR mixed-oxide fuel during reactor accidents. These will be in the form of modules of the SAS code, to ensure their ready availability for work on FFTF, demonstration plants, etc. The models will be based on experimental data where possible, and will be upgraded as new data or improved analytical models become available from other activities at ANL or other laboratories.

For these purposes, three aspects of the fuel behavior will be considered: (1) behavior while the fuel pins retain their integrity (i.e., up to the point of gross cladding failure), (2) explosive thermal interaction between molten fuel and liquid coolant ("vapor explosions"), and (3) motion of the fuel after the pins have lost their integrity, when the fuel moves under the influence of coolant and fission-product-gas flow and gravity (this is often known as "slumping").

Provision will be made (particularly by sensitivity studies) for recommending in-pile (and out-of-pile) experiments to remove the major uncertainties about fuel behavior, and also to analyze existing experimental results and make use of them.

Summary. Development of an improved SAS module to analyze the behavior of fuel up to the point of cladding failure was started. Study of the motion of fuel after gross failure was initiated. TREAT

experiments were analyzed, and recommendations were made for future TREAT experiments.

The revision of the fuel deformation module in SAS1A. The current DEFORM module in the SAS1A code is adequate for fresh unirradiated fuel pins. However, it is inappropriate for highly irradiated fuel pins near the end of their lives, so a revision is being made.

In the old model, it is assumed that the fuel always behaves elastically and that the cladding behaves first elastically, then perfectly plastically. The fuel and the cladding are initially stress and strain free and the fuel geometry is either a hollow annulus or a solid cylinder. No provisions are made for internal pressures due to fission-product gases.

The major revisions over the previous model are: (1) distinct metallurgical regions in the fuel are treated, each with its own material properties; in particular, the plastic stress-strain relations in both the fuel and the cladding are assumed to be given by general work-hardening laws that are also temperature-dependent, (2) the behavior of fission-product gases in the fuel matrix, the central cavity, and the plenum (assumed to be connected to the gap) is considered, (3) an option is provided to treat the columnar-grain region as a strengthless material that possesses only a bulk modulus but no shear modulus, (4) several different cladding-failure criteria are to be provided, based on data obtained from burst-tube experiments, and (5) the initial conditions required to start the transient are to be fed from a suitable steady-state lifetime code.

The major assumptions used in the model are: (a) the plane strain approximation is used and the stress-strain equations are treated quasi-statically, (b) the long-term effects, such as swelling or creep, are

negligible during the short transient, (c) each fuel and cladding region is treated as isotropic and homogeneous; in particular, the presence of cracks in the unrestructured region is ignored, (d) both the fuel and the cladding are incompressible, because the elastic regime covers a fraction of the total deformations, (e) the fuel and the cladding, when they are in contact, slip freely over each other; this restriction will be removed as soon as acceptable computational speed is obtained, and (f) melting of the fuel is restricted to start either from the inner cavity wall or from the centerline of the fuel; vaporization of fuel is ignored.

The mathematical formulation closely follows that of Landau *et al.*,[2] except for the modification of the work-hardening yield surface. For a cylinder with inner and outer radii, a and b, the stress and strain rates are given by

$$\dot{\varepsilon}_z = \dot{F}_z/3AG + \underline{M}(\dot{\psi}) + \underline{M}\,(\Lambda s_z) \tag{1}$$

$$\dot{\sigma} = (\dot{F}_z + 3\dot{F}_r)/3A + 4G\{\underline{M}(\dot{\psi}) - \dot{\psi}\} + G\{\Lambda s - \underline{L}(\Lambda s) - \Lambda s_z + \underline{M}\,(\Lambda s_z)\} \tag{2}$$

$$\dot{\varepsilon} = \dot{\psi} \tag{3}$$

$$r^2\dot{e} = 3r^2\underline{N}(\dot{\psi}) + ab\underline{K}(\Lambda s) + \pi a^2b^2(P_b - P_a)/AG \tag{4}$$

$$\dot{s} = 2G(\dot{e} - \Lambda s) \tag{5}$$

$$\dot{s}_z = 2G(\dot{\varepsilon}_z - \dot{\varepsilon} - \Lambda s_z) \tag{6}$$

where σ and ε are the mean stress and strain, s and e are the stress and strain parameters, s_z is the deviatoric axial stress, ε_z is the axial strain, F_z is the axial force, F_r is $\pi(a^2P_a - b^2P_b)$ with P standing for

pressures, G is the shear modulus, A is the cross-sectional area, ψ is the thermal expansion, and the flow parameter Λ is given by

$$\Lambda = 3/4\{s\dot{e} + 3s_z(\dot{\varepsilon}_z - \dot{\varepsilon})\}/Y^2 - 1/2\ G^{-1}\{\dot{\bar{\varepsilon}}Y^{-1}\ Y/\partial\bar{\varepsilon} + \dot{T}Y^{-1}\ Y/\partial T\},$$

unless the yield function f, defined below, is zero and Λ is positive. Otherwise Λ is zero. The yield surface is expressed by

$$f = (\bar{\sigma})^2 - [Y(\bar{\varepsilon},T)]^2$$

where $\bar{\sigma}$ and $\bar{\varepsilon}$ and equivalent stress and strain. The quadratures, $\underline{K}$, $\underline{L}$, $\underline{M}$ and $\underline{N}$ are defined, for a continuous function X(r), by

$$\underline{K}(X) = 2\pi ab\ A^{-1} \int_a^b dr\ r^{-1}\ X(r)$$

$$\underline{L}(X) = 2\pi\ A^{-1}\ \{a^2 \int_a^r dr + b^2 \int_r^b dr\}\ r^{-1}X(r)$$

$$\underline{M}(X) = 2\pi\ A^{-1} \int_a^b dr\ rX(r)$$

$$\underline{N}(X) = X(r) - 2\pi\ A^{-1}\ r^{-2}\{b^2 \int_a^r dr + a^2 \int_r^b dr\}\ rX(r)$$

The system of equations (Eqs. 1-6) is solved iteratively for the fuel and the cladding. When the two bodies come into contact, the contact pressure supersedes the gap pressure as the interface condition.

The cavity pressure is calculated accounting for the fission-product gases, strengthless fuel region, molten fuel, and the gas bubbles in the fuel matrix.

The program, TSDEF, has been programmed and is nearing its final correction stage. Preliminary iteration speed is estimated to be 0.12 sec per time step per axial segment for each axial iteration over 15 radial mesh points.

Analysis of Disassembly Accident, including Computer-code Development and Sensitivity Studies.

(R. B. Nicholson and J. F. Jackson)

Scope. An improved capability is being developed for calculating LMFBR disassembly accidents. Emphasis is on evaluating and improving the VENUS computer program. Improvements are being made in the equation of state, in the treatment of heat transfer to the coolant and structure (particularly to evaluate the postburst energy partition), and to use small weak explosion pressures. To examine postburst damage, VENUS is being linked with the REXCO-H code, which was developed in the Reactor System and Containment Structural Dynamic Response study.

The development of a SAS1B module is an important project because it combines two-dimensional space-time kinetics, hydrodynamics, and equations of state. A module is being developed to analyze weak-pressure anisotropic disassembly.

To exploit and test the capabilities of VENUS, various disassembly calculations will be performed, including an analysis of the KIWI-TNT reactor explosion test.

Sensitivity studies are being made, with emphasis on determining the influence of uncertainties in the equation of state on a total energy release in the disassembly accident. This work is being coordinated closely with related theoretical and experimental studies on equation of state being conducted in the Materials Behavior and Energy Transfer study

to provide guidelines for them, including specifying improvements that are most needed, as well as evaluating the consequences of new data or methods. Disassembly calculations are also being made in support of the FFTF and other related LMFBR safety activities.

Summary. The VENUS computer code was refined and improved. It was thoroughly tested, debugged, and examined for time and spacemesh stability conditions. Several equation-of-state options were added. The code was made available with ANL assistance for use on FFTF and demonstration-plant studies. A program of sensitivity studies was initiated and partially completed.

VENUS code development. The recently developed LMFBR disassembly code VENUS,[3] has been applied to a broad range of excursions on FFTF reactor models. As a result, various deficiencies in the program have been isolated and corrected. A considerable amount of experience has also been gained in the proper application of the code to different transient situations.

VENUS offers increased accuracy over previous disassembly codes, mainly because it calculates the movement of the core material by a direct finite-difference solution of a set of two-dimensional (r,z) hydrodynamics equations. Then changes in the fuel density associated with the disassembly motion are explicitly calculated. This allows a density-dependent equation of state (EOS) to be used. To exploit this increased sophistication, considerable effort has gone into developing as accurate an EOS as possible, based on available data. A brief discussion of this EOS is given in the next section, along with recent refinements in its evolution.

The results of some disassembly calculations that give insight into the proper application of VENUS are presented under "Time-step requirements

and pressure oscillations." This includes a discussion of time-step and mesh-interval requirements and their relationship to the numerical stability of the pressure calculations. Some of the factors that influence the production of pressure oscillations during disassembly are also discussed.

In the final section, some limitations of VENUS with respect to mild disassembly excursions are considered. Refinements to the code that attempt to overcome these difficulties are discussed.

Equation of state. Although several EOSs have been provided in VENUS, the following one is considered to be the most accurate (there is a possibility that the implicit heat capacity is somewhat too low). The temperature-energy relationship is given by

$$T = \begin{cases} \text{MAX}\ (T_1,\ T_2),\ \text{for}\ V_r \leq 0.6 & (7) \\ \text{MAX}\ [T_1,\ \text{MIN}\ \ (T_2,\ T_3)],\ \text{for}\ V_r > 0.6 & (8) \end{cases}$$

where

T = fuel temperature in °K

$$T_1 = 273 + 2287\ U \tag{9}$$

$$T_2 = (4272.5-1003\ V_r + 1699V_r^{\ 2})(U-0.237 - 1.882V_r) \tag{10}$$

$$T_3 = [4272.5-1003\cdot(0.6) + 1699\cdot(0.6)^2]\cdot[U-0.237-1.882\cdot(0.6)] \tag{11}$$

$V_r = \rho_c/\rho$ = reduced specific volume of fuel

ρ_c = critical fuel density

ρ = fuel density

U = internal energy of the fuel (kJ/gm)

The pressure-energy relationship is:

$$P = \begin{cases} \text{MAX}(P_1,\ P_2),\ \text{for}\ V_r \leq 1 & (12) \\ \text{MAX}(P_1,\ P_3),\ \text{for}\ V_r > 1 & (13) \end{cases}$$

where

P = fuel pressure in dynes/cm^2

$$P_1 = \exp(69.979 - \frac{76800}{T} - 4.34 \ln T) \tag{14}$$

$$P_2 = 1.554 \times 10^{12} \left(U_1 - 3.59 + 0.119V_r + \frac{0.0767}{V_r^{\,3}}\right)$$

$$\cdot \exp(-9.67V_r + 4.445V_r^{\,2}) \tag{15}$$

$$P_3 = 10^{10}(U_1 - 3.2213 - 0.173V_r)(1.9V_r - 0.704) \tag{16}$$

H_f = heat of fusion of fusion of the fuel in kJ/gm

A fictitious internal energy, U, is determined at the i-th time step in the calculation as follows:

$$U = \begin{cases} U_o + \sum_{i=1}^{I} \Delta U_i & \text{for} \quad U < U_m \quad (17) \\ U_m & \text{for} \quad U_m < U < U_m + H_f \quad (18) \\ U_o - H_f + \sum_{i=1}^{I} \Delta U_i = U_1 & \text{for} \quad U_m > U_m + H_f \quad (19) \end{cases}$$

where

$$U_o = \frac{T_o - 273}{2287} \tag{20}$$

T_o = initial temperature in °K

U_m = the internal energy required to raise the temperature of the fuel to its melting temperature in kJ/gm

ΔU = change in internal energy in the i-th time step

If the initial temperature is above the melting temperature, the internal energy, U, is just given by Eq. 17 and the U_1 in Eqs. 15 and 16 is replaced by U.

Before the fuel has expanded to fill all the space available to it, the pressure is given by the vapor-pressure expression in Eq. 14. The density-dependent one-phase pressure relationships in Eqs. 15 and 16 are used after all the available space is filled. These analytical expressions are fits to the corresponding states calculations of Menzies.[4] They differ significantly from Menzies' analytical expressions because of the inclusion of several refinements to the formulations.

One of the most important refinements was accounting for the energy required to melt the fuel (heat of fusion). Although this was ignored in Menzies' original calculations, it can have a significant effect on the total energy release in a disassembly calculation. It is accounted for through the calculation of the internal energy as outlined in Eqs. 17-19.

The density-dependent temperature and pressure expressions were also revised to give an improved fit to Menzies' data. His data cover the range of reduced specific volumes form 0.4 to 1.0. Later, the expressions were revised further to give a better extrapolation to reduced volumes larger than 1.0. This was found to eliminate some obviously nonsensical results for calculations carried out to relatively large core expansions.

The fuel density, ρ, and therefore the reduced specific volume, V_r, are calculated on the basis of the total volume available to the fuel for expansion. The presence of sodium and stainless steel is assumed to influence the pressure only because these materials occupy space that is thereby unavailable for fuel expansion. Because the one-phase pressure is on extremely sensitive function of the fuel density, it is important to account for the compressibility of the sodium when determining the fuel density. The difficulty in doing this lies in the fact that the density then becomes pressure dependent. Because the pressure is, in

turn, density dependent, the resulting set of coupled equations are transcendental.

Considerable effort has gone into developing s suitable iteration scheme to solve these equations. Because this calculation must be carried out at each mesh position for each time step, it is important that it be as efficient as possible. Initial attempts to iterate were frustrated by the extreme sensitivity of the one-phase pressure to the fuel density. In successive iterations, the pressure was often found to oscillate between extremely high one-phase pressure (>1000 atm) and relatively low two-phase vapor pressure (<50 atm).

After considerable experimentation with various transient calculations, a pressure iteration scheme that appears suitable has been developed. The basic approach is to restrict the pressure change between successive iterations to various amounts, depending on the pressure differences being obtained. The resulting technique gives sufficiently converged results within a few iterations (on the average). It has been found to increase only the computer time requirements by about 20% over formulations that ignore compressibility.

Time-step requirements and pressure oscillations. Pressure oscillations in both space and time have been observed when applying VENUS to various excursion calculations.[5] Initially, it was not clear whether these oscillations were the result of physical phenomena or numerical instabilities. Although a time-step control scheme is included in VENUS, its ability to properly control the time step had not been demonstrated.

For these reasons, as well as to check out VENUS further and gain experience with its operation, a series of excursions on a simplified FFTF-type reactor model were studied. The main objectives were to

determine the time-step requirements of the code, to study their relationship to the stability of the pressure calculation, and to isolate other factors that influence the production of pressure oscillations during the calculation.

The reactor model and initial conditions were chosen to comform to those used in some early FFTF disassembly work. These were rapid prompt-critical excursions initiated from high initial power, temperature, and reactivity conditions by a $100/sec ramp insertion. The sodium coolant was assumed to be present during the disassembly. The main simplifications were in considering a one-region core with smooth power and reactivity worth distributions. A uniform initial temperature distribution was also used in the nominal model. The time-step size requirements were investigated for various equations of state, spatial mesh spacings, power distributions, and initial temperature profiles.

The results of this study showed that pressure waves could be set up when a high-pressure one-phase condition exists in a given mesh cell, while an adjacent cell remains in a low pressure two-phase condition for a relatively long time. This allows the boundary of the high-pressure cell to accelerate virtually unrestrained until a one-phase condition is finally reached in the adjacent cell. The motion of the boundary continues until sufficient pressure develops in the cell being compressed for a long enough time to arrest the inertia of the expanding cell. In the meantime, the density in the expanding cell can decrease to the point where a low-pressure two-phase condition ensues. Thus, pressure oscillations can be set up. It should be noted that the pressure changes are largely a result of compression and expansion, as opposed to the changes in internal energy that occur during a given time step.

Some of the factors that can influence the formations of pressure oscillations become clear in light of the above. First, the severity of the one-phase pressure relationship in the EOS can have a strong influence. Severity in the sense of strong density dependence is especially important. In general, the density dependence increases greatly as the density itself increases. Thus, configurations in which there is little room for fuel expansion, as in cases where the sodium is present, are more vulnerable to oscillations.

This situation is aided considerably by accounting for the compressibility of the sodium. For example, no pressure oscillations were observed in the nominal problem with time steps of 25 μsec or smaller when the EOS described in the previous section was used. Further, converged pressure results were obtained for time steps of 10 μsec or less. Here, "converged" means that further decreasing the step size does not alter the results more than some acceptable amount. When the same transient was calculated using an EOS that did not account for the compressibility of the sodium, the pressure results would not converge even for time steps as small as a fraction of a microsecond.

Those factors that cause adjacent mesh cells to develop different pressures would also be expected to influence the production of pressure oscillations. Two examples of this are steep spatial gradients in the power and initial temperature distributions. Pressure waves were generally observed near the outer regions of the core where the power gradient was largest in the model being considered. When another power distribution was used that was more centrally peaked, pressure waves occurred nearer the center of the core. Using a centrally peaked initial temperature distribution was found to have a similar effect.

The influence of using different space-mesh interval sizes was also investigated. Calculations with mesh spacings of 2.5 and 10 cm carried out in addition to the 5-cm mesh used in the nominal model. Smaller time-step sizes were required for equivalent convergence as the mesh spacing was decreased, as expected. The results were qualitatively similar to those using the 5-cm mesh; however, the relationship between time-step sizes and mesh spacing is discussed in more detail later.

Pressure oscillations have also been observed in the reflector regions during some transients. The formulation used in VENUS to calculate the pressure in blanket regions assumes that such pressure arises solely from the compression of the blanket materials. This compression is caused by the expanding core moving the inner boundary of the blanket. After a preset amount of distortion has occurred in a given blanket mesh cell, the pressure is determined using an average compressibility for the materials present.

When there is no void space in the blanket, a slight distortion of the spatial mesh can result in a very large pressure change. This can give rise to pressure instabilities that propagate throughout the blanket.

It is intuitively clear that the Δt required for stability should be related to the spatial mesh interval and the speed of sound. For pressures to propagate smoothly through the space mesh, the time step must be somewhat smaller than the time required for s sound wave to traverse the distance between adjacent mesh points. For example, when using a 2-cm blanket mesh interval, the traverse time was estimated to be about 10 μsec for the FFTF reflector. With a 10-μsec time step, large pressure spikes were developed in the reflector region. Decreasing the time step to below a few microseconds, however, was found to eliminate them completely.

By increasing the blanket mesh intervals to 5 cm, no pressure waves were observed for step sizes up to at least 10 μsec. The pressure waves can also be eliminated by artificially decreasing the velocity of sound by making the blanket more compressible.

For a comparable mesh spacing, it appears that the blanket EOS has roughly the same time-step size requirements as the EOS described earlier. Time steps of about 10 μsec or less will provide good pressure convergence for a 5-cm mesh.

As a final point, it could be noted that VENUS provides an option whereby no pressure is generated in the blanket until a preset amount of distortion has occurred. This is included in an attempt to account for any void space that initially might be present in the blanket. If the amount of void space is quite large, say 5 to 10%, the effect is to just remove the blanket from the calculation until the first mesh cell in the blanket has been compressed by this amount. If the mesh is large this is late in the excursion. Thus, for sensible calculations containing void in the blanket, we must use small mesh spacing. Also, with large spacing, when pressures finally do start to build up, the effect is to worsen the pressure stability problem in the blanket, as the outer boundary of the core has been allowed to accelerate unrestrained throughout the initial time period. The net result is that if calculations are done with void space in the blanket the time-step size must be smaller.

In conclusion, we have found that the pressure calculations in VENUS can be very sensitive to the time-step size, especially whenever high one-phase pressures are encountered. We have also shown that the time-step size requirements to ensure stability of the pressure calculations are sensitive to several other factors, such as the EOS, the power and initial temperature distributions, the amount of space availabe for fuel expansion, and the spatial mesh spacing.

The time-step control scheme in VENUS does not appear adequate in terms of guaranteeing converged pressure results. In some instances where the pressure results were found to be not converged, the scheme was attempting to increase the step size, instead of decreasing it. Thus, considerable care must be used in time-step size selection.

It should be noted that the power and energy-release results are much less sensitive to the time-step size. For example, comparing the same transient as calculated with different step sizes, one often finds considerable differences in the detailed space-time history of the pressure, although the energy release continues to agree to within less than 1%. Therefore, the size of the time step required depends to an extent on the purpose of the calculation.

In general, we have found that reasonably well converged one-phase pressure results can be obtained with time steps of about 10 μsec, as long as the compressibility of the sodium is accounted for. When the fuel is in the two-phase domain throughout the core, considerably larger time steps can be successfully taken (say 50 to 100 μsec).

Although many of the pressure oscillations that were observed in the early applications of the code have been eliminated through proper time-step sizes and refinements to the EOS, it appears that some pressure waves might have a legitimate basis in some of the factors discussed earlier. At least, certain oscillations have persisted to the point where it became economically unfeasible to decrease further the time-step and space-mesh sizes.

Application to mild excursions. Some rather mild disassembly excursions were calculated as part of an FFTF safety study. The

maximum pressures during these transients remained below about 30 atm throughout the entire disassembly process. The power bursts were turned over and held down by Doppler feedback for a sufficient time to complete the disassembly, even though the pressures were relatively small.

In a situation such as this, two of the basic assumptions made in the formulation of codes such as VENUS become questionable. The first assumption is that the mixture of core materials can be treated as a homogeneous isotropic medium subject to the equations of hydrodynamics. The second assumption is that heat transfer can be ignored and, consequently, an EOS characteristic of the fuel material can be used to determine the pressure.

In rather severe accidents, the pressures usually get well above the residual structural strength of the core components and the periods involved are sufficiently short that heat transfer can be safely neglected. However, these conditions might not be met adequately in many transients of interest.

As a first step in evaluating the potential influence of structural restraints in low-yield excursion, VENUS was modified to suppress the buildup of pressure in each mesh cell until some threshold pressure is reached. This threshold is chosen to correspond roughly to the estimated structural restraint in the core at the beginning of the disassembly calculation.

As an example, a 10-atm threshold was used on a transient in which the maximum pressure had only reached about 16 atm when applying VENUS in the usual manner. The pressure went up to 50 atm and the energy release increased by 15% when using the threshold modification. Although the increase in the energy release is not large, it is nonetheless significant.

As a further refinement, the code was modified to suppress the radial motion of each mesh point until the pressure difference of the mesh cells on either side of it (radially) exceeds a preset threshold. This is still an oversimplification in the sense that coherency effects are ignored. However, it should provide a more accurate representation of the expected structural restraints than the simple pressure threshold described above.

This was applied to a mild FFTF flow-coastdown accident in which the pressure had risen originally to a maximum of 35 atm. When a 5-atm threshold was used, the total energy release increased by 12%. Next, the radial motion was suppressed completely throughout the entire disassembly by putting in an extremely high threshold. This was found only to increase the energy release by 15% over the original.

There appeared to be two main reasons why the energy release was not very sensitive to restraining the radial motion in this case. The most important was the fact that the transient was turned over primarily by Doppler feedback. The disassembly feedback becomes dominant only on the back side of the power burst, after most of the energy has been released. The second factor is that restraining the radial motion just results in accelerating the motion in the axial direction, thereby partially offsetting the effect of the restraint.

It is seen that the consideration of structural restraints can be significant in mild excursions. Although not dramatic in the above examples, there might be other transients where the effect is larger. An improved formulation for taking structural restraints into account is being considered. The scope of this effort includes other possible sources of anisotropic disassembly motion as well.

The problem of accounting for heat transfer from the fuel during disassembly is also being investigated. Potentially, this effect could influence a long-period transient by removing energy from the fuel, as well as producing additional disassembly pressure through the heating of non-fuel core constituents.

References

1. A. W. Cronenberg III, *Slug Expulsion of Boiling Sodium from a Reactor Coolant Channel*, M. S. Thesis, Northwestern University (Jun 1969).

2. H. G. Landau, J. H. Weiner, and E. E. Zwicky, Jr., *Thermal Stress in a Viscoelastic-plastic Plate with Temperature-dependent Yield Stress*, J. Appl. Mech. *27*, 297-302 (1960).

3. W. T. Sha and T. H. Hughes, *VENUS--A Two-dimensional Coupled Neutronics-Hydrodynamics Fast Reactor Power Excursion Computer Program*, ANL-7701 (Oct 1970).

4. D. C. Menzies, *The Equation of State of Uranium Dioxide at High Temperatures and Pressures*, TRG Report 1119, UKAEA (1966).

5. W. T. Sha and A. E. Waltar, *Fast Reactor Disassembly Calculation Utilizing a Temperature-Density-Dependent Equation of State*, Trans. Am. Nucl. Sci. *12*(2), 825 (Nov 1969).

6. J. C. Carter et al., *SAS1A, A Computer Code for the Analysis of Fast Reactor Power and Flow Transients*, ANL-7607 (Oct 1970).

7. A. K. Agrawal, *On the Analysis of Fuel Meltdown Studies with TREAT*, Trans. Am. Nucl. Soc. *12*(2), 865 (Dec 1969).

8. C. E. Dickerman et al., *First TREAT Loop Experiment on Oxide Fuel Meltdown*, Trans. Am. Nucl. Soc. *12*(2), 867 (Dec 1969).

9. A. M. Judd, *Calculation of the Thermodynamic Efficiency of Molten Fuel-Coolant Interactions*, Trans. Am. Nucl. Soc. *13*(1), 369-370 (Jun 1970).

10. D. R. MacFarlane, "Sodium Boiling Transients Leading to Disassembly in Oxide-fueled Fast Reactors," *Proc. of the Symp. on Dynamics of Nuclear Systems, U. of Arizona* (Mar 1970).

11. J. B. van Erp, D. R. MacFarlane, and H. K. Fauske, *Protection Against LMFBR Local Core Accidents*, Trans. Am. Nucl. Soc. *13*(1), 363-364 (Jun 1970).

12. A. E. Waltar (PNL) and W. T. Sha, *A New Computational System for Fast Reactor Accident Investigation*, Trans. Am. Nucl. Soc. *13*(1), 371 (Jun 1970).

13. E. R. Siegmann, *A Compressible Model for Transient Sodium Boiling*, Trans. Am. Nucl. Soc. *12*(2), 904 (Dec 1969).

14. T. J. Marciniak, L. J. Habegger, and H. Greenspan, *Summary Review of Neutronic Noise Techniques for Incipient Boiling Detection in Liquid Metal Fast Breeder Reactors*, ANL-7652 (Jan 1970).

Nuclear Safety Research and Development--LMFBR Safety

IV. REACTOR CONTROL AND STABILITY*

(W. C. Lipinski)

Overall scope. The technology of safety-related instrumentation and stability for future large LMFBR systems has been developed. This includes (1) stability analysis methods and stability design criteria for spatially dependent reactor systems, and (2) spatial transfer-function techniques for determining the dynamic characteristics of reactor systems. This work was terminated at the end of the reporting period as program emphasis shifted to investigation of the more immediate problems of core protection systems for the FFTF, demonstration plants, and 1000-MWe LMFBRs.

Reactor Stability and Stability Design Criteria for Spatially Dependent Systems (C. Hsu)

Scope. Stability analysis methods and spatially dependent reactor-simulation techniques were being developed to (1) analyze the stability of spatially dependent reactor systems using Lyapunov's and related methods, (2) develop sufficiency conditions for stability to provide guidelines in reactor design (for example, an upper bound for the combined reactivity feedback from Doppler, void, and fuel-expansion effects), (3) refine the design guidelines to account for typical operational and physical limits imposed on actual systems (for example, temperature and stress limits), and (4) simulate spatially dependent reactor systems for test and verification of the developed methods. Special emphasis was placed on the reference LMFBR core design concepts in the 1000-MWe Follow-on Studies.

Summary. The development of analytical techniques to obtain stability criteria for linear and/or nonlinear spatially dependent LMFBR systems was completed. The techniques investigated included: Lyapunov's method,

*For references for this chapter, see p. 72.

the spectrum-analysis method, the comparison-function method, and the maximum-principle approach. Necessary extensions and improvements were made to enhance practical application of these methods to realistic LMFBR systems. Numerical computational tools were also developed that made it possible to analyze reactor system stability in detail by: (1) estimating the system eigenvalues and eigenfunctions, and (2) solving nonlinear system steady-state and time-dependent equations. A terminal report summarizes the technical progress.[1]

Spatial stability analysis with linear model. The stability of linear spatially dependent LMFBR systems was analytically investigated by using: Lyapunov's method, spectrum analysis, comparison functions, and the maximum principle. The conclusion from this study is that, among all the methods investigated, the spectrum analysis is best suited for the study of linear reactor-system stability. Computational capability was developed for this method to analyze practical reactor systems.

A study of linear homogeneous LMFBR system stability also has been made using the root-loci method.[2] The objectives of this study were: (1) to determine the linear stability at operating conditions for an LMFBR system being studied, and (2) to determine the sensitivity of the stability condition (system relative stability) with respect to the variation of system feedback parameters.

Spatial stability analysis with nonlinear model. Necessary extensions and improvements were made to apply these methods to realistic LMFBR systems that are inherently nonlinear.

Based on the progress made to date and careful comparison of the various methods, the conclusions for applying these methods to nonlinear reactor systems are: (1) the theoretical development of methods for analyzing nonlinear reactor stability has reached a mature state; with the proper

development of computational capability, they can be applied effectively to practical reactor problems,[3] and (2) among the various methods studied, the spectrum-analysis method is believed to be most practical for detailed study of nonlinear reactor-system stability; however, for qualitative stability analysis, all the methods are equally effective.

For the reasons cited above, numerical computational tools were developed that made it possible to analyze reactor system stability in detail by: (1) estimating the system eigenvalues and eigenfunctions, and (2) solving the nonlinear system steady-state and time-dependent equations. A terminal report summarizes the work.[4]

Future program. Work terminated at the end of the report period.

Transfer-function Techniques to Measure Large Fast Reactor Stability

(L. J. Habegger)

Scope. Theoretical and experimental techniques were being developed to: (1) define the concept of spatially dependent transfer functions, (2) determine and evaluate the spatial effect of possible source-detector configurations, (3) devise feasible experimental measurement techniques, and (4) simulate and verify the experimental techniques. The definition and interpretation of spatially dependent transfer functions were considered for an LMFBR reference design developed in the 1000-MWe Follow-on Studies.

Summary. The development of computational methods to obtain spatially dependent transfer functions for realistic LMFBR systems and the study of the source-detector spatial effects were completed. The quasilinearization technique was applied to the spatially dependent reactor systems. Four important numerical programs were developed to obtain: (1) the nonlinear steady-state coupled neutronic-thermohydraulic system solutions, (2) the space-time nonlinear reactor system solutions, (3) parameter identification in space-time reactor systems, and (4) the eigenvalue and

eigenfunction reactor system solutions. The analysis of the spatial transfer function for a typical LMFBR system was initiated.

Source-detector spatial effects. The source-detector spatial effects were investigated with numerical examples. The model and method used are presented in the following sections. Five different types of input locations and configurations were simulated to obtain the spatial output responses. The computed spatial output can be analyzed for the various locations and configurations of the detector. From these analyses, significant spatial effects were observed. Typical spatial effects noted for the distributed-parameter model were both at high frequencies (due to neutron diffusion time) and at low frequencies (due to the thermohydraulic transit time). More detailed results are discussed in the terminal report.[5]

Computer programs for solution of spatially dependent systems. A computer code was written for solving one-dimensional nonlinear space-time equations. The forms of equations to which the code is applicable represent models of power reactors that include coupling of space-dependent reactor power densities with various nonlinear feedbacks, such as feedbacks from fuel and coolant temperatures. The intended applications of the code to the current LMFBR control and stability program are twofold: (1) in the analysis of transfer-function techniques to measure large fast reactor stability, the code is used in conjunction with Galerkin's method[6] for computing space-dependent transfer functions for various source-detector configurations (Galerkin's procedure is limited to linear systems), and (2) the code can be used for the verification of theoretical stability domains derived for nonlinear reactor systems.[7]

Analysis of spatial transfer function of typical 1000-MWe LMFBR systems. Galerkin's computational procedure was used to obtain spatially

dependent transfer functions for a large 1000-MWe LMFBR. The model for this system contains two energy groups, one delayed group, and two temperature feedbacks, and is multiregioned. The transfer functions were computed for zero power and for 20, 100, and 200% power with adjustments in power levels. These computer transfer functions are the simulation of measurements performed on a realistic reactor system. The objective is to determine the validity of gain and phase margins used to analyze the stability of the reactor system.

The results of this study can be summarized as:

(1) With the assumption that the input is located in the center of the reactor, the difference in the location of the output neutron-flux measurement resulted in a phase-margin discrepancy as much as 17° between the reflector and the core. However, the effect of the difference on the stability extrapolation depends on the specific reactor design.

(2) The computation of the gain margin required transfer-function measurements at high frequency. As a result, the gain margin from both the theoretical computations and experimental measurements is unreliable because (a) space dependence becomes more significant as frequency increases, and (b) the needed experimental accuracy is more difficult to obtain as frequency increases.

(3) In addition, the assumption used in the conventional point model for stability extrapolation is not always applicable in the spatially dependent calculations. For a point model, it is assumed that only the feedback function depends on the power level. That is, only the feedback transfer function changes with the power level. This is not so in the spatially dependent case because the temperature profile is also changing at various power levels, thus resulting in a change both in the forward transfer

functions and the feedback transfer function. The spatial effect due to this change was studied to determine the correct interpretation of stability extrapolation in actual measurements of spatially dependent reactor systems.

Future program. Work terminated at the end of the report period.

References

1. C. Hsu and L. Habegger, ANL Internal Memorandum.

2. C. Hsu and L. Habegger, *Root-Loci Approach in the Study of Stability of Linear Homogeneous Space-Time Reactors*, Trans. IEEE on Nucl. Sci. *NS-17*(1), 549-554 (Feb 1970).

3. C. Hsu and W. T. Sha, *Determination of Stability Domain of Nonlinear Reactor Dynamics*, Trans. Amer. Nucl. Soc. *12*(1), 295-296 (Jun 1969).

4. L. Habegger and C. Hsu, *The Use of Qausilinearization for the Solution of Nonlinear Space-Dependent Reactor Equations*, Trans. Am. Nucl. Soc. *12*(2), 830-831 (Nov 1969).

5. L. Habegger and C. Hsu, *Spatially-Dependent Transfer Function Analysis of Distributed Reactor Systems*, ANL-7788 (Mar 1971).

6. L. V. Kantorovich and V. I. Kryloff, *Approximate Methods of Higher Analysis*, Interscience, New York (1959).

7. *Reactor Development Program Progress Report for December 1967*, ANL-7403, p. 147.

Nuclear Safety Research and Development--LMFBR Safety

V. COOLANT DYNAMICS*

(H. K. Fauske)

The course of single-assembly, whole-core, and hypothetical accidents is largely affected by the coolant behavior, so the transient behavior of sodium under accident conditions is being studied experimentally and analytically. In the studies, mathematical models are being developed for incorporation into practical codes for analysis of initiating and hypothetical accidents. The Coolant Dynamics activity is a long-term development program reflecting overall anticipated LMFBR safety needs.

Sodium-superheat analyses and out-of-pile experiments involve stationary as well as flowing systems in single- and multiple-pin geometries. Sodium-expulsion and -reentry out-of-pile experiments involve static- and forced convection tests in single- and multiple-pin geometries. Analyses and experiments of liquid-vapor dynamics concern bubble growth, bubble collapse, liquid-film thickness and breakup, evaporation and condensation rates, void fraction, pressure drop, velocity of sound, pressure-wave propagation, and critical flow. Tests are being conducted with suitable nonmetallic fluids to simulate sodium behavior in single- and multiple-pin geometries. Realistic mathematical models will be obtained by combining information from all these studies.

Sodium Superheat

(R. E. Holtz and R. M. Singer)

Incipient superheat determines to a great extent the rate of expulsion and the choice of voiding models (flow patterns) used in accident evaluation, so analysis and experiments concerning incipient sodium superheat are employing static and flowing sodium so that methods can

*For references for this chapter, see p. 110.

be developed for predicting sodium superheat and the inception of boiling. Reactor accident situations, such as flow blockage, coastdown, or moderate power transients, are simulated. The studies include investigation of the effects of reactor environment (e.g., "old" sodium, oxide, gas bubbles, etc.) on the incipient-boiling conditions.

It has been well established in the past several years that nonflowing sodium must be superheated substantially above its saturation temperature in order to cause it to boil.[1-9] However, there has been much controversy concerning the limiting values of the superheat and the role of many parameters on the incipient boiling conditions. For example, it has been proposed or demonstrated that the following parameters all are of importance in determining the incipient superheat:[10] (1) pressure-temperature history, (2) pressure, (3) heat flux, (4) liquid purity, (5) dissolved gas content, (6) surface conditions, (7) nuclear radiation, (8) heating method, (9) length of time of operation, and (10) liquid velocity, and perhaps others. Additionally, in some cases (most noticeably in regard to the heat flux), the available data indicate conflicting results as to the roles of these parameters. Therefore, the primary thrust of our efforts in this area has been to understand the underlying physical phenomena that determine the incipient-boiling conditions so that a suitable nucleation model could be developed. In so doing, it was determined that several of the proposed parameters were interrelated or redundant.

For a liquid to nucleate (boil) from a preexisting vapor- and/or gas-filled cavity on a solid surface, the pressure within the vapor phase must exceed the liquid pressure and the surface-tension force. This criterion can be stated mathematically as

$$P_v(T_w) + P_G - P_L = \frac{2\sigma(T_w) \cos [\theta_a(T_w)]}{R} \tag{1}$$

Thus, the incipient-boiling wall temperature T_w can be determined if the following quantities are known: the vapor pressure-temperature behavior of the fluid $P_v(T)$, the inert-gas partial pressure in the cavity at the instant of nucleation P_G, the liquid pressure at the solid surface P_L, the surface tension of the liquid-vapor interface σ, the liquid-vapor-solid contact angle θ_a, and the size of the surface cavity R.

A theoretical model has been developed[11] that claims that the maximum size of an active surface cavity is determined by the conditions experienced by an experimental apparatus prior to incipient boiling. This model allows the calculation of R in Eq. 1 if the most severe cavity deactivation conditions are specified; i.e., the preboiling conditions at which the deepest penetration of liquid into surface cavities occurs. Thus, if the primed quantities denote these extreme conditions, R is simply computed as

$$R = \frac{2\sigma(T_L') \cos [\theta_r(T_L')]}{P_L' - P_v(T_L') - P_G'} \tag{2}$$

This concept was examined experimentally by carefully controlling the extreme deactivation conditions, P_L', T_L', and P_G' and conducting pool incipient-boiling experiments. In these tests, certain deactivation conditions were established, and then the variation of the incipient-boiling wall superheat, ΔT_w, with saturation temperature was measured. The results from a typical series of tests in which the inert gas pressure at nucleation, P_G, was minimized are summarized in Fig. 2.

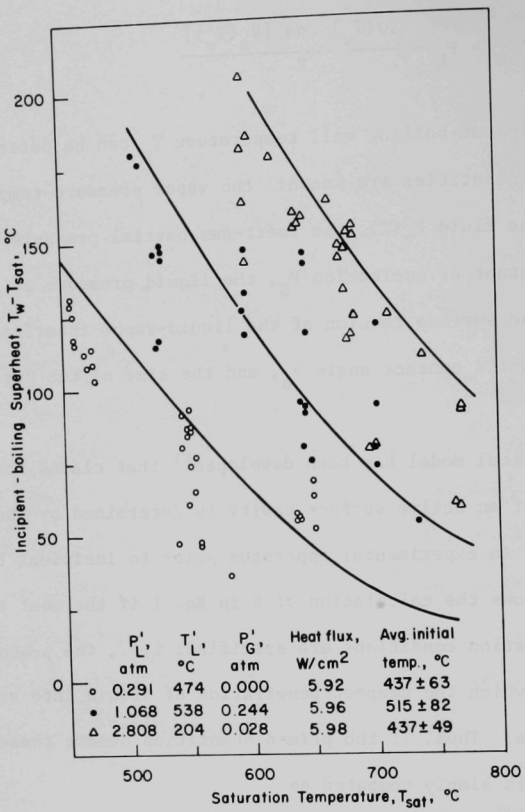

Fig. 2. Effect of Pressure-temperature History on Incipient-boiling Superheat. Solid lines are theoretical. Average surface roughness was 60 x 10^{-4} mm; the blanket gas was argon; height of sodium above the heater was 76 mm.

Although there is some scatter in the data, it is evident that there is considerable agreement between the measurements and the predictions of Eqs. 1 and 2. Some of the scatter might be attributed to the necessity of assuming a unity value of the ratio of the cosines of the contact angles, θ_a and θ_r, because of a lack of knowledge of their values.

The implications of the validity of this model are manifold. For example, the reported effects of surface conditions and length of time of operation are readily explained by variations in the deactivation conditions. These also were experimentally examined, the former by conducting tests on two distinctly differing surfaces. One surface was highly polished and another roughened by sandblasting so that the nominal surface roughnesses were about 0.2 and 6.0 μm. When these two surfaces were independently subjected to identical extreme deactivation conditions, the resulting incipient-boiling superheats were also identical (within the experimental scatter). Additionally, there was no general variation of the superheat with time that could not be attributed to changes in the deactivation conditions or the inert-gas pressure at nucleation. The details of these experiments and the results are reported in Ref. 12.

In the experiments, the inert-gas partial pressure in the cavities was minimized to independently study the validity of the pressure-temperature history nucleation model. However, it is clear from Eq. 1 that the gas pressure, P_G, can be an important parameter affecting the incipient boiling conditions. The gas pressure will vary during a heating transient as the gas dissolves into the liquid; thus an analysis of the combined heat and mass transfer occurring during such a transient is necessary to determine the value of P_G at nucleation. This was done in Ref. 11, and it was determined that P_G can vary markedly not only during heating transients but also during boiling and cooling. One of the primary results of this analysis was the identification of the heat flux effect being caused by inert-gas pressure variations. The analysis predicted that the wall incipient superheat would decrease as the heat flux was increased, if only the heat flux was varied.

However, it seemed quite likely that in most experiments, the cavity gas pressure was varying in an uncontrolled manner. This would make it possible for reported variations in the superheat to be misinterpreted. To examine this possibility, several series of incipient-boiling tests were conducted in which care was taken to vary only the heat flux, but to allow the cavity gas pressure to vary naturally. In such a sequence of tests, the cavity gas pressure would continually decrease to some level; thus, if the heat flux was successively increased or decreased, the superheat would always tend to increase. This in fact is what was observed, as is summarized in Fig. 3. These results clearly indicate the importance of the dissolved-gas transport and explain the past confusion on the effect of the heat flux.

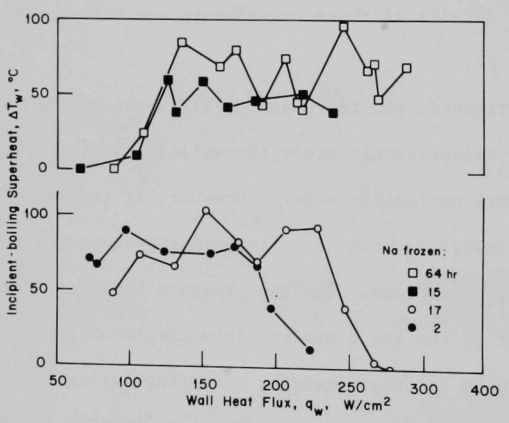

Fig. 3. Variation of Incipient-boiling Wall Superheat with either Increasing (upper curves) or Decreasing (lower curves) Heat Flux. Cover gas was argon; surface finish was approx. 10 μm; T_s was 829°C, the initial liquid temperature $T_{\ell 0}$ was 432°C, T'_ℓ was 502°C, $(\Delta T_w)_{theo}$ calculated from Eqs. 1 and 2 was 97°C, L_0 was 94.0 cm, L_h was 8.4 cm, P'_ℓ was 1.36 bar, and P'_ℓ was 0.14 bar.

Finally, this model of liquid-metal nucleation was applied to a realistic LMFBR accident: a single-subassembly blockage with continued heating.[13] It was found that, in this type of accident, boiling would always begin near the center of the enriched core, and incipient superheat would be in the range 50 to 100°C. The actual value of the superheat was found to depend strongly on the preaccident conditions in the core (i.e., flow velocity, pressure gradient, heat flux, etc.), as indicated in Fig. 4. Additionally, it was demonstrated that, due to the large axial temperature gradient existing during such an accident,

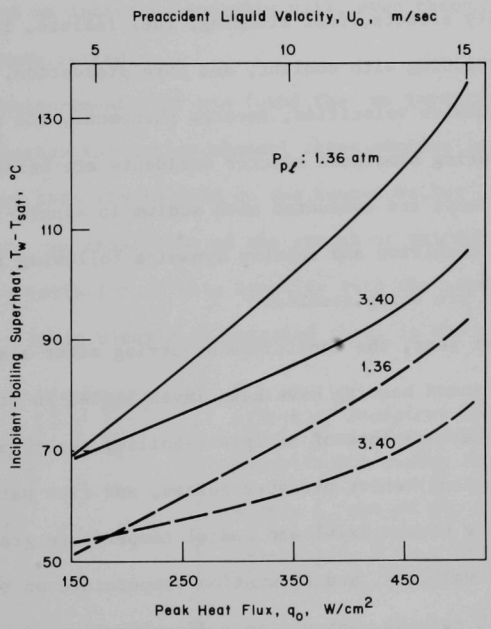

Fig. 4. Superheat Requirements for Various LMFBR Operating Conditions (for an EBR-II-type coolant circuit). Solid curves are for hydraulic diameter A of 4.0 mm; broken curves are for A of 7.0 mm. $P_{p\ell}$ is plenum pressure. Preaccident channel temperature rise was 174°C, heated length was 0.915 m, unheated riser was 0.600 m, and $q_w = q_0 \sin(\pi x/L_0)$.

it was quite unlikely that randomly located failures in fuel cladding would cause boiling to occur at a net zero liquid superheat.

Future program. These studies, both theoretical and experimental, will be continued. Primary emphasis is on the effect of liquid velocity on the superheat and on the prediction and measurement of the incipient superheat during realistic reactor accident conditions.

Sodium Expulsion and Reentry

(R. M. Singer and R. E. Holtz)

An understanding of expulsion and reentry behavior is required to evaluate reactivity effects, fuel slumping, fuel failure, interactions of molten fuel and cladding with coolant, and core disruption. Thus vapor growth rates, expulsion velocities, reentry phenomena, and pressure generation in sodium during simulated reactor accidents are being investigated experimentally. Tests are conducted with sodium in single- and multiple-pin systems. The expulsion and reentry dynamics following flow blockages and flow coastdown are being studied.

During the past year, the conditions occurring after a sudden flow blockage with continued heating have been investigated in static-sodium expulsion tests. Measurements of incipient-boiling superheat, rate of voiding, expulsion and reentry pressure pulses, and flow patterns have been made. The role of the axial and radial temperature gradient, gas-blanket pressure, heat flux, and saturation temperature on these phenomena were examined, with special emphasis on a determination of the range of validity of the single-slug ejection mechanism.

Analysis of the measurements of the liquid-column displacement and the transient location of the liquid-vapor interface indicated that the flow pattern during expulsion is that of a single vapor slug when

the incipient-boiling bulk liquid superheat is greater than about 10 to 15°C. However, the presence of an asymmetric radial temperature profile (normal to the heating surface) caused the vapor slug to only partially fill the channel cross section for superheats less than about 50°C. Under these conditions, relatively thick liquid films remained in the heated section, materially aiding the system's heat-removal capabilities, thus markedly reducing the possibility of the failure of the heated wall. It is expected that such conditions of an asymmetric radial temperature profile exist near the outer pins in a fuel subassembly and thus aid in the maintenance of an intact subassembly wall, even though the central fuel pins might have melted.

From these measurements, it was found that an important parameter in determining whether the entire channel cross section is voided (except for a very thin liquid film on the heated walls) is the incipient-boiling superheat. An indication of the extent of voiding is the void fraction, and the variation of this quantity with the superheat is shown in Fig. 5. It is clearly illustrated that, in the presence of

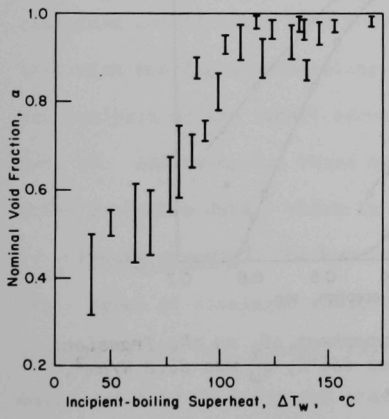

Fig. 5.
Effect of Incipient-boiling Superheat on the Nominal Void Fraction in the Two-phase Region during Expulsion. Height of liquid column above the top of the heater L_0 was 94 cm, length of the heated section L_h was 7.4 cm, saturation temperature T_s was 854°C, and the wall heat flux q_w was 67.1 W/cm^2.

an asymmetric radial temperature gradient, relatively large superheats are required to void the channel. In fact, only about 30 to 50% of the channel cross section was voided when the superheat was about 50°C.

In the case of an approximately radially symmetric temperature profile and/or a large incipient superheat, the flow pattern was that of a single vapor slug that essentially filled the entire channel cross section. The initial growth of this vapor slug was limited by liquid inertia, but due to the axial temperature gradient existing in the liquid (as would be present in a blocked-flow accident in an LMFBR) the slug quickly grew into cooler regions and eventually collapsed, allowing the liquid to reenter the heated zone. Thus, the maximum growth rate and displacement as well as the reentry were affected markedly by local thermal conditions. A summary of the transient column displacements illustrating the expulsion and reentry for various superheats is illustrated in Fig. 6; additional details are given in Ref. 14.

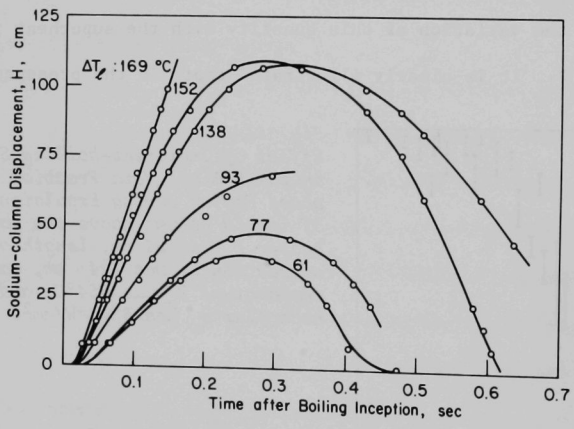

Fig. 6. Effect of Incipient Bulk Liquid Superheat ΔT_ℓ on the Transient Sodium-column Displacement. T_s was 855°C, q_w was 65.3 W/cm², L_0 was 94 cm, and L_h was 7.0 cm.

The pressure pulse that occurred during the initial vapor growth (expulsion) compared quite well to that predicted from the vapor pressure corresponding to the incipient wall superheat. Typical results from one series of tests are summarized in Fig. 7, where the measurements in general

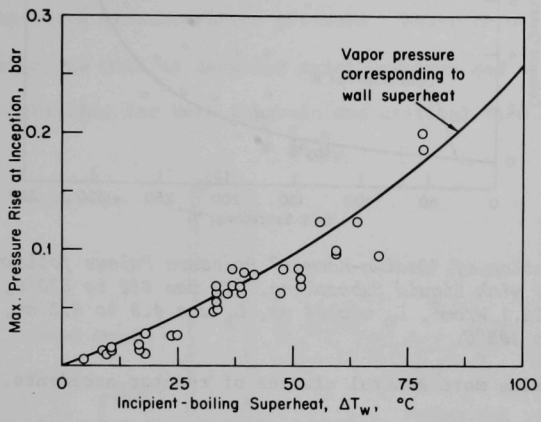

Fig. 7. Variation of Initial Pressure Rise in Liquid with Incipient Superheat. T_s was 681°C, q_w was 71.4 W/cm^2, L_0 was 94.0 cm, and L_h was 5.1 cm.

do not deviate from the predictions by more than the experimental accuracy of about ±0.1 bar. The pressures occurring at reentry (vapor collapse) exhibited considerably more scatter, but seemed to correlate reasonably well with the liquid subcooling. This correlation was based on a theoretical analysis of the impact occurring after vapor collapse and discussed in Ref. 14. Additionally, these measurements agreed quite well with the only other available data,[8] which is indicated in Fig. 8.

Future program. The expulsion and reentry dynamics occurring during other types of simulated reactor accidents (e.g., flow coastdown) will be studied in the Fuel Element Failure Propagation loop, whose design is being modified to carry out these tests. These future tests will provide a check of the results obtained in the static expulsion experiments, and

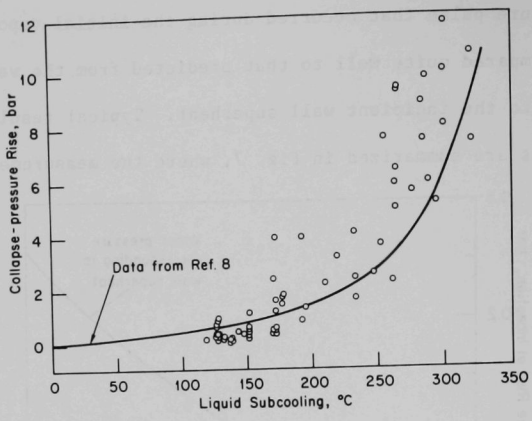

Fig. 8. Variation of "Sodium-hammer" Pressure Pulses following Vapor Collapse with Liquid Subcooling. T_s was 680 to 870°C, q_w was 53.5 to 122.1 W/cm^2, L_0 was 94 cm, L_h was 4.9 to 8.3 cm, and ΔT_w was 10 to 195°C.

also will examine more general classes of reactor accidents. In addition, in-pile tests to simulate reentry conditions are being planned.

Liquid-Vapor Dynamics

(H. K. Fauske, M. A. Grolmes, and R. E. Henry)

Analysis and experiments of bubble growth, bubble collapse, transient evaporation and condensation rates, liquid-film thickness in the slug-flow regime, liquid-film instability and breakup, slip ratio in two-phase-flow-pressure drop, velocity of sound, pressure-wave propagation, and critical flow are being performed. All these phenomena might affect the events following incipient boiling in a coolant channel, depending on the resulting flow regime(s), and therefore must be studied separately to understand them.

Critical flow, void fraction, and two-phase pressure drop. Much new data for the critical flow rates, liquid volume fraction, pressure gradients, and the extent of equilibrium in flashing sodium flow have been

obtained in the Sodium Flashing Facility shown in Fig. 9.[15-18] In this facility, sodium can be heated to various temperature levels at approximately atmospheric pressures and discharged through a test section into a blowdown vessel. The flashing of the liquid sodium was achieved by decreasing the system pressure below the saturation pressure. Measurements of flow rate and void fraction, as well as detailed axial pressure and temperature profiles, were obtained for both subsonic and critical-flow conditions.

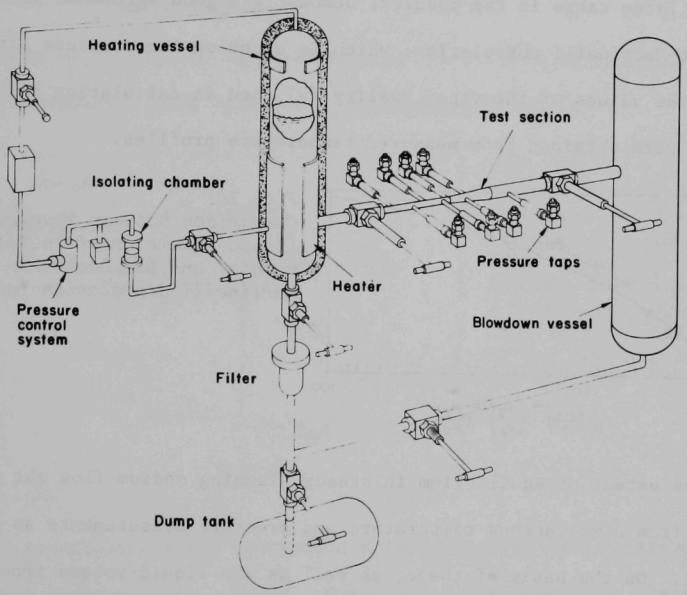

Fig. 9. Sodium Flashing Facility. ANL Neg. No. 900-6.

In the study of sodium liquid-vapor pressure drops, the average liquid-volume fraction at a conduit cross section is an important variable. While numerous liquid-fraction data and correlations are available for nonmetallic fluids, very few data exist for liquid metals. An electromagnetic flowmeter was used to measure the average liquid velocity in the two-phase region. Two-phase liquid-fraction data were obtained for sodium over a

temperature range of 1200 to 1500°F, vapor weight fraction of 0 to 3%, and flow rates of 0.4×10^6 lb/hr-ft^2.

Figure 10 shows the measured liquid-volume fraction $(1 - \alpha)$ as a function of the Lockhart-Martinelli flow modulus, $X_{tt} = [(1 - x)/x]^{0.9} (\rho_g/\rho_\ell)^{0.5} (\mu_\ell/\mu_g)^{0.1}$, where α is the void fraction, x is the vapor weight fraction, ρ is the density, μ is the viscosity, and the subscripts ℓ and g refer to the liquid and vapor phase, respectively. The measurements, which cover a large range in the modulus, demonstrate good agreement with the Lockhart-Martinelli correlation, which is based on low-pressure air-water data. The values of the vapor quality (x) used in calculating the flow modulus were obtained from measured temperature profiles.

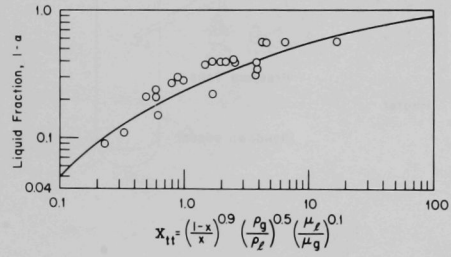

Fig. 10.
Comparison between Measured Sodium Liquid Volume Fraction (data points) and the Lockhart-Martinelli Correlation (curve).

The extent of equilibrium in steady flashing sodium flow was ascertained from simultaneous temperature and pressure measurements as shown in Fig. 11. On the basis of these, as well as the liquid-volume fraction measurements, thermodynamic equilibrium can be assumed for steady flashing in the annular, annular-dispersed flow regimes. However, data have also been obtained that indicate the extent of incipient liquid superheat before flashing in flowing sodium.

Figure 12 illustrates sustained liquid superheat up to 79°F at constant system velocity of 5 ft/sec. The system pressure is reduced stepwise until the inception of flashing is indicated by a rapid self pressurization

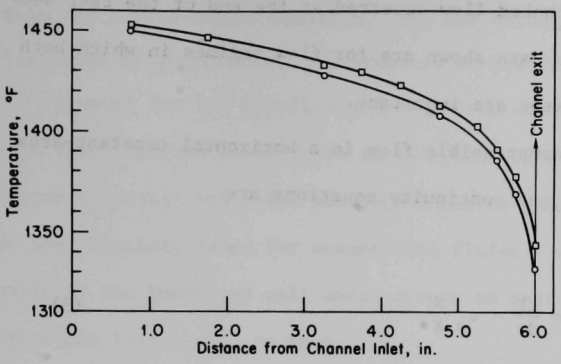

Fig. 11. Comparison of Measured Wall Temperatures (squares) and Saturation Temperatures (circles) Converted from Simultaneous Pressure Measurements. Mass flowrate G was 180 lb/sec-ft^2; stagnation temperature T_0 was 1503°F.

approaching P_{sat}. Steady flashing flow follows. Similar incipient superheats were observed with velocities approaching 20 ft/sec.

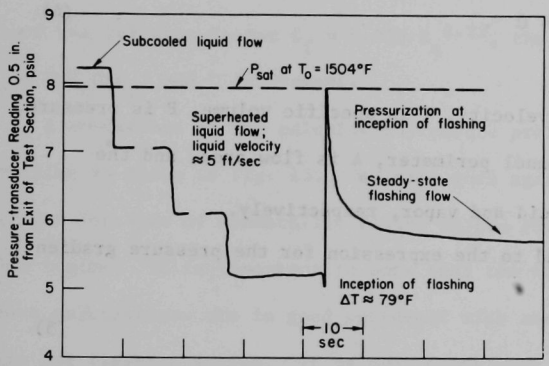

Fig. 12. Illustration of Incipient Superheat and Pressure Generation followed by Steady Flashing in Forced-convection Sodium Flow. A round test section was used in the 0.136-in.-ID Sodium Flashing Facility. ANL Neg. No. 113-3291, Rev. 1.

The so-called boiling hysteresis effect observed with nonmetallic fluids was observed here. While significant superheating was sustained when the system pressure was decreased from an initial highly subcooled state, negligible superheating was sustained when flashing was ceased as a result of increasing the system pressure.

Although numerous experimental data and correlations exist for pressure drop in nonmetallic two-phase flows, very little information is available for liquid metals.[15] In particular, detailed data of pressure drop in steady flashing sodium flow are lacking. For the data obtained in the

Sodium Flashing Facility, choked flow occurred at the end of the test sections, so the pressure-drop data shown are for flow regimes in which both momentum and frictional losses are important.

For steady two-phase compressible flow in a horizontal constant-area duct, the overall momentum and continuity equations are

$$\frac{d}{dz}\left\{\frac{\alpha u_g^2}{V_g} + \frac{(1-\alpha)u_\ell^2}{V_\ell}\right\} = \frac{dP}{dz} - \tau_w \frac{S}{A} \tag{3}$$

and

$$\frac{d}{dz}\left\{\frac{\alpha u_g}{V_g} + \frac{(1-\alpha)u_\ell}{V_\ell}\right\} = 0 \quad . \tag{4}$$

where z is distance, u is velocity, V is specific volume, P is pressure, τ_w is wall shear, S is channel perimeter, A is flow area, and the subscripts ℓ and g are liquid and vapor, respectively.

Equations 3 and 4 lead to the expression for the pressure gradient:

$$\frac{dP}{dz} = \frac{-\tau_w S/A}{1 - G\,(dv/dP)} \,, \tag{5}$$

where

$$G = \frac{\alpha u_g}{V_g \chi} = \frac{(1-\alpha)u_\ell}{V_\ell(1-\chi)}$$

$$v = \frac{\chi^2 V_g}{\alpha} + \frac{(1-\chi)^2 V_\ell}{1-\alpha}$$

and χ is quality and G is mass flowrate. The momentum losses can be evaluated using the Lockhart-Martinelli void fractions in agreement with

measured liquid-volume fraction. The use of equilibrium qualities is justified by simultaneous measurements of pressure and temperature profiles.

A model for the friction pressure drop was employed that proposes that the increased shear force in two-phase flow is due to the increased liquid velocity; the model has been found by numerous investigators to be approximately valid for nonmetallic fluids. At low qualities, the ratio of the two-phase wall shear stress to that of liquid alone is therefore $1/(1 - \alpha)^2$, so that

$$\tau_w \frac{S}{A} = \frac{2C_f V_\ell G^2}{(1 - \alpha)^2 D} \tag{6}$$

where the friction factor $C_f = 0.079\ R_e^{0.25}$, the Reynolds number $R_e = P_\ell U_\ell D/\mu_\ell$, and D is diameter.

A comparison of the calculated pressure profiles with measured profiles is shown in Fig. 13. The same good agreement has been demonstrated for flow of nonmetallic fluids in the annular, annular-dispersed flow regime. It is important to note that the flowrates used in the above calculations are in good agreement with measured critical-flow data for flashing sodium. It is consistent with the above equations that the critical flowrate is given by $G_c = (-\ dv/dp)^{-0.5}$ evaluated at the duct exit with the use of equilibrium quality and Lockhart-Martinelli void fraction. Numerous other equilibrium models have been proposed and these differ primarily in the void-fraction relationship used. Examples are the homogeneous-flow model, $\alpha = [1 + (\rho_g/\rho_\ell)\ (1 - x)/x]^{-0.5}$, and the slip-flow model, $\alpha = [1 + (\rho_g/\rho_\ell)^{0.5}\ (1 - x)/x]^{-0.5}$, as well as the Lockhart-Martinelli model in which the void fraction is a function of the parameter X_{tt}.

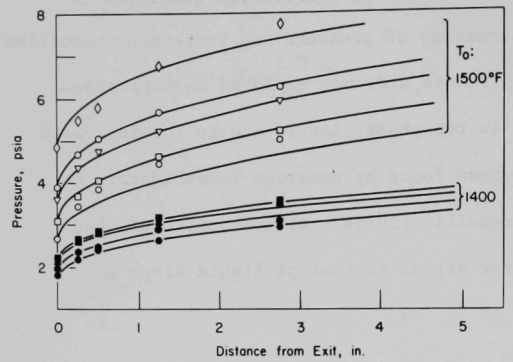

Fig. 13.
Typical Pressure Profiles for Flashing Sodium, and Comparison with Calculated Values (curves). ANL Neg. No. 900-911, Rev. 1.

Calculated values based on these three different methods for assessing the void fraction are compared with the sodium data in Fig. 14. Substantial agreement is noted between predicted values (based on the Lockhart-Martinelli void-fraction model) and the experiments, but the homogeneous-equilibrium model fails completely.

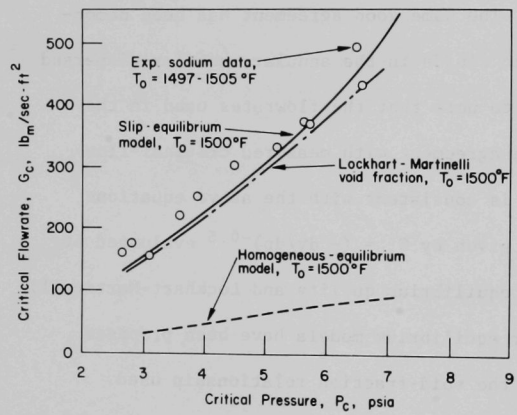

Fig. 14.
Measured Critical Flowrate of Sodium and Comparison with Several Models.

Attention to experimental details and previous experience were carefully considered in these studies.

Previous experimental investigations of two-phase steam-water critical flows showed that an abrupt expansion immediately downstream of the choking

plane significantly affects the two-dimensional pressure distribution in the region immediately upstream of the throat.[17] Such a distortion of the local pressure distribution means that a wall pressure tap located in the throat vicinity will record a value that is not representative of the centerline pressure where the critical conditions occur. Therefore, data taken under these circumstances will be misleading in terms of model interpretation, and in the case of simultaneous temperature-pressure measurements, can yield two-phase superheat data that are not representative of the bulk flow conditions. The adiabatic steam-water results showed that a test section with small angle of divergence downstream of the throat minimizes the two-dimensional effects described above. To determine if these geometrical factors are important in low-pressure compressible flow of two-phase sodium, two test sections were used in the Sodium Flashing Facility. Both test sections were circular constant-area ducts with downstream geometries as shown in Fig. 15.

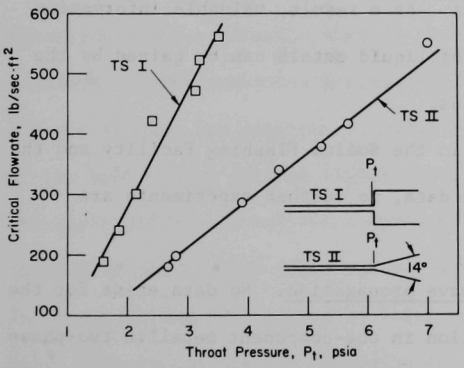

Fig. 15.
Comparison of the Critical Parameters for Different Downstream Geometries. Stagnation temperature T_0 was 1500°F.

Figure 15 compares the critical flowrates for the two geometries on the basis of the measured throat pressures for a stagnation temperature of 1500°F. The critical flowrate is independent of downstream geometry, hence the differences displayed in Fig. 15 result from comparing the flowrates

on the basis of the measured throat pressures. Because the 14° divergent geometry minimizes the two-dimensional effects, the throat pressures of TS II are more representative of the bulk flow behavior.

The same measurements taken on TS I would lead to conclusions directly opposite to those deduced from TS II. Hence the need and usefulness of such detailed measurements in outlining the mechanism of metallic two-phase flows is demonstrated.

The detailed results of TS II have shown that two-phase critical flow of sodium (annular flow regime) can be closely represented by equilibrium models[15] (Fig. 14).

On the basis of data obtained in the Sodium Flashing Facility, valuable conclusions can be drawn in regard to the similarity between the hydrodynamic behavior of sodium and nonmetallic fluids. No major differences are found if similar flow regimes are considered. Models developed for predicting void fraction, pressure drops, and critical flow of nonmetallic fluids can be used to predict metallic systems. As a result, valuable information concerning the two-phase behavior of liquid metals can be gained by the study of suitable nonmetallic fluids.

In view of the data obtained in the Sodium Flashing Facility and the successful interpretation of these data, no further experiments are scheduled in this facility.

Sonic velocity and pressure-wave propagation. No data exist for the velocity of pressure-wave propagation in one-component metallic two-phase systems. However, recent data[19,20] and analyses of the propagation velocity in nonmetallic mixtures indicate that extensive experimental verification is not required to describe the pressure-wave propagation in metallic two-phase media. Experiments have demonstrated clearly the dependence of

the propagation velocity on the mixture flow pattern, and analysis taking into account flow patterns indicate the following expressions for:

bubbly flow, $a_{tp}^{-2} = \rho_{tp} \left\{\alpha\, v_g/a_g^2 + (1 - \alpha)v_\ell/a_\ell^2\right\}$

slug flow, $a_{tp} = a_g a_\ell \left\{\alpha a_\ell + (1 - \alpha)a_g\right\}^{-1}$

annular or droplet flow, $a_{tp}^2 = [\alpha\rho_\ell + (1 - \alpha)\rho_g] - [\alpha\rho_\ell/a_g^2 + (1 - \alpha)\rho_g/a_\ell^2]^{-1}$

where a is propagation velocity in media and the subscript tp is two phase. These equations are compared with experimental data for one-component as well as two-component nonmetallic mixtures in Figs. 16 and 17. Because the above equations are not dependent on rate processes such as heat, mass, and viscous momentum transfer, the good agreement with data would indicate that these equations are quite general and equally valid for metallic systems as well. As a further check, the analysis of pressure-pulse propagation has been extended to include the effects of mass and momentum transfer between the phases. The deviation of the bubble flow data at higher void fractions [Fig. 16 (top)] and the small difference between compression and rarefaction waves in the stratified and droplet flow regime [Fig. 16 (bottom)] can be accounted for by including the effects of these rate processes.[21] Thus these small effects can also be accounted for in metallic two-phase systems.

With this basic understanding of pressure-wave propagation in equilibrium two-phase mixtures with well-defined flow patterns, studies are in progress to determine pressure-pulse propagation in one-component two-phase media with nonuniform flow patterns under conditions of bulk

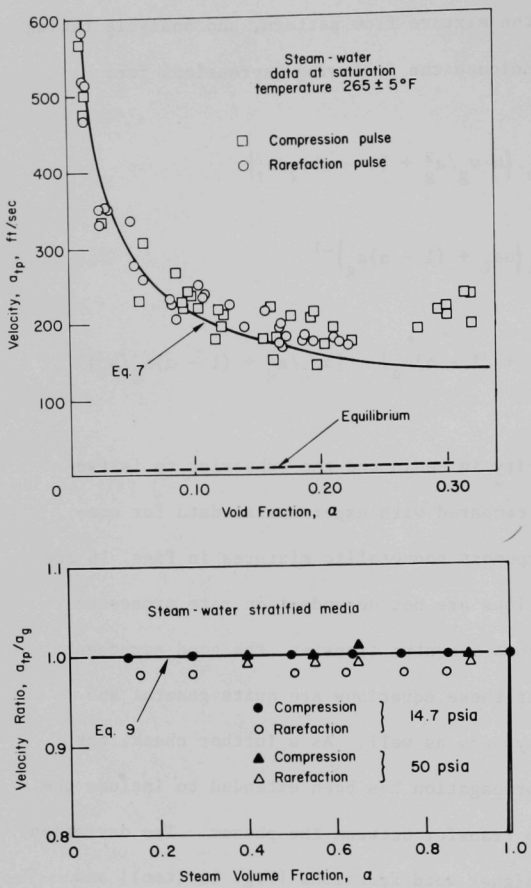

Fig. 16. Comparison between Predicted (curves) and Measured (data points) Pressure Wave Propagation Velocities in Bubbly (upper) and Stratified (lower) Steam-Water Mixtures. Upper-ANL Neg. No. 900-914, Rev. 1, lower-ANL Neg. No. 900-7, Rev. 1.

nonequilibrium such as local boiling. These conditions will be selected to correspond to conditions that might arise in potential LMFBR abnormal operation.

Techniques for flow-regime and gas detection. Techniques are needed to detect and identify various flow regimes in two-phase flows. It is also becoming increasingly important in reactor safety research to be able to detect the presence of minute quantities of inert gas in the coolant. This information is important to the problem of sodium superheat and the early

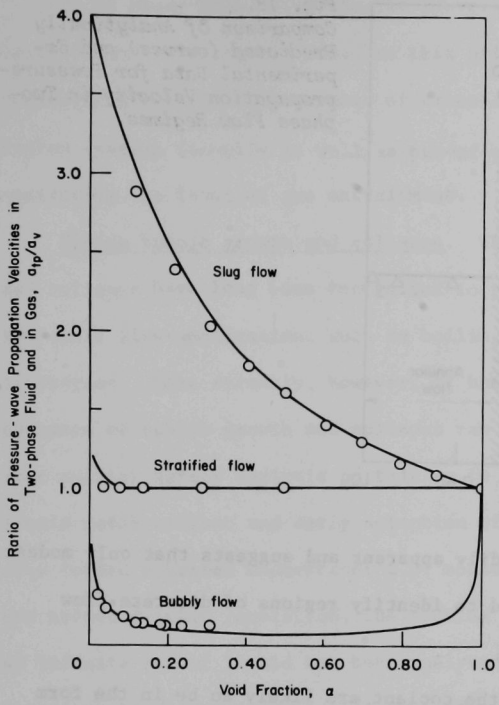

Fig. 17. Comparison between Predicted (curves) and Measured (data points) Pressure-wave Propagation Velocities in Air-Water Mixtures.

detection of fuel-pin failure. The acoustical properties of two-phase mixtures might have direct application to these problems.

As a result of ongoing research pertaining to pressure-wave propagation and sonic velocity in two-phase mixtures,[19,20] a technique has been devised that appears promising for use in identifying the major two-phase flow regimes in any particular apparatus.[22] This technique is based on the fact that the system compressibility is extremely sensitive to the distribution of the gaseous phase. This is illustrated in Fig. 18, where the characteristic propagation velocity is shown as a function of void fraction with approximate flow-regime bounds indicated. The analytical predictions have been shown to be in good agreement with experimental data including two- as well as one-component mixtures. The large difference in propagation

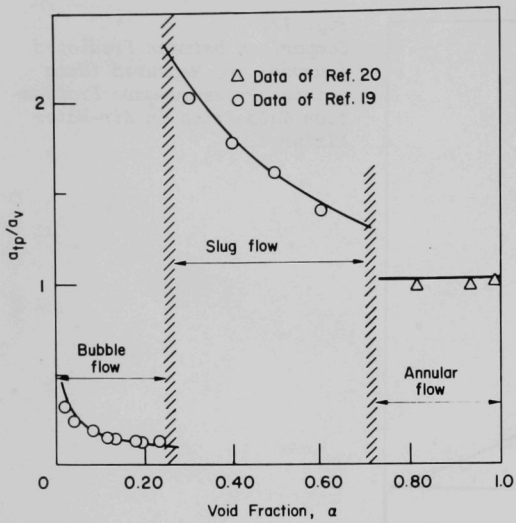

Fig. 18.
Comparison of Analytically Predicted (curves) and Experimental Data for Pressure-propagation Velocity in Two-phase Flow Regimes.

velocity with flow regime is readily apparent and suggests that only modest experimental accuracy is required to identify regions of discrete flow regimes.

Small quantities of gas in the coolant are likely to be in the form of bubbles. For this flow regime (Eq. 7) and typical LMFBR conditions, the sonic velocity is shown as a function of gas concentration in Fig. 19.

$$a_{tp} = \left[\frac{a\,\rho_{tp}}{\rho_g\,a_g^2} + \frac{(1-\alpha)\,\rho_{tp}}{\rho_\ell\,a_\ell^2}\right]^{-0.5} \tag{7}$$

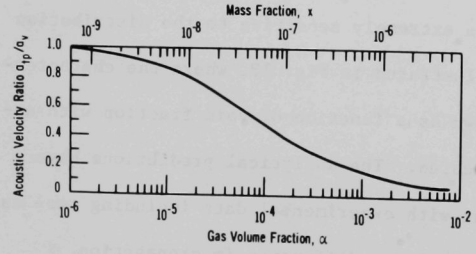

Fig. 19.
Propagation Velocity in a Homogeneous Two-phase Sodium-Argon System at 1200°F and 14.7 psia as a Function of Mass or Volume Fraction. ANL Neg. No. 900-527, Rev. 1.

It is clear that this velocity is very sensitive to low gas concentrations. A technique based on this principle is suggested for determining the first appearance of trace amounts of gas in liquid-sodium systems (in-pile as well as out-of-pile) or for continuously monitoring the level of gas entrainment.

Sodium bubble growth and collapse. The dynamics of bubble growth and collapse have long been recognized to play an important role in many two-phase flow applications such as boiling, flashing of liquids, and cavitation. More recently, however, it has become clear that the dynamics of bubble growth and collapse can play an important role in fast reactor safety analysis pertaining to the possible voiding of the liquid metal coolant and early detection of the accident.[23] As a first step toward a better understanding of sodium bubble growth, collapse, and pressure-pulse generation, the problem of a single vapor bubble in an infinite sea of liquid has been analyzed. A complete system of equations involving a minimum of simplifying assumptions has been specified and solved numerically.[24,25] This system of equations not only takes into account the effects of surface tension, inertia of the liquid, and heat conduction of the liquid, but also the effects of non-equilibrium at the liquid-vapor interface, and provides for complete coupling of the heat-conduction and liquid-inertia equations. The equations are also not limited by the assumption of saturated vapor within the bubble.

Typical analytical results for sodium are shown in Figs. 20-22. The growth behavior of a sodium bubble is shown in Fig. 20. The initial radius R_o is taken as the critical radius corresponding to the assumed initial superheat. The possible effects of nonequilibrium at the vapor-

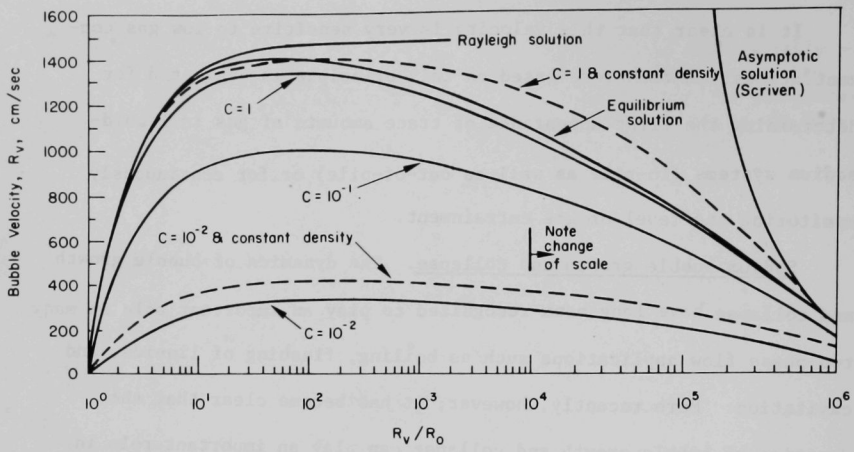

Fig. 20. The Growth Behavior of a Sodium Vapor Bubble in Highly Superheated Sodium at Atmospheric Pressure. R_v is bubble radius, R_0 is initial bubble radius, sodium liquid pressure P_∞ was 1 atm, superheat ΔT_s was 151.5°K, and initial bubble radius was 10^{-4} cm.

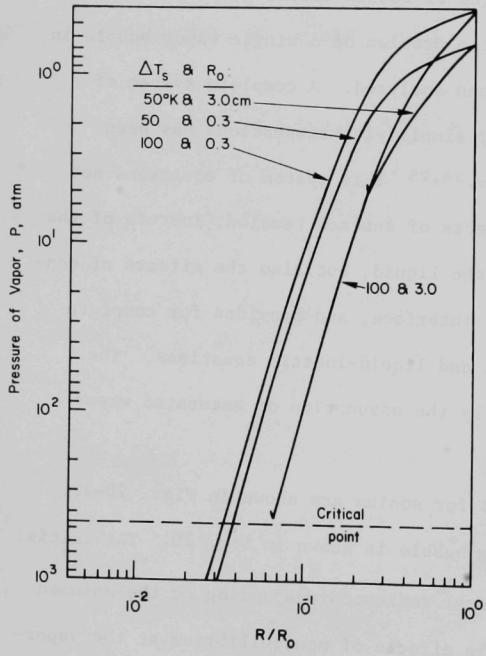

Fig. 21. Pressure of the Vapor P in a Collapsing Sodium Bubble as a Function of its Dimensionless Radius R/R_0 for a Range of Subcoolings ΔT_s and Initial Radii R_0. P_∞ was 1 atm. ANL Neg. No. 900-206, Rev. 2.

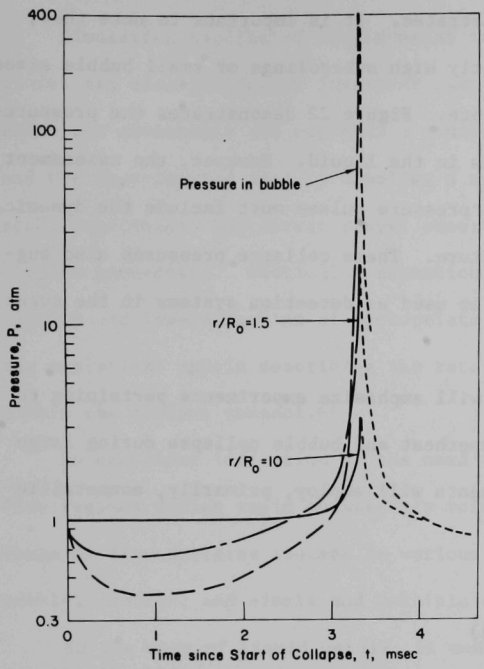

Fig. 22.
Pressure Distribution in the Liquid for a Typical Case. The initial bubble radius R_0 was 3 cm, r is distance from center of bubble, subcooling ΔT_s was 100°K, and initial pressure P_∞ was 1 atm.

liquid interface are shown by variations in the coefficient for condensation or evaporation, C. It is apparent that, for the sodium case considered, if nonequilibrium effects are negligible the early growth behavior is very close to the Rayleigh solution that considers only the inertia of the surrounding liquid. Nonequilibrium effects would diminish the early growth rate. It is also apparent that the sodium bubble reaches an extremely large size before the growth rate approaches the asymptotic solution in which the growth is governed by heat conduction into the surrounding liquid.

Numerical solutions for the collapse of sodium bubbles[26] are shown in Fig. 21, illustrating the separate effects of liquid subcooling and initial bubble size. The generation of large pressures as the

bubbles collapse is clearly demonstrated. It is important to note that, after a given time, for sufficiently high subcoolings or small bubble sizes the vapor reaches its critical state. Figure 22 demonstrates the pressure-time behavior at various locations in the liquid. However, the assessment of the potential damage from such pressure pulses must include the dynamic response of the surrounding structure. These collapse pressures also suggest that pressure sensors might be used as detection systems in the event of accident situations.

Continued work in this area will emphasize experiments pertaining to bubble growth with high liquid superheat and bubble collapse during large liquid subcooling. These experiments will employ, primarily, nonmetallic fluids.

Sodium Simulations

(M. A. Grolmes and H. K. Fauske)

Expulsion and reentry tests are conducted with nonmetallic fluids to obtain detailed local transient measurements that are needed to develop voiding models. The transient flow regimes in initially static and in initially flowing systems (with single and multiple pins) are studied experimentally to determine the details of expulsion and reentry. The experiments with nonmetallic fluids closely complement tests with sodium (p. 106); more information is obtained from combinations of tests than could be obtained with sodium alone.

In recent years, simulation, or experimental modeling, of boiling heat transfer and two-phase flow has become well established in nuclear reactor technology. The incentives for modeling are both technical and economic. Experimentation on a smaller scale at reduced operating temperatures, pressures, and power levels are obvious advantages.

Simulation studies of liquid-metal two-phase flow using nonmetallic fluids are also playing an important part in the LMFBR program, in which the advantages are not only a reduction in operating temperature and the experimental ease of handling a nonmetallic fluid, but, in this study especially, the direct visual observation of the phenomena in complex geometries. Particular attention is given to hydrodynamic simulation and identification of appropriate flow regimes for use in developing analytical models describing the rate of void growth and collapse within the coolant channel.[27]

An excellent indication of the need for identification of realistic flow regimes during rapid subassembly voiding can be found in the full range of flow patterns assumed in various published models, such as bubbly, annular, and single and multiple slug.

In the case of liquid metals, it would appear that at least the effects of high thermal diffusivities, the well-known superheating characteristics, and large liquid-to-vapor density ratios should be considered.

To obtain similarity of density ratio with liquid metals (LM) at atmosphere pressure, common nonmetallic fluids (NM) must be compared at subatmospheric pressures.

The ability of the alkali liquid metals to sustain large superheats prior to nucleation is a result of their intense wettability and physiochemical interaction with the heating surface as well as their thermophysical properties. From the well-known formula expressing the excess vapor pressure in a cavity required for nucleation, the following criterion can be considered to contribute to the similarity of liquid metal and nonmetallic fluid in the absence of entrained gas:

$$\left(\frac{\sigma T_{sat}}{h_{fg}\rho_v}\right)_{LM} \Bigg/ \left(\frac{\sigma T_{sat}}{h_{fg}\rho_v}\right)_{NM} \approx 1$$

where σ is surface tension, T_{sat} is saturation temperature, h_{fg} is latent heat, ρ is density, and the subscript v denotes vapor.

When this dimensional-property group is considered at the same ratio of liquid to vapor density it is found that Freon-11 appears to model sodium more closely than either water or methyl alcohol.

The large thermal diffusivities of liquid metals will result in rather shallow temperature gradients in the narrow coolant channel prior to nucleation and rapid vapor growth immediately following nucleation. This situation can be simulated with nonmetallic fluids if a method of rapid or slow depressurization is employed to superheat the fluid with no radial temperature gradients. The rapid vapor growth associated with liquid metals gives rise to local pressurization tending to deactivate other potential nucleation sites and, therefore, favor the growth of a single bubble. On the other hand, a fluid of low thermal conductivity might experience considerably slower vapor growth and, consequently, little or no pressurization might occur, resulting perhaps in the nucleation of many bubbles.

Therefore, the simulation of the early vapor growth rate appears necessary to model correctly the flow pattern in a superheated liquid metal. By considering the equation of motion of a liquid column of height L_o in a confined channel of equivalent diameter D_o (the motion of the column being due to a growing bubble), together with the well-known Plesset-Zwick equation for bubble growth rate (asymptotic conduction

solution), the following criterion appears to assure a similar initial vapor growth rate:

$$\left(\frac{Ja^2\alpha\rho_\ell L_o}{D_o^2(P_{sat}-P_o)}\right)_{LM} \Bigg/ \left(\frac{Ja^2\alpha\rho_\ell L_o}{D_o^2(P_{sat}-P_o)}\right)_{NM} \approx 1$$

where Ja is the Jacob number, α is thermal diffusivity, P is pressure, and the subscript ℓ denotes liquid.

Thus, while maintaining liquid-to-vapor density ratio, superheat, and geometric similarity, Table I illustrates to what degree nonmetallic fluids compare with sodium. As a result of the previous characteristics cited, together with the excellent vapor growth simulation illustrated in Table I, Freon-11 was used as the principal simulant in the experimental studies.

TABLE I. Illustration of Vapor Growth Rate Simulation

Na/NM	$\left(\frac{Ja^2\alpha\rho_\ell}{P_{sat}-P_o}\right)_{Na} \Big/ \left(\frac{Ja^2\alpha\rho_\ell}{P_{sat}-P_o}\right)_{NM}$
Na/Freon-11*	∿1
Na/H_2O	∿20
Na/CH_3OH	∿14

* Freon-113 is equally suitable.

Several stages of a single-channel (20 mm ID) expulsion event are shown in Fig. 23 that illustrate two markedly different modes of coolant ejection after sudden depressurization. The photographs are taken directly from individual motion picture frames of the same event. At

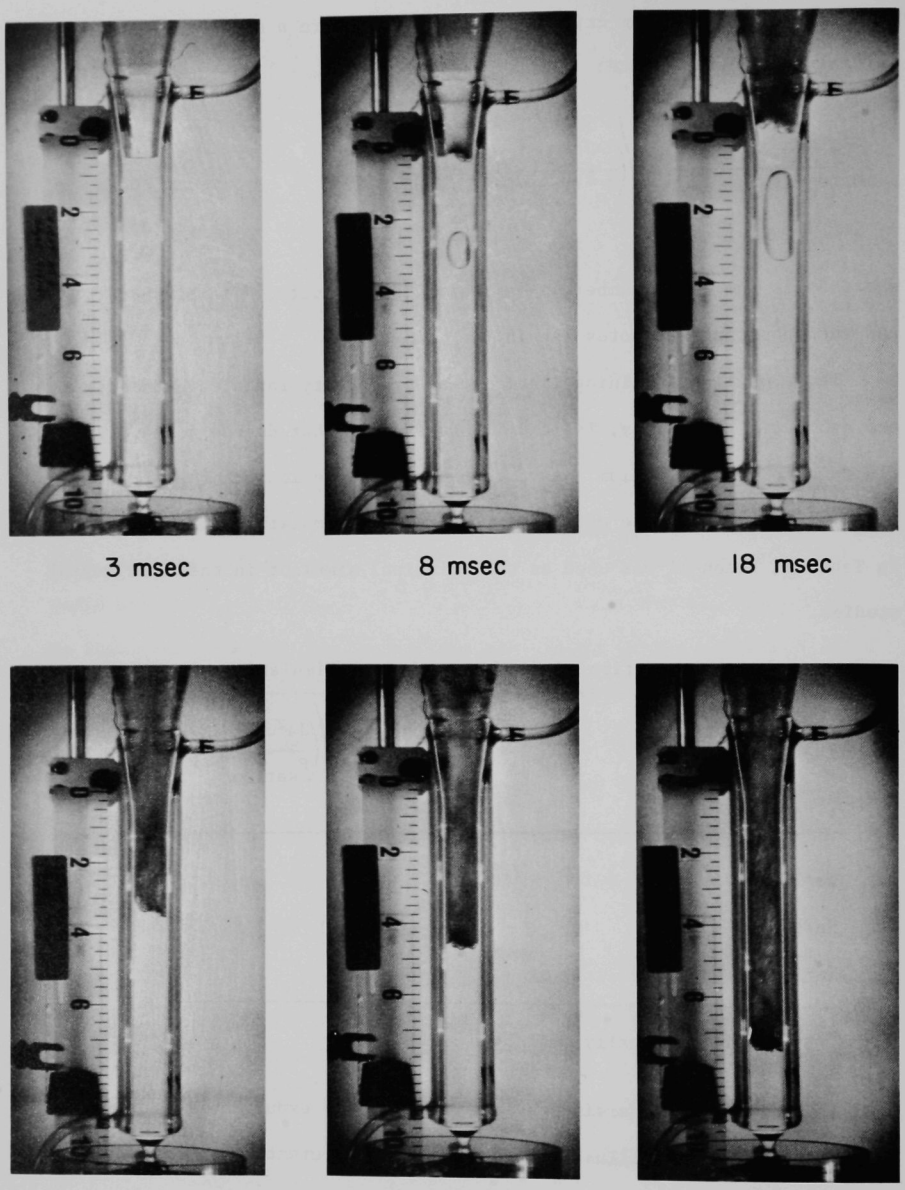

Fig. 23. Single-channel Expulsion Event Illustrating Rapid Bubble Growth, Slug Ejection, and Two-phase Flashing for Methyl Alcohol at 122°F, Depressurized to 0.4 psia. ANL Neg. No. 112-3242A.

3 msec, a single vapor bubble has grown from a wall nucleation site to a size slightly larger than 1/4 in. At 5 and 10 msec later (8 and 18 msec), a liquid wall film is evident (with distortion from curvature of glass) as the vapor expands. The rapid initial bubble growth to the channel diameter proceeds to complete ejection of the upper liquid slug into the reservior. The remaining lower liquid column is again depressurized, and, rather than additional bubble nucleation, a two-phase flashing action is initiated at the free interface. A dispersed two-phase mixture is expelled from a well-defined liquid two-phase interface that propagates downward into the liquid column. Three stages of this expulsion process, which proceeds to the base of the column, are shown at 80, 170, and 360 msec.

It is evident from the times indicated that this mode of ejection proceeds at a much slower rate than does the slug-type vapor expansion. In this instance, the upper slug ejection proceeds at a velocity in excess of 10 ft/sec; the two-phase interface propagates at approximately 1 ft/sec. Both modes of coolant expulsion have been interpreted from liquid-metal data in the absence of direct observation.

Although this second mode of expulsion would appear to have important consequences as far as the later stages concerning cooling action and coolant reentry in a blocked subassembly, the slug mode of ejection following the rapid growth of a single bubble is important because it initiates the expulsion event and was found in all Freon-11 tests from 2 mm ID up to 50 mm ID where a suitable nucleation site was present on the channel wall. In no event was nucleation within the bulk of the fluid observed, and it was evident that a liquid film was always adhering to the test-section wall during the vapor expansion.

This persistent single-bubble-type ejection in Freon-11 tests is in good agreement with interpretations of sodium and potassium experiments.

To verify the general applicability of current single-channel analytical models, it is necessary to demonstrate that single-bubble slug-type ejection is realistic in more complex geometries. This has been shown to be the case in both a 7- and a 19-pin assembly.[28] In these assemblies, the vapor bubble was observed to grow and occupy the total cross section within approximately one channel diameter. No appreciable resistance to radial expansion was observed due to the pins.

Experiments have also been performed in which an initial axial-temperature variation is imposed on the fluid. This is to achieve simulation of the subcooling in the upper plenum of a reactor with reference to the overheating within a blocked subassembly. Analytical models are being developed and improved on the basis of these simulation experiments. Future studies will be directed to both expulsion and reentry in single- and multiple-pin geometries.

Mathematical Models of Voiding and Reentry

(H. K. Fauske)

The experimental and theoretical results obtained in the other parts of the Coolant Dynamics program are being incorporated into a realistic model of sodium expulsion and reentry that will provide a firm basis for predicting voiding rate, reentry dynamics, pressure generation, and initial conditions for fuel-coolant interaction for various types of LMFBR accidents.

An expulsion model that satisfies all conservation conditions has been developed to predict the expulsion and reentry behavior of sodium coolant upon overheating of a reactor channel.[29] It is assumed that a

vapor slug forms over the entire channel cross section, which then pushes the liquid out. Experimental evidence (see p. 100) indicates that this physical picture would be descriptive of severe reactor accidents, such as blockage and pump failure. Parametric studies were made of the effects of the wall film thickness, of the liquid superheat at inception of boiling, point of bubble initiation, and magnitude and shape of the wall heat flux, as well as heat capacity, on the expulsion behavior. Reentry problems associated with blanket and plenum cooling were also studied.

The vapor is assumed to be in equilibrium with the surrounding liquid interfaces at all times. The heat conduction equation is solved in the end liquid regions and also in the liquid film adhering to the wall in the vapor zone. This allows expulsion and reentry to be calculated in both the presence and absence of wall film.

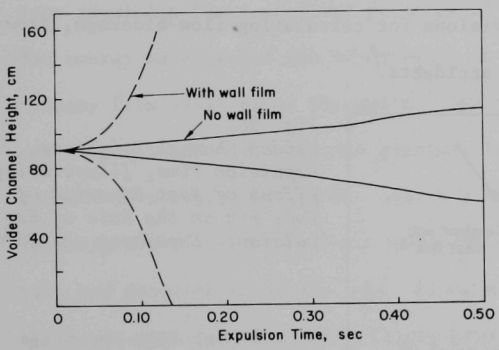

Fig. 24.
Voided Channel Height vs Expulsion Time, Illustrating Effect of Liquid Wall Film. Superheat was 20°C and power density was high.

Figures 24 and 25 indicate the strong effect of the presence of wall film. With a dry wall, the voiding rate is much slower and the pressure quickly drops nearly to the external pressure. Furthermore, energy storage in the wall film is significant for thicknesses >0.005 cm. The reduction in film thickness is negligible during expulsion, so that film dryout is not likely to occur during the initial expulsion phase if the wall is

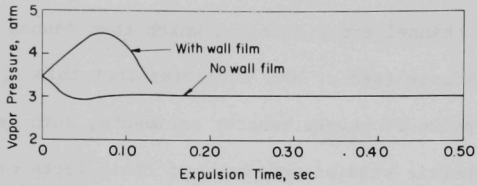

Fig. 25.
Vapor Pressure within Bubble vs Expulsion Time, Illustrating Effect of Wall Film on Pressure History. Superheat was 20°C and power density was high.

well wetted. Moreover, reentry of a liquid slug will not occur until the wall film has been largely evaporated. Finally, the superheat at which boiling is initiated governs the early voiding behavior, while for reasonable values of the wall heat flux (reactor conditions) the evaporation rate from the wall film dominates the expulsion rate during the later stages. The strong effect of heat capacity on the pressure buildup and the associated voiding rate has been demonstrated for typical flow-blockage accidents, as is indicated in Figs. 26 and 27. This version of the slug model, including several bubbles, is being incorporated into the SAS accident-analysis code, making provisions for calculating flow-blockage, flow-coastdown, and power-excursion accidents.

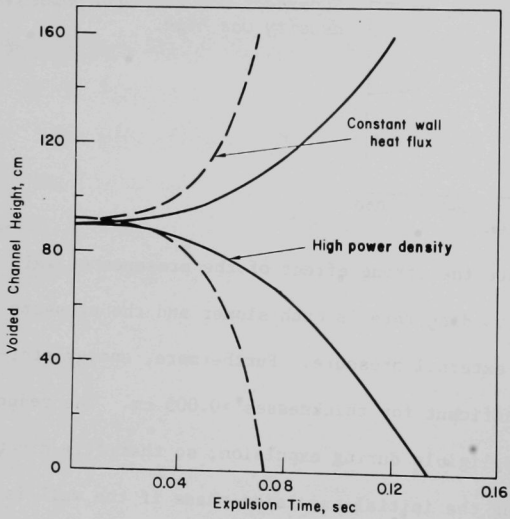

Fig. 26.
Voided Channel Height vs Expulsion Time, Illustrating Effect of Heat Capacity of Fuel Pin on the Rate of Expulsion. Superheat was 20°C.

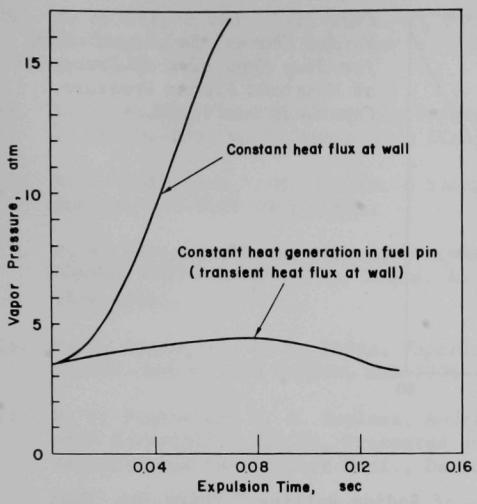

Fig. 27.
Vapor Pressure vs Expulsion Time, Illustrating Effect of Heat Capacity of Fuel Pin on Pressure History within Vapor Bubble. Superheat was 20°C.

The slug model has been generalized to permit direct comparison with nonmetallic fluids (p. 100). This has resulted in an analysis of the slug-type expulsion based on first principles[30,31] (no empirical constants). The energy balance for the vapor space is written assuming a uniform stationary film existing on the walls. The temperature gradient at the upper and lower liquid slugs and the gradient at the film-vapor interface are evaluated in a similar manner, assuming the existence of a thin thermal-boundary layer within the film, whose thickness as a function of exposure time and position along the vapor space was taken into account. Excellent agreement with experimental data has been demonstrated, including both voiding rate and pressure variation (Fig. 28). Development of improved methods for describing liquid-film thickness, breakup, and condensation rates are in progress to evaluate reentry and chugging behavior.

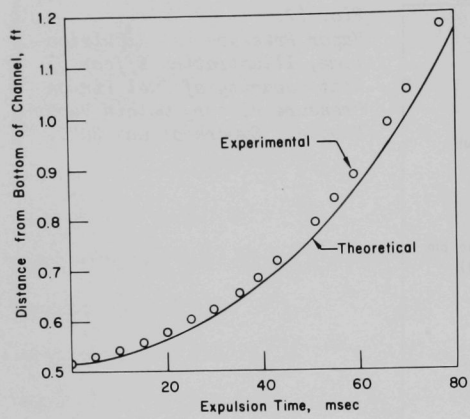

Fig. 28.
Voided Channel Height vs Time for Slug Expulsion of Freon-113 at Constant Plenum Pressure. Superheat was 109°F.

References

1. B. S. Petukhov et al., "Study of Sodium Boiling," *Third Int. Heat Transfer Conf.*, Chicago, *5*, pp. 80-91 (Aug 7-12, 1966).

2. R. E. Holtz and R. M. Singer, "On the Superheating of Sodium and the Generation of Pressure Pulses," *Proc. Int. Conf. on the Safety of Fast Reactors*, Aix-en-Provence, France, Ses. IIb-5 (Sept 19-22, 1967).

3. R. E. Holtz and R. M. Singer, *Incipient Pool Boiling of Sodium*, AIChE J. *14*, No. 4, pp. 654-656 (Jul 1968).

4. J. C. Chen, *Incipient Boiling Superheats in Liquid Metals*, Trans. ASME, Series C, J. Heat Transfer *90*(3), pp. 303-312 (Aug 1968).

5. G. C. Pinchera et al., "Liquid Sodium Superheat and Water Ejection Experiments," *Proc. Symp. Two-phase Flow Dynamics*, Eindhoven, The Netherlands (Sept 4-9, 1967).

6. R. E. Holtz and R. M. Singer, *On The Initiation of Pool Boiling in Sodium*, Chem. Eng. Progress Symp. Series No. 92 (Heat Transfer, Philadelphia), *65*, pp. 121-128 (1969).

7. G. C. Pinchera et al., "Experimental Boiling Studies Related to Fast Reactor Safety," *Proc. Int. Conf. on the Safety of Fast Reactors*, Aix-en-Provence, France, Ses. IVa-2 (Sept 19-22, 1967).

8. K. H. Spiller et al., *Überhitzung und einzelblasenejektion von stagnierendem Natrium*, Atomkernenergie *13*, pp. 245-251 (1968).

9. B. LeGonidec et al., "Experimental Studies on Sodium Boiling," *Proc. Int. Conf. on the Safety of Fast Reactors*, Aix-en-Provence, France, Ses. IIb-3 (Sept 19-22, 1967).

10. R. M. Singer and R. E. Holtz, *On the Role of Inert Gas in Incipient Boiling Liquid Metal Experiments*, Int. J. Heat Mass Transfer *12*(9), pp. 1045-1060 (Sept 1969).

11. R. E. Holtz, *The Effect of the Pressure-Temperature History upon Incipient-boiling Superheats in Liquid Metals*, ANL-7184 (Jun 1966).

12. R. E. Holtz and R. M. Singer, *A Study of the Incipient Boiling of Sodium*, ANL-7608 (Oct 1969).

13. R. E. Holtz and R. M. Singer, *Incipient Boiling Conditions in a Blocked LMFBR Subassembly*, Trans. Am. Nucl. Soc. *12*(2) pp. 912-913 (Nov 1969).

14. R. M. Singer and R. E. Holtz, *Vaporization Dynamics of Initially Static Superheated Sodium*, ANL-7706 (Sept 1970).

15. H. K. Fauske and M. A. Grolmes, *Modeling of Liquid-Vapor Metal Flows with Nonmetallic Fluids*, Presented at ASME Fluids Engineering, Heat Transfer and Lubrication Conf., Detroit (May 1970).

16. H. K. Fauske and M. A. Grolmes, *Pressure Gradient in Flashing Sodium Flow*, Trans. Am. Nucl. Soc. *12*(2) pp. 908-909 (Nov 1969).

17. H. K. Fauske and R. E. Henry, *On the Measurement of Throat Pressure in Flashing Sodium Critical Flow*, Trans. Am. Nucl. Soc. *13*(1) pp. 330-331 (Jun 1970).

18. H. K. Fauske and M. A. Grolmes, *Incipient Liquid Superheat, Hysteresis Effect and Equilibration in Forced Convection Flashing Sodium Flow*, Trans. Am. Nucl. Soc. *13*(1) pp. 331-332 (Jun 1970).

19. R. E. Henry, M. A. Grolmes, and H. K. Fauske, "Propagation Velocity of Pressure Waves in Gas-Liquid Mixtures," *Cocurrent Gas-Liquid Flow, 1*, Plenum Press, pp. 1-18 (1969).

20. M. A. Grolmes and H. K. Fauske, *Propagation Characteristics of Compression and Rarefaction Pressure Pulses in One-Component Vapor-Liquid Mixtures*, Nucl. Eng. & Design *11*, pp. 137-142 (1969).

21. R. E. Henry, *Pressure Wave Propagation in Two-phase Mixtures*, Chem. Eng. Progress Symp. Series, 102, *66* (1970).

22. M. A. Grolmes and H. K. Fauske, *Acoustic Techniques for Flow Regime and Gas Detection*, Trans. Am. Nucl. Soc. *12*(2) pp. 832-833 (Nov 1969).

23. J. B. van Erp, D. R. MacFarlane, and H. K. Fauske, *Protection Against LMFBR Local Core Accidents*, Trans. Am. Nucl. Soc. *13*(1) pp. 363-364 (Jun 1970).

24. T. Theofanous et al., *A Theoretical Study on Bubble Growth in Constant and Time-dependent Pressure Fields*, Chem. Eng. Sci., *24*, pp. 885-897 (1969).

25. T. Theofanous et al., *Nonequilibrium Bubble Collapse: A Theoretical Study*, Chem. Eng. Prog. Symp. Series, 102, *66*, pp. 37-47 (1970).

26. T. Theofanous, H. S. Isbin, and H. K. Fauske, *Sodium Bubble Collapse and Pressure Generation*, Trans. Am. Nucl. Soc. *12*(2), pp. 909-911 (Nov 1969).

27. M. A. Grolmes and H. K. Fauske, *Modeling of Sodium Expulsion with Freon-11*, Presented at ASME Fluids Engineering, Heat Transfer and Lubrication Conf., Detroit (May 1970).

28. M. A. Grolmes, H. K. Fauske, and G. A. Lambert, *Superheat Expulsion in Single and Multipin Channels - Simulation of Blocked Subassembly Voiding*, Trans. Am. Nucl. Soc. *12*(2), pp. 907-908 (Nov 1969).

29. A. W. Cronenberg et al., *A Single-bubble Model for Sodium Expulsion from a Heated Channel*, Nucl. Eng. and Design, in print.

30. W. D. Ford, H. K. Fauske, and S. G. Bankoff, *The Slug Expulsion of Freon-113 by Rapid Depressurization of a Vertical Tube*, Int. J. Heat and Mass Transfer (1970) (in press).

31. W. D. Ford, H. K. Fauske, and S. G. Bankoff, *Analysis of a Slug Expulsion for a Nonmetallic Fluid*, Trans. Am. Nucl. Soc. *13*(1) p. 372 (Jun 1970).

Nuclear Safety Research and Development--LMFBR Safety

VI. CORE STRUCTURAL SAFETY*

(C. K. Youngdahl)

Overall scope. The responses of cylindrical shell structures (particularly with circular and hexagonal cross sections) to both internal and external impulsive loads, and the influence of the structural response (as feedback) on the course of the pressure-time function, are investigated by mathematical analyses of elasticity and plasticity. The information applies to core-region structural components such as fuel cladding, fuel-element subassemblies, and control-rod shrouds or guides.

Summary. The analysis of the dynamic plastic response of a circular cylindrical shell to an axially varying load was concluded and equivalence parameters were proposed. Strain-hardening effects were estimated. The study of dynamic plastic response of a hexagonal shell was continued.

Dynamic Plasticity Analysis of Circular Shells

The dynamic rigid-plastic analysis of a circular-cylindrical shell acted on by an axisymmetric load with an arbitrary axial and time variation over a fixed axial region was concluded.[1] A set of three equivalence parameters was proposed. The first indicates the force of the loading, the second is an axial load-shape factor, and the third is a time load-shape factor. The use of the equivalence parameters will provide a means of correlating analytical and experimental results of LMFBR safety studies. The parameters were found to be applicable also to other reactor structural-component configurations.[2,3]

*For references for this chapter, see p. 120.

To determine the localized plastic deformation of a pipe or tube produced by a dynamic loading that exceeds the yield load only briefly, it is important to know the effect of the spatial and temporal shapes of the pressure pulse on the final deformation. This is particularly true in computer or laboratory simulations of reactor accidents, where it is impossible or impractical to reproduce the actual loading conditions.

It had been hypothesized[4] previously that the final deformation for any load shape was essentially dependent only on the impulse and peak load. However, this was shown to be reasonable only for loadings greatly in excess of the yield load;[5,6,7] the errors for loadings that produce only small plastic deformations are quite large. Initially it was found[6,7] that the final plastic deformation of a long tube loaded by a dynamic concentrated ring load with arbitrary time history is well correlated by two parameters--the impulse and the effective load. Both parameters are defined in terms of simple integrals of the load-time shape. It then was found that a third parameter can be added to account for the effect of the axial variation of a pressure pulse on the dynamic plastic deformation of a long tube or pipe.

Consider a long circular cylindrical shell made of a rigid perfectly plastic material (Fig. 29). The shell is loaded axisymmetrically by a dynamic pressure $P(z,t)$ applied over an axial region $|z| \leq L$. It will be assumed that the pressure is symmetric about $z = 0$ and can be written as the product of spatial and temporal shape functions, i.e.,

$$P(z,t) = \Phi(z)\Psi(t) \quad . \tag{1}$$

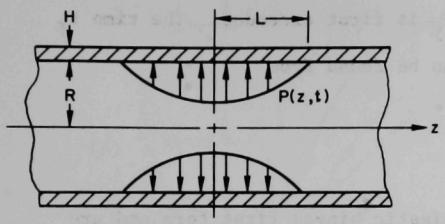

Fig. 29.
Circular Cylindrical Shell Loaded by an Axially Varying Pressure.
ANL Neg. No. 113-3506.

The partial differential equations governing the dynamic plastic deformation can be integrated in closed form with respect to z, resulting in sets of coupled nonlinear differential equations in time.[1,8] These are solved on a computer for combinations of various assumed load shapes Φ and Ψ.

The results for $U_o\ (t_f)$, the final plastic deformation at z = 0, are well correlated by

$$U_o(t_f) = I\ f(\Psi_e,\ \Phi_e) \tag{2}$$

where I is the impulse [the integral of P(z,t) over z and t] and Ψ_e and Φ_e are effective values of Ψ and Φ defined by

$$\Psi_e = \frac{\left[\int_{t_y}^{t_f} \Psi(t)dt\right]^2}{2\int_{t_y}^{t_f}(t - t_y)\Psi(t)dt},$$

$$\Phi_e = \frac{\left[\int_{o}^{z_y} \Phi(z)dz\right]^2}{2\int_{o}^{z_y} z\Phi(z)dz}. \tag{3}$$

The time t_y is when the yield load Ψ_y is first exceeded. The time t_f is when the deformation stops; it can be found from

$$\int_{t_y}^{t_f} \Psi(t)dt \approx \Psi_y \, (t_f - t_y). \tag{4}$$

The axial positions $\pm z_y$ are where plastic hinges first form and are known from the yield load analysis. The half-length L of the loaded region is replaced by an effective half-length L_e defined by

$$L_e = \frac{1}{2\Phi_e} \quad . \tag{5}$$

If Ψ and Φ are both rectangular, the problem can be solved in closed form,[1,8] so that the function f in Eq. 2 is known. The quantities Ψ_e, Φ_e, and L_e given in Eqs. 3 and 5 specify a rectangular distribution equivalent to arbitrarily prescribed $\Psi(t)$ and $\Phi(z)$, as shown in Fig. 30.

Some typical results are shown in Figs. 31 and 32; R, H, and ρ are the tube radius, thickness, and surface density, respectively, and

$$P_o = \sigma_y \frac{H}{R}, \tag{6}$$

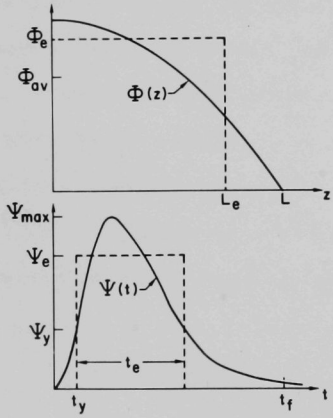

Fig. 30.
Load Shape $\Phi(Z)$ and Pulse Shape $\Psi(t)$.
ANL Neg. No. 113-3501.

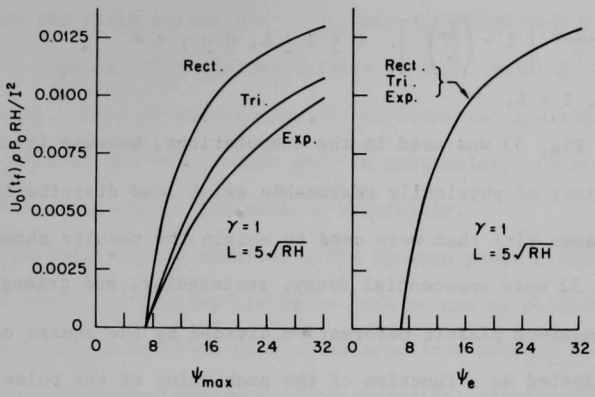

Fig. 31. Maximum Plastic Deformation as a Function of Ψ_{max} and Φ_e for Various Pulse Shapes. ANL Neg. No. 113-3498.

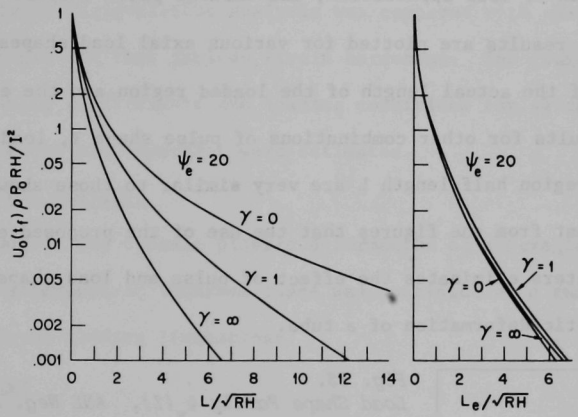

Fig. 32. Maximum Plastic Deformation as a Function of L and L_e for Various Load Shapes. ANL Neg. No. 113-3495.

where σ_y is the yield stress of the tube material. The nondimensional quantity ψ is defined in terms of Ψ by

$$\psi = \frac{2L\Phi_{av}}{P_o\sqrt{RH}}\,\Psi, \tag{7}$$

where Φ_{av} is the average value of Φ. The load shape family Φ_γ defined by

$$\Phi_\gamma = \frac{\gamma + 1}{\gamma}\left[1 - \left(\frac{Z}{L}\right)^\gamma\right], \quad 0 \leq Z \leq L, \; 0 \leq \gamma < \infty \tag{8}$$

$$= 0, \; Z > L,$$

and shown in Fig. 33 was used in the computations, because it compasses a variety of physically reasonable axial load distributions. The pulse shapes $\Psi(t)$ that were used to obtain the results shown in Figs. 31 and 32 were exponential decay, rectangular, and triangular. In Fig. 31, the maximum plastic deformation divided by the square of the impulse is plotted as a function of the peak value of the pulse and of the effective value for a fixed axial distribution ($\gamma = 1$ in Eq. 8), a fixed region of load application, and various pulse shapes. In Fig. 32, the results are plotted for various axial load shapes as a function of the actual length of the loaded region and the effective length. Results for other combinations of pulse shape Ψ, load shape Φ and load region half-length L are very similar to those shown here. It is apparent from the figures that the use of the proposed equivalence parameters eliminates the effect of pulse and load shape on the maximum plastic deformation of a tube.

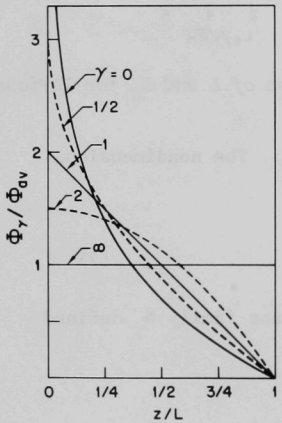

Fig. 33.
Load Shape Family $\Phi_\gamma(Z)$. ANL Neg. No. 113-3499.

Because the three parameters I, Ψ_e, and Φ_e depend only on integrals of the loading, they are insensitive to small perturbations in pulse shape. This is encouraging for experimental applications because details of the pulse shape and, in particular, its peak value are difficult to reproduce and measure accurately.

Work was initiated on predicting the dynamic plastic deformation produced by realistic loading histories such as can be obtained from the Coolant Dynamics and Fuel-Coolant Interactions studies in order to provide a preliminary estimate of the potential significance of feedback effects.

The dynamic rigid-plastic analysis was compared with crude models for ring deformation that include strain hardening. The ranges of strain-hardening coefficients and loading conditions for which strain-hardening effects are important were estimated.

Hexagonal-shell Analysis

The study of the dynamic plastic deformation of a hexagonal shell produced by axisymmetric internal loads was continued at a reduced level because of funding limitations.

Future Program

The development of dynamic plasticity analysis of circular shells will continue, with particular emphasis on predicting the deformation produced by realistic loading histories as provided by other ANL programs. The analysis of the dynamic plastic deformation of hexagonal shells produced by axisymmetric internal loads will continue and the deformation produced by some realistic loading histories will be determined.

References

1. C. K. Youngdahl, *Correlating the Dynamic Plastic Deformation of a Circular Cylindrical Shell Produced by an Axially Varying Pressure*, ANL-7738 (Oct 1970).

2. C. K. Youngdahl, *Correlation Parameters for Eliminating the Effect of Pulse Shape on Dynamic Plastic Deformation*, J. Appl. Mech. *37* (3), pp. 744-752 (Sept 1970).

3. C. K. Youngdahl, *Load Equivalence Parameters for Dynamic Loading of Structures in the Plastic Range*, ANL-7677 (Sept 1970).

4. P. S. Symonds, *Dynamic Load Characteristics in Plastic Bending of Beams*, J. Appl. Mech. *20*, pp. 475-481 (1953).

5. P. G. Hodge, Jr., *The Influence of Blast Characteristics on the Final Deformation of Circular Cylindrical Shells*, J. Appl. Mech. *23*, pp. 617-624 (1956).

6. C. K. Youngdahl, "The Equivalence of Dynamic Loads for the Final Plastic Deformation of a Tube," *Proc. First Internatl. Conf. on Pressure Vessel Technology*, CONF-690906, Pt. 1, Design and Analysis, 89-100, Delft, The Netherlands, Sept. 29 - Oct. 2, 1969, ASME, New York (1969).

7. C. K. Youngdahl, *The Dynamic Plastic Responses of a Tube to an Impulsive Ring Load of Arbitrary Pulse Shape*, ANL-7562 (April 1969).

8. G. Eason and R. T. Shield, *Dynamic Loading of Rigid-Plastic Cylindrical Shells*, J. Mech. Phy. Solids, *4*, pp. 53-71 (1955-1956).

Nuclear Safety Research and Development--LMFBR Safety

VII. FUEL ELEMENT FAILURE PROPAGATION*

(J. F. Schumar, B. D. LaMar, R. O. Ivins)

Overall scope. The propagation of fuel-element failures is of serious concern to both the safety of an LMFBR and its operation. Rapid pin-to-pin propagation could potentially lead to cascading failure of a magnitude that threatens the integrity of a subassembly. Potential failure of a subassembly leads to concern of damage to the surrounding assemblies. The implication to safety is serious if the time for failure propagation is shorter than the time required for detection and reactor shutdown. The concern in the operation of an LMFBR is related to the importance of being able to continue operating a reactor safely with a number, as yet undetermined, of failed fuel elements.

This program is addressed to resolution of these problems. It includes out-of-pile simulations of the phenomena involved in fuel-element failure propagation and in-pile tests simulating LMFBR conditions. Failure thresholds and mechanisms of propagation are being studied in these tests and will culminate in the development of calculational methods required for the safety evaluation of conceptual designs and for the preparation of safety analysis reports of proposed LMFBR plants and fast-reactor test facilities. The calculational methods also are needed for the development of the functional requirements for core protective systems, safety instrumentation, containments, and consequence-limiting safety systems. These methods provide the means to evaluate the expected performance of such systems.

Out-of-pile experiments are conducted: (1) to study the phenomenology of the modes of propagation, (2) to assist in the design and

*For references for this chapter, see p. 229.

performance of the in-pile tests, and (3) to provide information to aid in the analysis and interpretation of the in-pile test results. The analytical studies develop predictive mathematical descriptive models for failure propagation, and aid in planning and designing the out-of-pile and in-pile tests.

The in-pile experiments are integral simulations of conditions expected in an operating reactor when a well-characterized initiating fuel-element failure is induced. Planned tests, in flowing-sodium loops in a thermal test reactor, will provide engineering data for developing predictive analytical descriptions of fuel-element failure propagation.

The in-pile loops (FEFPLs) are designed to be major safety vehicles capable of performing a wide range of tests. It is planned to conduct the tests in the Engineering Test Reactor (ETR). The development of the loop involves combined effort by ANL and Idaho Nuclear Corp. (INC).

Out-of-pile Studies

Scope. Experimental efforts concerned with providing information leading to a better understanding of the basic nature of failure propagation modes constitutes a continuing effort in this task. Experiments are planned using both an out-of-pile sodium test loop and test loops using nonmetallic fluids, as well as other small-scale experiments. In support of the in-pile tests, techniques to provide specific modes of failure (i.e., to initiate the in-pile failures on demand) are being developed and tested.

Gas-jet impingement experiments in heated channel. The experiment described here is the first of several out-of-pile experiments directed toward the study of potential propagation of failure from one fuel pin to another in an LMFBR fuel subassembly.

During reactor operation, the fission process produces a number of fission gases in the fuel, with xenon being the most abundant. A portion of this gas remains in the fuel; the remainder diffuses out of the fuel and is retained by the cladding. Fission-gas plenums are designed into the fuel pins to limit the pressure buildup due to this fission-gas production. Even so, the internal pressure might reach values as high as 1000 psi near the "end-of-life" of the fuel. This high-pressure gas represents a source of stored energy that could provide the driving force for propagation of failure once a break has occurred in the fuel-pin cladding. The release of stored fission gas has, in fact, been the potential mode of failure propagation receiving the most attention to date.

The present series of experiments were intended to scope the problem of gas-jet impingement and to provide some preliminary insight into the heat-transfer mechanisms associated with it. The specific experimental objectives were: (1) obtain data relative to the temperature transients induced in a heated wall by the impingement of a high-velocity gas jet, (2) deduce information about the heat-transfer phenomena occurring when the jet impinges on the surface (e.g., is the surface truly gas blanketed or does the gas jet entrain sufficient liquid to spray-cool the surface?), (3) obtain transient flow, pressure, and photographic data to characterize the hydrodynamic phenomena associated with the gas release, and (4) investigate the effect of bypass flow around a channel subjected to a rapid gas release.

The experiment was performed in a water-cooled electrically heated rectangular flow channel 0.050 x 0.578 x 18 in. The test section was

designed to allow a fixed volume of gas to be discharged through an orifice and impinge on the opposite wall. Thermocouples measured the resulting wall-temperature transients. The test parameters were: coolant velocity of 10, 20, and 30 ft/sec, orifice diameter of 0.016, 0.025, and 0.051 in., plenum gas pressure of 500, 750, and 1000 psia, and surface heat flux of 0.5×10^6 and 1.0×10^6 Btu/hr-ft^2. Tests were run with and without bypass flow around the channel.

Additional data were obtained from an unheated Lucite channel with flow-channel dimensions identical to the heated channel. Gas releases were initiated and high-speed motion pictures were obtained of the resulting gas jets and flow transients. Transient pressures and flowrates were recorded and compared with similar measurements from the heated section.

Analysis of the photographic data shows the channel was completely voided only for gas releases from the 0.051-in. orifice. Flow-recovery times varied from 0.14 sec (30 ft/sec and 500 psi) to 0.89 sec (10 ft/sec and 1000 psi). The peak pressure pulses, measured 1 in. from the orifice, had a magnitude of about 100 psi for tests with the 1000-psi plenum pressure.

Gas releases from the 0.025-in. hole produced a small flow reversal with a rapid recovery. The gas jet holds a fairly stable liquid interface on the wall at a position about 0.5-in. upstream from the orifice. A typical flow pattern is shown in Fig. 34. The jet persisted for about 2 sec.

Tests with the 0.016-in. orifice produced very minor flow perturbations of the coolant, but, as with the 0.025-in. orifice, they also produced a stable liquid interface on the wall at a point upstream of the jet. The jet persisted 4 to 5 sec.

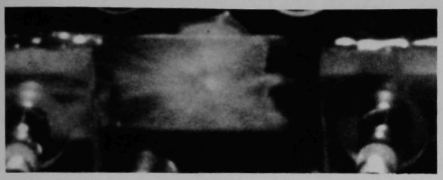

Fig. 34.
Spray Pattern and Interface between Gas Jet and Coolant.

Data from the heated tests revealed that in every case the surface directly opposite the jet was cooled as a result of the improved heat transfer due to spray cooling. The heat-transfer coefficient at the point of impingement was best correlated with the gas flowrate. This is shown in Fig. 35. The effects of the coolant velocity and orifice diameter were less than the scatter of the data. Only for cases where the channel was blown completely dry did the wall temperature rise to values that exceeded its initial steady-state value; e.g., for a velocity of 20 ft/sec, gas pressure of 1000 psi, and an orifice diameter of 0.051 in., the wall temperature peaked at 130°F above the steady-state temperature 0.8 sec after the gas release was initiated. Figure 36 is a reproduction of the strip chart obtained for test conditions of 0.025-in. orifice, 20-ft/sec coolant velocity, and 750-psi gas pressure.

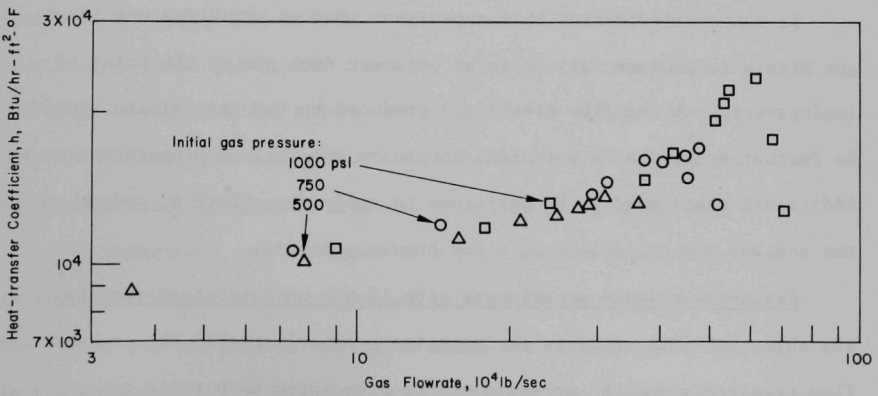

Fig. 35. Heat-transfer Coefficient at Point of Gas-jet Impingement. Coolant velocity was 30 ft/sec and orifice diameter was 0.025 in.

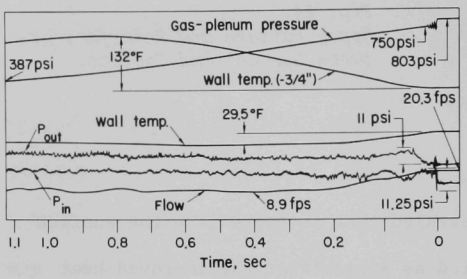

Fig. 36. Test with 0.025-in. Orifice, 20-ft/sec Coolant Velocity, and 750-psi Gas Pressure. ANL Neg. No. 113-3259, Rev. 1.

While the wall directly opposite the jet was cooled, temperature measurements 0.75-in. upstream of the jet indicated the wall temperature increased during every transient. This can be seen in Fig. 36. It is postulated that this temperature transient was produced by the coolant flow transient because the observed temperature transients agreed well with calculated temperatures obtained by using the transient flow data from the experiments. The flow transients observed in these tests are believed to be far more severe than would occur in an actual subassembly because of the very small flow area in the test section. As would be expected, the flow transients were far less severe for the experiments with no bypass flow.

It was concluded from this experiment that an impinging gas jet is not likely to produce failure in an adjacent fuel pin at the point of impingement, but the flow transients produced by the gas release should be further studied as a potential mechanism for failure propagation. Additional tests need to be performed to study the effect of sodium as the coolant and the effect of a rod-bundle geometry.

Rapid-gas-release experiments with 19-pin unheated test section. The object of this study is to investigate experimentally the coolant flow transients and the pressure pulses associated with rapid gas release (total release time <∿50 msec) from a single pin. Two of the

effects of rapid gas release that might result in propagation of the failure to the neighboring pins are: (1) thermal insulation of the adjacent pins as a result of coolant transients that temporarily void the region, and (2) generation of pressure pulses. The sudden release of fission gas causes separation of the liquid column in the fuel subassembly in two parts in such a way that the lower liquid column experiences a rapid deceleration and the upper liquid column is rapidly accelerated. These rapid flow transients result in generation of pressure pulses of considerable intensity and width.

The first mechanism could result in overheating of the cladding due to the poor heat transfer characteristics of the gas phase, whereas the second mechanism might result in rupture of the adjacent fuel pins due to excessive deflection caused by the pressure pulses traveling radially from the source point. In addition, the pressure pulses might also cause some deformation of the hexagonal can containing the fuel assembly.

The present study has the following objectives: (1) provide quantitative data regarding hydraulic transients, (2) study the effect of variables such as gas plenum pressure, rates of coolant flow, and type and size of the cladding breach (holes, slots or rips), (3) observe intensity and half width of the pressure pulses, and (4) formulate an analytical model consistent with the experimental observations.

The experiment was performed in a test section consisting of a triangular array of 19 pins enclosed in a plexiglas hexagonal channel. The center pin was made of stainless steel and had a hole of the selected size and at the location desired for the gas release. A pressure-actuated piston-type valve opened the hole on demand and released

the argon gas stored in the pin. The remaining 18 pins were made of clear plexiglas to allow observation of the resulting gas bubble. The dimensions of the pins were 1/4-in. OD x 71.5-in. length and were wrapped with 0.05-in. OD spacer wire at 12-in. pitch. The whole pin bundle was supported at the bottom by a perforated plate (grid).

The test section was mounted vertically in a forced-circulation water loop shown in Figs. 37 and 38. The discharge flow from the simulated fuel subassembly rose vertically about 10 ft to a tank (plenum) with a free surface open to the atmosphere. A bypass flow channel was connected in parallel with the simulated fuel subassembly. The range of parameters for the tests were: 0, 5, 10, 18, and 30 ft/sec coolant velocity, 500 and 1000 psia plenum-gas pressure, and a 0.063-in.-dia hole or a slot 0.062 in. x 0.125 in. The breach was in the center of the rod bundle.

Results pertaining to a typical transient are given in Figs. 39-41 for coolant velocity of 30 ft/sec and gas plenum pressure of 900 psia. Figure 39 indicates that the flow into the test section is rapidly reduced to about half its value in about 35 msec and recovers its original value in about 115 msec, while the gas from the gas plenum is discharged almost completely in about 30 msec. The peak pressure pulse measured at the point of release and at the wall of the test section has a maximum magnitude of about 100 psi above the local system pressure and a half width of 15 msec. The intensity of these pressure pulses falls off very quickly along the length of the test section; e.g., the peak value measured in a typical transient is about 50 psi above the local system pressure just above the grid and about 15 psi below the grid. Figure 40 shows typical flow patterns at various time intervals; it is

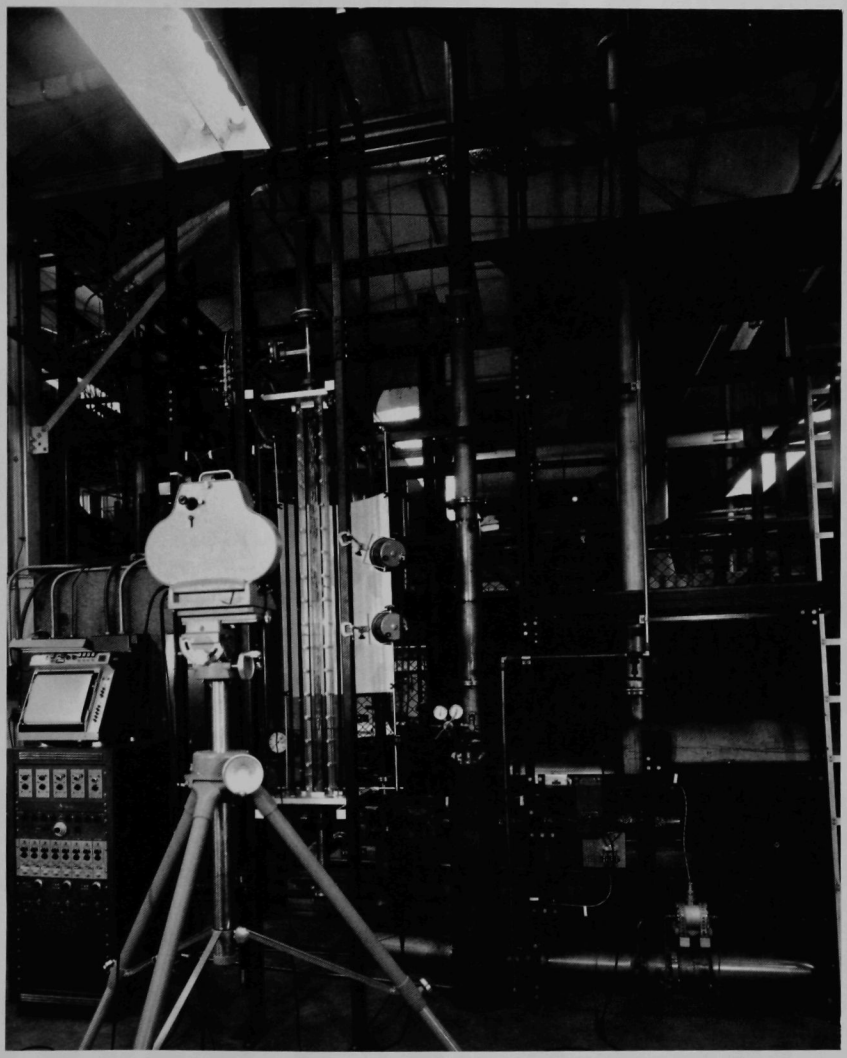

Fig. 37. 19-pin Test Section Mounted Vertically in Forced-circulation Water Loop. ANL Neg. No. 113-2572.

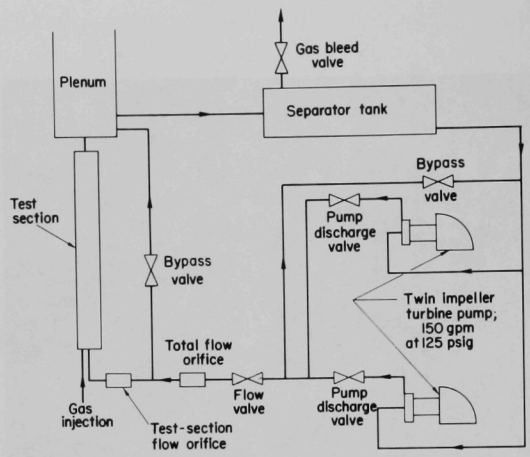

Fig. 38.
Water Test Loop.

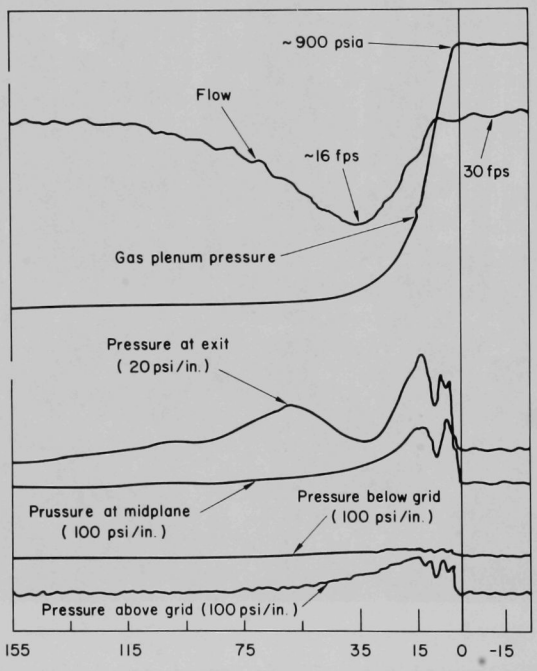

Fig. 39.
Typical Transient for Test with Coolant Velocity of ~30 fps, Plenum Pressure of 900 psia, and a Slot of 1/16 x 1/8 in.

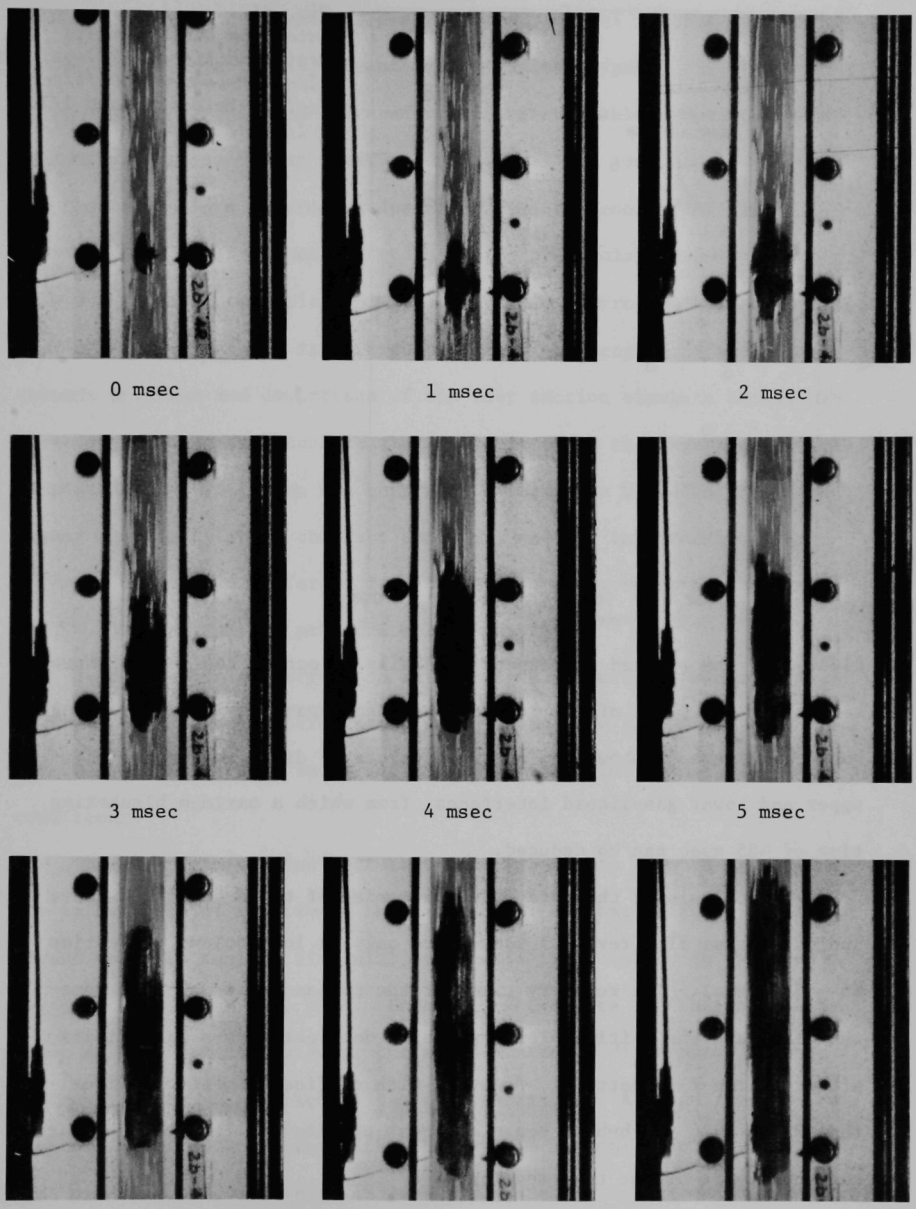

0 msec 1 msec 2 msec

3 msec 4 msec 5 msec

6 msec 7 msec 8 msec

Fig. 40. Sequence of Bubble Expansion at Various Time Intervals for Typical Transient. ANL Neg. No. 900-490.

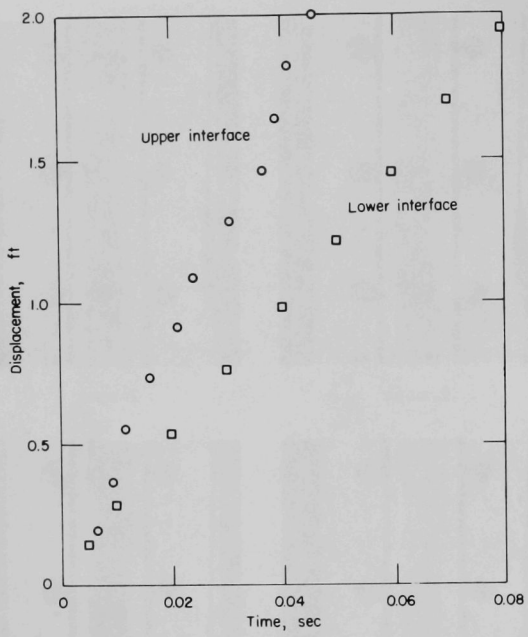

Fig. 41. Interface Displacements for Test Conditions: 900-psi Gas-plenum Pressure, 30-ft/sec Coolant Velocity, and 1/16 x 1/8-in. Slot.

clear that the ejected gas expands radially to occupy the entire cross section at the point of the release and then expands axially as a single bubble. Figure 41 shows the measured values of displacements of the upper and lower gas-liquid interfaces, from which a maximum blanketing time of ∿35 msec can be deduced.

The analysis of the data from the series of tests described above indicates that flow reversal took place only at low coolant velocities (0 - 5 ft/sec). The recovery time for the coolant flow was then somewhat longer. The initial plenum pressure does not have a significant effect on the flow pattern. However, with orifice diameters smaller than 0.065 in., the bubble began to break up into smaller bubbles near the upper part of the test section.

Detailed analysis of the data of these experiments is still underway. In particular, attention is being given to those aspects where

the experiments did not simulate very closely actual reactor conditions. These are: (1) in the experiment only a limited bypass flow was provided because of the limited capacity of the available pumps; this led to some variations in the pressure drop across the test section during the flow transients, whereas under actual reactor conditions the pressure drop would be nearly constant, (2) the coolant expulsion process due to rapid gas release is predominantly controlled by the inertia of the liquid phase, so it is important that the lengths of the fluid columns upstream and downstream of the test section simulate adequately those encountered in actual reactor conditions (in the experiment a considerable fluid column was comprised between the branchpoint of the bypass and the inlet to the test section), and (3) the acoustic properties of water are different from those of sodium, which has an effect on the magnitude of the pressure pulses generated.

In the analytical effort an attempt is being made to account adequately for the above differences, so as to be able to predict with required accuracy voiding rates and pressure pulses for actual reactor conditions.

These experiments indicate that flow transients induced by rapid gas release are of relatively short duration, so that it might be expected that the coolant flow will be re-established prior to overheating of the adjacent fuel pins. However, no definite conclusions can be drawn at this point in view of the above-mentioned differences between the experiments and the actual reactor conditions. Also, as regards the possibility of failure propagation through mechanical loading of adjacent pins due to pressure-pulse generation, no definite conclusions are possible at this point, amongst others because of the lack of data

regarding the mechanical properties of cladding material at end-of-life conditions. Analysis in this latter area is also continuing.

Pressure distribution in the coolant plenum during coolant expulsion. The possibility of initiating fuel failure propagation by fission-gas release depends to a large extent on the resulting flow transient. Consequently, it is important to account properly for the inertial effects of the coolant present in the inlet and exit plenums during an expulsion process due to rapid gas release. An analytical study of the effects of the presence of the plenum has application in the coolant-expulsion process due to sudden vaporization of superheated coolant in the reactor fuel assembly.

When describing thermal and hydraulic transients in reactor coolant channels of fixed cross-sectional area, it often is adequate to use a one-dimensional formulation of the laws of conservation of mass, momentum and energy. When there are sudden and large changes in cross-sectional area of the coolant channel, such as at the exit plenum, the accelerated fluid at the location of area transition assumes a "jet" action in almost "stationary" fluid; this results in the exchange of the momentum between the incoming fluid and stationary fluid. As a consequence of the large transition in cross-sectional area at the inlet to the plenum, the resulting flow in the plenum can no longer be considered to be one-dimensional; a one-dimensional formulation of the conservation laws to describe the flow in the plenum is not suitable. In some applications, such as coolant expulsion due to rapid fission-gas release or due to the sudden vaporization of superheated coolant in the reactor fuel assembly, the transient times of the event are very short and the expulsion process is inertia dominated.[1] Consequently it is proper to include the inertial contribution of the fluid in the plenum to the

expulsion process. Thus an investigation was made to determine the significance of the above-mentioned inertial effects.

Assuming the flow in the plenum to be incompressible, irrotational, inviscid, and axisymmetric, the governing equations[2] are:

Euler's equation,

$$\nabla\left(\frac{P}{\rho} + \frac{q^2}{2} + gz + \frac{\partial\phi}{\partial t}\right) = 0 \tag{1}$$

and Laplace's equation in cylindrical coordinates (see Fig. 42)

$$\frac{\partial^2\phi}{\partial r^2} + \frac{1}{r}\frac{\partial\phi}{\partial r} + \frac{\partial^2\phi}{\partial z^2} = 0 \ , \tag{2}$$

where $\phi(r,z,t)$ is the velocity potential related to the velocity vector $q(r,z,t)$ through the relation $q = \nabla\phi$, $P(r,z,t)$ is the axisymmetric pressure at a point, ρ is the density of the fluid, g is the gravitational constant, r and z are coordinates of a point as shown in Fig. 42, and t is the time. The boundary conditions for Eq. 2 are

(i) $\left.\frac{\partial\phi}{\partial r}\right|_{r=a} = 0$

(ii) $\left.\frac{\partial\phi}{\partial z}\right|_{z=0} = u(r,t) \begin{cases} = U_o(t) \text{ for } r < b \\ = 0 \text{ for } r > b \end{cases}$

(iii) $\left.\frac{\partial\phi}{\partial z}\right|_{z=H\to\infty} = U_o \frac{b^2}{a^2}$,

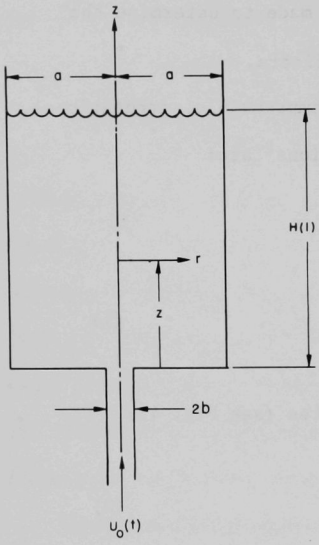

Fig. 42.
Description of the Coordinate System.

where a is the radius of the plenum, b is the radius of the inlet section, and $U_o(t)$ is the influx velocity at the plenum inlet at any time t. The choice of boundary conditions (i) and (ii) is fairly obvious, and the boundary condition (iii) implies that at large enough heights, H, the flow is essentially a parallel flow.

To determine the pressure distribution in the plenum as a function of time and space from Eq. 1, we must first solve Eq. 2 with boundary conditions (i), (ii), and (iii). The solution[3] to Eq. 2 is

$$\phi(r,z,t) = U_o(t)\,\frac{b^2}{a^2}\,z - \frac{2U_o b}{a^2}\sum_n \frac{J_1(\alpha_n b)e^{-\alpha_n z}}{\alpha_n^2\, J_o^2(\alpha_n a)}\, J_o(\alpha_n r)\ . \qquad (3)$$

In the above solution of Eq. 2, the first term represents a uniform flow; quite clearly, at large enough values of z, the second term becomes vanishingly small and the flow essentially becomes a uniform flow.

Integrating Eq. 1 between z = z to z = H and subsequently substituting for ϕ and $q(=\nabla\phi)$ from Eq. 3, we obtain

$$P(r,z,t) = \rho g(H-z) + \left[(H-z) + \frac{2}{b} \sum_n \frac{J_1(\alpha_n b) e^{-\alpha_n z}}{\alpha_n^2 J_o^2(\alpha_n a)} J_o(\alpha_n r) \right]$$

$$\cdot \rho \frac{d}{dt} \left(U_o \frac{b^2}{a^2} \right) - \frac{1}{2} \rho \left\{ \frac{4b^2}{a^4} U_o^2 \sum_m \sum_n \frac{J_1(\alpha_m b)\, J_1(\alpha_n b) e^{-(\alpha_m + \alpha_n) z}}{\alpha_m \alpha_n J_o^2(\alpha_m a)\, J_o^2(\alpha_n a)} \right.$$

$$\left[J_o(\alpha_m r)\, J_o(\alpha_n r) + J_1(\alpha_m r)\, J_1(\alpha_n r) \right]$$

$$\left. + \frac{4b^3 U_o^2}{a^4} \sum_n \frac{J_1(\alpha_n b) e^{-\alpha_n z}}{\alpha_n J_o^2(\alpha_n a)} J_o(\alpha_n r) \right\} + P_a \,, \qquad (4)$$

where P_a is the pressure at the top of the plenum. In the above expression, the second term represents the inertial contribution to the pressure in the plenum and the third term is the kinetic-energy equivalent of the pressure in the plenum. The pressure distribution as given by Eq. 4 when averaged over the inlet flow area at z - 0 becomes

$$P_{av}(0,t) = \rho g H + \rho \left[H + \frac{4}{b^2} \sum_{n=1}^{\infty} \frac{J_1^2(\alpha_n b)}{\alpha_n^3 J_0^2(\alpha_n a)} \right] \frac{d}{dt} \left(U_0 \frac{b^2}{a^2} \right)$$

$$- \frac{1}{2} \rho \left\{ \frac{8b^2}{a^4} U_0^2 \sum_{n=1}^{\infty} \frac{J_1^2(\alpha_n b)}{\alpha_n^2 J_0^4(\alpha_n a)} \left[J_0^2(\alpha_n b) + J_1^2(\alpha_n b) \right. \right.$$

$$- \frac{1}{\alpha_n b} J_0(\alpha_n b) J_1(\alpha_n b) \Bigg] \Bigg\}$$

$$- \frac{1}{2} \rho \left\{ \frac{16b}{a^4} U_0^2 \sum_{m=1}^{\infty} \sum_{n=m+1}^{\infty} \frac{J_1(\alpha_m b) J_1(\alpha_n b)}{\alpha_m \alpha_n (\alpha_m - \alpha_n) J_0^2(\alpha_m a) J_0^2(\alpha_n a)} \right. \tag{5}$$

$$\times \left[J_1(\alpha_m b) J_0(\alpha_n b) - J_0(\alpha_m b) J_1(\alpha_n b) \right]$$

$$\left. + \frac{8b^2}{a^4} U_0^2 \sum_{n=1}^{\infty} \frac{J_1^2(\alpha_n b)}{\alpha_n^2 J_0^2(\alpha_n a)} \right\} + P_a \ .$$

where α_n is a positive root of the equation

$$J_1(\alpha_n a) = 0 \ .$$

The above average pressure is now in the proper form to be utilized as the plenum boundary condition for a rapid coolant expulsion process; an example of its application can be found in Ref. 1. In this application, if one were to consider that the flow in the plenum is one-dimensional, the pressure boundary condition at $z = 0$ is obtained by integrating a one-dimensional equivalent of Eq. 1 between the limits $z = 0^-$ to $z = H$ and including in the resulting expression the pressure loss due to sudden expansion; the result is

$$P_{1D}(0^-,t) = P_a + \frac{\rho}{2} \left(U_o \frac{b^2}{a^2} \right)^2 - \frac{\rho}{2} U_o^2 + \rho g H$$

$$+ \rho H \frac{d}{dt} \left(U_o \frac{b^2}{a^2} \right) + K \frac{\rho}{2} U_o^2 , \qquad (6)$$

where K is the pressure loss coefficient for sudden expansion given by the relation

$$K = \left(1 - \frac{b^2}{a^2} \right)^2 .$$

Introducing the above expression into Eq. 6, we obtain after some algebraic simplifications

$$P_{1D}(0^-,t) = \rho g H + \rho H \frac{d}{dt} \left(U_o \frac{b^2}{a^2} \right) - \rho \frac{U_o^2}{2} \left(2 \frac{b^2}{a^2} \right) \left(1 - \frac{b^2}{a^2} \right) + P_a . \qquad (7)$$

To bring out a comparison between the pressure boundary condition given by Eqs. 5 and that given by above expression, we next proceed to give an illustrative example.

The temporal distributions of velocity and acceleration in the inlet section to be used in the computation of pressures from Eqs. 4, 5, and 7 are shown in Fig. 43. Figure 44 shows axisymmetric pressure distribution as a function of radius of the plenum at z = 0 and at various time intervals. Typical behavior of these curves can easily be understood if we consider first the time interval, say at t = 0.0015 sec, where the maximum of acceleration occurs (see Fig. 43); then, with reference to Eq. 4, we can easily see that accelerating fluid in the "jet" makes a positive contribution to the plenum pressure. Next, let us consider the time interval between t = 0.02 and 0.03 sec; we find that in

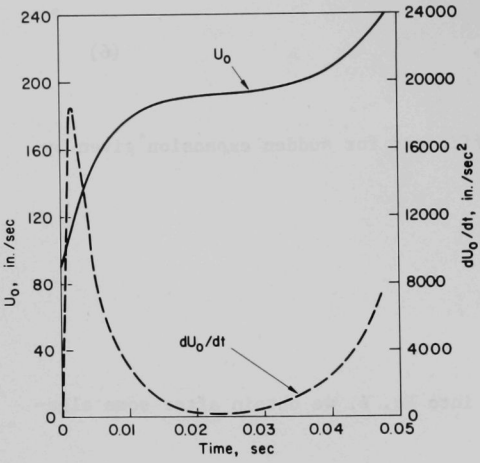

Fig. 43.
Velocity and Acceleration Distributions in the Inlet Section (Transition Piece between Fuel Assembly and Exit Plenum) during Coolant Expulsion due to Rapid Fission-gas Release (breach size = 1/4 x 1/16 in.) at the Center of 19-pin Fuel Assembly. Initial gas plenum pressure was 1000 psia, initial coolant velocity in the fuel assembly was 30 ft/sec.

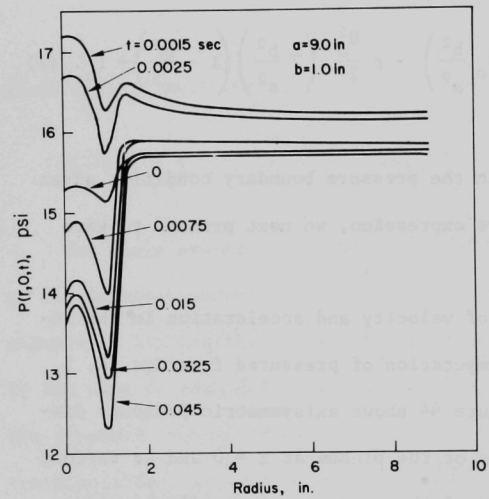

Fig. 44.
Axisymmetric Two-dimensional Pressure Distribution in the Plenum at z = 0.

this time interval acceleration is the least but fluid in the "jet" achieves a considerable velocity. Once again with reference to Eq. 4, we find that increased kinetic energy of the fluid in the "jet" has a negative contribution to the pressure distribution in the plenum; in addition, we can state that, as r becomes greater than the radius of the inlet section, the fluid is relatively "stationary" and we notice a rapid recovery of the pressure.

A comparison between pressure as given by Eq. 5 and that given by Eq. 7 is shown in Fig. 45. This plot is indicative of a quantitative difference between the two pressure distributions in a typical coolant-expulsion process.

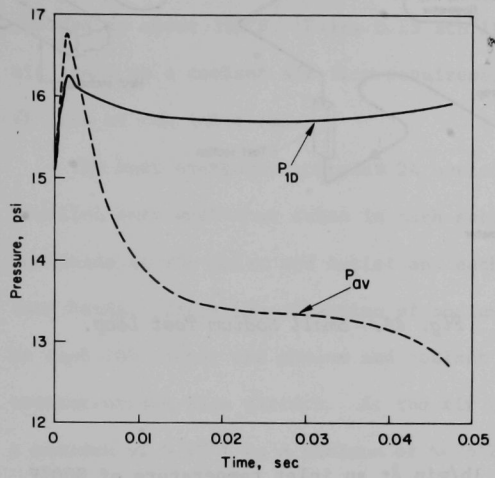

Fig. 45.
Comparison of the Spatially Averaged (over the inlet section) Pressure with the One-dimensional Pressure Distribution.

Design and fabrication of a small sodium test loop. A small sodium test loop was designed and fabricated to permit study of the fluid-flow and heat-transfer problems associated with possible fuel failure propagation, making use of electrically heated test sections. In addition, this loop will be used for the sodium experiments planned in ANL's Coolant Dynamics program which require a high degree of similitude with actual reactor geometries.

The principal components of the main loop consist of a dump tank, an electromagnetic pump, a test section and a heat exchanger (see Fig. 46). The loop's main piping is 1-in. Schedule-40, Type-304 stainless steel. The piping system is welded except for the test section, which is installed with Conoseal couplings to permit ready replacement. A linear velocity of 20 ft/sec in the main piping results in a flow in the

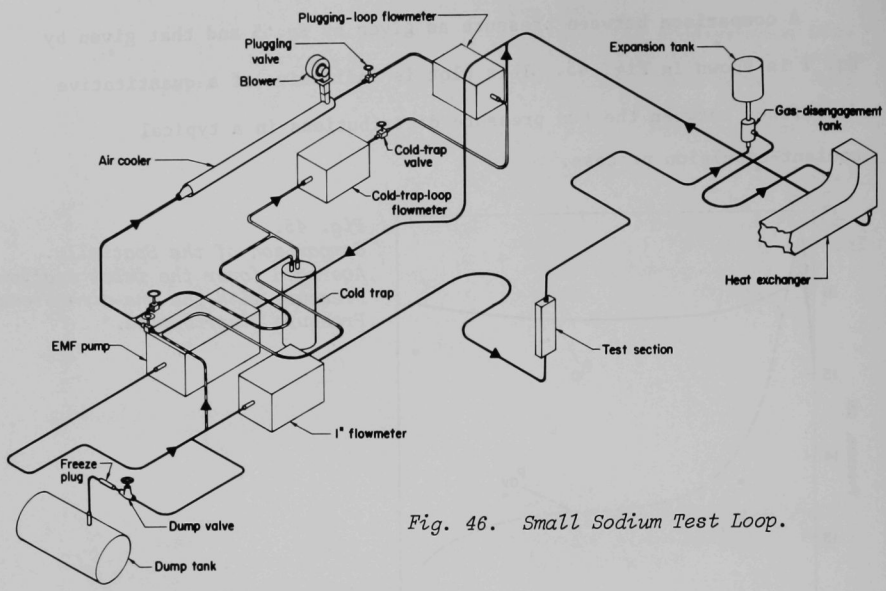

Fig. 46. Small Sodium Test Loop.

test section of 29.8 gpm, or 204 lb/min at an inlet temperature of 800°F. The power connectors to the heaters are installed at the bottom of the test section to provide maximum sodium cooling to the connection zone.

At a power input of about 15 kW/ft, the total heat input to the test section will be about 10^6 Btu/hr. Using 0.3 Btu/lb-°F as the heat capacity of the sodium, the temperature rise in the sodium will be 275°F and the outlet temperature will be about 1075°F. The outlet sodium flows to the heat exchanger through a small gas-disengaging section. This section is designed to remove from the sodium any entrained gas that subsequently might accumulate in the heat exchanger and obstruct the sodium flow. (It is intended that small quantities of gas will be injected into the test section to simulate fission-gas release from a failed fuel element.) The air-cooled heat exchanger is designed to remove 10^6

Btu/hr from 204 lb/min of sodium that enters at 1075°F and leaves at 775°F. (There is a temperature rise of about 25°F in the electromagnetic pump before the recycled sodium enters the test section.) The coolant air enters at about 80°F, flows parallel to the tubes, and discharges at about 350°F. Using 0.25 Btu/lb-°F as the heat capacity of air leads to a coolant air flow requirement of 246 lb/min or ∿3200 ft^3/min at the inlet end.

The heat exchanger contains 24 horizontal tubes arranged in six parallel sets with four tubes in each set. The tubes are connected to manifolds at the inlet and outlet and each set contains three 180° return bends. Since the direction of sodium flow in the tubes reverses at each 180° bend, the sodium and coolant air do not follow a true countercurrent flow pattern. At the air outlet end, the ΔT ranges from a maximum of ∿725°F to a minimum of ∿425°F, and at the air inlet end the ΔT ranges from a maximum of ∿920°F to a minimum of ∿770°F. An average ΔT of 700°F was used for heat-transfer calculations. The 24 tubes are 1-in.-OD x 0.143-in.-wall Type-304 seamless stainless steel. Each tube has 20 longitudinal fins, 6 ft long, 1/2 in. high, and 0.035 in. thick. Overall fin efficiency was estimated to be 50%, giving an effective heat-transfer surface of 1 ft^2/ft of tube length. The tubes are arranged in a rectangular array on 3 x 3-in. centers (with a slight pitch toward the outlet end to facilitate draining). To increase the air velocity around the finned tubes, 15 dummy tubes, of 1.75-in. OD, are positioned in the void spaces between the finned tubes. The net free air flow area is 1.23 ft^2, resulting in air velocity of 43 ft/sec at the inlet end. Under these conditions, an overall heat-transfer coefficient of 10 Btu/hr-ft^2-°F can reasonably be expected. The

heat-transfer surface required is: $A = Q/H\Delta T = 10^6/(10 \times 700) = 143$ ft^2. The 24 finned tubes, each 6-ft long, provide the equivalent of 144 ft^2 of surface. If necessary, increased heat-removal capability can be obtained by increasing the air-blower output. Coolant air is supplied to the heat exchanger by a centrifugal fan equipped with a 7.5-hp motor. It can deliver up to 4000 cfm against 4-in.-of-water static pressure. A motorized damper in the air duct to the heat-exchanger plenum will be controlled by the temperature of the sodium leaving the heat exchanger and will regulate the air flow.

The main loop was designed with large-radius bends to achieve a low pressure drop, which was calculated to be 12.5 psi at rated flow. The pressure drop through the heat exchanger was calculated to be about 3 psi.

The loop is at present provided with an electromagnetic pump rated 29 gal at 27-psi pressure drop so that 11.5 psi remains available for the pressure drop in the test section. The present pump is suitable for checking the performance of the loop, but provision is being made in the loop piping layout for later installation of larger pumps. Sodium flowrate through the main loop will be measured by magnetic flowmeters.

A combination dump and charging tank, having a capacity of 25 gal, is installed at the lowest point of the loop. The total sodium holdup in the entire loop system is about 15 gal. Approximately 20 gal of sodium will normally be charged to the tank to provide an excess heel in which impurities can settle out from the sodium. The tank is equipped with high- and low-level probes and a well for subsequent use of an induction-type level probe. The dump valve is a manually operated

1-in. IPS bellows-seal globe valve. The loop is normally operated with this valve open, the Na being held by a freeze plug that is electrically operated. A small surge tank of about 1-gal capacity is installed at the highest point in the system. This tank is equipped with a high-level probe. In addition, both the dump tank and the surge tank are connected to an argon blanket system. To prevent plugging of the argon lines with condensed sodium, connections to the tanks are made through sodium vapor traps.

The secondary loop system contains a sodium cold trap and plugging valve. The pipe lines are 3/8-in. IPS Schedule 40 and the valves are 3/8-in. IPS manually operated bellows-seal globe valves. The cold trap is 24-in. high and 6 in. in diameter with a holdup capacity of about 3 gal. A 4-in.-dia tube is located concentrically within the 6-in.-dia-tube, providing an outer annulus through which the hot sodium flows downward and an inner tube through which the cold sodium flows upward. The two concentric zones thus provide for heat exchange between the inlet and outlet sodium. The outer tube is surrounded by a spiral air duct through which coolant air is blown from bottom to top. The cold trap is designed to operate at a flowrate of 0.5 gal/min of sodium entering at 800°F and leaving at 650°F. A minimum sodium temperature of about 250°F is expected to be reached at the bottom of the trap when approximately 60 cfm of coolant air is flowing through the air duct. Both the annular sodium flow zone and the 4-in.-dia inner tube are packed with stainless-steel wool for collection of precipitated oxide.

The parallel section of the secondary loop contains the plugging valve. The plugging valve itself is a modified globe valve in which small slots were machined in the valve-stem adapter to provide a set of

fine orifices for collecting precipitated oxide. The system has an air-cooled finned-tube heat exchanger for precooling the sodium stream and an E-M flowmeter for detecting the change in sodium flowrate at plugging temperature.

The secondary-loop system does not have its own pump. Sodium flow through the secondary loop will be established by the pressure differential in the primary sodium loop across the points of connection of the two loops. Valves are provided in the secondary loop so that, in addition to measuring the plugging temperature of the sodium in the main loop, it will be possible to test the quality of the sodium passing through the cold trap.

The entire loop system and tanks (except for the heat exchanger) is traced with heaters and covered with pipe insulation. The individual tubes in the heat exchanger are not traced with heaters. Resistance-heater elements are installed in the air duct in the exchanger and the entire air plenum is covered with block insulation to permit preheating the heat exchanger as a unit.

Design and fabrication of a 19-pin heated test section for use in water. The design of this test section was completed and fabrication was initiated. Thermocouples will be installed to measure coolant temperatures and wall temperatures at various axial locations.

As a consequence of FFTF-related commitments, requiring a preliminary evaluation of the overall fission-gas release problem by mid FY 1971, the heated-pin experiment was moved up in priority. Experiments on the 19-pin heated test-section are expected to start in September 1970. Primary emphasis will be on slow gas release.

Design and fabrication of 91-pin test section. Design of this test section was completed and fabrication was initiated. However, in view

of the reassignment of priorities as a consequence of FFTF-related commitments, the fabrication was temporarily interrupted. It is tentatively foreseen that tests using a 91-pin test-section will be initiated in late FY 1971 in the Transient Flow Simulation Loop, which is to be used jointly with the Coolant Dynamics program.

Design of externally heated test sections for study of gas-jet impingement in sodium. The design of two externally heated test sections for the study of heat-transfer phenomena in the immediate vicinity of the impingement area of a gas jet was initiated. Both test sections are planned to have only a limited heated area. The first test section will have a rectangular cross-sectional flow area; the second test section will have a convolute cross-sectional area and simulate five coolant subchannels with internal bypass. The experiments with the first test section are planned to begin in the second quarter of FY 1971.

Testing of heaters for simulation of fuel pins in sodium. A number of heaters designed at ANL were tested. Problems were encountered, amongst others, with insufficient cooling of the lead wires. In view of the recent successful operation of ORNL-designed heaters, it was decided to adopt the ORNL design for future experiments.

Design of transient flow simulation loop. A preliminary sketch of the proposed Transient Flow Simulation Loop is shown in Fig. 47. This facility will be designed to provide up to 60 sec full flow through a 91-pin full-axial-scale subassembly mockup. The facility will consist of a supply reservoir, a discharge reservoir, and flow controls for the supply reservoir and temperature and pressure controls for both supply and discharge reservoirs. Refrigeration equipment will maintain

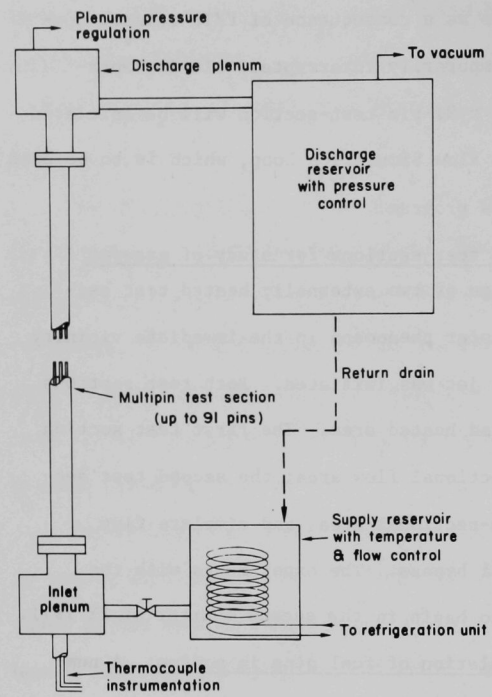

Fig. 47.
Transient Flow Simulation Loop.

subambient temperatures. A power supply capable of providing up to 100-kW DC power to the 91-pin section will be available. Existing instrumentation for this facility includes a magnetic-tape data-acquisition system compatible with the computer facilities of the FEFP Sodium Loop. This facility will be used jointly for the out-of-pile fuel element failure propagation studies with nonmetallic fluids as well as for the flow-transient expulsion and reentry studies and the local blockage studies.

Attention is being given to using Freon as a coolant. The primary reason for this is the fact that Freon has a low specific heat, resulting in small requirements for the power supply (in fact, the power supply, to be used for the 19-pin heated test section in water, suffices for the 91-pin heated test section in Freon), and thus in a small probability for

destruction of the test section through burnout. Joint use of the Transient Flow Simulation Loop and the 91-pin test section with the Coolant Dynamics program results in better utilization of the equipment involved, as well as in substantial savings to both programs.

In-pile Studies

(J. Tessier)

Scope. This work includes in-pile experiments using a recirculating-sodium package loop simulating an LMFBR environment. It is contemplated: (1) to perform the experiments in an operating thermal test reactor, (2) to test initially a maximum of 19 pins simultaneously, (3) to employ primarily UO_2 and mixed-oxide fuels and a sodium coolant, and (4) to test initially elements typical of the Fast Test Reactor (FTR) design.

The initial in-pile tests are to establish limits for failure propagation and provide data in support of FFTF. These and subsequent tests will provide data for developing analytical models, obtain engineering data on the failure propagation of specific designs, find thresholds of propagation under normal reactor power or mild accident conditions, determine the "margin of safety" for continued operation with one or several failed elements, and study the rate and extent of failure propagation.

When the preliminary tests are finished, more sophisticated tests can begin. The goal of these tests is to develop data for predictive models of failure propagation that will determine analytically the possibility and consequences of fuel-element failures in a reactor. Ideally, any subassembly design would be described by this model; initially, however, the analysis will be limited to specific fuels, claddings, and reactor operating parameters of a particular design.

An important part of this task is the design, development, fabrication, and operation of both the package loops and the sample test trains. Idaho Nuclear Corp. (INC), under an ANL subcontract, is responsible for engineering design, component testing, and operation of the package loops.

In-pile experiments using recirculating-sodium package loops are planned to be performed in a steady-state thermal reactor, possibly the ETR. Normal and near-normal LMFBR operating conditions will be integrally simulated and a well-characterized initiating fuel-element failure will be induced. Initial tests, with variations in experimental parameters, will be performed on oxide-fueled stainless-steel-clad fuel elements typical of the FTR design. Engineering data from these tests will be used to help develop a predictive mathematical description of fuel-element failure propagation and fuel failure propagation. These data: (1) determine the likelihood of fuel-element failure propagation and fuel failure propagation, (2) determine "thresholds for propagation" under normal and near-normal operating conditions, and (3) determine the margin of safety of continued operation with one or several failed elements.

Design description of FEFPL. The Fuel Element Failure Propagation Loop (FEFPL) is being designed to conduct experiments that lead to fuel-element failure and interaction of fuel and coolant. It is envisioned that FEFPL will be operated in the Engineering Test Reactor (ETR) and occupy grid position J-13, a 6 x 6-in. core position, with G-7 as the backup position. Figure 48 illustrates the FEFPL inserted in the ETR.

A complete description of the loop design, fabrication, stress analysis, testing, and applicable codes and standards for design,

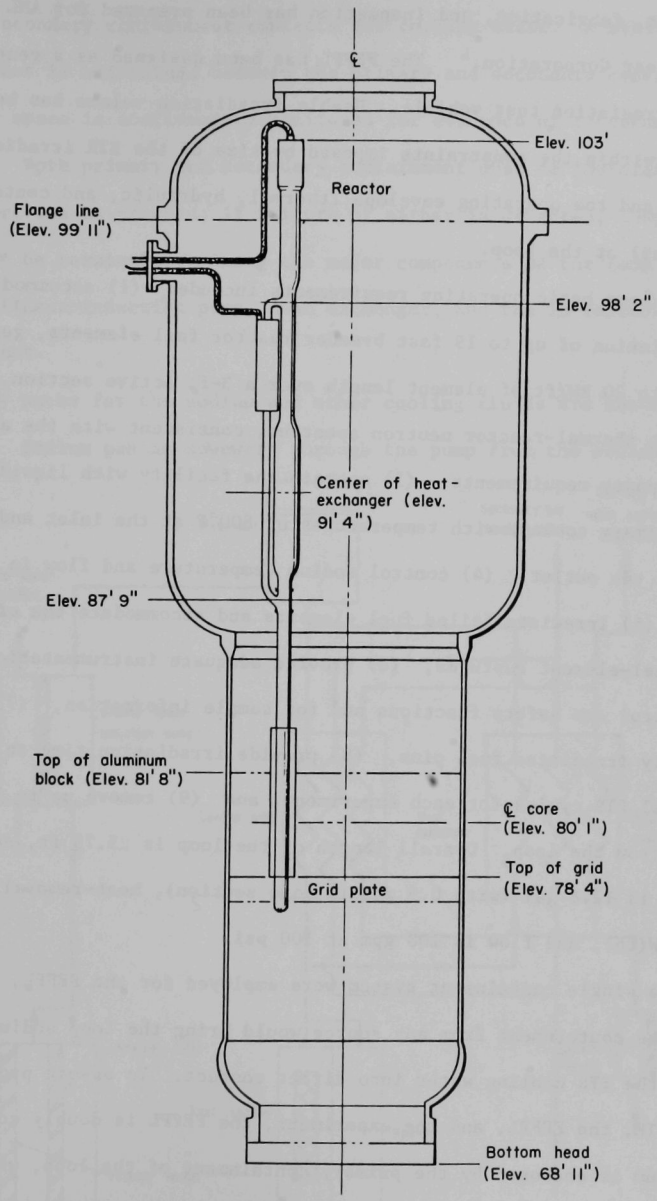

Fig. 48. FEFP Loop within ETR. ANL Neg. No. 113-2820, Rev. 2.

procurement, fabrication, and inspection has been prepared for ANL by the Idaho Nuclear Corporation.[4] The FEFPL has been designed as a general-purpose irradiation test vehicle. Usable irradiation volume has been maximized within the constraints imposed by size of the ETR irradiation locations and the operating envelope (thermal, hydraulic, and containment limitations) of the loop.

FEFP loop basic operating requirements include: (1) accommodate the irradiation of up to 19 fast breeder reactor fuel elements, generating up to 20 kW/ft of element length over a 3-ft active section, (2) harden thermal-reactor neutron spectrum, consistent with the above specific power requirements, (3) operate the facility with liquid sodium as the primary coolant with temperatures of 800°F at the inlet and 1300°F at the outlet, (4) control sodium temperature and flow in the facility, (5) irradiate failed fuel elements and accommodate the effects of severe fuel-element ruptures, (6) provide adequate instrumentation for loop control and safety functions and for sample information, (7) handle previously irradiated fuel pins, (8) provide irradiation time on the order of several ETR cycles for each experiment, and (9) remove up to 1.5 MW of heat from the loop. Overall length of the loop is 25.75 ft, sodium capacity is 17.8 gal (with 0.9 gal in core section), heat-removal capacity is 1.5 MW(th), and flow is 100 gpm at 100 psi.

If a single containment system were employed for the FEFPL, a failure of the containment from any source would bring the loop sodium coolant and the ETR cooling water into direct contact. To ensure protection of the ETR, the FEFPL, and the experiment, the FEFPL is doubly contained. All sodium is enclosed by the primary containment of the loop, which is completely enclosed within a secondary containment. The outer surface

of the secondary containment contacts ETR cooling water. A static-gas environment is maintained between the primary and secondary containment. This gas space is continuously monitored for evidence of containment failure. Both primary and secondary containment must be inviolate for loop operation to proceed; if failure of either is detected, loop operation must be terminated. Among the major components of the loop are the annular linear-induction pump, heat exchanger, and the in-reactor containment.

Flow paths for the sodium and other cooling fluids are shown in Fig. 49. Sodium passes downward through the pump from the sodium

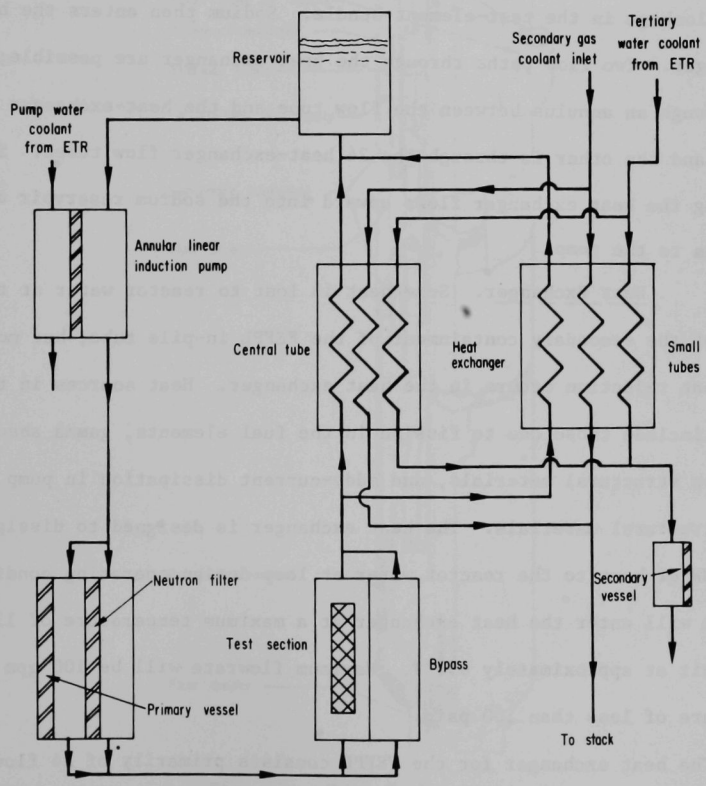

Fig. 49. System Diagram for Fuel-element Failure-propagation Loop.

reservoir at the top of the loop and enters the outer annulus of the re-entrant in-pile tube. It then flows downward between the outer surface of the flow divider and the inner surface of the primary containment. At the bottom of the in-pile tube, after having passed by both inner and outer surfaces of the neutron filter, the coolant flow reverses direction. Upward-flowing coolant then splits; most of it passes through the test-element bundle, but a portion is diverted through a bypass path. The bypass is provided to cool the inner surface of the flow divider, to moderate the temperature of the hot sodium leaving the test section, and to assure a coolant passage for continued loop operation in the event of flow blockage in the test-element bundle. Sodium then enters the heat exchanger. Two flow paths through the heat exchanger are possible; one is through an annulus between the flow tube and the heat-exchanger center tube, and the other is through the 24 heat-exchanger flow tubes. Sodium exiting the heat exchanger flows upward into the sodium reservoir and returns to the pump.

Heat Exchanger. Some heat is lost to reactor water at the surface of the secondary containment of the FEFPL in-pile tube, but most of the heat rejection occurs in the heat exchanger. Heat sources in the FEFPL include those due to fission in the fuel elements, gamma absorption by loop structural materials, and eddy-current dissipation in pump coolant and structural materials. The heat exchanger is designed to dissipate ∿1.5 MW of heat to the reactor water at loop design operating conditions. Sodium will enter the heat exchanger at a maximum temperature of 1300°F and exit at approximately 650°F. Maximum flowrate will be 100 gpm at a pressure of less than 100 psig.

The heat exchanger for the FEFPL consists primarily of 24 flow tubes and a center tube, primary and secondary tubesheets, and a cooling-water

shroud, as illustrated in Fig. 50. Because the heat exchanger is concentric with the vertical axis of the loop in-pile tube, the test train must pass through the heat exchanger during its insertion into and removal from the loop. This is accomplished by moving the test train within the flow divider. A piston-ring seal is provided between the flow divider and the

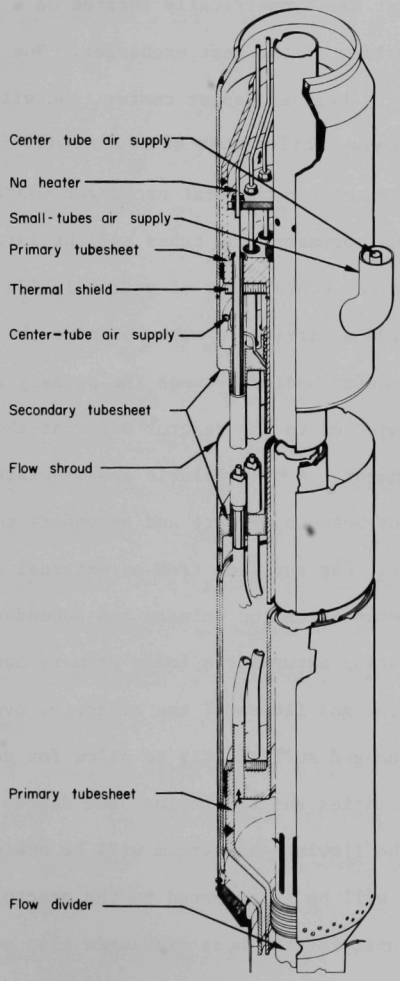

Fig. 50. Heat Exchanger.

lower portion of the heat exchanger to separate the sodium flowing toward the test section from the heated sodium leaving the test section. The heated sodium coolant travels upward through the loop into the lower plenum chamber of the heat exchanger. The high-temperature sodium coolant is distributed through the lower primary tubesheets into a series of 24 individual primary tubes that are symmetrically located on a diametral circle about the axial centerline of the heat exchanger. The flow region between the flow divider and the heat-exchanger center tube will be suitably orificed such that only a small amount of sodium will flow through it.

Secondary containment for the heat exchanger consists of tubes that surround the individual primary flow tubes and the large center tube. Primary tubes provide for containment of sodium inside the flow tubes, secondary tubes provide a barrier to water outside the heat exchanger, and gas acts as a transfer medium between the primary and secondary containment. Heat is rejected to the reactor water at the outer surface of the secondary containment. A controllable gas flowrate will be maintained in the 0.1-in. annulus between primary and secondary containment tubes to promote heat transfer. Gas supplied from an external source will enter the heat exchanger between the top primary and secondary tubesheets and flow downward, exhausting between the lower primary and secondary tubesheets. By varying the gas flowrate, the effective overall heat-transfer coefficient can be changed sufficiently to allow for design, assembly, and operating uncertainties and to provide some degree of loop temperature control. Although the flowing gas stream will be heated significantly, the bulk of the heat will be transferred to the reactor cooling water.

The gas supply unit for the heat exchanger also serves as the source of gas that occupies the volume between the primary and secondary

containment in the remainder of the loop. This static gas region is separated from the gas-flow region in the heat exchanger by seal rings located outside the upper and lower primary tubesheets. Gas enters the static intercontainment volume by leakage past the seal rings prior to loop power operation.

Heat-exchanger gas serves a dual purpose; it acts as a heat-transfer medium while flowing and as a thermal barrier when stagnant. This latter insulating effect reduces heating requirements to keep the sodium molten when the reactor is shut down. Principal FEFPL heat sources during reactor down time are electrical heaters and the operating pump. Heating capacity greater than 8.5 kW is provided by 24 two-element heaters, one located within each primary tube in the heat exchanger. Each element is rated at 700 watts, but the heaters are arranged in a three-wire configuration and will operate at about 350 watts per element. If failure of one element occurs, the heater changes to single-element operation at 700 watts. Heater power will be supplied from the ETR commercial-diesel bus and converted to 100 V D.C. Thermocouples located in the heat-exchanger region will provide operating data to the loop operator. The heating capability of 8.5 kW (minimum) complemented by heat generation in the pump is sufficient to maintain the sodium in a liquid state without any test-section power generation.

During a reactor scram or rapid power setback, the heat exchanger might experience a rate of change in sodium temperature as great as 500°F/sec. Therefore, thermal shields are provided on the air side of both the upper and lower primary tubesheets to moderate thermal shocks. Also, the outer surface of the secondary center flow tube is flame-sprayed with an insulating nickel-aluminum prime coat and a zirconium-oxide secondary coat.

Sodium pump. Flow in the FEFP loop will be maintained by an annular linear-induction pump (ALIP) that is designed to produce 100 gpm flowrate of 800°F sodium at 100 psi differential pressure. This pump uses the same basic core, coil, and containment configuration as smaller pumps in service in other in-pile experimental programs. Double containment between the loop sodium and the reactor cooling water is provided in the pump. As shown in Fig. 51, both the primary and secondary containment are within the laminated-stator section of the pump.

The pump consists of a solid Armco-iron core located within the primary containment, and a laminated stator that contains the pump coils located outside the secondary containment. Three-phase electrical power to the pump coils produces a magnetic field that travels along the pump axis. Pumping action is produced by the interaction of the moving magnetic field and the resulting eddy currents developed in the sodium.

A total of 63 coils are utilized in the stator of the pump for the FEFPL. The delta-connected stator coils are connected in a series-parallel arrangement such that the occurrence of an open circuit in any coil will cause only seven coils to go out of service. In this condition, the pump would continue to operate, but at reduced flow and efficiency.

Power to the pump will be supplied from the three-phase 480-volt ETR failure-free supply, which is diesel-backed commercial power. About 48 kW will be required to operate the pump at rated design conditions. This power will be distributed approximately as follows:

Resistance heating of the windings	8 kW
Hysteresis loss in laminations	1
Eddy-current heating in outer pipe	4
Eddy-current heating in inner pipe	3
Resistance heating of sodium	14
Core losses (eddy current and hysteresis)	12
Hydraulic losses	1
Output power	5
Total	48 kW

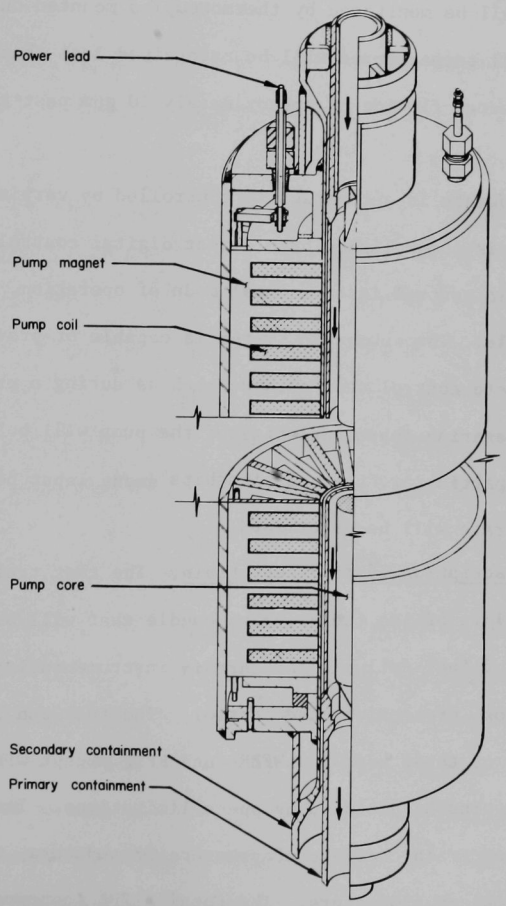

Fig. 51. Annular Linear-induction Pump.

The expected pumping efficiency is approximately 10%, and, as can be seen from the above data, the pump produces a considerable amount of fluid heating. Continued operation of the pump during periods of reactor shutdown or low-power operation will produce heat to supplement the 8.5 kW delivered by the resistance-heating units.

Coil current will be approximately 40 amp at rated design conditions. Temperatures will be monitored by thermocouples mounted on four of the pump coils; coil temperatures will be maintained less than 500°F by reactor cooling water flowing at approximately 10 gpm past the outer pump housing.

Sodium flowrate is automatically controlled by varying pump input power; control is accomplished by a direct digital control system. Although automatic control is the normal mode of operation, manual override is possible. The automatic system is capable of providing precise variable-flowrate control when needed, such as during a programmed flow transient. Operating characteristics of the pump will be measured in a test loop; in particular, the relationships among input power, developed head, and flowrate will be determined.

Design description of FEFP test train. The test train is the device that consists of the fuel-element bundle that will be subjected to various modes of fuel failure, and certain instrumentation required for data acquisition, protection, and control. The fuel bundle will be representative of those used by LMFBRs and FFTF except with a reduced number of fuel pins as dictated by space limitations. Instrumentation used in the test train consists of pressure transducers, thermocouples, and permanent-magnet flowmeters. The total FEFPL instrumentation system is described in detail in the following section.

Each test train will be specifically designed as dictated by the type of experiment to be conducted. Generally, each experiment will require a new test train. The test trains are designed to be removable from the FEFP loop, which allows reuse of the loops, depending on the severity of the experiment. At the height of the experimental program, it is expected that approximately six test trains will be required per year.

Test-train development is being undertaken at ANL and the early test trains will be fabricated and assembled by ANL. The test train is being designed with sensors placed at strategic locations, the number of sensors being limited by space available for lead connections. Instrumentation requirements will vary with the various experiments, so the complement of instruments in a given test train can vary accordingly. At the completion of the initial test-train development, a set of specifications, drawings, descriptions, and manufacturing procedures will be produced based on a reference test train. These documents can be used in conjunction with design modifications to produce test trains to meet the continuing needs of the FEFP program.

Design requirements. The test train is designed to the following general requirements: (a) sodium flowrate of 100 gpm, 70 gpm through the fuel bundle and 30-gpm bypass flow, (b) temperature of sodium into fuel bundle 800°F, leaving 1300°F, (c) design life of two ETR cycles, (d) test train to fit in a 2-5/8-in.-ID tube, (e) fuel bundle to contain as many as 19 fast breeder reactor fuel elements that generate a maximum of 20 kW/ft of element length over 3-ft active section, (f) provide instrumentation for measurement of system flowrates, temperatures, and pressures, and provide for pressure measurement in fuel-pin plenums.

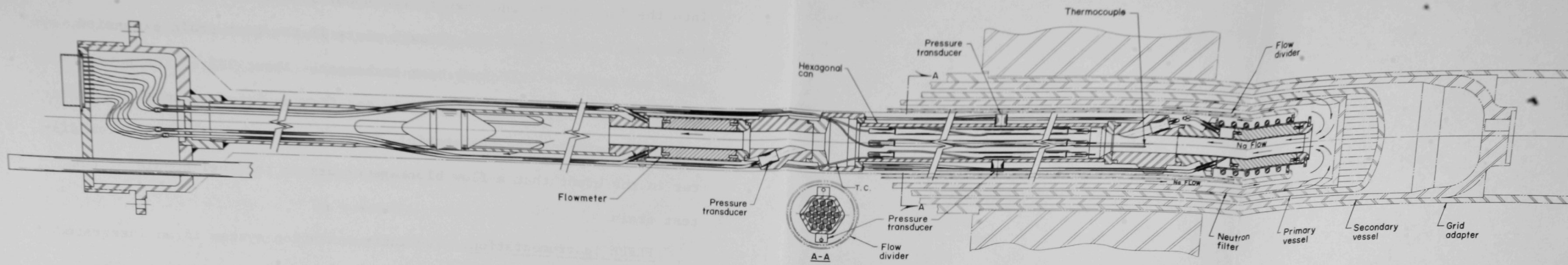

Fig. 52. FEFP Test Train. ANL Neg. No. 113-3257 A-C.

the fuel subassembly; 20 are thermocouples and seven are fuel-element-plenum pressure-transducer leads. These are joined by 17 additional leads for a total of 47 sheaths that are sealed at the top closure and stripped of the sheaths in the closure plug where three connectors are located. A total of 110 leads are connected to the pins of the connectors. The FEFPL instruments will have only electrical connections; no pneumatic lines or mechanical devices are permitted.

The flow path of sodium through the test train can be seen in Fig. 52. Sodium enters at the bottom through the lower flowmeter, continues into the fuel bundle and then to the upper flowmeter. From the upper flowmeter, sodium flows out through slots in the test-train extension piece and into the FEFP-loop heat exchanger. About 30% of the total loop flow will bypass the test train and flow up between the flow divider and the outside of the test train. This flow is to cool the neutron filter in the event that a flow blockage occurs in the fuel bundle of the test train.

FEFPL instrumentation. The instrumentation system is an integrated design intimately coupled with the loop and test-train designs. The system is designed to provide the greatest possible flexibility within the limits of loop and test-train design, consistent with safe operation. The instrumentation system for a test train and loop operating in the reactor is made up of three subsystems: the protection system, the control system, and the data-acquisition system.

Figure 53 shows the major components of the instrumentation system: the test train, the loop, the protection system, the process-control system, the data-acquisition system, the reactor, a computer, and the operator.

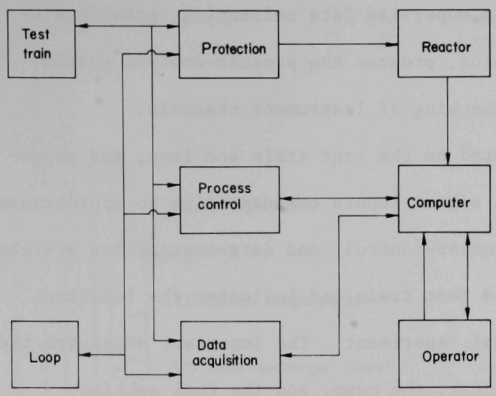

Fig. 53. Instrumentation System.

The function of the protection system is to provide for the safe operation of the loop. The safety requirements determine the outer bounds of the set points of the protection circuitry. The experimenter is free to operate the loop within these bounds with set points determined by the needs of the experiment. The protection system consists of high-speed circuitry that continuously monitors the appropriate sensor outputs. Reactor scrams will be generated from a standard two-out-of-three coincidence system to provide for reliable operation. Component failures in a single channel lead to a set condition of that channel.

The process-control system will control two primary parameters: (1) sodium flow through the fuel section of the test train, and (2) sodium temperature at the inlet to the fuel section. The flow will be controlled by regulating the power to the ALIP pump. Inlet temperature will be controlled by regulating the air supply to the heat exchanger. In the case where insufficient heat is generated by the fuel, heaters in the heat exchanger will maintain temperature in the loop.

The purpose of the data-acquisition system is to record experimental data. It consists of a high-speed analog recording system and a digital recording system.

The computer will be used to supervise data collection, provide display of information to the operator, program the process-control system, and do on-line calibration and checking of instrument channels.

Sensors. Sensors located on the test train and loop, and external to the reactor, will provide signal inputs corresponding to appropriate parameters to the protection, process-control, and data-acquisition systems.

Figure 54 shows the loop and test train and indicates the locations and types of sensors for a typical experiment. The important areas are the test train, the loop, heat exchanger, the pump, and the fuel section.

Many of the sensors are located on the test train. Table II lists and briefly describes the sensors. Three basic parameters will be measured: flow, temperature, and pressure. The flow, temperature, and pressure sensors are discussed in the following paragraphs.

A test train will include two permanent-magnet flowmeters that will monitor the flow at the inlet and outlet of the fuel subassembly. The design is a modification of the EBR-II instrumented-subassembly flowmeter design. The major mechanical changes are in the end pieces, the width of the flow tube, and the outer case. The magnet configuration, signal-lead connection, signal cable, and evacuation tube are the same. The characteristics are: sodium flowrate of 70 gpm nominal, range 0.5 to 500 gpm, expected accuracy ± 2 gpm or better, magnet material Alnico-V or Alnico-VIII, material in contact with sodium is 316 SS, sensitivity approximately 0.2 mV/gal/min at 800°F, inlet-flowmeter operating temperature 800°F, and outlet-flowmeter operating temperature 1300°F maximum.

Temperatures throughout the test train will be measured using Chromel (P)-Alumel thermocouples. The thermocouple is designed with an extension wire that extends beyond the hot junction. This allows the thermocouple to

Fig. 54.
Loop and Test-train Sensors.

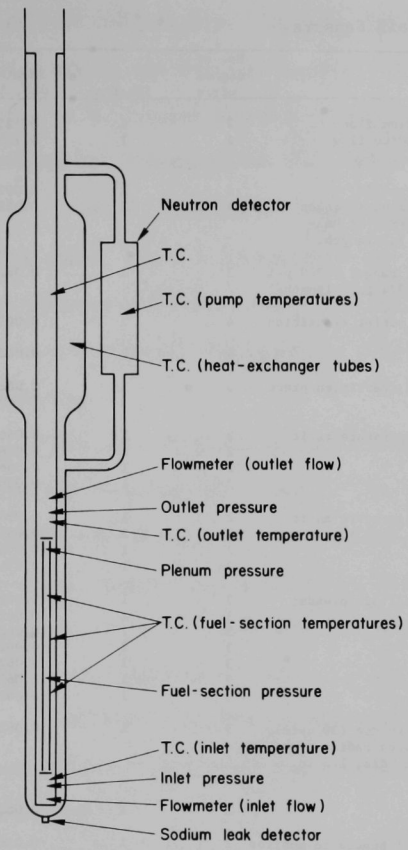

be used as a spacer wire within the fuel subassembly. The thermocouple characteristics are: junction is ISA-type grounded or insulated, accuracy has special limits of error of $\pm 3/8\%$, sheath and extension-wire material is 316 SS, and the insulation is alumina.

Four thermocouples will be located at the inlet to the fuel subassembly. These will be used to control inlet temperature. Four thermocouples will be located in the outlet sodium stream above the fuel subassembly. These thermocouples will be used to determine temperature profiles within

TABLE II. Test-Train Sensors

Sensor no.	Description	No. of signal wires	Sheaths	Sheath dia, in.
FM-1-1	Permanent-magnet flowmeter for inlet sodium flow	2	1	0.125
FM-2-1	Permanent-magnet flowmeter for outlet sodium flow (Ranges 0-100 gpm, 0-500 gpm)	2	1	0.125
PT-1-1	Strain-gage pressure transducer, fast response (30 μsec), inlet; range: 0-1500 psi. Located in inlet transition piece above inlet flowmeter (FM-1-1) Maximum size: cylinder 1/2 in. dia, 3/4 in. length.	4	2	0.062
PT-1-2		4	2	0.062
PT-2-1	Eddy-current pressure transducer, inlet; range: 0-200 psi. Maximum size: cylinder 1/2 in. dia, 3/4 in. length.	3	1	0.062
PT-3-1	Same as PT-1-1 and 2, except located in outlet transition piece below outlet flowmeter (FM-2-1).	4	2	0.062
PT-3-2	Same as PT-3-1, except range 0-5000 psi.	4	2	0.062
PT-4-1	Same as PT-2-1, except located in outlet transition piece below outlet flowmeter (FM-2-1).	3	1	0.062
TE-1-1	Thermocouples to monitor bulk sodium temperature as it enters fuel bundle. (Range 0-1800°F).	2	1	0.056
TE-1-2		2	1	0.056
TE-1-3		2	1	0.056
TE-1-4		2	1	0.056
TE-2-1	Thermocouples to monitor bulk sodium temperature as it exits fuel bundle. (Range 0-1800°F).	2	1	0.056
TE-2-2		2	1	0.056
TE-2-3		2	1	0.056
TE-2-4		2	1	0.056
PT-5-1	Eddy-current pressure transducers for fuel-pin plenum; range: 0-1500 psi.	3	1	0.062
PT-5-2		3	1	0.062
PT-5-3		3	1	0.062
PT-5-4		3	1	0.062
PT-5-5		3	1	0.062
PT-5-6		3	1	0.062
PT-5-7		3	1	0.062
PT-6-1	Strain-gage pressure transducer, fast response (30 μsec), located in middle of fuel bundle. Measures radial pressure pulses. Maximum size: cylinder 1/2 in. dia, 1/2 in. length. Range: 0-1000 psi.	3	1	0.062
PT-7-1	Same as PT-6-1 except range 0-200 psi.	3	1	0.062
TE-3-1	Thermocouples distributed throughout fuel bundle to monitor temperature profiles within the fuel bundle (range: 0-1800°F).	2	1	0.056
TE-3-2				
.		.	.	.
.		.	.	.
.		.	.	.
TE-3-15		2	1	0.056
TE-4-1	Thermocouples located on test train near the top plug. (Range: 0-1800°F).	2	1	0.056
TE-4-2		2	1	0.065
TE-4-3		2	1	0.056
		110	47	
Lead-wire and sheath breakdown				
2 flowmeters		4	2	0.125
26 thermocouples		52	26	0.056
9 eddy-current pressure transducers		27	9	0.062
4 strain-gage pressure transducers		16	8	0.062
2 strain-gage pressure transducers PT-6-1, PT-7-1		6	2	0.062
Ground pin		1		
Spares		4		
TOTAL		110	47	

the fuel subassembly. In this region the thermocouple is used as a spacer wire within the fuel-pin bundle. The extension wire allows the hot junction to be located anywhere along the length of a fuel pin. Three additional thermocouples will monitor temperatures near the top plug.

A set of 15 pressure sensors will be mounted on the test train. The range, size, location and type are given in Table II. Seven fuel-pin-plenum pressure sensors will monitor fission-gas pressure in the fuel-pin plenum. The pressure transient during a gas release will be measured.

Two sets of three pressure transducers will be mounted at the inlet and three at the outlet of the fuel subassembly. Two of these at each location will be fast-response pressure transducers for measuring pressure pulses generated within the fuel subassembly. The third at each location will be a slower-response sensor for measuring steady-state operating pressure at the inlet and outlet.

Two fast-response pressure sensors will be mounted through the subassembly wall for measuring radial pressure pulses in the fuel subassembly.

Some of the pressure-sensor characteristics are: strain-gage and eddy-current types, fast-response rise time is less than 30 μsec, slow-response rise time is less than 10 μsec, maximum operating temperature is 1300°F, accuracy is ± 5% of full scale, fast-response ranges up to 10,000 psi full scale, slow-response range is 200 psi full scale, and case materials are compatible with the sodium environment.

All test-train signal cables will be brought to the top and the sheaths will be brazed at a bulkhead above the sodium level. The sheaths will be terminated above the bulkhead. Signal lead wires will

be prepared and joined to insulated lead wire and run to two 55-pin connectors.

The sensor list indicates a representative set of sensors that could be included in a typical FEFP experiment. Different types of sensors may be included. The basic limitations on a single sensor are size and environment. The total number of sensors is limited by the total number of sheaths that can be accommodated (approximately 50) and the total number of lead wires than can be handled (110).

Trade-offs between certain types of sensors can be made to fit the needs of a given experiment. Table II gives a breakdown of 2 flowmeters, 26 thermocouples, 9 eddy-current pressure sensors, and 6 strain-gage pressure sensors.

Loop sensors are those sensors physically attached to the loop. Table III lists these sensors. Thermocouples are located on the heat-exchanger tubes to provide secondary control for matching temperatures of heat-exchanger tubes. These have the same design as the test-train thermocouples.

Two sets of sodium leak detectors are mounted on the loop. The sodium leak detectors are eddy-current devices that detect the presence of liquid sodium.

One set of these sensors (eddy-current) will detect the presence of liquid sodium on the inside of the outer containment shell. The measurement will indicate a leak from the primary containment tube to the annulus between the primary and secondary containment.

The other set will detect the presence of liquid sodium in the plenum (secondary) side of the heat-exchanger inlet. The measurement will indicate a leak in the primary containment. A gamma-compensated

TABLE III. FEFPL Loop Containment Sensors

Sensor no.	Function: Protection	Function: Fast data	Function: Digital data	Description
TE-5-1	X		X	Thermocouples located on alternate heaters in heat exchanger.
TE-5-2	X		X	
TE-5-3	X		X	
TE-5-4	X		X	
TE-5-5	X		X	
TE-5-6	X		X	
TE-5-7	X		X	
TE-5-8	X		X	
TE-5-9	X		X	
TE-5-10	X		X	
TE-5-11	X		X	
TE-5-12	X		X	
NaE-1-1	X		X	These sensors (eddy-current) detect the presence of liquid Na on the inside of the outer containment shell. The measurement will indicate a leak from the primary containment tube to the annulus between the primary and secondary containment.
NaE-1-2	X		X	
NaE-1-3				
NaE-2-1	X		X	These sensors (eddy-current) detect the presence of liquid Na in the plenum (secondary) side of the heat-exchanger inlet. The measurement will indicate a leak in the primary containment.
NaE-2-2	X		X	
NaE-2-3	X		X	
DN-1-1	X		X	Fission-product detector located at inlet to ALIP pump.
TE-6-1	X		X	Thermocouples to monitor ALIP pump. Stator temperatures.
TE-6-2	X		X	
TE-6-N	X		X	
NaE-3				These sensors (eddy-current) detect the sodium level when charging the loop.

BF_3 counter system will be located at the inlet to the ALIP pump to detect delayed neutrons from fission products in the sodium stream. Thermocouples will measure pump stator temperatures.

Standard commercially available sensors will be used for the functions described in Table IV. Pump flow designated as FM-3-1 will be calculated from parameters determined from pump performance tests on the test stand. This will give a measure of total sodium flow, which can be correlated with flow readings from the test-train flowmeters.

Protection system. The protective instrumentation monitors specific experiment parameters and will initiate a corrective action if the specified limits are exceeded. Design of each protective channel will be in conformance with RDT C16-1T, "Supplementary Criteria and Requirements for Reactor Plant Protection Systems." Because of the limited number of sensors that can be located in the loop due to space and access restrictions, the sensors must provide a multifunctional signal. The signal from a single sensor will provide information to the data-acquisition, control, and protective channels. Independence of the protective channel, however, will be maintained from the signal-conditioner output to the protective signal or trip. Isolation amplifiers will be designed or procured with the capability of preventing any failure or malfunction in the control of data-acquisition channels from affecting the protective-channel function. Certain protective channels will utilize logic elements to initiate an action when a prescribed combination of protective trips occurs. Other channels will initiate a protective action on occurrence of a single trip. Redundant channels are provided for each protective function. A means will be provided for testing, monitoring, and servicing a protective channel without compromising the protective action from the redundant channel.

TABLE IV. FEFPL Sensors External to the ETR

Sensor no.	Function: Protection	Function: Fast data	Function: Digital data	Description
FM-3-1	X	X	X	Flow signal derived for ALIP pump electrical power (voltage, current, phase). The measurement will be used to implement sodium flow control. Pump power continuity signals will be used for protection.
AP-1-1	X		X	Heat-exchanger air-supply pressure monitor.
AP-1-2	X		X	
AP-1-3	X		X	
AF-1-1	X		X	Heat-exchanger air-supply flow monitor.
AF-1-2	X		X	
AF-1-3				
WP-1-1	X		X	Sodium-pump cooling-water pressure monitor.
WP-1-2	X		X	
WP-1-3	X		X	
WF-1-1	X		X	Sodium-pump cooling-water flow monitor.
WF-1-2	X		X	
WF-1-3				
WT-1-1	X		X	Sodium-pump cooling-water temperature monitor.
WT-1-2	X		X	
WT-1-3	X		X	

Control system. Control of the loop sodium flow is required to achieve specific loop operating requirements, such as sample differential temperature, sample flowrate, or loop flowrate. To obtain the desired flow condition, the ALIP's output is controlled by varying the input potential to the pump. The control function will be accomplished either manually or automatically by a direct digital control (DDC) system. Manual control is the normal control mode, and manual override of the automatic control mode is possible. Automatic control is used whenever precise variable control of the flow is required; i.e., a programmable flow transient.

The pump is supplied 480-volt, 3-phase, electrical power from the ETR commercial diesel bus. A 3-phase variable autotransformer or induction voltage regulator will be used to control the pump input power. Control will be accomplished by varying the voltage regulator output with a motor controller, which can be controlled either manually from the control station or directly by the computer. The controller will be capable of varying the pump input power over the range of 0-60 kW required to change the flow from 0 to 100%. Initial response requirements of the control system will be based on obtaining changes in flowrate that will approach the loop sodium flow-coastdown curve. Actual loop flow-coastdown characteristics will be measured during prototype-loop operation and will provide the basis for finalizing the control-system design.

Control signals and information required for controlling the sodium flow will be derived from loop and sample conditions monitored by the computer. The computer will be programmed to process data from specified loop parameters on a time-shared basis, and will provide control information to the operator and the automatic control system. Loop flow will be based on the test-sample differential temperature, sample sodium

flow, or loop sodium flow requirements. The sample differential temperature and the sample sodium flow will be determined directly from the sensor signals. The gross sodium flow will be calculated by the computer from sodium temperature, pump input power, and derived constants.

Adequate instrumentation to provide for protection of the reactor and the loop will be included in the pump control circuit. The pump will continue to run under all conditions of loop abnormalities, such as fission-gas release to the sodium, pressure transients, and loss of reactor power. However, if a primary-tube rupture occurs, the pump will be automatically stopped and the reactor shut down. This protective action is initiated by two-out-of-three logic circuits that monitor the three heat-exchanger and the three lower secondary sodium leak detectors. A reactor shutdown will also be initiated on loss of pump power by undervoltage and underfrequency relays. To prevent possible damage to the pump and a pressure shock to the loop, switches will be installed on the voltage regulator to prevent starting the pump unless the output voltage is near zero. Thermocouples located on four selected pump windings provide the operator with information for adjusting the cooling water. Loss of cooling water will be monitored by a pressure switch and a pump-winding overtemperature alarm. A manual emergency on-off pushbutton station will be located in the loop control area for initiating a reactor shutdown and pump stoppage if the need should occur.

The loop heat exchanger removes the fission and gamma heat generated in the loop and provides the means for controlling the loop sodium temperature. Heat generated in the loop is primarily due to the test fuel elements, and will vary due to fuel content, number of fuel pins, and reactor power. Reactor-core flux variation as a function of fuel-cycle time is also a source of sample heat variation. Removal of this

heat requires changing the heat-exchanger heat-transfer rate over a wide range. Control is accomplished by regulating the gas flow through the heat-exchanger annulus, which changes the overall heat-transfer coefficient from the sodium flowing through the heat exchanger to the reactor primary coolant. In addition to controlling the sample inlet temperature, the differential temperature between the heat-exchanger tubes must be controlled between set limits to prevent excessive heat-exchanger stresses.

Gas at 275 psi and up to 6 lb/sec can be supplied to the heat exchanger from existing facilities at the TRA. The flow of this gas through the heat exchanger will be controlled by two air-operated control valves. Thermocouples monitor the sample-inlet sodium temperature and the differential temperature between the inner and outer heat-exchanger tubes. The derived signals are fed to the computer, which is programmed to process them and provide information to the operator and the automatic control system. Automatic control will be provided for by interface instrumentation between the computer and the control valve, so that the required temperature control will be accomplished through direct, DDC, adjustment of the control valves by the computer. The inlet temperature to the sample will be controlled by adjustment of the bulk gas flow. Control of the tube differential temperature between the required limits will require regulating the flow split between the inner tube and outer tubes. Manual control will be accomplished by overriding the automatic system and manually adjusting the signal to the digital controller for each valve.

A postulated air flowrate of 0-5 lb/sec is required to control the heat exchanger over the range of loop heat-removal requirements. The

actual gas flow required will be determined from test data obtained from the heat-transfer tests being performed and heat-exchanger operation in the prototype loop. The control-system final-design performance and response will be established by analog-computer studies of a control-system model.

Instrumentation for protection of the reactor and loop will be provided for in the heat-exchanger air control system. A loss of air flow or pressure will actuate protection relays that are tied into the reactor safety circuit. Loss of heat from the heat exchanger will be minimized whenever the reactor is shut down by actuation of a fast-action valve to shut off the air flow.

Data acquisition. A 14-track continuous-loop analog tape recorder will be used to record high-frequency signals from the test-train transducers. These signals will include the flowmeters, pressure transducers, and some thermocouple outputs. This loop will provide an approximately 25-sec delay to enable a logic system that monitors the fast signals to decide whether an interesting event has occurred and bring a second (not continuous loop) analog recorder up to speed and transfer and information to it. This second recorder will be capable of storing approximately 1/2 hr of the fast-signal outputs. Provision will be made for slower signals from signal converters to be used as inputs to the logic system, which also will accept digital signals from the computer or reactor scram circuits to initiate fast-signal recording.

A digital recording system will be used to record data from the signal-transmitter current loops. This system will have a number of modes of data collection. The digital system includes input filter networks, a 56-channel low-level (50-mV input) solid-state multiplexer,

programmable amplifier, high-level multiplexer, an analog-to-digital converter, and a PDP-15-20 computer. The computer is an 18-bit word machine with 8K word core with an 800-nanosec cycle time. Peripherals include: KSR-35 teletype, 2 DEC tape transports and control unit, high-speed papertape reader/punch, extended arithmetic-element for high-speed arithmetic operations and register manipulation, magnetic-disk storage, cathode-ray-tube display, and high-speed (800 bpi, 75 ips) 9-track digital tape recorder.

There will be two basic digital modes of operation. The first (low-speed digital) will read every multiplexer input once a second, and make this data available for display on the CRT. Average values will be calculated and recorded on the DEC tape units every 10 min. These rates are subject to computer and operator control. The second mode (high-speed digital) will be initiated when the analog recording system is started in the permanent record mode. In this mode, the computer will initiate a complete scan of the multiplexer inputs every 10 msec. This data will be recorded on the high-speed digital tape recorder. This will provide approximately 1/2 hr of digital recording time, which matches the high-speed analog recorder permanent-record length.

FEFPL-ETR interface study. An investigation was made to show the physical and operational interfaces between the FEFPL experiment and the ETR and between the FEFPL experiment and other in-tank experiments. The results obtained serve as a reference to the probable effects of the FEFPL experiment on the operation of the ETR. The study was designed to investigate all aspects of installation, operation, and removal of the FEFPL facility in the ETR regarding ETR operation and the effects to other experimenters.

The ETR is designed to accommodate large experiments and provide a high thermal- and epithermal-neutron flux. It is located at the National Reactor Testing Station, Idaho, and operated by Idaho Nuclear Corp. The FEFPL is a packaged system designed to circulate sodium to experimental in-pile test trains and to remove up to 1.5 MW of generated heat. The test trains are designed to develop information on fuel-failure propagation in fast breeder reactors.

The entire sequence of operation of the FEFPL loop is either of two ETR reactor positions has been evaluated, including initial installation, startup, normal and abnormal operation, and removal. Included in the evaluation were the effects of: safety (regarding personnel, the ETR, and the experiment), scheduled reactor downtime, interference with operation of other facilities, flux perturbations, and equipment and shielding requirements. This required that the study include estimates for: reactor work schedules, reactor outfitting, conceptual design of special handling equipment, and use of and modifications to existing reactor equipment. All the foregoing aspects were treated in an appropriate manner, thereby yielding a set of critical interface parameters that must be met to assure a safe and efficient life during its occupancy in the ETR facility.

A delineation was made of all processes, procedures, requirements, and interface needs of the FEFPL and the ETR during the entire residence period of the experiment, including initial installation and removal. Two positions in the ETR suited for FEFPL, J-13 and G-7, were investigated. Results indicate that both positions are usable; however, they differ substantially in initial installation time and requirements, equipment needs, flexibility in regard to ease of reactor refueling,

shutdown operations associated with neighboring experiments, and ease of removal of the test train and loop. The main conclusions are:

Safety. Reactor safety with respect to handling operations is not compromised by the FEFPL.

Flux perturbations. Small flux perturbations that could be caused by the FEFPL can be balanced by core loading adjustments.

Position selection. The FEFPL can be operated successfully in either the J-13 (6 x 6) position or in the G-7 (6 x 9) position of the ETR core.

In the J-13 position: (a) no changes are required to existing in-pile tubes, (b) approximately 70 man-hours of in-tank work will be required to reposition existing lead experiments, experiment support clamps, and other equipment, (c) FEFPL must be removed from the reactor before removal of Naval Reactor (NR) experiments if temporary shielding is used to reduce reactor downtime, and (d) minor modifications to FEFPL design will eliminate any possible physical interference between FEFPL and J-10 or L-12 experiments.

In the G-7 position: (a) redesign and installation of in-pile tube supports for H-10 and J-10 in-pile tubes are required to eliminate interference; H-10 cooling lines and other experiment lead-out tubes must be relocated; approximately 300 man-hours are required to modify the equipment, (b) Remote Positioning Mechanism (RPM) cans cannot be used with H-10 or J-10 experiments; there is insufficient clearance to accommodate the cans; in the past, the RPM cans were not used every cycle, (c) use of the G-7 position allows more flexibility for in-tank work, including refueling, after FEFPL loading than does operation in J-13, and (d) all but three NR loop experiments (C-7, F-10, H-10) can be removed prior to

removal of FEFPL; temporary shielding, required for FEFPL, will prohibit removal of experiments from those three positions.

Installation and removal. Satisfactory procedures are available for installation and removal of FEFPL. FEFPL experiments utilizing either unirradiated or preirradiated fuel can be inserted in the ETR with normal procedures and normal time expenditures. Reactor downtime required to insert FEFPL is 23 hr. With proper planning, this work can be accomplished with no major effect on reactor schedule. Reactor downtime required to remove the FEFPL is estimated to be 19 hr. This work can be accomplished by extending the normal shutdown schedule up to 23 hr. High radiation levels from the loop might cause postponement of in-tank work, causing normal downtime to be increased by three days.

Startup. The FEFPL will require stepwise approach to full power. Existing ETR Standard Operation Procedures startup power levels might be satisfactory.

Normal operation. FEFPL is expected to cause fewer power reductions during reactor operation than caused by existing loops because of the coincident-circuitry design used for protection circuits. Midcycle shutdowns requested by other experimenters should not detrimentally affect FEFPL operation. It is preferable to eliminate midcycle shutdown if temporary removal of FEFPL would be required.

Abnormal operation. High radiation levels from potential FEFPL experiments might delay removal of the ETR top dome for several days after shutdown. Abnormal operation causing reactor scram and FEFPL removal will have no physical effect on ETR. There will be a time delay prior to reactor startup.

Special equipment. Special insertion, handling, and removal tools and equipment must be designed and built for use with FEFPL. Temporary shielding will be required to reduce radiation at work locations during reactor shutdown. The shielding will weight between 5800 and 18,700 lb, depending on loop radiation level and loop position in the reactor core. This amount of temporary shielding is required if work in the reactor tank must be performed immediately after shutdown. If work in the tank can be delayed, the shielding weight can be reduced.

Plans for initial test sequence. A proposed set of reference in-pile experiments for the Fuel Element Failure Propagation (FEFP) program has been planned. This set is representative of the first series of experiments that are to be run in the FEFP Loops (FEFPL). The reference experiments serve three general purposes: (1) to act as a starting point for the development of an experimental plan in support of FFTF, (2) to provide a basis for the design of test loops, and (3) to establish a plan consistent with the philosophy of the FEFPL safety study.

A preliminary plan for the first series of tests is to be developed by the end of calendar 1970. This plan is being developed in collaboration with Hanford Engineering Development Laboratory (HEDL) so that the tests will directly support the FFTF Project.

The reference experiments are based on a draft proposal that was presented to RDT in February 1970, during the review of the FEFP Program held in Washington. It is expected that the experiments will be revised considerably before they are conducted. However, the philosophy of experimentation is expected to remain constant in spite of possible changes in experimental order, types of fuel elements used, methods of initiating failure, and severity of test conditions.

The philosophy adopted is that the design of each experiment builds on the knowledge gained from the totality of preceding tests. Also, results of experiments made in other facilities, such as the TREAT tests with the Mark-II loops and static autoclaves, tests in GETR with capsules and the GE Loopsul, and possibly tests being planned for PBF, will provide the additional experience necessary to conduct later, more severe tests. Hence the first series of experiments are planned to be conservative with respect to risk; they will not approach the design-requirement conditions for the loop. These conditions will only be approached in succeeding experiments when the necessary knowledge is gained that allows more accurate estimation of the results expected in each test.

The design basis, conforming to this approach, is to construct the FEFPL as strong as is practical, consistent with the ETR environment, cost, and the basic performance requirements for the testing of fuels in an LMFBR-like environment. Total capability limits of the loop are then defined and each experiment is planned such that these limits bound the possible test results. If certain experiments require higher performance limits, modifications to the loop to increase its capabilities will be made. In describing the test conditions and anticipated results, an objective estimate of all quantities involved was made. No attempt was made to bias results by either a worst- or best-case analysis. Where accurate computations could not be made due to present lack of technological basis, estimates have been made; thus some of the quantities presented here are subject to change as more complete analyses and refined calculations are made.

Purpose. In addition to the general purposes cited in the introduction, the reference experiments are designed to supplement information derived from TREAT tests. In particular, they are directed toward the goal of improved understanding and eventual resolution of key uncertainties in possible single-subassembly accidents in the FFTF. The results will form a base for an initial assessment of related assumptions and analyses made in support of the design and operation of FFTF from the standpoint of safety.

Planning bases. Selection of the set of reference experiments is based on the results of an LMFBR "accident delineation" study at ANL. They are consistent with the In-Pile Safety Experiments as presented in the Studies of LMFBR Safety Test Facilities, Vol. II,[5] where accident delineation is also described in detail.

The more detailed planning is based on considerations directly related to FFTF, including core geometry, nominal operating conditions, postulated accidents and specific steps in accident sequences for that reactor. Therefore, the experimental results should be applicable to the support of FFTF safety analyses. Test conditions, the design of test assemblies, and instrumentation will be selected so as to provide significant checks on, and data for, analytical models of the postulated accidents and associated phenomenological events. Each of these considerations are further elaborated later in this document.

A similar experimental program will be developed later for demonstration plants and target plants.

FEFPL experiments. Subsequent to initial loop and instrumentation checkout, a total of 11 reference experiments has been developed as a planning base. These experiments are designated as PA, PB, or PC and

have the following general characteristics: experiments PA simulate the effects of gas release from fuel elements due to cladding failure, experiments PB simulate the effects of release of small amounts of molten fuel from within fuel elements, and experiments PC simulate the conditions of loss of coolant flow and the effects of large and complete coolant-flow blockages. These experiments are described further below and in Table V.

PA. Fuel Element Propagation Series - Tests PA-1, PA-2, and PA-3, in which defected central fuel elements will be intentionally failed during operation.

PB. Rate of Propagation Series - Tests PB-1 and PB-2, in which several pellets of overenriched fuel in the central fuel element will be melted when the system is brought to full power, Tests PB-3 and PB-4, in which a partial assembly blockage, equivalent to two coolant channels, will be caused, and Test PB-5, in which several coolant channels will be blocked.

PC. Fuel Failure Propagation Series - Tests PC-1 and PC-2 in which two loss-of-flow simulations will be made, one simulating a pump coastdown, and the other a pipe rupture, and PC-3, the last and most severe test, in which total blockage of coolant flow through a bundle of seven fuel elements will be caused.

Schedule. Examination of the schedule information of Table V shows that an appropriate sequence of testing is planned; i.e., milder tests are performed first, followed by step-by-step accomplishment of the more severe tests.

ETR runs on a cycle of approximately 6 weeks. Ideally, a new experiment would be inserted for each cycle. However, the nature of the

TABLE V. Summary of FEFPL Reference Experiments

Test series and key uncertainties	Test		Schedule	
	Type	No.	First year	Second year
Checkout				
Proper operation	Steady-state operation and instrument performance.	P-CK	1	
Fuel-element Failure Propagation				
Effects of gas release.	Gas-release test--moderate leakrate.	PA-1	2	
Behavior of released solid fuel.	Pressurized-pin cladding rupture & rapid leakrate.	PA-2*	5	
Behavior of sodium-logged pins.	Continued operation with defected cladding.	PA-3*	6	
Rate of Propagation				
Behavior of small amounts of molten fuel.	Melting of 20 pellets in central pin with rapid shutdown.	PB-1	3	
	Melting of central pin with continued operation.	PB-2*		7
Maximum rate of flow reduction due to propagating blockage.	Blockage (2 channels) with scram on adverse flow.	PB-3	4	
	Blockage (2 channels) with later scram based on results of PB-3.	PB-4*		8
	Blockage (5 channels) with scram on adverse flow.	PB-5		11
Failure propagation				
Actual work-energy release from FCI and capability to contain.	Loss of flow--simulated pump coastdown with scram on failure.	PC-1		9
Characterization of Na expulsion and potential reentry processes.	Loss of flow--simulated pipe rupture with delayed scram.	PC-2*		10
Ability of assembly cans to resist meltthrough.	Total blockage of simulated assembly (one out of three).	PC-3*		12

*Preirradiated fuel.

reference experiments requires that they be staggered so as to allow time to analyze their results before performing the next of the same type. That is, the design of each successive experiment depends on the success of the preceding experiments. This is particularly true with respect to the initiating mechanism used, instrument data obtained, and the ability to analyze the data. To allow adequate time between the sequentially planned experiments, a tentative rate of five experiments per year is assumed.

Loop usage. It is fully expected that several FEFP loops will be required to complete the experiments. Each loop will be used until either an experiment is performed that renders it unfit for further service or succeeding experiments require significant loop modification. Improvements in the initial loop design will be made to meet design requirements for each series of tests. This is necessary because it is impractical to design a loop (test trains must be designed specifically for each test) that will allow the necessary simulation of the LMFBR environment for the various test series. Also, the current state of the art does not allow a reasonably accurate assessment of the containment necessary for the more severe tests. The possible need for changes in loop design was a major factor in the selection of a package-loop concept rather than a through-loop concept.

Operational tests will be performed outside the reactor to assure that each loop functions properly before its insertion in the core. The determination of the total number of loops required for each series, and possibilities for repeated use of a loop, require thorough planning of the entire experimental program.

Test-assembly design. Test-assembly designs are intended to provide the best practicable simulation of conditions in an FFTF subassembly for each experiment, consistent with the constraints imposed by loop design and flux source. They are particularly influenced by the anticipated relative sensitivity of the experiments to the following factors, arranged in order of decreasing importance: (1) primary temperatures, (2) coolant hydrodynamics, and (3) fuel-element properties. Thus, the proposed test-assembly designs reflect the assignment of highest priority to simulation of fuel temperatures (coolant inlet temperatures and average mass flowrates are relatively easy to control), next highest priority to simulation of coolant hydraulics, and final priority to simulation of the state of fuel elements as affected by their history in a reactor environment.

Major limitations on experiment design imposed by the Fuel Element Failure Propagation Loop on geometry (cross-sectional area and length of the test section), heat-removal capacity, and pumping capability. Among the basic design requirements of the FEFP Loop are: (1) to accommodate the irradiation of up to 19 fast breeder reactor fuel elements, generating up to 20 kW/ft of element length over a 3-ft active length, (2) to operate with liquid sodium coolant at inlet and outlet temperatures of 800 and 1300°F, respectively, and (3) to remove up to 1.5 MW of heat from the loop.

With certain restrictions on the sample train, the loop can accommodate up to 37 FFTF fuel elements, but the linear power ratings of the test elements would be limited by heat-exchanger capacity.

The pump in the FEFP Loop is designed to circulate 100 gpm of 800°F sodium at a delivery head of 100 psi.

Some of the FFTF fuel-element design and operating conditions are shown in Table VI. These data indicate that the FEFP Loop can properly duplicate the temperature and coolant mass flow per fuel element in FFTF.

Although irradiation of FFTF fuel elements in the ETR will require significant flux-spectrum and fuel-enrichment adjustments, the Fuel Element Failure Propagation Loop, when installed in the J-13 location of the ETR core, should adequately simulate the FFTF fuel operating conditions for the proposed fuel-element failure propagation experiments.

The experimental program requires the use of different test-section configurations. Because the proposed tests in the initial series are concerned primarily with failure propagation from element to element and from subassembly to subassembly, it is desirable to use the largest number of elements possible within the range of obtainable power density and power distribution needed for an authentic FFTF-type experiment.

It is expected that the defected-element gas-release experiments and the molten-fuel-release experiments will employ test sections using a pin-centered geometry similar to that shown in Fig. 55. The 19-element hexagonal can or the 19-element scalloped cylindrical shroud configuration with a defective center element is the most desirable configuration for these series of tests.

Blocked-coolant-channel experiments will probably be conducted in coolant-channel-centered test sections of the type shown in Fig. 56. The 12-element test section would be most attractive for these tests, but initial investigations on failure phenomenon might be best tested in the 6-element configuration.

Subassembly-to-subassembly fuel failure propagation experiments in the 2.625-in.-ID FEFP test region are difficult to mockup. Figure 57

TABLE VI. FFTF Fuel-element Design and Operating Conditions

Fuel Composition, w/o (PuO_2 - UO_2)	Inner core zone:	18-82
	Outer core zone:	26-74
Cladding material		316SS
Fuel-element OD, in.		0.230
Cladding thickness, in.		0.015
Fuel smeared density, % of T.D.		85.5
Element lattice geometry		Triangular
Element pitch, in.		0.286
Active fuel length, in.		36
Reflector length (above and below fuel), in.		6
Gas-plenum length, in.		41
Elements per fuel subassembly		217
Subassembly wall thickness, in.		0.120
Subassembly across-flats dimension, in.		4.615
Average linear power, kW/ft		7.16
Peak linear power, kW/ft		12.43
Maximum coolant velocity, ft/sec		25
Bulk coolant inlet temp, °F	Initial:	600
	Design max:	850
Bulk coolant outlet temp, °F	Initial:	850
	Design max:	1050
Subassembly pressure drop, psi		∿100
Average target burnup, MWd/kg		45
Power distribution, peak to average		
Radial		1.40
Axial		1.24
Overpower		1.15

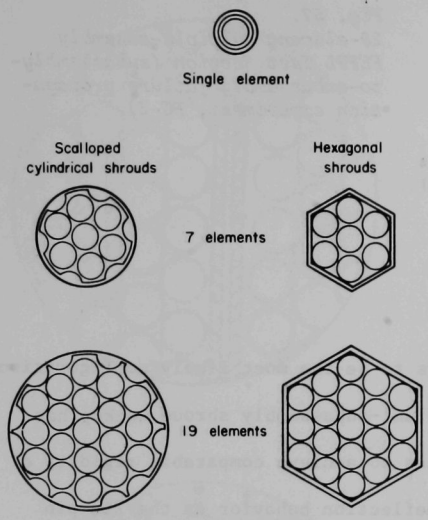

Fig. 55.
Typical Element-centered FEFPL Test Sections.

Fig. 56.
Typical Channel-centered FEFPL Test Sections (partial-flow-blockage experiments).

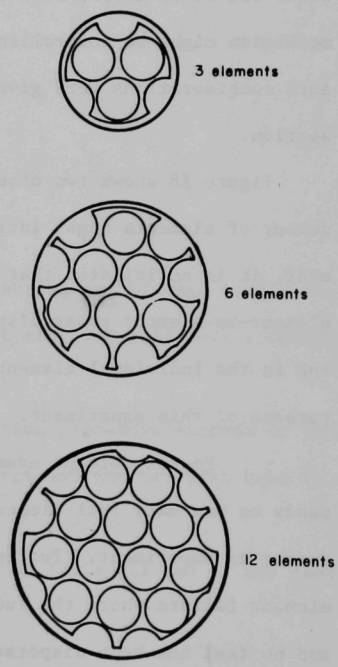

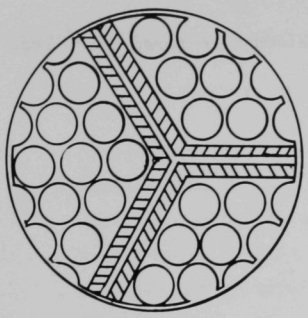

Fig. 57.
29-element Multiple-assembly FEFPL Test Section (subassembly-to-subassembly failure propagation experiment, PC-3).

shows a 19-element section that appears to be the most likely configuration to be used. The 0.120-in.-thick FFTF fuel-subassembly shroud mockup has been reduced to about half the thickness to achieve comparable rigidity of structure (i.e., comparable pressure-deflection behavior as the 217-pin assembly shroud). The thinner section represents a 50% reduction in heat sink, but it is anticipated that the pressure component of the failure mechanism might be controlling. Therefore, for these initial tests, pressure considerations were given first priority in the design of the test section.

Figure 58 shows two other alternate section designs, but the larger number of elements might introduce a serious flux-depression problem. However, it is anticipated that varying enrichments will compensate for the element-to-element power disparity and that the resultant severe flux skewing in the individual elements can be kept to a tolerable value for the purpose of this experiment.

Postexperiment examination. The postexperiment examination depends on how many fuel elements have failed and how badly they have failed during an experiment. Two extreme cases are examined: (1) mild fuel-element failure where the fuel elements are still intact, can be separated, and no fuel has been dispersed, and (2) severe fuel-element failure with

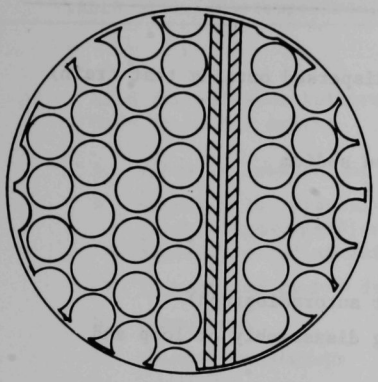

27 elements
(18-9)

Fig. 58.
Multiple-assembly FEFPL Test Sections (subassembly-to-subassembly failure propagation, future experiments).

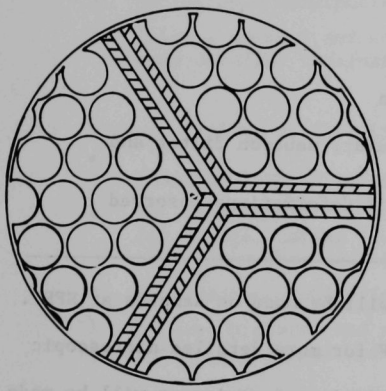

29 elements
(13-8-8)

the fuel elements melted together through the shroud and binding inside the flow divider. The actual condition of the test sections will fall somewhere in between.

In all cases, the disassembly and examination procedure depends on the condition of the test train and loop. Procedures and choices will have to be made as one disassembles.

The examination of the loop is summarized in Table VII and of the test train is summarized in Table VIII.

TABLE VII. Postexperiment Examination of FEFP Loop

I. Mild fuel-element failure (no UO_2 dispersed outside test train)

- A. Visual examination of loop
- B. Sample and analyze cover gas and sodium

II. Violent failure of fuel

- A. Same procedure as I
- B. Activity of loop (gamma scan or autoradiograph)
- C. Photographic record made during disassembly of loop and test-train removal
- D. Recover fuel from sodium (dispersed in loop)
  1. Visual examination and photographs
  2. Weight
  3. Particles size

III. Loop data for feedback into design

- A. Visual examination (in particular, neutron filter and primary containment)
- B. Full destructive examination if deformations observed

Macroscopic examinations and tests will be made on samples at HFEF. Specific samples will be prepared at HFEF for more detailed microscopic examinations. These tests requiring sophisticated equipment will be made at the Argonne, Illinois site.

Analytical Studies

(E. W. Barts)

Scope. The analytical studies encompass two general primary areas of work: (1) support of the in-pile program, including design, performance and safety analyses related to the FEFPL and its subsystems, and (2) the development of predictive mathematical models of fuel-element failure propagation based on results obtained from out-of-pile and in-pile

TABLE VIII. Postexperiment Examination of FEFP Test Train

I. Mild fuel-element failure (test-assembly fuel elements do not have to be cut apart)

A. Visually inspect and photograph

B. Disassemble, visually examine, and low-magnification photograph (high-magnification photograph of suspicious-looking places, including failure points)

C. Inspect and record dimensions and weights

D. Gamma scan

E. Neutron radiograph

F. Analyze fuel-element plenum gas (mass spectrograph)

G. Selectively cut up and visually inspect fuel and cladding

H. Macroscopic examinations, including some metallography

I. Select, prepare, and ship to Argonne, Illinois samples for more detailed examinations

II. Violent failure of fuel (gamma scan and neutron radiograph)

A. Visually inspect and photograph

B. Cut open flow divider and carefully dissect, watching out for damage, taking low-magnification photographs (high-magnification when necessary)

C. Macroscopic examinations, including some metallography

D. Select, prepare, and ship to Argonne, Illinois samples for more detailed examinations

III. Instrument and test-train data for feedback into design

A. Visual examination for possible reuse

B. Destructive examination for design improvement

experiments. A consequent ancillary responsibility is to provide continuous guidance to the experimental programs so that critical information needs are satisfied.

The ultimate goal of this activity is the successful accomplishment of (2) above, viz., the characterization of phenomena that occur, subsequent to fuel-element failures of various types and degrees of severity, suitable for incorporation in LMFBR accident-analysis codes. These mathematical models depend strongly on the results of in-pile and out-of-pile tests, from which empirical relationships are being formulated. To the extent practical, the models are divided into manageable analytical units. Thus, they will consider separately: (1) how a fuel element spontaneously fails, (2) the effects of fuel-element failure or motion on the coolant, and (3) the determination of thresholds for fuel-element failure from external loads.

Because of the anticipated complexity of physical phenomena accompanying fuel-element failure propagation, a definitive description of the analytical program for the determination of predictive models cannot be written at the present time. Actual models will depend strongly on the results of in-pile and out-of-pile tests. Empirical relationships based on the tests will probably be preferred over mathematical solutions derived from basic physical principles. To enhance the chances of success by this approach requires well-designed aid in planning and designing the experiments. The experimental results will be correlated and specific analytical models developed. It is expected that these models will suggest future experiments and indicate the critical parameters to be measured.

Test fuel-pin performance and neutron-filter requirements. The initial analysis was based on LMFBR-type fuel that was positioned in an assembly designed as part of a loop that would allow the liquid-metal coolant to remain isolated from the materials that normally comprise any thermal reactor. A cross section of the system designed for the calculations is shown in Fig. 59. A similar test section would be used for a 7-element test. The transformation of the model to aid the initial calculations is shown in Fig. 60. The transformation replaced the hexagonal packing of fuel elements with the more tractable geometry of the concentric cylinders. Based on this model and using transport theory, the relation between the neutron-energy spectra to be found in representative fast reactors and in a filtered neutron-energy spectrum as exists in a thermal reactor was analyzed.

The data are presented in Fig. 61 to show the effective energy of the neutrons in FFTF, a typical LMFBR, and in a high-flux thermal reactor.

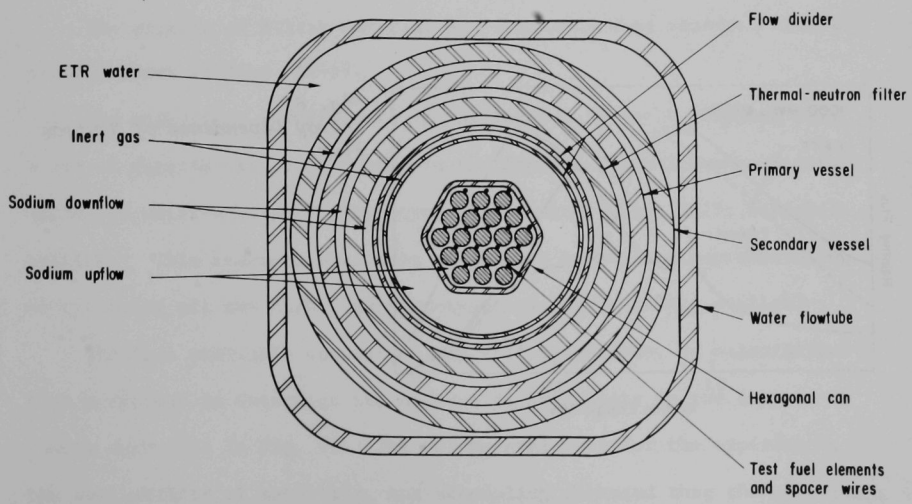

Fig. 59. In-core Test-train and Loop Cross Section.

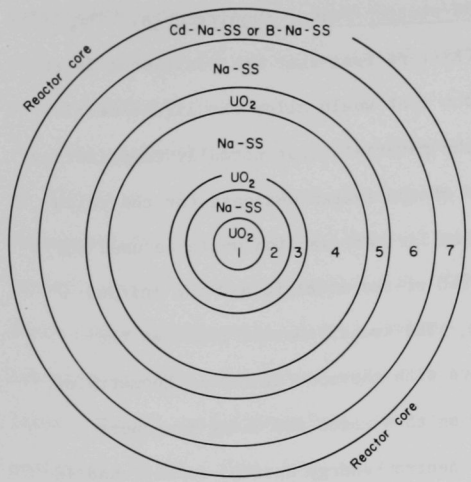

Region:	Radius:
1	0.548 cm
2	1.298
3	1.868
4	2.950
5	3.438
6	4.656
7	5.204

Fig. 60.
Analytical Model of FEFP Test.

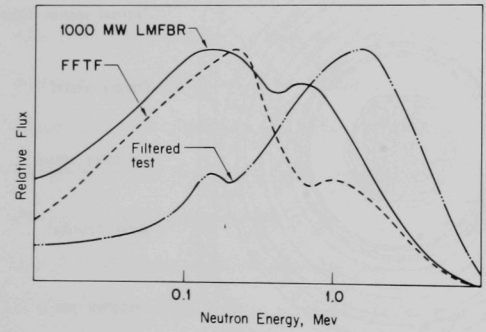

Fig. 61.
Energy Dependence of Neutron Flux.

The results of the initial series of calculations showed that it would be possible to duplicate the design power of 20 kW/ft of fuel ($\sim$3 kW/cm^3 UO_2) using a thermal-reactor driver, and that the power in the different rows could be adjusted to compensate for self-shielding effects by varying enrichments of fuel. However, if the flux incident on the filter is spectrally representative of a water-moderated fully enriched system, then magnitude of the thermal flux incident on the filter must be equal to or greater than 10^{14} neutrons/cm^2-sec. After the feasibility was demonstrated by the initial calculations, additional analyses were performed to scope the required enrichments for a constant power generation per fuel element and to determine the influence of the type of filter on the operation of the experiment. These results are shown in Tables IX and X and in Figs. 62-66. The calculational technique used in obtaining these results was the 16-energy-group SNARG-1D code.[6] This is a transport-theory code developed by ANL for one-dimensional calculations.

The effects of filter material and thickness were examined with the results shown in Figs. 67-69.

The analytical results were of sufficent interest to suggest that a set of experiments be performed in the Argonne Thermal Source Reactor (ATSR), a water-moderated plate-type-fuel reactor using fully enriched uranium.[7] This reactor, available at ANL, is reasonably representative of virtually all the high-flux-test-type reactors currenty available.

The fuel available was not of the FFTF dimensions, so calculations were performed to determine the neutron distributions in the test assembly described in Fig. 70. The volume available for the experiment, the availability of materials, and scheduling dictated that the experiment be only a 19-element assembly and that the fuel enrichment be a

TABLE IX. Power Density* in Assemblies Containing 7, 19, and 37 UO_2 Fuel Elements; 35-mil Cadmium Filter

Center fuel element		Ring of 6 fuel elements		Ring of 12 fuel elements		Ring of 18 fuel elements	
Enrichment, %	Power density, W/cm^3 UO_2	Enrichment, %	Power density, W/cm^3 UO_2	Enrichment, %	Power density, W/cm^3 UO_2	Enrichment %	Power density, W/cm^3 UO_2
93	4117	93	4886				
93	3175	93	3520	93	4495		
93	2641	93	2817	93	3256	93	4172
70	3099	70	3678				
70	2390	70	2649	70	3383		
70	1988	70	2120	70	2451	70	3140
50	2213	50	2626				
50	1707	50	1892	50	2417		
50	1420	50	1515	50	1751	50	2243
30	1328	30	1576				
30	1024	30	1135	30	1450		
30	852	30	909	30	1050	30	1346

*Power density was computed for the midpoint of 91.44-cm-long fuel elements with the assemblies so positioned in a reactor that the incident thermal-neutron flux is $10^{14}/cm^2$-sec.

TABLE X. Power Gradients in Fuel Elements

Case No.:	I		II		III		IV			V		
No. of fuel elements:	7		7		7		19			19		
Filter material:	Cadmium		Cadmium		Cadmium		None			Cadmium		
Filter thickness, mils:	35		35		96		-			35		
Fuel element in:	Center	Ring of 6	Center	Ring of 6	Center	Ring of 6	Center	Ring of 6	Ring of 12	Center	Ring of 6	Ring of 12
Enrichment:	50	44	30	26	93	93	93	93	93	93	93	93
W/cm^3 of UO_2:	2420	2472	1547	1537	2290	2370	4421	5147	11360	3159	3511	4336
Radii, cm	Power-density ratio											
0.2740	1.081	1.000	1.070	1.000	1.043	1.000	1.085	1.000	1.000	1.065	1.000	1.000
0.2055	1.039	1.001	1.034	1.002	1.021	1.001	1.040	1.002	1.020	1.032	1.001	1.010
0.1370	1.017	1.006	1.015	1.005	1.009	1.002	1.018	1.010	1.093	1.014	1.002	1.022
0.0685	1.004	1.023	1.003	1.020	1.002	1.005	1.005	1.025	1.150	1.004	1.012	1.043
0	1.000	1.036	1.000	1.031	1.000	1.012	1.000	1.049	1.297	1.000	1.023	1.067
0.0685	1.004	1.060	1.003	1.050	1.002	1.024	1.005	1.072	1.500	1.004	1.040	1.102
0.1370	1.017	1.091	1.015	1.080	1.009	1.037	1.018	1.121	1.666	1.014	1.065	1.138
0.2055	1.039	1.138	1.034	1.112	1.021	1.055	1.040	1.165	2.350	1.032	1.098	1.187
0.2740	1.081	1.179	1.070	1.159	1.043	1.078	1.085	1.262	3.465	1.065	1.131	1.237

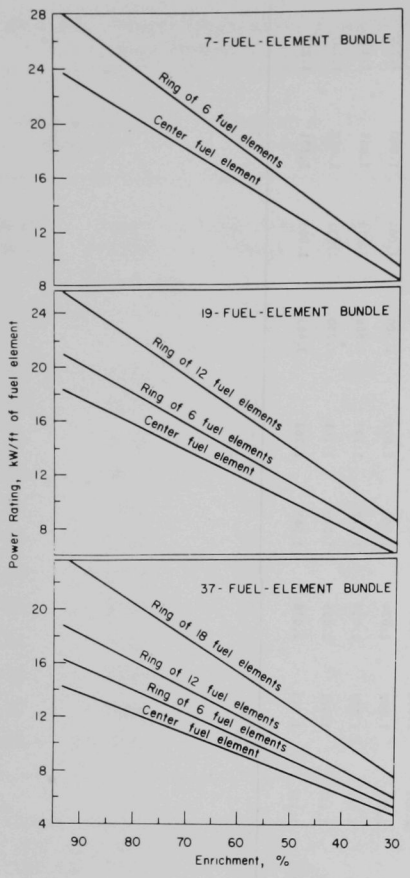

Fig. 62.
Heat Generation and Enrichment.

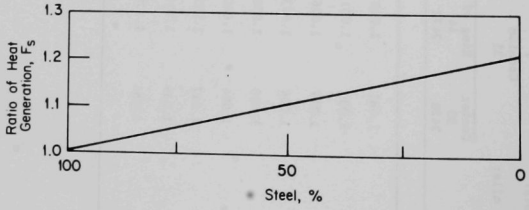

Fig. 63. Effect of Quantity of Steel in Test Section.

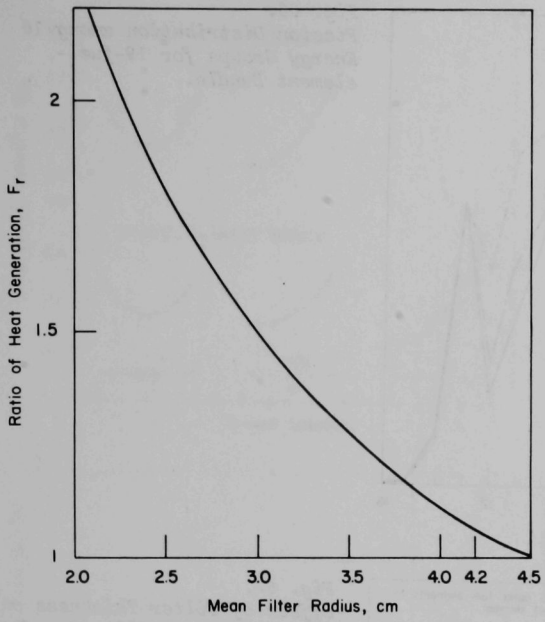

Fig. 64.
Effect of Neutron-filter Mean Radius.

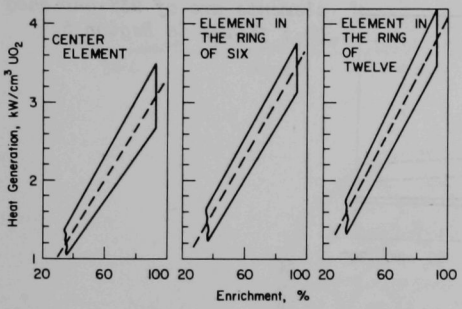

Fig. 65.
Heat Generation vs Enrichment for a 19-fuel-element Assembly in a Thermal Reactor with 10^{14} n/cm^2-sec Incident on the Neutron Filter.

selection from 50, 60, or 75%-enriched UO_2 pellets. The enrichments were estimated from the results presented in Tables IX and X.

ATSR experiment description and results. The experiments were designed to determine the relative power generation for each element in the 19-element bundle and to examine the detailed power generation within each fuel element.

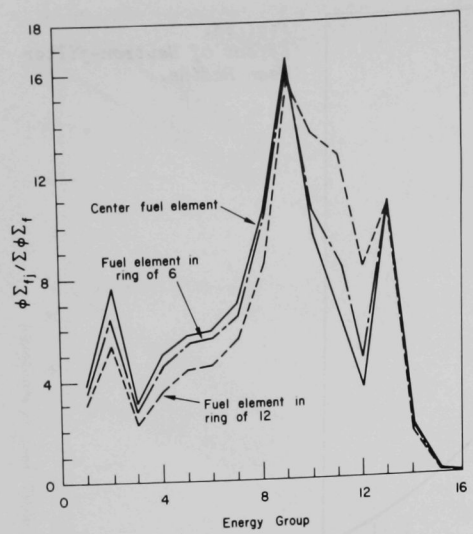

Fig. 66.
Fission Distribution among 16 Energy Groups for 19-fuel-element Bundle.

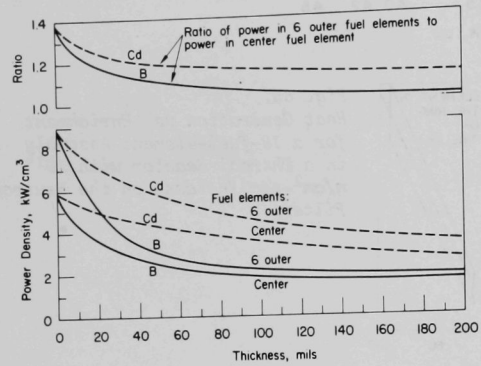

Fig. 67.
Effect of Filter Thickness on Power Density. All seven fuel elements are of 93%-enriched UO_2; filter is Region 5.

As is shown in Fig. 70, the ATSR irradiation test section is composed of 19 tubes. These contain UO_2 pellets positioned in a hexagonal array in a matrix of Grade-1100 aluminum. A sketch of an element comprising the test section is seen in Fig. 71. Surrounding the aluminum matrix is the filter composed of either metallic cadmium or a high-boron compound. In this case, the boron filter was a boron-loaded resin coating

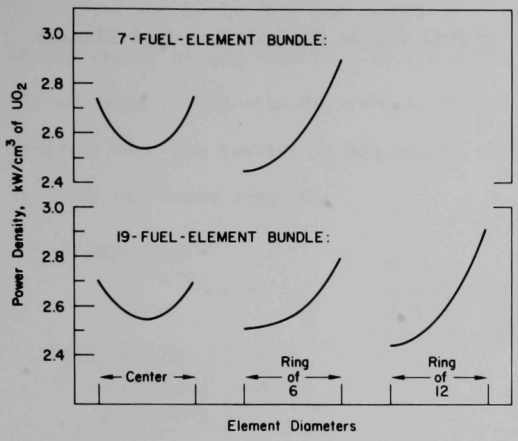

Fig. 68.
Power Gradient on the Diameter of Fuel. The average power density in all fuel elements is 2.6 kW/cm^3; the diameter of all fuel elements is 0.548 cm.

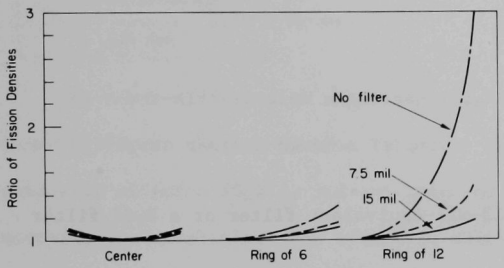

Fig. 69.
Fission Distribution inside Fuel Elements. A 15-mil boron filter is used in the design.

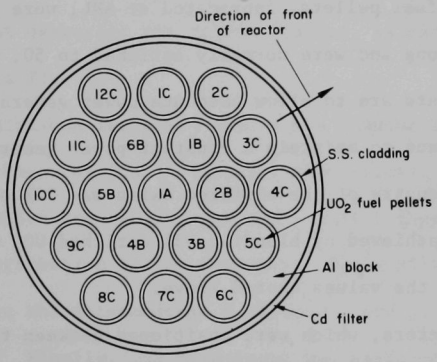

Fig. 70. ATSR Experiment Cross Section.

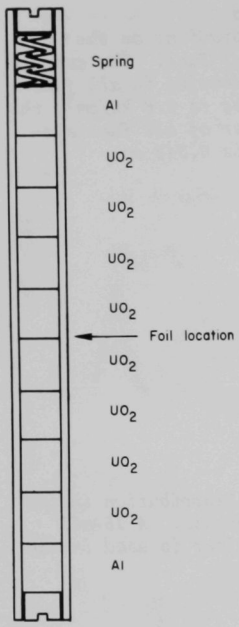

Fig. 71.
Location of Foil inside Typical Test Fuel Element.

with boron density that gave a 13-mil-equivalent filter or a B_6Si filter entrained in a steel mesh.

The UO_2 fuel pellets, fabricated at ANL, were 0.25 in. in diameter and 0.5 in. long and were normally enriched to 50, 60, and 75% ^{235}U. These high enrichments are to allow adequate power generation in the filtered neutron flux and to maintain a constant power generation in each element. The nominal density of the sintered oxide was 94% of theoretical and the enrichments, achieved by blending 93%-enriched UO_2 with normal UO_2, were approximately the values quoted above.

The detectors, which were positioned between the UO_2 pellets, were either 0.002-in.-thick foils of fully enriched uranium or were 0.003-in.-thick Lexan foils similarly positioned in the test assembly.

After the foils were positioned in the test assembly, it was placed at the center of the void tube in the ATSR. The void tube, shown in Fig. 72, contains a 2-in.-dia dry tube in which the assembly is exposed to neutrons when the reactor is operating. For these tests, a power of 5 to 10 watts was found adequate.

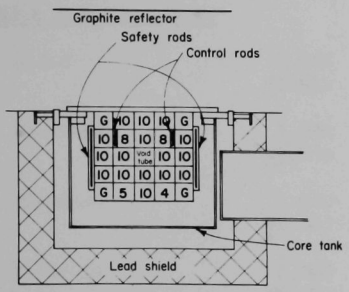

Fig. 72.
ATSR Loading. The numbers 4, 5, 8, and 10 indicate the number of fuel elements in the box; G indicates graphite plug.

The power-distribution experiments using the uranium foils included three different thermal-neutron filters: one of 40-mil cadmium, one of nexaboron silicide (B_6Si), and one composed of amorphous boron is a polymerizing resin vehicle. The effective thicknesses of the boron filters were approximately 15 mils each. However, the B_6Si was entrained on a stainless-steel mesh that decreased the filter density, as can be seen in the neutron radiograph in Fig. 73.

The different irradiations performed inside the cadmium filter were first with uniform enrichment of 50% ^{235}U in all the pellets, then with a distributed loading in which the enrichments approximated those required for a constant power distribution in the assembly: 50% enrichment in the outer 12 elements, 60% in the intermediate 6 elements, and with the central element enriched to 75%. Finally, the experiment was performed with aluminum pellets replacing the fuel to determine the neutron distribution in the absence of the absorbing fuel.

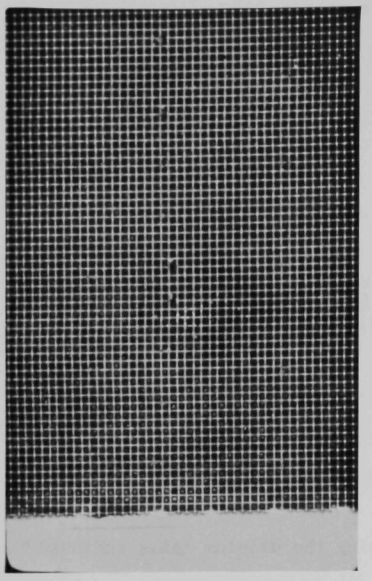

Fig. 73.
Neutron Radiograph of B_6Si Neutron Filter.

After the foils were positioned in the cadmium-clad assembly, the test assembly was positioned in the ATSR, then exposed to approximately 1 watt-hour of reactor power. After removal, the foils were placed on planchettes, then loaded into the automated counting equipment and repetitively counted.

The counting was done on a 2x2 NaI(TI)-crystal spectrometer biased to reject all events below 550 keV. The output from the preamp was split between two channels of amplifier and analyzer so that the major problems in electronics could be recognized and to compare the data-acquisition systems. The times and the counts were stored until there were a sufficient number of counts to determine statistics and decay times, then the data were typed onto IBM cards. The counting data, including foil weights and gross decay times, were analyzed using standard ANL computer programs[8] with the results in Table XI. The results have

TABLE XI. Fast-fuel Irradiations in ATSR

Enrichment, %	Relative power density				
A - B - C	A	B	C	C(face)	C(corners)
With cadmium filter					
0-0-0	1.008 ±0.017	1.024 ±0.006	1.000 ±0.007	1.002 ±0.005	0.998 ±0.010
50-50-50	1.000 ±0.006	1.066 ±0.010	1.269 ±0.049	1.240 ±0.029	1.307 ±0.033
75-60-50	1.000 ±0.003	0.876 ±0.006	0.891 ±0.029	0.865 ±0.010	0.918 ±0.008
75-60-50	1.000 ±0.002	0.881 ±0.006	0.092 ±0.032	0.872 ±0.005	0.931 ±0.013
With hexaboron-silicide filter					
50-50-50	1.000 ±0.001	1.236 ±0.017	2.150 ±0.168	2.008 ±0.082	2.292 ±0.086
75-60-50	1.000 ±0.005	0.992 ±0.017	1.524 ±0.137	1.405 ±0.059	1.645 ±0.061
With boron-loaded resin filter					
75-60-50	1.000 ±0.002	1.061 ±0.127	1.298 ±0.247	1.293 ±0.271	1.315 0.258

been normalized to unity for the central element to display the power distribution in a conventional fashion.

Similar experiments were performed using the two boron-loaded filters. The foils were irradiated, counted, and analyzed in a manner similar to that discussed for the cadmium-clad test assembly. These results are also shown in Table XI.

An examination of the data from irradiations inside the B_6Si filter shows a much higher relative value for the power generation in the outer

ring than for the other measurements. The rapid change is attributed to the leakage of thermal neutrons into the fast fuel. Since the thermal neutrons have such short mean free paths, the outer elements capture the bulk of the thermal neutrons, resulting in the observed augmented fission rate.

The detailed fission distribution within the fuel elements was determined by examining the density of fission-product tracks in Lexan foils.[9-11] Each Lexan foil, 0.003-in. thick, was sandwiched between two enriched-uranium foils, each of which was 0.002-in. thick, then positioned between the fuel pellets composing an element.

After the test assembly was loaded, it was positioned in the central void and irradiated in the ATSR. After removal, the Lexan was washed in alcohol, etched with NaOH, then washed with dilute NH_3. A photomicrograph of an etched foil is shown in Fig. 74. The track density of from 4 to 6 x $10^6/cm^2$ corresponds to an irradiation of approximately 1000 watt-sec in the ATSR.

Counting the tracks was too laborious, so the counting was automated by using a microphotometer coupled to a digital voltmeter and a printer. It was determined that an approximately linear relationship existed between 0.3 and 0.8% optically dense as shown in Fig. 75. A track density on the order of 5 x 10^6 tracks per unit area was used so as to have enough clumping to eliminate diffraction effects from the individual tracks.

The microphotometer was a Jarrell Ash Model 23-050. The adjustable slit was positioned to scan an area 0.05 mm by 1 mm with a scanning rate of 25 mm/min. The statistical deviation for an integrating time of 1 sec is then 0.83%. The output from the digital voltmeter was printed

Fig. 74.
Typical Etched Fission-particle Tracks in Lexan.

out on paper tape and the results were manually reduced for an average value at each of 37 points in the element.

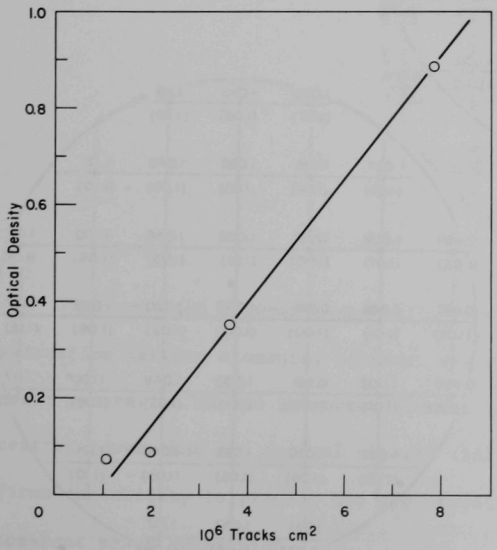

Fig. 75.
Optical Density vs Number of Tracks.

The fission distribution was calculated for a similar geometry using the SNARG-2D Code. The stacked cylinders were transformed into equivalent square cylinders to solve the problem, then the results were transformed back to the cylindrical geometry.

Comparisons between the analytical and experimental results are displayed in Figs. 76-79. It is seen that there is a maximum difference at a few points of as much as 10%, with an average difference between the analysis and the measurement of less than 5%.

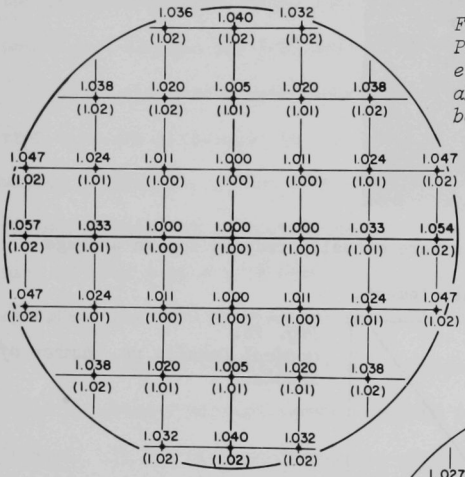

Fig. 76.
Power Generation across Fuel-element 1A. Calculated values are above points; measured values are below points and in parentheses.

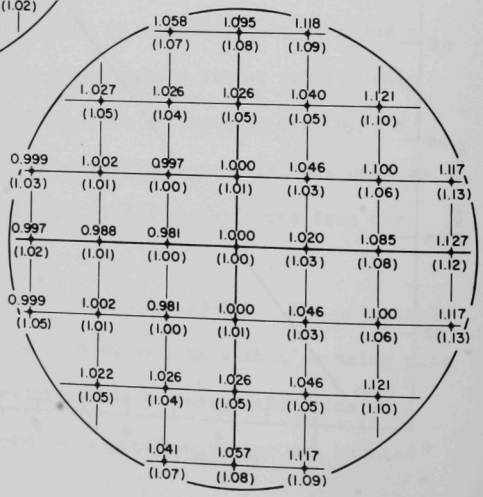

Fig. 77.
Power Generation across Fuel-element 2B.

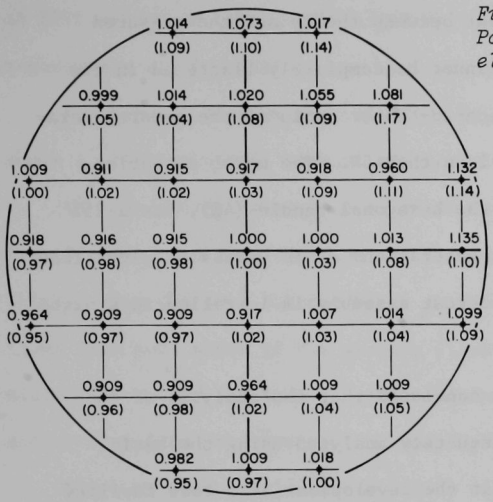

Fig. 78.
Power Generation across Fuel-element 3C.

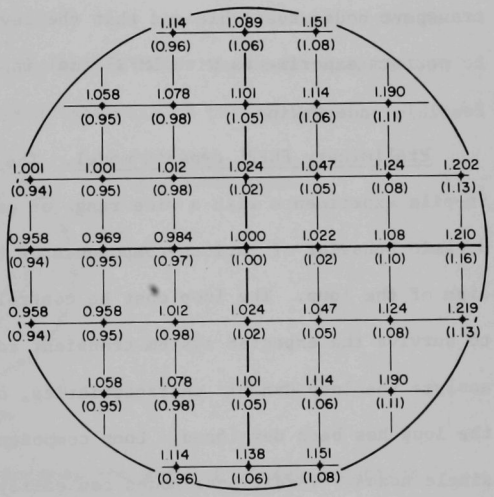

Fig. 79.
Power Generation across Fuel-element 4C.

The variation between Lexan foils prohibits relating the power generation between elements; however, the calculated values for the power generation showed the outer element (4C) to have a 3.2% higher central power than the central element (1A). The small difference confirms the ability to predict the appropriate enrichment to allow a constant power generation.

It is seen that the agreement between theory and the measured values is adequate. The power cannot be completely flattened in the fuel element; however, the surface-to-center ratio of the power generation for the central element is less than 5%. The worst situation, i.e., at the corner elements in the hexagonal bundle (4C), has a 25% variation in the volumetric heat generation. This variation might lead to local heating in the event the test assembly is installed in a high-flux thermal reactor.

From the experiments, it is concluded that the analysis of the filtered test assembly can be adequately analyzed using the basic transport codes available and that the development of a test facility to perform experiments with LMFBR fuel in a thermal reactor is a feasible undertaking.

Preliminary FEFPL dynamic model. The FEFPL will be used to perform in-pile experiments with a wide range of experimental conditions. The dynamic behavior of various components of the loop is critical in the design of the loop. The loop most be controllable and it must be designed to survive the expected system transient caused by an experiment. To analyze the loop dynamic characteristics, a preliminary dynamic model of the loop has been developed. Loop components are assumed lumped into single nodes. (Additional nodes can easily be added to the present setup when needed.) The power generated in the loop is determined by the operating conditions of the ETR, and there is assumed to be no neutronic coupling between the loop and the ETR in the present model.

The model will be used to provide transient information in the areas of component design and loop safety studies. Also, for the experiments to be meaningful, it is important to simulate closely the operating conditions

of FFTF and/or an LMFBR. The model will aid in planning and designing the experiments and in choosing the best control scheme for the loop.

A schematic diagram for the FEFPL is shown in Fig. 49. Figure 59 shows a cross-sectional view of the test train and the loop.

Thermal energy balance is taken at each node around the loop. The flow divider is filled with gas and is assumed to act as a heat barrier. This is also the case for the outer surface of the primary vessel. Sodium flows from both sides of the neutron filter are assumed to have perfect mixing in the lower plenum. Perfect mixing in the upper plenum of the sodium flow from the test section and the bypass flow is also assumed.

The heat exchanger, which consists of a central tube and 24 small tubes with heaters in them, is shown in Fig. 80. Heat generated in the heaters is assumed to transfer instantaneously to the sodium.

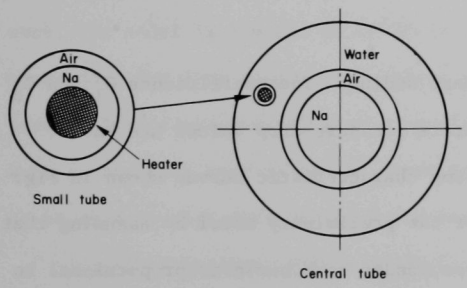

Fig. 80.
Heat Exchanger.

A variable transport delay between the annular linear-induction pump (ALIP) and the neutron filter is simulated by

$$T_{ci} = T_{cip}(t - \tau) \tag{8}$$

where T_{ci} is the sodium temperature entering the neutron filter, T_{cip} is the sodium temperature leaving the ALIP, and τ is the total mass in the section where time delay occurs/mass flowrate of the loop.

The model for the primary-coolant-loop hydraulics is derived by applying Newton's second law of motion to a viscous incompressible fluid in nonsteady flow:[12]

$$\ell' \frac{dW_{cp}}{dt} = g_c H - g\int \rho dz - g_c \Delta P_f \tag{9}$$

where W_{cp} is the mass flowrate of sodium, ℓ' is $\sum \frac{(\Delta L)_i}{A_i}$, the sum of the length/area ratio over the entire loop, g is the acceleration of gravity, g_c is a conversion factor, H is the pump head, and ΔP_f is the total loop friction pressure drop, which is the friction pressure drop across the core plus the friction pressure drop across the rest of the loop.

The pressure drop is assumed to have the form

$$\Delta P_f = C_1(\alpha W_{cp})^{1.8} + C_2 W_{cp}^{1.8} \tag{10}$$

where α is the fraction of the bypass sodium. The coefficients C_1 and C_2 can be determined if some steady-state pressure-drop values are known. The pump head H is obtained from pump characteristic curves shown in Fig. 81. These curves are generated for the preliminary model by assuming that they are parabolic and that the area under each curve is proportional to

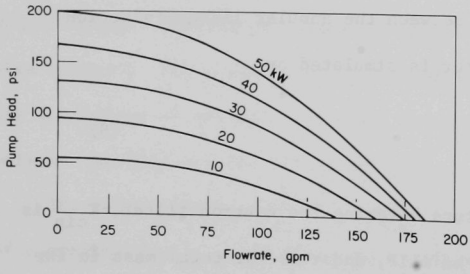

Fig. 81.
FEFPL - ALIP Performance Curves.

the input kW.[13] A natural-circulation head, $\int \rho dz$, is obtained by summing the products of density and length over the entire loop.

Only the primary-coolant (sodium) loop hydraulics are included in the present model. The secondary coolant (air) and tertiary coolant (water) appear as parameters.

The initial conditions from which the system is perturbed are obtained from steady-state calculations. The properties of the system are calculated based on average steady-state temperatures and are assumed to remain constant during a transient.

The IBM System/360 Continuous System Modeling Program (S/360 CSMP) is used for solving the dynamic model.[14]

Sample problems were run to demonstrate the model performance. All portions of the simulation seem to respond in a reasonable manner. However, the model is limited in application by lack of design and performance data for loop components. Also, better representations than the present "lumped-parameter" approximations of certain critical regions, such as the test section and the heat exchanger, are needed for the model to be able to give more detailed and accurate information.

In-pile experiment safety studies. The reference set of in-pile experiments for the FEFPL are described in an earlier section (p. 182). As stated there, each experiment builds on the knowledge gained from preceding tests. In addition, experiments run in other facilities, such as the TREAT tests with the Mark-II loops and static autoclaves, tests in GETR with capsules and the GE Loopsul, and possibly tests being planned for PBF, will provide the experience necessary to conduct later more severe tests. Hence, the first series of experiments are planned to be conservative with respect to risk and will not approach the conditions set forth

in the design requirements for the loop. It is expected that succeeding experiments will only approach these conditions as knowledge is gained that allows more accurate estimation of the results expected in each test.

The basis for this approach is to design the FEFPL as strong as practical consistent with the ETR environment, cost, and basic performance requirements of testing fuels in an LMFBR-like environment. The total capability of the loop is defined and each experiment is planned such that these limits bound the possible test results. If experiments require higher performance limits, modifications will be made to the loop to increase its capabilities.

Basis for loop design and safety of FEFP experiments. The primary concern in the safety of FEFPL experiments is the accumulation of energy in the test fuel following a loss of cooling capability within the loop. This energy could later be transferred to the sodium coolant in a manner that results in high-pressure pulses. Such pressure pulses could possibly cause damage to the containment vessels. The calculation of these pressures is based conservatively on the thermodynamic limit because adequate physical models are not available to describe the complex phenomena involved. Indeed, it will be, at least in part, the purpose of the reference experiments to be performed in this loop to determine the pressures that are generated from various simulated accident situations. The primary problem is that conservative calculations for potential pressures and work energy exceed those that can be shown by analysis to be accommodated in the design of the test assembly and yet achieve the desired test performance at this time. The current "state of the art" for calculations of loop containment structures is to use a Hicks and Menzies type (thermodynamic maximum) calculation[15] to obtain the maximum work and pressures expected from the

molten fuel-coolant interaction and then apply the Proctor and Wise empirical relationship[16] to determine the allowable deformations of the cylindrical containment vessels.

A necessary criterion in the design of FEFPL is the containment by the primary vessel of any pressure pulse generated in the loop during an experiment. Therefore, to build a useful in-pile loop, more realistic analysis techniques must be used.

Experimental and analytical work is being carried out at ANL that will provide better techniques in the future. Experiments are being conducted in which molten fuel and sodium are contacted to measure the work-energy produced.

Table XII summarizes the conversion efficiencies of thermal energy to work energy observed experimentally in these tests. The experimental conversion efficiencies were estimated, considering the final pressure of expansion to be of the order of 1 atm. In this case, the thermodynamic limit of the conversion efficiency is about 30 to 50%. Table XII clearly shows that the experimental conversion efficiencies are orders of magnitude lower than the thermodynamic limit. Even the highest value (about 1%) is only 3% of the thermodynamic limit.

As a result of these low conversions of thermal to mechanical work, it appears that the energy released to do work on the loop vessel will be several orders of magnitude less than that which can be calculated from Hicks and Menzies criteria. The pressure-time functions also appear to be very dissimilar to a chemical explosive (e.g., TNT) energy release and thus not modelled well by the Proctor and Wise relationship. Indeed, the resultant shock wave is much different than that of a chemical explosive. A large fraction of the work is done by coolant vaporization

TABLE XII. Experimental Conversion Efficiencies of Thermal Energy to Work

Method	Conversion efficiency, %
TREAT UO_2-Na experiment (piston autoclave, S-series, 500 cal/gm UO_2)	
With bond gas	0.0014
Without bond gas (evacuated pins)	0.15
Laboratory experiment of dropping molten UO_2 into sodium	<0.01
Laboratory experiment of injecting water into molten salt (NaCl)	0.4 - 1.0

at a rate controlled by the heat-transfer processes between fuel and coolant. Thus, a large fraction of the work is done at relatively low pressures, typically near or below 100 atm. However, in the case of a chemical explosive, most of the work is done at high pressures, typically above 100 atm. The difference is shown qualitatively in Figs. 82 and 83, where P* is the pressure at or below which a large fraction of the work is done by molten fuel-coolant interactions. If P* is below the design pressure of a pressure vessel, the difference between a molten fuel-coolant interaction and a chemical explosion is significant.

Recent calculations based on a rate-limited model developed at ANL also indicate that most of the work due to a fuel-coolant interaction is done by coolant vaporization at pressures of the order of 100 atm. The calculations indicate that high shock pressures occur during the liquid-phase heating and expansion and that the shock energies are much smaller than those calculated by thermodynamic considerations alone.

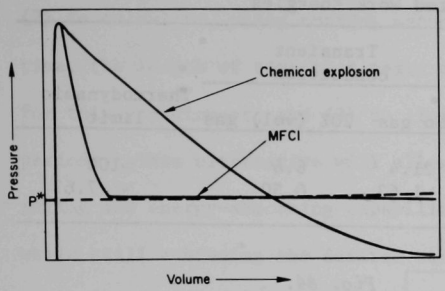

Fig. 82. MFCI vs. Chemical Explosion; P-V Plot.

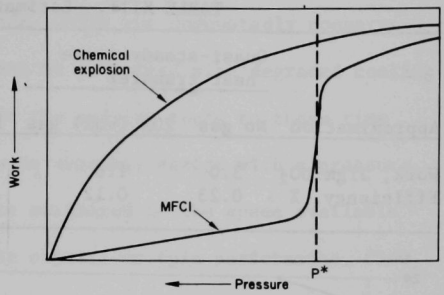

Fig. 83. MFCI vs. Chemical Explosion Work is Given as a Function of the Final Pressure of Expansion.

Time-histories of the energy release were derived from the calculations and are shown in Fig. 84. Clearly, the energy-release histories depend much on the approximations made for the process of coolant heating. The calculations assumed a one-dimensional acoustic constraint of infinite extent. However, for a finite loading-column length, the initail shock wave is effectively terminated when the unloading rarefraction wave returns from the free surface. For the FEFP loop, the unloading time is 5-6 msec. Suppose the unloading time is 6 msec. The pressure at this time is of the order of 100 atm. Table XIII gives the shock energies (work done up to the unloading time) estimated from Fig. 84. Corresponding conversion efficiencies of thermal energy to work are also given. The conversion efficiencies are based on the total thermal energy of the UO_2 above 25°C.

In the present state of knowledge, the case of quasi-steady-state heat transfer appears more realistic than the transient-conduction case. For experimental safety purposes, however, the transient-conduction case is preferred because it represents a more conservative approximation.

TABLE XIII. Estimated Work Energies

Approximation	Quasi-steady-state heat transfer: No gas	Quasi-steady-state heat transfer: 20% (vol) gas	Transient conduction: No gas	Transient conduction: 20% (vol) gas	Thermodynamic limit
Work, J/gm UO_2	3.0	1.6	21.4	6.6	∿100
Efficiency, %	0.23	0.12	1.63	0.50	∿ 7.63

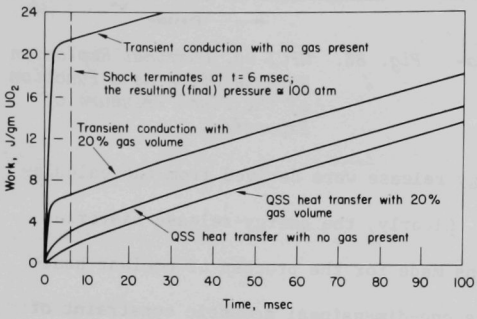

Fig. 84. Energy-release Time Histories Based on ANL Rate-limited Model.

Continued experimental and analytical work is being carried out to define better the nature of the fuel-coolant interaction, pressure-time functions, and magnitude of energy releases, and can be expected to provide better analysis methods in the future.

The dynamic plastic response of a pressure vessel to pressure-time functions is also under investigation at ANL. This approach might be expected in the future to improve the determination of the allowable deformations of cylindrical containment vessels due to arbitrary pulses.

The present problem is to define the consequence of the in-pile experiments before carrying them out. Because this is difficult to accomplish, only one procedure seems available: (1) to build the strongest containment possible from economic, neutronic, and reactor-geometry considerations, (i.e., gamma heating and reactor experimental hole size),

(2) to calculate, using current methods, which are undoubtedly conservative, the length of time that tests can be performed with degraded cooling for this containment, and (3) to limit the initial tests to these time periods. This alternative will allow an assembly design with a pressure rating and energy-absorbing capability maximized to the space available while still achieving the desired test objectives (pin performance, flow, etc.).

The current FEFPL design capabilities are summarized in Table XIV. The planned series of tests must be within the FEFPL loop capabilities. This is accomplished by limiting the test parameters such that loss of coolant does not occur in the initial test. The parameters of the second test would be based on the results of the first test, etc. Gradually, step by step, the final desired test parameters are approached. Finally, when these tests are completed, the energy-release mechanism and loading function on the containment will be known in a fashion that enables the desired condition to be reached within the FEFPL design limits. This "bootstrap" approach is slow and costly, but it appears to be the only method of safeguarding the test reactor while performing needed tests. In addition, considerable related experimental backup both in- and out-of-pile has been planned before each proposed FEFPL experiment.

As a part of the study of LMFBR safety test facilities, ANL performed an accident-delineation study and recommended a program of in-pile safety experiments. Table XV outlines the proposed program using capsules, autoclaves, and loops in TREAT, as well as the forced-convection capsule in GETR. This testing program will also provide experimental backup to the FEFPL experimental series.

TABLE XIV. FEFPL Design Capabilities

Objective: Develop a high-performance irradiation facility for LMFBR safety tests.

Basis: Optimized pressure capability with respect to loop operating temperatures and gamma heating, reactor experimental hole size, and other space limitations, and the use of austenitic stainless steel.

Current safe static design pressures:

Test Section		Remainder of loop	
Primary vessel	1500 psi	Primary vessel	500 psi
Secondary vessel	2100 psi	Secondary vessel	500 psi

An experimental plan will be submitted before each FEFPL experiment in which the test limits will be established. These limits will be based on pertinent prior experiments. For example, the direct backup to P-CK and the PA series is primarily planned as part of the FEFP out-of-pile tests. The PB series is a direct extension of the D series performed in the Mark-II loop in TREAT that studies the short-term effects of the release of a small amount of molten fuel in a 7-pin cluster. The PC series depends on the results of all past experiments, in particular the RA, RB, C10, F, and L experiments that study assembly blockage or loss of flow. In addition, the SA and I series will provide needed data on fuel-coolant interactions and the G series will study the containment of molten fuel by the assembly duct.

Safety requirements for instrumentation and scram systems. In each test, the safe performance depends on the length of time in which energy is accumulated in the fuel from an imbalance between the rate of energy generated in the fuel and the rate of energy removed by the coolant. In the ETR tests, the imbalance results primarily from a disturbance in

TABLE XV. Experimental Backup to First Twelve Experiments

Facility Test vehicle Key uncertainty	Series	No. pins
TREAT		
Static capsules		
Failure thresholds and coherence of failure of elements for power excursion.	C4,C6,A	1-3
Column autoclave		
Work-energy release from molten fuel-coolant interaction.	SA	7
Characterization of expulsion and reentry for power excursion.	SB	7
Modified autoclave or loop		
Characterization of expulsion and reentry for assembly blockage.	RA	7
Characterization of expulsion and reentry for loss of flow.	RB	7
Impact capsule		
Work-energy release from molten fuel-coolant interaction.	I	Pool
Transparent autoclave		
Fuel movement for loss of flow.	F	3
Mark-II loop		
Effects of release of a small amount of molten fuel.	D	7
Ability of duct to resist meltthrough.	G	3
Fuel movement for loss of flow.	L	7
Failure thresholds and coherence of failure for power excursion.	H	7
Fuel movement for power excursion.	E	7
GETR		
Forced-convection capsule		
Characterization of expulsion and reentry for assembly blockage and loss of flow.	C10	3-7
Behavior of failed fuel.	B	3-7

the coolant flow. Overpower transients are limited by the reactor safety circuits.

Because the energy accumulated is equal to the difference in the rate of energy generated and the rate of energy removal multiplied by the period of time over which this imbalance exists, a limit to the time can be established as an operating safety limit. This requires special instrumentation to detect the imbalance and a scram signal to scram the test reactor.

Such scram circuitry is necessary to simply run the loop in ETR. For each test the set points (with a time delay in appropriate circuits) will be established based on prior experience to limit the pressures during the test. It is the determination of these time delays that establishes the safety and usefulness of these experiments.

The loop checkout could be performed today because scram set points could be established within the present state of knowledge. No time delay is required. Actually, all the proposed tests could be run, although some would be limited to relatively short periods of time. The TREAT tests will provide backup experiments for testing times on the order of 10 sec. The role of the ETR tests is to extend the duration of tests and to conduct large-scale tests in an environment more closely simulating an LMFBR.

As stated above, the early fuel-element failure propagation tests do not require limitations on operating times as long as loop conditions remain within the scram setpoints. The main concern is the ability to run the more severe transients called for later in the program.

An estimate has been made from SAS calculations of the times available following a complete loss of coolant flow before significant melting

occurs. Times for fuel operating at 20 kW/ft are given in Table XVI. These times do not consider the reentry of the sodium and the continued heat transfer that will occur. Estimates of the time for reentry to occur after expulsion vary from about 0.1 to 1.0 sec after sodium boiling initiates the expulsion. Thus, it can be seen from the events vs. times shown above that reentry would occur before significant fuel melting. More detailed analyses of this type are being carried out.

TABLE XVI. Time Estimates L/C Event Sequence (SAS calculations for 20 kW/ft)

Event	Time
	0 sec
Sodium flow reduced to zero	|
Sodium boils	|— — —| (1/2 to 1 sec)
Cladding failure (melting or loss of strength)	|——— — — — — —| (1 to 3 sec)
	(3 to 4 sec)
Significant fuel melting (>1%)	|———— — — —|
	(5 to 7 sec)
Complete fuel melting	|———————— — — — —|
	(6 to 8 sec)
Molten fuel reaches boiling point	|———————————— — — — —|
	(0.6 to several seconds)
Sodium reenters	|——— — — — — — — — — — — — — — — —?

The times involved with the scram circuitry are given in Table XVII. Thus, a loss-of-flow or total blockage experiment could be performed with a scram on loss of flow (e.g., 50%) with a time delay on the order of 3 sec allowing a complete expulsion and reentry to occur without risk (no significant fuel melting).

Times longer than 3 sec could be defended based on the thermodynamic calculations. Using the conservative analyses, the primary vessel

TABLE XVII. Time Estimates for Reactor Scram

Instrument response	
Pressure and flow	<10 msec
Thermocouples	20 to 50 msec
Scram delay	20 msec
Rod insertion	250 msec
Total	∿300 msec

will absorb 20,000 Joules in expanding out to just touch the secondary vessel. Using the Hicks and Menzies[15] approach, expanding to a final pressure of 100 atm gives an energy available for mechanical work of 100 J/gm of UO_2 starting with molten UO_2 at the boiling point. Thus, 200 gm of molten UO_2 can be obtained. One test fuel element could contain approximately 180 gm of UO_2.

From the more recent calculational and experimental results, the thermodynamic limit of the energy conversion appears overly conservative, as has been discussed previously. A more realistic, but still conservative, estimate can be obtained from the ANL calculations based on the transient-conduction approximation. When there is no noncondensable gas present in the fuel-coolant mixing zone, the shock energy is 21.4 J/gm of molten UO_2 (See Table XIII). Thus, almost six test fuel elements could become fully molten and still be within the capability of the containment. The presence of a compressible gas would further reduce the efficiency of energy conversion. When the initial volume of a noncondensable gas in the mixing zone is 20% of the sodium (liquid) volume, the shock energy is 6.6 J/gm of molten UO_2. The 20% initial volume of noncondensable gas was chosen since this is approximately the void volume, or bond gas, relative to the total sodium volume present in the test section of the

loop. At this shock energy almost all the fuel in all 19 fuel elements could become fully molten. The final pressure of expansion would be about 100 atm, which is well within the FEFP-loop test-section capabilities.

Model development. In conjunction with the LMFBR Program Plan,[17] a basic accident tree for fuel-element failure propagation was developed. Based on the accident tree, the complex problem of failure propagation can be simplified by subdivision into smaller separate problems consisting of the various events that can occur. These individual events can be more readily analyzed than the total phenomenon of failure propagation. Then the models of separate events can be used to develop a hierarchy of models.

A literature search was initiated to determine the availability and suitability of existing computer codes for use in analyzing failure propagation. In addition, preliminary analyses were started for several of the events to scope the problems involved in model development. In particular, the rate of release of fission-gas from a failed fuel element, the effect of flow blockages, and the effect of external loads on fuel elements were examined.

References

1. T. C. Chawla and B. M. Hoglund, *A Study of Coolant Transients During A Simulated Fission Gas Release in a 19-pin Array*, ANL-7651 (Jan 1971).

2. J. M. Robertson, *Hydrodynamics in Theory and Application*, p. 155, Prentice-Hall, Inc., Englewood Cliffs, New Jersey (1965).

3. T. C. Chawla and B. M. Hoglund, *Pressure Distribution for Axisymmetric Two-Dimensional Flow in a Plenum During Coolant Expulsion*, submitted to J. Nucl. Science and Engr. for publication.

4. S. Cohen, Idaho Nuclear Corporation, personal communication (May 1970).

5. L. Baker, ANL, personal communication (Aug 1970).

6. G. J. Duffy et al., *SNARG ID, A One-Dimensional, Discrete Ordinate, Transport Theory Program for the CDC 3600*, ANL-7221 (Jun 1966).

7. R. J. Armani, *The Argonne Thermal Source Reactor*, ANL-6440 (Mar 1962).

8. G. S. Stanford, *The Codes NURF, COMBO, and TWOSORCE for Processing Foil Counting Data*, ANL-7356 (Aug 1967).

9. J. W. N. Tuyn, *Solid State Nuclear Track Detectors in Reactor Physics Experiments*, Nucl. Appl. *3*(6), 372-374 (Jun 1967).

10. R. Gold, R. J. Armani, and J. H. Roberts, *Absolute Fission Rate Measurements with Solid State Track Recorders*, N. Sci. and Engr. *34*(1), 13-32 (Oct 1968).

11. P. F. Rago, N. Goldstein, and E. Tochilin, *Reactor Neutron Measurements with Fission Foil-Lexan Detectors*, Nucl. Appl. and Tech. *8*(3), 302-309 (Mar 1970).

12. C. D. Flowers and L. H. Gerhardstein, *Analog-Hybrid Dynamic Simulation of the FFTF Reactor and Heat Transport System*, BNWL-707 (Apr 1968).

13. Roger Carlson, ANL, personal communication (Apr 1970).

14. *H_2O-0367-2, System/360 Continuous System Modeling Program* (360A-CX-16X) Users Manual, IBM.

15. E. P. Hicks and D. C. Menzies, "Theoretical Studies on the Fast Reactor Maximum Accident," *Proc. of the Conf. on Safety Fuel and Core Design in Large Fast Power Reactors, Oct 11-14, 1965*, ANL-7120, pp. 671-685.

16. W. R. Wise, Jr. and J. F. Proctor, *Explosive Containment Laws for Nuclear Reactor Vessels*, NOL-TR-63-140 (Aug 1965).

17. *LMFBR Liquid Metal Fast Breeder Reactor Program Plan, Vol. 10, Safety*, WASH-1110 (Aug 1968).

Nuclear Safety Research and Development--LMFBR Safety

VIII. FUEL DYNAMICS STUDIES IN TREAT*

(C. E. Dickerman)

Overall scope. Studies are being made of fast-reactor fuel and coolant behavior under transient conditions associated with fuel failure.[1] The study consists of in-pile experiments in the TREAT facility[2] and the necessary analytical and engineering support. These experiments are directed primarily to the study of fuel and coolant movements accompanying fuel-element failure. Information concerning many other phenomena (such as prefailure movements, secondary movements, mechanisms of failure, fuel-coolant interaction, coolant ejection, and pressure generation in both fuel and coolant) is also obtained in the course of these tests. These studies include the testing of both fresh and preirradiated fuel.

Mathematical models are being developed or verified, on the basis of the experimental results, for use in LMFBR accident analysis.

The development, procurement, use, and upgrading of experimental apparatus consistent with applicable codes, standards, engineering and operating procedures, quality control, and quality assurance procedures are significant parts of this activity.

Transient In-pile Tests with Oxide Fuel

Scope. In-pile experiments are conducted, in support of near-term reactors, on oxide-fuel behavior under transient heating, including: movements prior to failure, mechanisms of failure, movements associated with failure, secondary movements and the degree of coherence in their occurrence, and the energy transfer from fuel to vaporizing coolant under conditions approximating actual core-channel geometry. This work

*For references for this chapter, see p. 272.

is coordinated closely with TREAT autoclave experiments on Fuel-Coolant Interactions and with the out-of-pile and in-pile Coolant Dynamics studies. Consulting services are provided, as needed, for related safety programs.

Summary. Safety experiments began with five tests (E1, E2, E3, H1, and H2) on the behavior of oxide fuel under transient heating in a flowing-sodium environment. The experiments, with Mark-II loops[3,4] in TREAT, consisted of survey-type tests designed to provide guidance for the analysis and planning of future experiments. Results demonstrated the capability of flowing-sodium coolant to protect cladding against meltthrough under some conditions, provided checkpoints on conversion of thermal energy in the oxide (both unirradiated and irradiated) into kinetic energy in a flow-channel geometry permitting sodium expulsion and reentry, and illustrated the role of axial heat transport by flowing sodium in sample response to a power transient.

Checkout Tests E1 and E2 on Mark-II-loop experiments on oxide-fuel movement during a power excursion. Experiments E1 and E2 were the first TREAT-loop tests performed using oxide fuel. Both experiments used the prototype Mark-II loop, developed specifically for safely performing destructive tests on oxide fuel pins in flowing sodium.[4]

Test-sample design for the experiments was based on that for 19 oxide pins under irradiation in EBR-II in the first subassembly for unencapsulated oxide pins, X040. The TREAT pin consisted of a stack of 13%-enriched UO_2 pellets of 90% smeared density, approximately 27.9-cm long, inside a Type-304 stainless-steel jacket with 0.737-cm OD and 0.635-cm ID. A plenum space, 11.4-cm long, was inside the cladding above the fuel stack. A spiral spacer wire, 0.14 cm in diameter, was

wound around the jacket. The test pin inside the test section was surrounded by a ring of six dummy pins (hollow jacket tubes), to mockup the space in a real cluster that would be available for fuel-coolant mixing.

Radiochemical analyses of a test pin from a calibration run inside a Mark-II loop yielded a calibration of 3.45 J/gm-UO_2-MW-sec of TREAT energy.

Test E1.[5] Test E1 was the checkout Mark-II-loop TREAT experiment. TREAT produced a sample energy input of 1732 J/gm UO_2 in the E1 power burst with 0.27-sec width at half-maximum. This sample energy input is approximately 34% greater than required for oxide melting under adiabatic heating. Loop temperature at the start of the transient was 400°C, and sodium flow through the test section was approximately 3.8 m/sec.

Analyses have been performed using the SAS1A code system. The heat-transfer module predicts, depending on axial position, a maximum sample melting of 78 to 80%. Plastic strain of the cladding was calculated using the fuel-deformation module of the code, assuming neither axial motion nor restraint of the molten fuel. Cladding failure due to oxide expansion, with a 4% plastic strain, would correspond to an energy input equivalent to 1610 J/gm UO_2 (above central fuel melting). The maximum rise in the midpoint cladding and the bulk coolant temperatures were calculated to be about 370 and 200°C, respectively. These temperatures were near the top end of the active part of the fuel pin.

No flow or pressure events were recorded by the loop instrumentation. Maximum outlet coolant rise was approximately 68°C. Transient

instrument data are shown in Fig. 85. The rapid drop in both inlet and outlet flow resulted from shutdown of the annular linear-induction pump (ALIP). "Pressure" signals shown for the inlet and outlet pressure transducer have the characteristic shapes of response of these two sensors to the high transient radiation levels in TREAT and qualitatively were in satisfactory agreement with the responses recorded in preliminary transients.

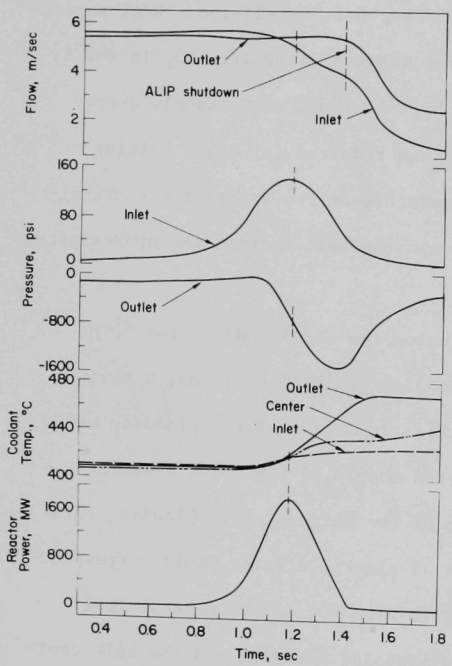

Fig. 85. Transient Data from Checkout-1 Oxide Meltdown Experiment in the Mark-II TREAT Sodium Loop (Transient 1281). Sample fission energy of 1.72 x 10^3 J/gm. ANL Neg. No. 113-2618, Rev. 1.

Posttransient neutron radiographs showed no fuel in the coolant channels, but extensive axial movement of molten fuel inside the fuel jacket. Individual oxide pellets were clearly shown in the pretransient radiographs, but no remnants of the pellet structure were apparent after the experiment. The maximum radial extent of fuel melting, as determined from maximum radial fuel voids, was in good agreement with the

SAS1A calculations for temperature. Figure 86 is a sketch of the posttransient fuel radiographs. The voids and the presence of some fuel at the top of the cladding show that extreme motion of fuel did occur. After radiography, the unfailed pin was removed from the loop and returned to the ANL Illinois hot laboratories for inspection. Postmortem inspection confirmed the radiographic data and showed that molten fuel had come into contact with the cladding, "wetting" it and solidifying. Meltthrough of the cladding did not occur. Pre- and postexperiment measurement of the cladding diameter showed no appreciable cladding strain. An upper limit of 0.3% strain was assigned, conservatively, to the measurement.

This experiment produced results significantly less severe than anticipated. Relief of oxide loading of the cladding by extreme axial motion of the fuel was clearly demonstrated. Absence of any extreme deformation of the cladding during the transient indicates that the axial motion of the fuel in an unrestrained-fuel case should be included in future analyses. The large discrepancy in the calculated and observed coolant temperatures was due to test-section steel adjacent to the test pin, and cross-channel mixing with the sodium around the dummy pins.

Test E2.[6] The loop experiment described above gave guidance on modeling fuel failure, demonstrated the effectiveness of axial motion in relieving radial loading of cladding, and gave support to calculations indicating that the flowing sodium coolant can effectively cool cladding during some meltdown incidents. However, it did not provide guidance on the consequences of oxide meltdown into flowing sodium with transient vaporization of the coolant, impact-

pressure pulses, expulsion, and reentry, like those found in earlier loop experiments on meltdown of metal fuel. Consequently, a backup pin was modified and loaded into a test section as the second checkout, or E2 experimental sample, for a run at higher energy. The modified pin contained a natural-UO_2 pellet at the top of the 13%-enriched fuel stack to prevent axial meltthrough. Then a 5-cm-long steel rod was placed between the natural-oxide pellet and the steel retainer spring to provide inertia to resist upward axial movement. These two changes were specified in collaboration with the group working on the Accident Analysis program to reflect some typical features of the current FFTF fuel design, while avoiding rigid axial restraint.

In the E2 checkout test, the test pin, as before, was contained inside a ring of dummy pins, and the initial sodium flow was about 4 m/sec through the test section. TREAT supplied about 2.59×10^3 J/gm of oxide, in a power pulse of about 0.24-sec half-width. Failure was marked by anomalies on the three (inlet, center, and outlet) test-section thermocouples, on the two (inlet and outlet) flowmeters, and on the two (inlet and outlet) pressure transducers.

Figure 87 shows the instrument data from the transient. Shown are output from test-section inlet and outlet flowmeters, inlet and outlet pressure transducers, and thermocouples at inlet, outlet, and center. The large relatively smooth signal for the outlet (variable reluctance) pressure transducer is the radiation response of the instrument. Superimposed on this signal are three prominent spikes. (Figure 87 shows the radiation response of the outlet transducer in the correct polarity. The E1 data graph, Fig. 85, has the outlet transducer response negative.) The maximum pulse recorded by either transducer was only about 35 atm.

Fig. 86.
Artist's Rendering of the Posttest Neutron Radiographs of the E1 Test Pin, Showing Extensive Movement of Molten Fuel Inside the Unfailed Cladding during the Transient. ANL Neg. No. 113-2996.

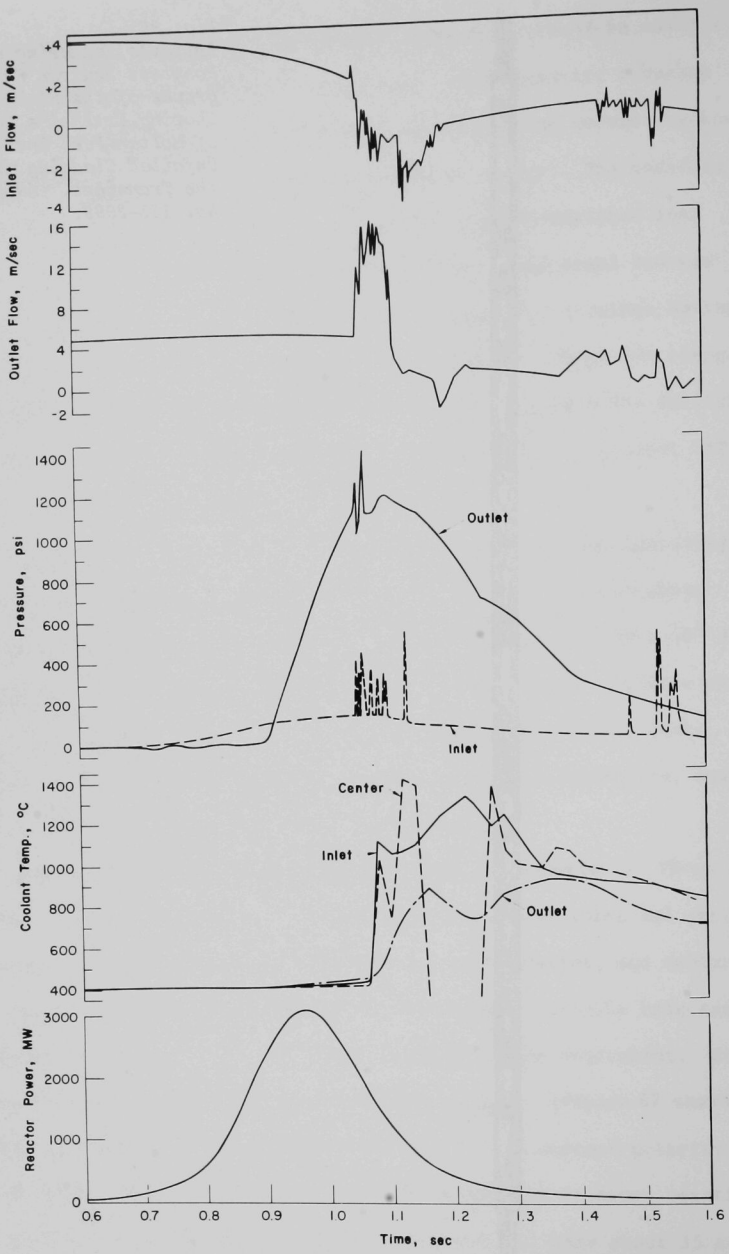

Fig. 87. Instrument Data from Checkout-2 Mark-II Loop Experiment (Transient 1283). ANL Neg. No. 113-2997, Rev. 1.

Conversion of thermal energy to kinetic at the time of failure can be estimated from the flowmeter data. Detailed analysis of the work done in accelerating coolant out of the test section, in compressing the gas in the plenum space at the top of the loop,and in forcing coolant back against the pump head indicated the total kinetic energy resulting from fuel failure was $\sim$100 J. Total energy added to the pin (above the reference level of 400°C) at the time of failure was about 1.88×10^3 J/gm. Thus, the energy conversion was less than 0.1%. Neutron radiographs taken of the loop after the transient did not reveal any detectable fragments of fuel, indicating that extreme dispersal occurred.

After sufficient cooling time to permit shipping the loop containing the failed pin, the prototype Mark-II loop was returned for removal of the test sample specifically developed for operations with the loops.[7] No difficulty was experienced with the glovebox transfer port or its accessories during the withdrawal operation. The loop was not contaminated or damaged.

No external damage to the test section was visible, but the top of the center (fueled) pin had moved upward about 1.5 in. The spades of all pins were still attached in place at the bottom of the fuel holder, but the top portion of the fuel-pin cladding slid out easily; the center portion had melted.

After the test section was removed, the loop was moved to the sodium scrubber for recovery of the sodium and fuel residues. It had been noted previously that it was not possible to create sodium flow in the loop, so it was thought that the top pump flange was blocked by meltdown products. However, with the test section out, flow was attained, indicating that the blockage was in the region of the test section.

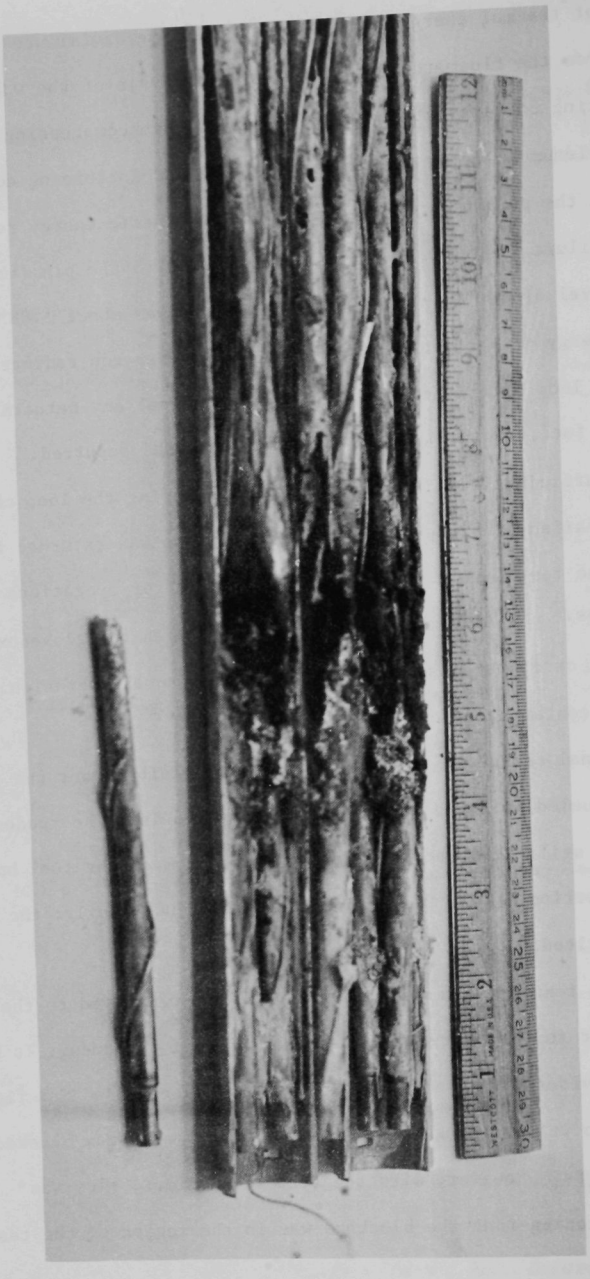

Fig. 88. View of E2 Test Section after Being Cut Open during Posttransient Inspection. ANL Neg. No. 900-98A.

The test section was slit open in the glovebox. Figure 88 shows the test section after being cut open, showing the two halves of the split section. Figure 89 indicates the orientation of the test pin in Fig. 88, prior to cutting. Extensive fuel fines were found inside the test section, tightly packed between the cladding-tube remains of the central fueled pin and the surrounding ring of six dummy pins. The appearance was in good agreement with the hypothesis that packed fines had clogged the test-section flow channels. Careful reexamination of the post-TREAT test-section neutron radiograph disclosed some white streaks (originally identified with cladding and minor steel structure such as flow guide wires and pin spacer wires) that could represent fuel in the flow channels. Examinations revealed no evidence for

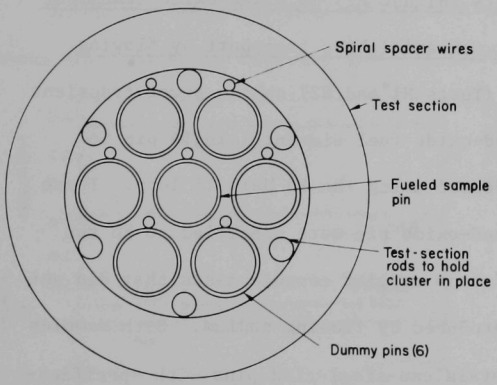

Fig. 89. Orientation of Test Pins for E2 Test Section. ANL Neg. No. 900-292, Rev. 1.

pressure failures. All cladding ruptures--both in the fueled pin and the dummy pins--appear to be simple meltthroughs.

During the loop-reclamation operations, the loop was examined carefully over its entire length; fines were discovered throughout the loop, including between the flanges for the pressure-transducer stand-off subassemblies (no fines were outside the stainless-steel O-rings--

this refers only to the space within the sealed loop envelope), and the short loop drain line at the bottom loop bend. The annular linear-induction pump was sacrificed during reclamation operations, but the loop proper appears to be in satisfactory condition. It will be reoutfitted and prooftested as part of the schedule of regular operations. The sample remains are being examined in detail.

Test E2 showed that the top internal structure added after E1 did not lower the sample failure threshold below the E1 energy level. Although sharp pressure spikes and coolant voiding occurred, the energy conversion from thermal energy to work was very low. However, very extensive subdivision and movement of the oxide resulted from the fuel failure.

First two Mark-II-loop tests (H1 and H2) on mixed-oxide transient fuel-element failure threshold with axial heat transport by flowing sodium. The first experiments (Tests H1 and H2) on the power-transient threshold for failure of a mixed-oxide fuel element (single pin in FFTF-cell simulation) were conducted using the B3 Mark-II loop. These first loop experiments on a mixed-oxide pin were specified to be run close to failure, as a "bridge" from earlier capsule tests that did not have the axial heat transport produced by flowing sodium. Both samples were 0.230-in.-OD. Type-316 stainless-steel-clad pins with specifications similar to those of the FFTF fuel (one pin was actually supplied from the UKAEA fuel development program for the Prototype Fast Reactor). Sodium flow through the test section was 4 m/sec. Because neither experiment was run to investigate the postfailure fuel-movement regimes, the sample was contained inside an adiabatic flow tube that simulated the cell-like environment of a single pin inside an FFTF or PFR subassembly.

Because both test pins were highly enriched, the loop was run using a thermal-neutron filter.[8]

Test H1. Test H1 was run using PFR test pin 726. Figure 90 shows the test data. The transient, of 975 J/gm of oxide, carried the sample sufficiently close to the failure threshold to produce some local boiling (see outlet-flowmeter and pressure-transducer traces), although gross channel burnout did not occur and the pin did not fail. Calculated and measured outlet coolant temperatures were in good agreement, as shown in Fig. 91. The comparison of Fig. 91 is the first true test of the SAS1A transient-temperature module, including the detailed calculation of change in the fuel-cladding gap heat-transfer coefficient as the fuel heats up and the gap contracts.

After the test, the test section was removed from the sodium loop using the Fuel Cycle Facility (FCF) at EBR-II. Analysis of samples

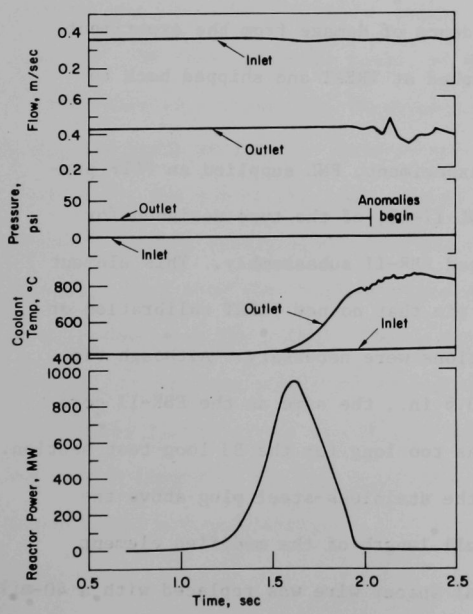

Fig. 90. Transient Data for the Fuel-failure-threshold Test H1 (Transient 1298).

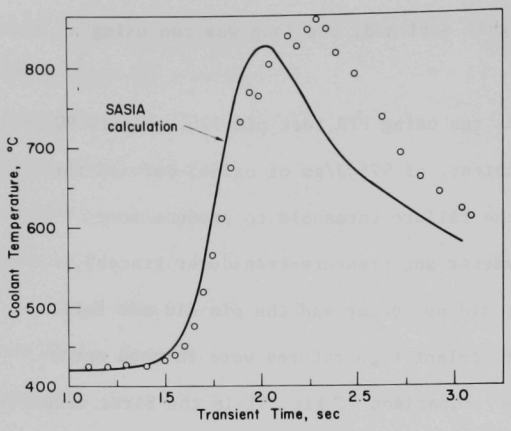

Fig. 91.
Comparison of Calculated and Experimental Transient Outlet Coolant Temperatures from Test H1.

from the loop plenum gas and sodium, before removal of the test section, indicated no detectable fission products. An inert-gas adapter tube was attached to the loop head for the removal of the test section so that the hot sodium was not exposed to air. After an overnight alcohol rinse of the test section, the pin was removed. Visual inspection and radiation monitoring found no evidence of damage from the experiment. Then the pin was neutron-radiographed at TREAT and shipped back to Illinois for further examination.

Test H2.[9] For the H2 experiment, PNL supplied an FFTF prototypical mixed-oxide element, PNL-17-42, of the type designed for use with the Mark-E37A instrumented EBR-II subassembly. This element is similar enough to the H1 test pin that no new TREAT calibration or significant fuel-holder modifications were necessary. Although the active length of PNL-17-42 was 13.5 in., the same as the EBR-II core height, the overall pin length was too long for the B3 loop test section. The pin was modified by cutting the stainless-steel plug above the upper plug weld so that the overall length of the modified element was reduced to 31 in. The initial spacer wire was replaced with a 40-mil

spacer, so that the pin could fit into the circular flow channel that mocks up the flow "cell" of a single pin in an FFTF fuel subassembly.

The principal goal of Test H2 was to carry the test pin just past the failure threshold. On the basis of preliminary SAS1A calculations, a TREAT transient was specified that would produce a sample energy input of 1435 J/gm of oxide. The actual energy input for H2 was 1485 J/gm. Initial flow was 7 m/sec. Pretest SAS1A calculations for a comparable transient, with a sample integrated power of 1528 J/gm, predicted coolant boiling in the test section at 85% of the transient energy input with the sample failing by melting of the cladding at 90% of the energy input. The experimental results verified the reliability of that analysis. Failure, which was indicated by flow, pressure, and temperature anomalies, occurred at approximately 85% of the transient energy input. After the test, it was found that flow through the test section could be reestablished. Figure 92 shows the transient data for Test H2. The first pressure pulse, of about 8 atm, precedes immediately a rapid rise in test-section thermocouple temperature to 1100°C, before going off scale at 1400°C. This thermocouple, which was located axially 1 in. below the top of the fuel column, apparently detected hot fuel. Posttest neutron radiographs have been taken of the pin in its test section. They show that failure occurred at the top of the fuel column, in agreement with the calculations. Further, about 3 in. of fuel are missing from the top of the column and the optical densities of the radiographs indicate that significant quantities of fuel were lost over the entire length of the test pin. The test section will be removed and returned for examination.

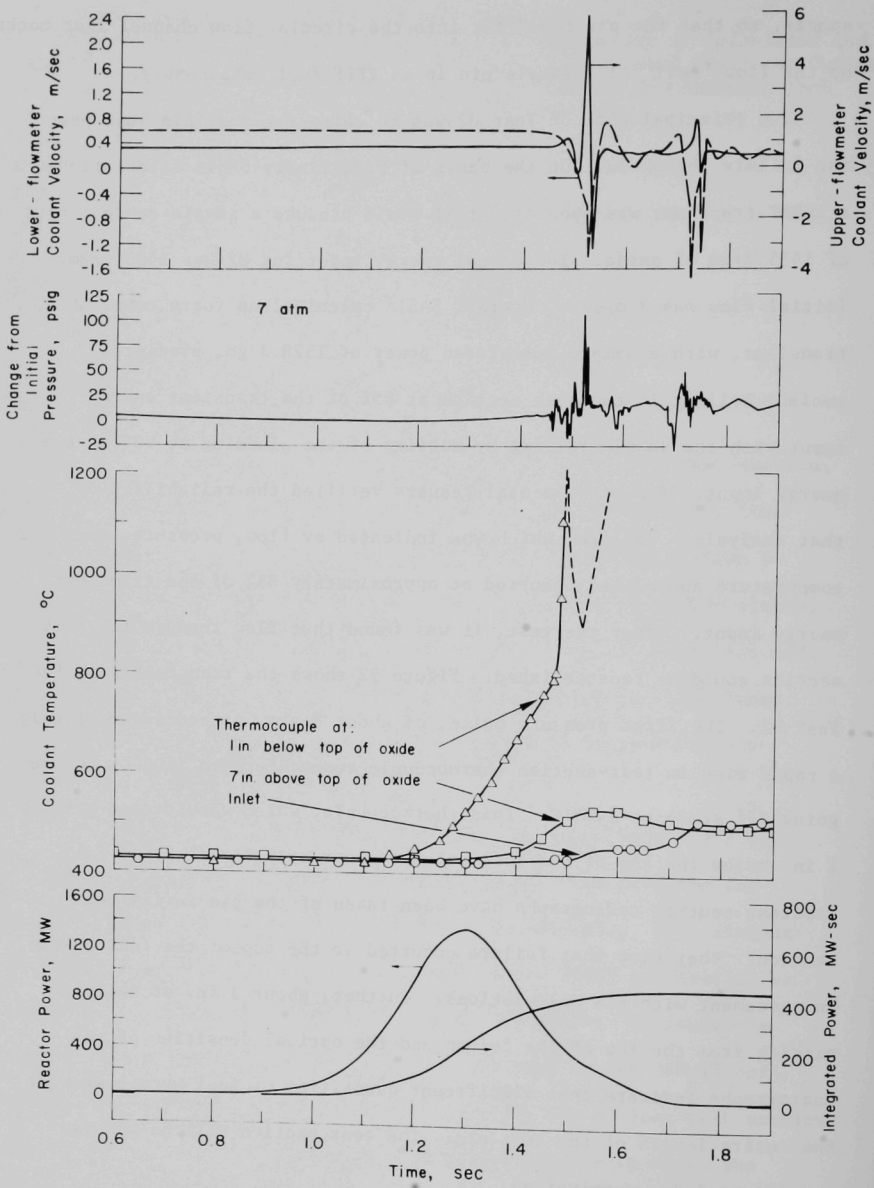

Fig. 92. Transient Data for the Fuel Failure Threshold Test H2 (Transient 1317). ANL Neg. No. 900-409, Rev. 2.

First Mark-II-loop test (E3) on fuel-movement failure of irradiated oxide pins during a power excursion.[10] This experiment, designated E3, was the first Mark-II-loop test on meltdown of preirradiated fuel pins. It was a survey experiment, in which the pins were failed near the peak of the TREAT power transient, with the objective of providing an early indication of the severity of events associated with failure of preirradiated oxide fuel elements when subjected to a severe overpower transient in flowing sodium. The fuel sample used in the E3 experiment consisted of three gas-bonded UO_2 pins, having a 14.5-cm-long stack of fuel cylinders, 0.381 cm in diameter, with a cladding OD of 0.442 cm and ID of 0.396 cm. Overall length of the pins was about 22.5 cm. The nominal burnup of the pins was 6 a/o. The B1 Mark-II loop was used for this test.

The pins were originally fabricated of 13%-enriched UO_2 to minimize internal power depressions during steady-state irradiation, while maintaining sufficiently high sample power generation in TREAT to meet experimental objectives. Nominal burnup of the pins was 6 a/o, resulting from irradiation in the Materials Testing Reactor. Destructive examination of an identical pin has been reported,[11] as have results of a TREAT transient performed on another identical pin in the absence of coolant[12] to permit direct observation by high-speed photography.[13,14] The destructive examination indicated that the fuel pellets had become annular, with a typical inner diameter of 0.058 cm and outer diameter of 0.388 cm. Cladding dimensions were unchanged by irradiation. The estimated fission-gas volume for 100% release from the oxide is 21.4 cm^3 (STP); 23% release was found in the destructive examination.[6] Pretest fission-gas pressure was estimated to be about 7.7 atm at room temperature.

The E3 test section maintained the pins in an equilateral triangular geometry and incorporated spacer rods to simulate adjacent fuel pins. Five coolant-temperature thermocouples were provided; four were at the outlet of the fuel section about 1/4 in. above the tops of the pins. These were in addition to the standard loop instrumentation of pressure transducer and flowmeter at both inlet and outlet of the test section. Due to the lack of a licensed shipping cask large enough to ship a loaded Mark-II loop, the test section was loaded into the loop by semiremote means using an auxiliary loading fixture.

For the E3 test, the initial sodium temperature was 400°C, and the initial coolant velocity past the test pins was 4 m/sec. A sample energy input of about 2100 J/gm was realized, producing evidence of failure near the peak of the power transient. Sodium expulsion and transient inlet flow reversal occurred. Pressure pulses of about 56 atm maximum were recorded. Figure 93 shows the transient data. Posttest neutron radiographs showed no detectable fragments of oxide pellets in the test section, indicating that extensive oxide fragmentation had occurred. However, the conversion of thermal energy to work was relatively small. The loop has not yet been returned for postmortem examinations.

Future program. The initial TREAT experiments to provide safety base technology for near-term LMFBRs, such as FFTF, will continue. The first experiments will be performed on loss of flow, effects of release of small amounts of molten fuel, modeling of fuel slumping after loss of coolant, and irradiated mixed-oxide failure threshold with axial heat transport by flowing coolant. Work will continue on fuel movement and failure resulting from a power excursion.

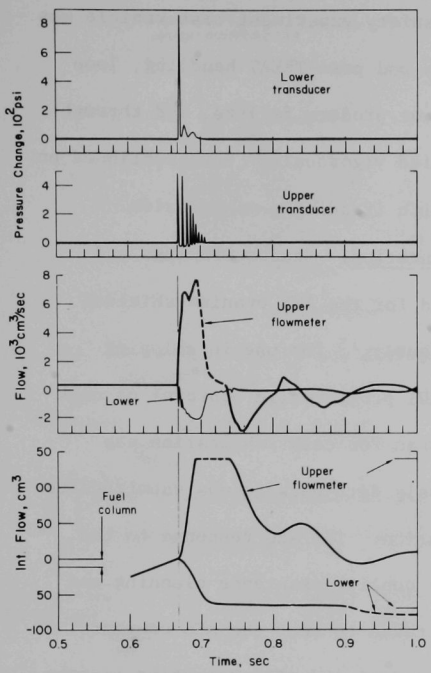

Fig. 93.
Transient Data from Irradiated-oxide-fuel Test E3 (Transient 1322). ANL Neg. No. 900-474, Rev. 3.

Experimental Support

(L. E. Robinson)

Scope. Basic experimental capabilities are being provided for the transient in-pile experiments with oxide fuel (see p. 231), except that fuel specimens are supplied by RDT. Loops, capsules and the shipping cask are being developed and fabricated. Also included are glovebox fabrication, core accessories, and support of work to enlarge the capabilities of experiment instrumentation. Throughout the development and fabrication, use is made of applicable codes and standards, established engineering procedures, and quality-control and quality-assurance procedures. Consulting services are provided as needed to related safety programs.

Summary. Mark-II-loop use as a safety experiment test vehicle was demonstrated through TREAT experiments and post-TREAT handling, loop reuse following a transient that did not produce failure, and through operations with a sample that had failed vigorously. Work continued on providing capability for operations with irradiated mixed oxide.

Shipping-cask procurement documentation. Vendor drawings and associated documentation were prepared for the ANL uranium-shielded shipping-cask design, described previously,[15] for use in shipping Mark-II TREAT loops, in accord with RDT programmatic approval of cask procurement. The quality-assurance plan for cask fabrication was completed. The cask design-and-analysis data package was submitted to the AEC for approval to begin fabrication. The AEC response to the cask data package specified action on quality-assurance planning and additions to the design. Action was taken to meet the AEC comments. The cask closure-flange assembly was redesigned, incorporating energy-absorbing structure to provide greater capability to meet a drop criterion; a diffusion barrier was specified between the uranium shielding and the steel structure to satisfy concern over possible steel-uranium eutectic formation during exposure to a fire; provisions were made to facilitate the future addition of a vent and drain if they should be required; and integral "legs" were added to the cask to eliminate the need for a separate skid to hold the cask during shipment. Figure 94 shows the revised cask configuration. Figure 95 shows the cross section of the cask package. In addition, the quality-assurance plan was augmented and rewritten in accord with RDT standard F2-2T. The complete new package was under final review at the end of the report period, before submittal to AEC for approval.

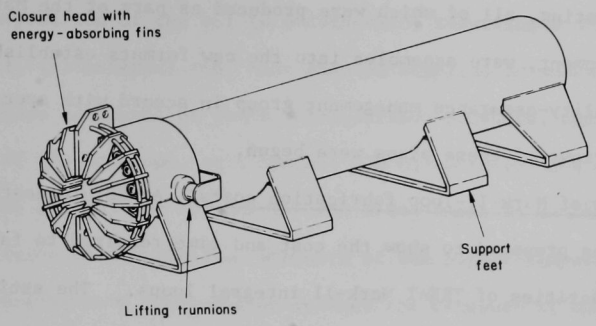

Fig. 94. Configuration of the Revised Shipping Cask. ANL Neg. No. 900-367, Rev. 1.

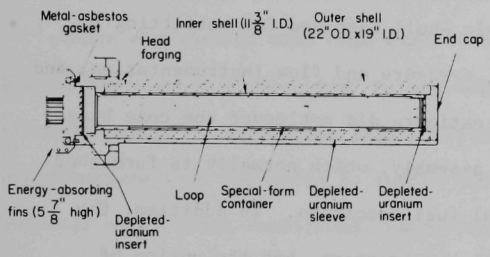

Fig. 95. Cross Section of Shipping-cask Package. Overall length is 128 7/8 in. ANL Neg. No. 900-366, Rev. 1.

To use the shipping cask, it will be necessary for the Mark-II loop (or other experiment) to first be sealed inside a "special form" container (see Fig. 95). A detailed review was made, analyzing the loop shipping container used for shipping the prototype loop to TREAT for the first (E1) test. This review showed that, with a minor change in the closure-flange design, the loop shipping container would qualify for service as a special-form container or as a Spec. 7A container for shipping Type-A quantities of "nonfissile" radioactive material. The change was made.

Revision of Mark-II loop quality-control package into new QAM format. The detailed quality-control package of the loop for Mark-II material specifications, fabrication procedures, inspection procedures, inspection specifications, outfitting procedures and inspections, and

the loop testing, all of which were produced as part of the Mark-II loop development, were assembled into the new formats established by the ANL quality-assurance management group in accord with specification F2-2T. Reviews of these plans were begun.

Review of Mark-II-loop fabrication costs. At RDT request, an estimate was prepared to show the cost and time required to fabricate various quantities of TREAT Mark-II integral loops.[4] The estimate was based on using prior experience in fabricating these loops at ANL, and projected FY 1971 labor rates and material costs. The estimate showed the cost for fabricating the basic shell loop and for outfitting a typical loop with trace heaters, pressure and flow instrumentation, and other ancillary equipment. The estimate did not cover the cost breakdown for making the fuel-holder assembly, which normally is furnished by the user with the experimental fuel specimens. In addition, the user, depending on the experiment requirements, has the option of either adding or removing subsystems from the basic shell loop, which also would affect the cost.

Safety aspects of the elevated-temperature behavior of DC-200 silicone cooling oil used with the Mark-II loop. DC-200 dimethylpolysiloxane (silicone) oil is used as an auxiliary coolant for the Mark-II sodium loop, to cool the Annular Linear Induction Pump (ALIP) and the loop freeze plugs. As part of the loop development, an analysis was made of the chemical stability of the silicone oil under "operating accident" conditions of (1) rupture of silicone lines with dispersal of silicone on hot loop parts, and (2) silicone flow stoppage in the ALIP. After review of the available chemical data, it was concluded that the oil presented no hazards of overpressure or overheating of loop parts due to silicone decomposition and combustion for the following reasons:

(a) the decomposition of the oil is endothermic, requiring a heat source to sustain it, (b) external heat must also be supplied to sustain combustion of these compounds or their decomposition products, and (c), the surface of the loop can, at a nominal 200°C, represent the coldest portion of the system, and as such affords a condensation surface for the decomposition or distillation products of the higher-temperature oil--consequently, this condensation reduces the pressure of the loop system. It was concluded under these assumptions that the pressure from the decomposition of the coolant oil would be less than 15 psi.

These conclusions were supported by results of a test performed during the testing period prior to the high-pressure prooftest of the prototype loop.[16] During the safety review of the E1 experiment, the experimenters were requested to supply additional information on silicone behavior under these conditions. Accordingly, a simple quantitative survey experiment was performed on pressure generation by silicone oil in a closed system. A given quantity of silicone was heated in a closed copper tube with argon cover gas above the silicone surface. The nominal room-temperature volume of the silicone for each run was 36.9 cm^3, and the nominal room-temperature value of argon was 73.9 cm^3. The silicone occupied a cylindrical volume about 15 cm long, with a thermocouple well extending down from the top surface half way (i.e., to 8 cm from the bottom of the cylinder). To effect good contact between the thermocouple and well, some silicone oil was added to the well. The thermocouple was always wet after removal from its well after each run, even though some smoking of the oil in the well was noted at temperatures above 340-400°C. Pressures were measured as a function of oil temperature during each run. The pressure of the compressed heated

cover gas was computed and subtracted from the total to obtain the partial pressure of the hot silicone. Pressures were measured after posttest cooling. After the last run (maximum temperature of 473°C) the posttest pressures were measured to be in excess of the original argon pressure of 1 atm by only 1.2, 1.0, and 0.6 psi at cooling times of 1.5, 2, and 18 hr, respectively.

These tests showed that the pressure due to the vapor or decomposition products from the ALIP coolant was about 25 psi at a temperature below 425 to 473°C. Consequently, the total pressure that could be attributed to the vapor and decomposition products from the pump-cooling oil was moderate for the temperatures studied.

Thermal-neutron filter for Mark-II-loop experiments.[8] A large radial power depression is produced in a mixed-oxide TREAT test pin by the thermal-neutron spectrum of the reactor. This power depression is sizable for a single highly enriched pin even when proper allowance has been made for the neutronic effects of the loop. For TREAT power pulses having a duration of the order of or less than the thermal time constant for heat transfer from the pin, this power depression can cause a sizable departure in sample temperature distribution from that which would be produced in an actual fast-reactor incident. Accordingly, in advance of the H1 test, provisions were made for a thermal-neutron filter that would remove the thermal-neutron flux on the test pin. A 1/v thermal-neutron-absorbing shield was fabricated as an inner liner to fit within the outer containment can of the Mark-II loop. The liner was designed as a piece of interchangeable hardware to be used in calibration runs and with actual test loops, as needed.

The shield was constructed by coating a substrate, consisting of a 16-mesh 20-mil wire screen spotwelded to the 25-mil stainless-steel

liner can, with a mixture of equal parts by weight of B_6Si and Pyromark paint. Several coatings were applied. After the last coating, the surface was polished evenly down to the grid wires (which served both as a reference marker and a mechanical reinforcement for the B_6Si). Then the shield was baked and coated with a protective surface layer of Pyromark paint.

Measurements of epithermal-neutron transmission, both on preliminary small samples as well as on the completed shield, were used to determine the "effective B_6Si thickness" at an assumed density of 1.7 gm/cm^3 (70% theoretical density). The small samples had an effective B_6Si thickness of 22.4 mils, while the completed liner had an effective thickness of 19 mils. Neutron-transport calculations indicated that such a Mark-II TREAT-loop liner would yield a ratio of H1 sample centerline to maximum TREAT power density of about 65 to 1. Measurements of thermal-neutron transmission indicated uniform surface coatings for the samples as well as for the completed shield. Analyses were performed to determine the in-pile thermal heating of the shield under various conservative assumptions. The heating from the n,α reaction is small in light of the high-temperature stabilities of the B_6Si and the Pyromark binder.

Suppression of sodium-slug impacts in the Mark-II loop.[17] Before test E2, modifications were made to the upper part of the loop test-section subassembly to reduce the potential for loop damage from "sodium hammer" under certain limiting case conditions of transfer of thermal energy to kinetic energy using sodium in the vicinity of the test pin as a working fluid (see p. 262).

Stress analysis of Mark-II loop with dump tank. The B3 Mark-II TREAT loop, used for the first loop experiment (H1) on mixed-oxide-fuel

meltdown in TREAT, was the first of the Mark-II loops to be equipped with a dump tank. A stress analysis was performed to show that the loop design with dump-tank piping was acceptable from the standpoint of thermal stresses in both normal operation and in the event the loop rupture disk breaks, dumping hot sodium into the blowout line.

The analysis of the dump piping, comprised of the blowout line from the loop proper to the safety tank, the safety tank, and the fill and overflow lines from the tank to the loop proper, results in a conservative estimate of the system stresses, because the model used was two-dimensional, while the actual loop is three-dimensional and more flexible. The smaller 5-ft-long overflow tube was neglected because of its high flexibility. Throughout the analysis, the rectangular valve bodies and their weldable port projections were considered to be essentially rigid because of their massive geometry.

Two cases were considered for analysis. Case I corresponds to the steady-state condition of the Mark-II loop, with the blowout line maintained at 205°C, the mechanical valve and lower fill line at 52°C, and the burst disk intact.

Case II serves as a limiting calculation, with the blowout line at 900°F, and the temperatures of the remainder of the auxiliary loop unchanged. This case corresponds to the limiting condition to be realized in the event that an overpressure ruptures the burst disk and discharges the molten sodium from the loop into the dump tank.

In both cases, the highest stresses occur at the segment of the auxiliary loop containing the mechanical valve in the fill line. For the steady-state Case I, the maximum stress calculated was 9,407 psi at the fill-line valve, with a stress of 6,370 psi at the rear of the burst-disk

housing, and a stress of 3,401 psi at the weldment of the fill line to the lower bend of the loop proper. None of these stresses is comparable to the yield strength of the stainless steel; hence, there would be no distortion in the system as a result of normal steady-state operation of the loop at temperature. In Case II, the resultant stresses calculated were 33,317 psi at the fill-line valve, 21,563 psi at the burst-disk housing, and 11,510 psi at the fill line-loop weldment.

The stresses realized in the auxiliary system in Case II are secondary stresses resulting from the thermal expansion of the blowout line during a thermal excursion from 400°F to the temperature of the loop sodium. Because the valve releasing the sodium from the loop into the blowout line is a simple rupture disk, the excursion is not a cyclic operation.

The ASME Boiler and Pressure Vessel Code,[18] for cases not requiring analysis for cyclic operation, specifies that the limit of stress intensity for secondary stresses plus bending is to be defined as $3S_m$, where $S_m = [(S_m \text{ @ } 400°F) + (S_m \text{ @ } 900°F)]/2 = [19,400 + 14,000]/2 = 16,700$ psi. Thus, $3S_m = 50,100$ psi, and the Case-II stresses are acceptable.

The USAS B31.1.0 Power Piping Code[19] specifies that the allowable stress, S_A, for cyclic operation must not exceed $S_A = f(1.25S_c + 0.25S_h)$, where S_c is the allowable stress as tabulated at the minimum temperature (100°F), S_h is the allowable stress at the maximum temperature (1000°F), and f is stress-range reduction factor for cyclic operation (f = 1, for less than 7000 full temperature cycles). This yields $S_A = (1.25)(18,750) + (0.25)(14,000) = 23,438 + 3500 = 27,000$ psi. Hence, the stress at the burst-disk housing ($\sigma_H = 21,563$ psi) is well below the limiting stresses allowed under both codes.

Prooftests of B1, B2, and B3 loops for use in Tests H1, E3, and L1. Mark-II Loops B3, B1, and B2 were readied for use in Tests H1, E3, and L1, respectively. Loops B3 and B1 were prooftested; Loop B2 was readied for its prooftest to be conducted early in FY 71.

Before experimental use in the meltdown studies of fast-reactor fuels in the TREAT facility, each of the Mark-II integral sodium loops is subjected to a prooftest, as prescribed by the ASME code.[18] For this test, the loop must be fully outfitted with external heaters, annular linear-induction pump, cooling lines, insulation, and sensor circuits, to permit pressure testing the loop to 125% of its rated pressure, while operational at the device's rated temperature. The pressurization is pneumatic, using high-purity argon gas. During the test, the contained sodium is pumped through the loop proper at a low flowrate, sufficient to ensure the establishment and maintenance of the distribution of temperature to be realized during experimental operation of the facility.

During the pressurization of each loop, the argon pressure was raised from the full-bottle value by means of the DYNAIR gas-pressure intensifier. The full pressure of a bottle of argon gas was applied to the dump tank, to prevent pressuring the burst disk when the test pressure exceeded the disk-rupture rating. The differential pressure across the burst disk between the loop and the dump tank was held to a maximum of 3000 psig. The first prooftest of the B1 loop was terminated prematurely at a test pressure of 4500 psi when the rupture disk burst at a differential pressure of 2500 psi between loop and dump tank. A new disk was attached to the loop in an installation meeting the full loop quality-assurance specifications of material, welding, and full-

radiography inspection. Then the B1 loop was prooftested satisfactorily at 5000 psi and 538°C.

Pressure transducers for Mark-II loops. At the time of the preparation of the Mark-I Integral Sodium TREAT loops, the pressure transducers considered to offer the best overall characteristics for adaptation to the sodium-filled flow system were unbonded strain-gage bridge sensors. There were several competitive transducers, essentially of the same type, and differing only in the method of strain-gage support within the transducer body. The 1/2- to 5/8-in.-diameter transducers selected were attached to the system by means of a tubular NaK-filled stand-off technique, to provide physical isolation of the sensor diaphragm, and a thermal isolation of the transducer as a whole from the high-temperature environment of the loop.[20]

During meltdown experiments in the TREAT facility using the Mark-I loops, these transducers furnished usable pressure-pulse data,[21] but exhibited spurious electrical signals as high as 40% of full scale as a result of the extreme transient radiation levels.

Thus, for the Mark-II integral sodium loop, a variable-impedance transducer, developed for blast instrumentation and checked in TREAT, seemed to offer the desired properties, including: low radiation sensitivity (∿3% at 10^{16} nvt), high-frequency response (>40 kc, natural frequency), high-temperature rating (600°F, operational), high electrical output (∿40 mv FS), and sodium compatibility (no mechanical coupling).

The variable-impedance model chosen was a standard unit, modified with the inlet nozzle jacketed with a copper radiator, for use with the NaK-filled loop stand-off.

Calibrations of the transducers with NaK eddy-current coupling, and subsequent bench tests, indicated the devices to perform as specified

and predicted. However, in the application of the sensors to the Mark-II loops extreme problems were encountered in calibration, drift, reliability, and shelf life. Further, the very low sensitivity to high transient radiation levels in TREAT shown in trials with a prototype was not sustained in tests with one of the units purchased subsequently for Mark-II-loop use. Accordingly, a used, "obsolete" transducer with well-known out-of-pile characteristics was obtained; this unit was originally designed to resist radiation effects. It is an unbonded strain-gage bridge transducer, similar to the ones used earlier on the Mark-I loops,[20] but with a case having a higher pressure rating than those used previously.

For the E1 and E2 tests with the Prototype Mark-II integral loop,[5,6] the variable-impedance transducer was used at the test-section outlet, and the strain-gage transducer was used at the test-section inlet. The latter sensor showed ∿10% full-scale radiation sensitivity (a small fraction of the sensitivity shown by the other unit: see Fig. 87). This strain-gage sensor proved to be uncomplicated in use, with low sensitivity to thermal gradients, and was run without auxiliary cooling.

Because the inlet transducer on the prototype loop had been replaced in the manufacturer's line by a more "advanced" device, one of the newer transducers was subjected to a TREAT power transient. Although the manufacturer's data showed that this unit had surpassed, in all respects, the earlier model in performance in steady-state nuclear-reactor testing, the new device with its thin-film strain bridge responded to the short-time very high radiation of TREAT with a wildly erratic electrical output signal of extreme amplitudes. Apparently, the

high radiation levels of the TREAT transient caused the thin ceramic substrate of the thin-film strain element to act as a semiconductor, producing successive avalanches of charge between input and output.

Additional models of the older strain-gage transducer were obtained and are now in routine use on the Mark-II loops. These were the transducers used in the H1, H2,[9] and H3[10] tests.

Adaptation of accessories for minimal cave usage of Mark-II loops with irradiated mixed oxide. Work was begun to adapt the cave accessories for minimal cave usage with Mark-II loops. The glovebox operations were checked through the cycle of operations with the prototype loop and the test section from Checkout Test E2. Work was begun to adapt previously used equipment designs and operating procedures with only minor modifications for use in minimal FCF air-cell operations with the Mark-II loop and mixed-oxide fuel.

Future program. Provision of experimental support for the transient in-pile tests (see p. 231) will continue on an expanded basis. Mark-II loops from the FY 1970 stocks will be finished, outfitted, and proof-tested for use. Loops will be provided for use as test vehicles for experiments in early FY 1972. Some loop reuse will be possible. The acquisition of the loop shipping cask will expedite performance of experiments, make possible experiments with previously irradiated mixed-oxide specimens, and permit post-experiment examinations of failed mixed-oxide pins. Capability for cave operations on loops involving irradiated mixed-oxide will be established and used.

Analytical Support

(A. B. Rothman)

Scope. Direct analytical support is provided for calculations used in planning the transient safety experiments (see p. 231) and in analyzing the results. Basic calculational techniques, computer-code modifications for specific experiment applications, and new programming of a minor nature are included. Automation of hodoscope readout and hodoscope data reduction and analysis are also being accomplished.

The end product of the experimental work is verification of predictive mathematical models for fuel-element behavior in transients large enough to cause fuel movement. These models are developed jointly by this activity and the Accident Analysis and Safety Evaluation study.

Summary. Analyses in support of the experimental program included reactor-physics calculations, transient-temperature calculations,[22] and programming analysis for the reduction of data for the fast-neutron hodoscope.[23] Completion of the first oxide loop experiments provided opportunities to check calculations.[24] Problems were apparent in modeling transient heat transfer where transfer to structure was important, but calculations were in good agreement with experiment for the cell-like geometry of a single flow channel.

Evaluation of SAS1A modeling of loop Checkout Tests E1 and E2.[5,6] Calculation by SAS1A[25] of the extent of fuel melting was confirmed by postmortem inspection of the unfailed pin from Checkout Test E1. This inspection also indicated the ability of axial fuel motion to release cladding stress. Coolant-outlet-temperature rises in Checkout Tests E1 and E2 up to the time of pin failure were well below calculated values.

Provisionally, this was attributed to the relatively slow radial heat transport of a gas-bonded oxide giving time for much more heat transport to surrounding structure in the checkout pseudocluster geometry than had occurred in earlier loop tests with EBR-II driver fuel.[21,26]

For both tests, the fuel-cladding deformation subroutine[25] calculated that the cladding began to be deformed plastically even before any fuel melting began. No significant plastic strain was found in the E1 pin, apparently demonstrating the effectiveness of axial movement in relieving strain. A large residual (i.e., plastic) strain of the stainless-steel E2 cladding is calculated after maximum reactor power, due to the large change in fuel volume occurring with UO_2 melting. The maximum cladding strain at the time of pin rupture (1880 J/gm of UO_2) is calculated to be 5.3%. This value of the cladding strain is very close to the threshold strain calculated for the autoclave experiment S3.[24] At the close of the report period, extensive efforts were being made to check this prediction for E2, using the cladding remains.

Evaluation of SAS1A modeling of first mixed-oxide-pin loop experiment with single pin in simulated FFTF cell (Test H1). In the evaluation of SAS1A modeling of Test H1, the measured and calculated rise of coolant outlet temperature agreed well. Check of the shape of the outlet-coolant-temperature curve confirmed the form of the SAS1A model for variable heat conductance, U, across the fuel-cladding gap. Parameter studies were performed using a constant value of U as a parameter. These showed that a constant U could not reproduce the shape of the outlet-temperature curve. Agreement between experiment and calculation indicates that the principal calculational problem in analyzing transient outlet-coolant temperatures of Checkout Tests E1 and E2 was the modeling of the complicated three-dimensional geometry around the pin.

Careful postexperiment metallurgical examinations showed residual strain in the cladding to be significantly lower than predicted using the nominal design fuel-cladding gap. Increasing the gap thickness by an amount within realistic fabrication tolerances resulted in a calculated strain in good agreement with measurements. This sensitivity to relatively small changes in as-fabricated fuel-cladding gap should not, in principle, occur for irradiated fuel because of closure of the gap.

Analysis of impacts inside Mark-II sodium loops under assumed limiting-case hazards conditions.[17] During the safety review of the El Mark-II-loop test, questions were raised concerning potential damage to the loop arising from sodium impacts at the top of the loop expansion volume, and secondary impacts if the sodium were to rebound downward after the original upward acceleration. These concerns arose from hazards calculations for a limiting case in which conversion of about 10% of the thermal energy input to the sample appears in kinetic energy of a sodium "slug." Calculated velocities at impact for this case are typically about 400 m/sec. (The maximum sodium velocity actually measured by a flowmeter in a Mark-II-loop test thus far is less than 20 m/sec.) Because the loop tests currently represent exploratory experiments into a relatively unknown regime, the test-section support member inside the loop expansion space was modified to provide a design margin in the event the actual experimental conditions were to approximate the conditions of the hazards calculations. Four reinforced orifice plates were placed on the support member to limit the sodium slug velocity at impact. The bottom orifice was placed high enough that sodium expulsion could proceed unimpeded, until the test section was voided past the upper flowmeter. Thus, there would be no compromise

of experimental objectives, at least on expulsion. Detailed sizing and placement of the orifice plates were made on the basis of an analysis of sodium-slug displacement, velocity, and acceleration, using a non-linear resisting force, for sodium of known (and constant) mass, density, and viscosity moving through a duct of variable area. Calculations were performed for a driving pressure of 410 atm (sodium critical pressure). The transient pressures resulting from the impacts of the sodium slug with the orifice plates and the top of the loop were calculated using results from Streeter and Wylie[27] and from Wright.[28] It was concluded that addition of the orifice plates would accommodate the conditions of the assumed accident.

Analysis of radiation effects on superheating of liquid sodium. Results of calculations, indicating that the radiation environment of a fast reactor should have negligible effect on the superheat of liquid sodium coolant, were reported.[29,30]

Demonstration of basic capability for automated handling of hodoscope data. The basic capability for automated handling of hodoscope data was demonstrated.[31] The TREAT hodoscope is a device developed to "follow" the movement of fuel during a TREAT experiment with a loop or steel capsule, by detecting fission neutrons emitted from the test section. These neutrons are then detected by an array of detectors outside the reactor core, and the data are recorded.[32,33] As a test of the hodoscope system, it was run, at the same time with the standard TREAT high-speed optical camera system, during a fuel-pin meltdown experiment conducted with a transparent capsule.[13] Data from the hodoscope were "read" by the ANL CHLOE scanning system, analyzed, and used in a computer reconstruction to produce "photos" of a test pin as the pin

slumped during a TREAT transient. Good agreement was found between the computer reconstruction of the fuel sample and the optical photography.

Analysis of transient data has shown that the transient signal-to-background ratio is better (by about a factor of three) than that recorded in steady-state checkouts. This appears to arise in a straightforward fashion from the core delayed gamma rays that contribute to background much more during a steady-state run than in a short reactor transient that lasts a few seconds or less. On the other hand, the delayed gammas from both core and sample persist after the burst, decaying much more slowly than the neutron signal. This effect tends to maintain the hodoscope counting rates at higher levels (though at a signal-to-background ratio comparable to steady state) than would be indicated by the reactor fission levels.

Future program. Analytical support for experiments will be expanded to provide routine data reduction from the TREAT fast-neutron hodoscope, the specialized calculations needed for detailed planning and analysis of the experiments performed, and associated fuel dynamics development.

Hot Laboratory Examinations

(L. Neimark)

Scope. Specialized examinations of both fresh fuels and preirradiated fuels are providing data needed to analyze the effects of transient tests on FFTF oxide fuel. Fresh fuel and irradiated fuel are examined nondestructively; destructive examinations are made of selected preirradiated pins that are to be used as references for comparison with post-TREAT examinations on preirradiated fuel. Nondestructive and destructive techniques are used in the study of post-TREAT fuel condition.

These examinations supply data for analyses in support of the TREAT experiments, and of the Accident Analysis work that is developing predictive analytical descriptions.

Summary. Postmortem inspections were performed on samples from Checkout Tests E1 and E2. Unirradiated PFR pins were nondestructively tested before they were used in TREAT tests, as were PFR pins that had been irradiated to 5% burnup. The 3%-burnup "lead" pin from the first unencapsulated oxide assembly run in EBR-II was examined.

Postmortem inspection of pin from Checkout Test E1. In the postmortem inspection of the pin from Checkout Test E1, the pin cladding was found not to have been deformed by the transient, although extensive motion of molten fuel had occurred inside the unfailed cladding. Molten oxide had been frozen in place against the cladding without significant attack of the sodium-cooled jacket. Maximum extent of fuel melting was approximately 80% of the pellet cross section.

Nondestructive test of unirradiated PFR mixed-oxide pins. The nondestructive characterization of 66 unirradiated PFR mixed-oxide fuel elements has been completed in preparation for tests in TREAT. The characterization included profilometry, eddy-current inspection, balance-point determinations, length measurements, and radiographs.

Nondestructive test of PFR mixed-oxide pins irradiated to 5% burnup in DFR. Nondestructive tests were performed on seven UKAEA mixed-oxide PFR-type pins that had been irradiated to 5% burnup in DFR. Two new results were obtained: neutron radiography disclosed internal oxide fragmentation and structural changes on one pin not seen on UK radiographs, and eddy-current inspection of the cladding showed anomalies associated with the inner surface of the cladding that might

represent fission-product penetration of the stainless steel. Destructive examination was not permitted, so direct investigation of the source of this anomaly could not be performed.

Examination of the 3%-burnup "lead" pin from the first unencapsulated oxide assembly run in EBR-II. The oxide pin removed from unencapsulated EBR-II Subassembly X040 at 3% burnup as a "lead" pin was examined in detail, both nondestructively and destructively.

Subassembly X040 was the first EBR-II subassembly to contain unencapsulated experimental mixed-oxide fuel pins. The subassembly consisted of 19 ANL pins along with 16 pins from General Electric Co. The 19 ANL pins were specified for exposure to 5a/o burnup, to provide a stock of domestic mixed-oxide pins irradiated in unencapsulated environment for use in fast-reactor safety transient meltdown experiments in the TREAT reactor. Subassembly X040 was removed from EBR-II at the 3a/o burnup level for an interim examination[34] so that the EBR-II project staff could ascertain the condition of the fuel in this first unencapsulated oxide-pin subassembly, to verify that the condition of the pins was in accord with expectations based on earlier encapsulated EBR-II oxide-pin irradiations, and to confirm that the irradiation could proceed from the standpoint of EBR-II safety and availability. No conditions were found that would bar continued irradiation of the subassembly to 5 a/o burnup. One of the 19 pins (012) appeared to have a minor surface defect. This pin was set aside for detailed destructive examination as a "lead" pin from Subassembly X040. The reconstituted subassembly, with Pin 012 replaced by a dummy pin, was reloaded into EBR-II as Subassembly X040A. Irradiation of X040A was completed without incident shortly before the end of the report period.

Upon close examination, the surface defect of Pin 012 appeared to be a surface scratch rather than an incipient crack. Detailed metallography confirmed this conclusion.

After removal of the spacer wire, the area covered by the wire in the fuel section of Pin 012 was readily discernible, as shown in Fig. 96. Also visible were shallow scratches where the wire rubbed against the cladding.

Fig. 96.
Fretting Scratches under Spacer Wire in Fuel Region of Pin 012 from Subassembly X040.

The maximum diameter increase (based on a nominal preirradiation diameter of 0.290 in.) of Pin 012 was 1.5 mils and occurred about 5.7 in. above the bottom of the fuel column. The diameter increase was not uniform around the circumference of the element; the "minimum" maximum was 0.8 mil. The diameter change along the length of the element

conformed only generally to the flux profile, and had a number of peaks and valleys. There was no evidence of "pellet ridging" or "bambooing" along the element.

Figure 97 shows a transverse section from 5/8 in. below the top of the fuel column of Pin 012, where gamma spectrometry indicated a high concentration of cesium. The section is typical of others along the

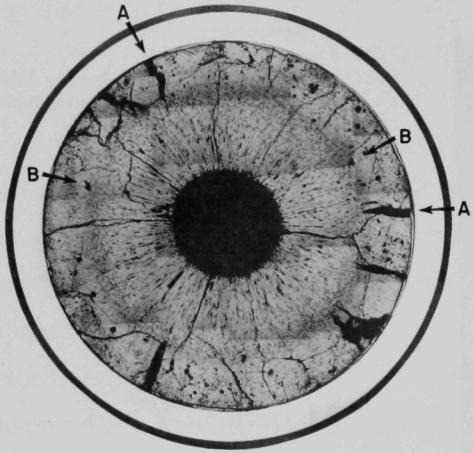

Fig. 97. Transverse Section 5/8 in. from Top of Fuel Column in Pin 012. U-Pu-Cs material is at the fuel-cladding interface. Healed cracks are at A and molybdenum deposits are at B.

length of the fuel column, except for a gray phase clearly evident between the fuel and the cladding. This gray phase is of substantially different morphology than the body of the fuel and appears to be free of porosity. Microprobe analysis showed that the phase contains uranium, plutonium, and cesium, with the uranium and plutonium in the same ratio and almost the same quantities as in the fuel pellet. Although not visible in the microstructure, a very high concentration of cesium was found by the microprobe between the gray phase and the cladding; there apparently was no penetration of cesium into the cladding at this position. The gray phase bears a resemblance to the U-Pu-Na reaction

products previously found in failed mixed-oxide fuel elements. The microprobe results indicate that the phase is a U-Pu-Cs reaction product.

Other noteworthy features in Fig. 97 are the cracking pattern and the apparent healing of these cracks in the columnar-grain region (at A). These cracks suggest that the initial 0.004-in. fuel-to-cladding gap has been closed by the outward movement of large segments of the pellet, and then the crack-healing process in the columnar-grain zone, above a temperature of about 1800°C, essentially locked the segments against the cladding. The perfect circular shape of the central void indicates that the segments did not move inward, by shear along cracks, on cooldown. This cracking behavior suggests that the mechanism for closure of the gap is related to thermal expansion and thermal-shock cracking of the pellets rather than to fuel swelling.

Nondestructive eddy-current examination had indicated that, at about 2.5 in. from the top of the fuel column, a possible defect existed on about 180° of arc on the inner surface of the cladding. The metallographic examination of this area showed no gross cracks. However, in half the circumference of the cladding, a number of grains of the stainless-steel cladding had fallen out during metallographic preparation. On further grinding, there was clear evidence of fission-product penetration into the grain boundaries of the cladding to a depth of approximately 0.002 in., the approximate depth indicated by the eddy-current examination. The calculated cladding temperature in this region was between 490 and 535°C.

No evidence was found for any significant attack of the cladding by sodium, or for any detrimental effects of the sodium-cleaning procedures at EBR-II.

Alpha autoradiographs of the sections indicated that plutonium had migrated up the thermal gradient. An intense band of alpha activity was found around the central void, with a depleted zone toward the colder ends of the columnar grains.

Fission-gas analysis showed 56% release from the fuel.

Postmortem inspection of sample from Checkout Test E2. The sample remains from the high-energy oxide-failure experiment of Checkout Test E2 was examined in detail. Fuel-structure and macroscopic characterization were combined with checks on melting of stainless-steel components from the cluster to provide a reconstruction of the course of the experiment complementary to the direct-observation data from the fast-neutron hodoscope. Detailed checks are underway to test the cladding-strain calculations of SAS1A.

Future program. Pins will be examined both before and after the in-pile tests to assist in analysis of the results. It is assumed that the preirradiated fuel pins supplied will be significantly closer to the FFTF fuel design specifications than were the pins from the first EBR-II experimental subassembly of unencapsulated oxide pins (X040). Examinations will be performed on pins from X040 only to the extent necessary to assist in evaluating the true condition of the actual TREAT specimens. At that point, the 17 identical X040 pins will serve only as backup pins that have been irradiated unencapsulated in a fast flux; they will be used only if needed.

References

1. C. E. Dickerman, *Studies of Fast Reactor Core Behavior Under Accident Conditions*, Nucl. Safety *11*(3), 195-205, May-June 1970.

2. C. E. Dickerman et al., "Use of the Thermal TREAT Reactor for Fast Reactor Safety Studies," *Proc. Natl. Symp. on Developments in Irradiation Testing Technology, Sandusky, Ohio*, USAEC CONF-690910, 52-58 (Sept 1969).

3. L. E. Robinson, R. O. Ivins, and C. E. Dickerman, "Capsules and Sodium Loops Used in Argonne National Laboratory Reactor Safety Experiments in the TREAT Reactor," *Proc. Natl. Symp. on Developments in Irradiation Testing Technology, Sandusky, Ohio,* USAEC CONF-690910, 38-51 (Sept 1969).

4. L. E. Robinson, R. Purviance, and K. Schmidt, *The Mark-II Integral Sodium TREAT Loop,* Trans. Am. Nucl. Soc. *13*(1), 354-355 (Jun 1970).

5. C. E. Dickerman et al., *First TREAT Loop Experiment on Oxide Fuel Meltdown,* Trans. Am. Nucl. Soc. *12*(2), 867-868 (Nov 1969).

6. C. E. Dickerman et al., *First TREAT Experiment on High-Energy Fuel Failure of an Unirradiated Oxide Fast Reactor Fuel Pin in Flowing Sodium,* Trans. Am. Nucl. Soc. *13*(1), 370-371 (Jun 1970).

7. C. E. Dickerman et al., "Low Level Activity Plutonium Handling Facility for Transient Reactor Test (TREAT) Facility Experimental Apparatus," *Reactor Physics Division Annual Report July 1, 1967 to June 30, 1968,* ANL-7410, 261-262 (Jan 1969).

8. A. B. Rothman et al., *Neutron Filter for TREAT Safety Studies on Fast Reactor Fuel,* Trans. Am. Nucl. Soc. *13*(1), 356-357 (Jun 1970).

9. A. B. Rothman et al., *Failure Threshold TREAT Experiment with an Unirradiated Prototypical FFTF Fuel Element,* Trans. Am. Nucl. Soc. *13*(2), 652 (Nov 1970).

10. L. W. Deitrich et al., *High-Energy Transient Meltdown of Irradiated UO_2 in a TREAT Mark-II Loop,* Trans. Am. Nucl. Soc. *13*(2), 652-653 (Nov 1970).

11. R. R. Stewart et al., *A Study of the Physical Properties of Nominal 0.7, 3, and 6 a/o Burnup UO_2 Fast-Reactor Fuel Pins Preparatory to Transient TREAT Exposure,* ANL-7571 (May 1969).

12. R. R. Stewart et al., *Studies of Fast Reactor Fuel Element Behavior Under Transient Heating to Failure III. In-pile Experiments on Irradiated UO_2 Fuel Pins in the Absence of Coolant,* ANL-7552 (Mar 1969).

13. J. J. Barghusen et al., "Observation of Fuel Failure Behavior During In-pile Meltdown Tests Using High-Speed Photography and a Transparent Autoclave," *Proc. Natl. Symposium on Developments in Irradiation Testing Technology, Sandusky, Ohio,* USAEC CONF-690910, 378-400 (Sept 1969).

14. L. E. Robinson and C. August, *Apparatus for High Speed Photographic Safety Experiments on Irradiated Fast Reactor Fuel Specimens,* ANL-7578 (Jan 1971).

15. C. E. Dickerman et al., "Design of an Advanced Shipping Cask for Transient Reactor Test (TREAT) Facility Experiments," *Reactor Physics Division Annual Report July 1, 1967 to June 30, 1968,* ANL-7410, 260-261 (Jan 1969).

16. L. E. Robinson, "Testing of the Prototype Mark-II Integral Sodium Transient Reactor Test (TREAT) Facility Loop," *Reactor Physics Division Annual Report July 1, 1968 to June 30, 1969*, ANL-7610, 261-264 (Jan 1970).

17. L. W. Deitrich, *Suppression of Sodium Slug Impacts in the TREAT Mark-II Loop*, Trans. Am. Nucl. Soc. *13*(1), 341-342 (Jun 1970).

18. *ASME Boiler and Pressure Vessel Code* (1968 Ed.) Section III, Nuclear Vessels.

19. *United States of America Standards B31.1.0 Power Piping Code* (1967), Chapter II, Sections 102.3.2C and 119.6.4.

20. L. E. Robinson and R. T. Purviance, *Pressure Transducers for TREAT Sodium Loops*, ANL-7107 (Jun 1969).

21. C. E. Dickerman et al., *Power Pulse Meltdown Experiments Performed in the Mark-I TREAT Sodium Loop on Clusters of 7 EBR-II Mark-I Type Pins*, Nucl. Eng. and Design *12*(3), 391-406 (Jun 1970).

22. C. E. Dickerman, *Transient Temperature Measurements and Analyses in TREAT Reactor Experiments*, Presented at the Natl. Heat Transfer Conf., Minneapolis, Minn. (Aug 1969).

23. A. DeVolpi, *Deciphering and Processing Digital Photographic Data*, Presented at Ninth Int. Congress on High Speed Photograph, Denver, Colo. (Aug 1970).

24. A. K. Agrawal, *On the Analysis of the Fuel Meltdown Studies with TREAT*, Trans. Am. Nucl. Soc. *12*(2), 865-866 (Nov 1969).

25. J. C. Carter et al., *SAS1A, A Computer Code for the Analysis of Fast Reactor Power and Flow Transients*, ANL-7607 (Oct 1970).

26. C. E. Dickerman et al., *TREAT Sodium Loop Experiments on Performance of Unbonded Unirradiated EBR-II Mark-I Fuel Elements*, Nucl. Eng. and Design *12*(3), 381-390 (Jun 1970).

27. V. L. Streeter and E. B. Wylie, *Hydraulic Transients*, McGraw-Hill, New York (1967).

28. R. W. Wright, *Pressures and Jets from Water Impacts Upon Open Structures*, Trans. Am. Nucl. Soc. *12*(1), 363 (Jun 1969).

29. L. W. Deitrich, *Radiation Effects on Superheating of Liquid Sodium*, Trans. Am. Nucl. Soc. *13*(1), 368-369 (Jun 1970).

30. L. W. Deitrich, "Radiation Effects on Superheat in Liquid Sodium," *Reactor Physics Division Annual Report for July 1, 1968 to June 30, 1969*, ANL-7610, 329-332 (Jan 1970).

31. A. DeVolpi, C. E. Dickerman, and J. F. Boland, *Preliminary Performance Data from Fast Neutron Hodoscope at TREAT*, Trans. Am. Nucl. Soc. *12*(2), 868 (Nov 1969).

32. A. DeVolpi, *Fast Framing Cameras Provide High-Speed Multi-channel Data Recording*, AEC-NASA Tech. Brief 69-10102 (Apr 1969).

33. A. DeVolpi, "The Recording of Transient Nuclear Data at 10^9 Counts/Second," *Internatl. Sym. on Nuclear Electronics, Versailles, 1968* (Proceedings, Paris, Documentation Francaise 1968) CONF-680906, 2, 112-1 - 112-11.

34. C. E. Dickerman, "Interim Examination at 3 a/o Burnup of the First Unencapsulated Mixed Oxide Pins from EBR-II," *Reactor Physics Division Annual Report for July 1, 1968 to June 30, 1969*, ANL-7610, 274-282 (Jan 1970).

IX. MATERIALS BEHAVIOR AND ENERGY TRANSFER*

(M. G. Chasanov)

Overall scope. This program is aimed primarily at providing high-temperature physical-property data for materials used in an LMFBR. The properties to be studied are chosen on the basis of their importance in fast-reactor safety analysis--ranging from steady-state and mild transients to core-meltdown situations. Among the properties being studied are heat capacity, enthalpy, compressibility, vapor pressure, and speed of sound; other properties, such as density, viscosity, surface tension and thermal conductivity, might be studied later. Presently, the emphasis is on obtaining information relating to fuel materials; however, future plans call for similar studies on coolant, cladding, and structural materials.

The experimental programs involving the fuel materials are being pursued to the maximum temperatures possible using tungsten containment vessels-- $\sim 3600^{\circ}K$. However, these temperatures are still markedly less than some of the temperatures of interest to reactor-safety analysts. Thus, coupled with our experimental program, we have an analytical effort that is investigating various types of correlative and extrapolative techniques for use in extending the temperature range of utility for the data obtained by us and by other investigators.

Theoretical Extrapolation of Measured Physical Properties to Very High Temperatures

(S. D. Gabelnick and M. G. Chasanov)

Scope. The high-temperature physical-properties program will, in general, provide physical-property data for fuel materials, cladding,

*For references for this chapter, see p. 288.

coolant, and structural materials at temperatures that are extremely high from an experimental point of view (∿3300°K), but are still markedly less than temperatures of interest to reactor-safety analysis. To correlate and extrapolate satisfactorily the experimental data for utilization at these significantly higher temperatures (∿6000°K), recourse to existing theory such as corresponding states, scaled particle, significant structures, etc., is necessary. Calculational studies based on these theories will be performed to assess consistency and validity of such extrapolation and correlation of the available data.

Summary. Efforts have been devoted to development of a basic computer program to calculate vapor pressures of fuel and fission products at temperatures for which thermodynamic data are presently available; extrapolation techniques are being incorporated to allow the program to be used at temperatures for which experimental thermodynamic data do not exist.

Correlation of experimental data obtained from high-temperature physical-property studies with corresponding states theory and other pertinent theories; development of useful equations of state for reactor materials. Knowledge of the pressure within an operating fuel pin is of importance to the reactor safety program. At normal operating temperatures, pressure from the buildup of gaseous fission products in the void, crack, and plenum regions of the fuel pin significantly contributes to the stresses placed on the cladding materials. Under accident conditions, the combined vapor pressure of fission products and fuel might serve as a ballast force causing molten fuel to be extruded through a rupture in the cladding, if such a rupture should occur. The vapor pressure is thus one of the factors that needs to be considered in determining the extent of fuel-coolant interaction.

The thermodynamic data needed for the calculation of partial vapor pressures of the fission products and of the fuel at the very high temperatures that might be reached during a reactor accident cannot be obtained directly by experimental means. Consequently, it is necessary either to find some basis on which to extrapolate existing experimental data taken at low temperatures to higher temperatures or to perform statistical mechanical calculations of the thermodynamic properties based on observed spectroscopic parameters.

Efforts initially have been placed on the development of a basic computer program suitable for calculating vapor pressures of fuel and fission products at normal operating temperatures; this same program will later be applicable to calculations of vapor pressures at very high temperatures when appropriate thermodynamic data are available.

For a fixed temperature, fuel density, relative void volume, percent burnup, and preburnup O/M ratio of the fuel, a set of simultaneous equations must be solved. These consist of (1) nonlinear equilibrium relations between the vapor species, oxygen, and the stable condensed phase of each fission-product element and of the fuel, (2) mass constraints imposed by initial quantities and preburnup O/M ratio of the oxide fuel and by fast-neutron fission-product yields, and (3) an equation relating oxygen pressure to the O/M ratio of the fuel. The assumptions made are (1) that all vapor species are released to the void volume, which is at constant and uniform temperature, and (2) that the condensed fuel and fission-product phases are immiscible and have unit activity coefficients. Although there are as many unknown quantities as equations, it is found that the concentrations of all species depend

simply on the O/M ratio of the condensed fuel. By estimating the final (after burnup) fuel composition, the concentrations of all species and a revised value of the final O/M ratio are obtained. Successive iterations are performed until the estimated and revised values of the after-burnup O/M ratio agree to within any required accuracy. Then partial vapor pressures of fission products and fuel are calculated from this final value.

Future program. Necessary thermodynamic data will be updated and extended to higher temperatures,the possibility of compound formation between several fission-product elements will be accounted for, and attempts will be made to improve on the simplifying assumptions enumerated above. In addition, use of existing theory to correlate and extrapolate experimental physical-property data to higher temperatures will be continued. Preliminary emphasis will be on corresponding states theory. However, these results also will be compared with scaled-particle and significant-structures theories. The results of these preliminary comparisons will indicate which approaches should be suitable for treatment of reactor-safety data.

High-temperature Physical-property Studies

(L. Leibowitz, S. D. Gabelnick, M. G. Chasanov, G. T. Reedy, and D. F. Fischer)

Scope. Those physical properties of interest because of their need in fast-reactor safety analyses are our prime consideration. These include pressure-energy relationships for the fuel materials, energy content of molten fuels, cladding, and structural materials, and transport properties. Equation-of-state data for fuel materials and coolant are of primary interest. Enthalpy and heat-capacity data for molten oxide fuel materials are

being determined up to ∿3600°K. Evaluation of pressures over molten fuel at up to ∿3500°K is being pursued by transpiration measurements and beyond this temperature by matrix-isolation spectroscopy. These parameters can be coupled to give pressure-energy relationships needed for Bethe-Tait-type calculations. Compressibility data for molten fuel materials and coolant, for use in conjunction with the Gruneisen equation of state, will be available from measurements of speed of sound. These data of speed of sound will be also of value in assessing shock propagation through molten fuel and coolant. Heat-content and heat-capacity data for molten cladding materials will be investigated by levitation calorimetry and, in addition, emissivity of molten fuel materials will be studied. It is expected that density and surface tension data might be obtained as byproducts of the other experimental investigations. These studies can be expanded to include future fast-reactor materials.

Summary. Enthalpy data for UO_2 (relative to 298°K) were obtained up to 3475°K. The liquid data fit a straight line whose slope is 33.6 cal/mol-°K (the heat capacity). The apparatus has been modified for use with mixed-oxide fuel materials; testing is in progress. Data were obtained for the total pressures over UO_2 at high temperatures. Several temperatures in the solid and liquid range have been investigated; the results agree well with extrapolation of lower-temperature ANL data. The ultrasonic apparatus for determination of speed of sound in liquid sodium and molten UO_2 has been assembled and is under test. The matrix-isolation spectroscopy apparatus is virtually completed; preliminary testing is under way.

Experiments to determine enthalpies and heat capacities of molten UO_2. Work is continuing on the program to determine the heat capacity of liquid uranium dioxide, an important quantity in fast-reactor safety calculations.

Accurate values of the heat capacity and heat of fusion of molten UO_2 will facilitate estimation of the total energy released and the temperatures attained in the reactor core during destructive nuclear excursions. Induction heating in conjunction with a drop calorimeter is being used for measurements at temperatures that previously have not been explored.

In an experiment, a sample sealed in a tungsten capsule is suspended by tungsten wire in an induction coil and is heated to the desired temperature. For the temperature measurement, a disappearing-filament-type optical pyrometer is sighted on a blackbody cavity (length-to-diameter ratio of ten) extending into the capsule. When temperature equilibrium has been reached (∿20 min), the suspension wire is vaporized by means of a condenser discharge and the hot capsule falls into a modified Parr adiabatic calorimeter. The temperature rise is measured with a quartz thermometer. The procedure is repeated with an empty capsule and the enthalpy of the sample found by difference.

Data have already been reported on the enthalpy of tungsten[1] (a calorimetric standard) to 3594°K and of UO_2[2] to 3329°K. The UO_2 enthalpy measurements have now been extended to 3475°K; the data obtained to date at temperatures above the melting point are shown in Fig. 98.

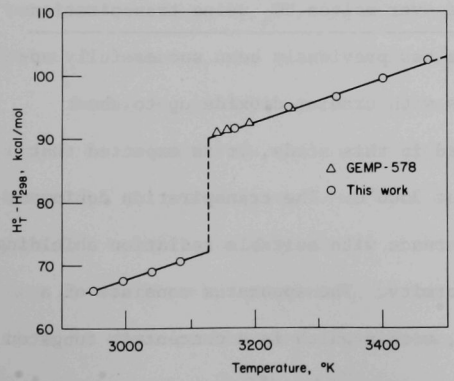

Fig. 98.
Enthalpy of UO_2.

The liquid-UO_2 enthalpies are in good agreement in the region of overlap with those reported by other workers.[3] These measurements extend previously available data by over 200°K. The heat of fusion of ∿18 kcal/mol is also in good agreement with the literature[3] value of 18.2 kcal/mol. A straight line fits our liquid enthalpy data within about 1% and the heat capacity of 33.6 cal/mol-°K we obtained can probably be used for moderate extrapolations.

Experimental determination of enthalpies and heat capacities of solid $(U_{0.8}Pu_{0.2})O_2$. The apparatus used for the UO_2 calorimetric studies has been modified for semiremote operation for use with mixed-oxide fuel materials and a walk-in hood has been constructed around it for plutonium containment. The equipment is being tested.

$(U_{0.8}Pu_{0.2})O_{1.980}$ pellets are being prepared for these studies. These cylindrical pellets are annular in shape, having an OD of 0.465 in., and ID of 0.175 in., and a length of 0.900 cm. Each experiment will involve dropping a tungsten capsule containing two of these pellets.

The tungsten capsules to be used in these experiments have been fabricated. A contract has been negotiated for the electron-beam welding of these capsules loaded with plutonium-containing materials.

Determination of total pressure over molten UO_2 using transpiration method. The transpiration technique has previously been successfully applied to vapor-pressure measurements with uranium dioxide up to about 2700°K.[4] In the experiments planned in this study, it is expected that measurements will be made up to about 3500°C. The transpiration equipment is being operated in an induction furnace with suitable radiation shielding included to ensure temperature uniformity. The apparatus consists of a tungsten susceptor-sample container, within which is a concentric tungsten

condenser; this assembly is positioned within the induction heating coil of a 25-kW generator. The coil and susceptor are inside a high-vacuum chamber equipped with a prism and viewports for determining the sample temperature using optical pyrometry. The carrier gas can be either high-purity argon or a selected mixture of hydrogen and water vapor.

A number of preliminary vapor-pressure measurements have been made with urania by means of the transpiration technique. These measurements have served to evaluate such factors as inert carrier-gas flow rates, choice of operating techniques, and hot-zone geometry, as well as the effect of the vaporization on sample stoichiometry. Two sets of measurements were made with solid urania, one at 2615°K, the other at 2860°K. From these preliminary measurements, the total pressures of uranium-bearing species obtained were 4.45×10^{-4} and 6.55×10^{-3} atm, respectively. These are in good agreement with literature values.

Preliminary vapor-pressure measurements on liquid urania have been carried out up to approximately 3400°K. These preliminary measurements, made with an inert carrier gas for the transport of urania vapor, establish guidelines for experimental procedure and yield approximate values for the total pressure at the temperature measured. For temperatures above the melting point of urania, and below the melting point of tungsten, the total urania pressure approaches 1 atm.

During a typical measurement, an appreciable fraction of the sample is converted to vapor with attendant changes in the unvaporized material. In measurements where the starting material was of composition O/U = 2.00, the composition of the charged urania was found to vary as vaporization proceeded, moving toward lower O/U ratios. The first of these preliminary measurements on the liquid, at 3175°K, gave a tentative value of 7.1×10^{-2} atm.

For two measurements at 3390°K, where the O/U ratio at the start of the run was 2.00 and the final composition was 1.94, the vapor pressure was measured to be 0.18 atm. Measurements at the same temperature with a starting O/U ratio of 1.94 showed no apparent further reduction in O/U ratio and gave a somewhat lower total pressure of 0.15 atm. However, it is possible that this apparent trend of decreasing pressure with lowering of O/U ratio is the result of scatter in the data.

Presently, work is under way to extend the preliminary measurements to approximately 3500°K, to examine further the effect of composition prior to starting final measurements over the range 2600 to 3500°K.

Construction and testing of speed-of-sound apparatus. The electronics of the ultrasonic apparatus for determination of speed of sound in molten UO_2 and liquid sodium were assembled and tested at room temperature. A vacuum-furnace system capable of attaining 3300°K has been adapted for use in these studies and is being tested. Cell design for these studies has been completed, and a stainless-steel version constructed for use with sodium up to about 1300°K. For the sodium experiments above that temperature, a tantalum-10% tungsten cell will be used. For the UO_2 studies, a tungsten cell of similar design should be adequate. To test the equipment, the stainless-steel cell was loaded with mercury and the speed of sound at 298°K was determined by the pulse-echo method using our experimental setup; the results agreed with the literature value to within 0.4%. The signals were extremely clear with little interference from stray reflections.

Speed-of-sound measurements in molten sodium to 1800°K. The cell used in the mercury test, described above, has been cleaned thoroughly,

loaded with high-purity sodium, and welded shut. Testing of an electrical-resistance-heated furnace and its control system are in progress. Speed-of-sound measurements on liquid sodium should commence shortly,

Construction of apparatus for matrix-isolation spectroscopy. The matrix-isolation spectroscopy apparatus involving a vacuum furnace which heats a Knudsen effusion cell, and a helium cryostat, has been completed. The system is undergoing preliminary testing.

Future program. Experimental determination of enthalpies and heat capacities of solid $(U_{0.8}Pu_{0.2})O_2$ should be completed in FY 1971; determination of these data for the molten mixed oxide should be under way. Speed-of-sound measurements in molten sodium up to 1800°K should be virtually completed. Vapor-pressure measurements over molten UO_2 by the transpiration method should be completed. Determination of the vibrational spectra of uranium oxides should be nearly completed in FY 1971.

Segregation of Pu in Fast Reactor Fuels under a Thermal Gradient

(M. G. Chasanov and D. F. Fischer)

Scope. Migration and segregation of fissile and fertile materials within a fast-reactor fuel during its operational lifetime could have significant effects on the operational safety of the fuel. Redistribution of plutonium in $(U,Pu)O_2$ fuels might change the chemical and physical properties of the affected regions enough to alter the neutronics of the system, affect fuel-cladding compatibility, and change the resultant fission-product distribution. Investigation of mixed-oxide fuels in a thermal gradient has been under way to evaluate the extent of migration of plutonium and fission products and elucidate the mechanisms involved in the migration processes. The variables considered to be of importance in these studies were departure from stoichiometry, plutonium content, density, magnitude of the

thermal gradient, and maximum sample temperature. The program also considered similar studies with carbide fuels.

Summary. Experiments in which hypostoichiometric oxides were maintained in gradients of 1100°K/cm for ∿100 hr showed no apparent changes in plutonium concentration. Hyperstoichiometric pellets created under the same conditions showed measurable increases in plutonium concentration at the hotter end of the sample. A carbide sample heated with a vaporization barrier showed no significant redistribution of plutonium. A topical report covering the program's results was completed.[5]

Study of segregation of Pu in mixed-oxide and carbide fuel materials under an impressed thermal gradient. Experiments on mixed-oxide specimens were carried out with right-circular cylindrical pellets, 1/2-in. high by 1/2-in. in diameter, that were prepared from coprecipitated UO_2-PuO_2; the pellets are all nominally $(U_{0.8}Pu_{0.2})O_{2\pm x}$. The studies were performed in the thermal gradient furnace described earlier (p. 167 of Ref. 6). Samples were annealed in the gradient furnace for the desired time, after which they were sectioned and analyzed for uranium and plutonium using an electron microprobe analyzer.

Results reported previously (p. 94 of Ref. 7) indicated that for specimens (initial O/M ratios of 2.01) heated in thermal gradients of the order of 1000°C/cm, enhancement of plutonium concentration occurred in the hottest regions. The concentration increases observed were small (∿2 wt % PuO_2 absolute increase) and the annealing times required were quite long (1020 hr for a sample with a top surface temperature of 1970°C, and 123 hr for a sample with a top surface temperature of 2350°C).

Additional experiments were performed using similar specimens whose initial O/M ratios were 1.97. Each pellet was heated in inverted tungsten

crucibles that served as a barrier to evaporative losses during the annealing period; a similar procedure had been used with the hyperstoichiometric specimens. The samples were annealed at the temperatures and times indicated:

P-10 (T_{top} = 2330°C, T_{bottom} = 1120°C, 262 hr),

P-11 (T_{top} = 2360°C, T_{bottom} = 1310°C, 125 hr),

P-12 (T_{top} = 2350°C, T_{bottom} = 1180°C, 97 hr).

Then electron-microprobe analyses were performed on these specimens; there appeared to be no significant plutonium concentration changes throughout these specimens' longitudinal sections.

Thus, in our experiments with mixed-oxide specimens, we have observed apparent changes in plutonium concentration at the hotter end of hyperstoichiometric pellets annealed in a thermal gradient, but no such change for slightly hypostoichiometric samples. This implies that the oxygen activity of the specimen could be involved in the mechanism for plutonium-concentration enhancement. It also might imply that vaporization processes play a significant role in the observed changes.

Several preliminary experiments were performed in a similar fashion using mixed-carbide fuel pellets of approximate composition $(U_{0.85}Pu_{0.15})C$. These cylindrical pellets were of 0.43-in. diameter and 0.42-in. length, just slightly smaller than the oxide specimens used earlier. The composition of the carbide pellets was 80.99 wt % U, 14.4 wt % Pu, and 4.61 wt % C. Four experiments similar to those performed on the oxide pellets were carried out. Sample top surface temperatures averaged around 2000°C and the gradients were about 700°C/cm. To date, electron-microprobe analytical data is available on the two longest-term annealed specimens. These are P-14 (T_{top} ~2000°C, T_{bottom} ~1370°C, 437 hr) and P-16 (T_{top} ~2000°C,

T_{bottom} ~1320°C, 460 hr). P-14 was annealed without a vaporization barrier, while P-16 used the aforementioned inverted tungsten crucible. The probe results indicated that considerable loss of plutonium occurred in the upper (hottest) region of P-14 (Pu concentrations reduced to a few percent) while virtually no loss was observed for P-16. This is not too surprising, since it is known that Pu is the chief high-temperature vapor species over such mixed carbides. Ceramographic examination showed considerable densification and columnar grain growth in the top portion of P-14, with little evident change in P-16.

A topical report covers the work.[5]

Future program. This program was completed in FY 1970.

References

1. L. Leibowitz, M. G. Chasanov, and L. W. Mishler, *Enthalpy of Solid Tungsten from 2800°K to Its Melting Point*, Trans. Met. Soc. AIME *245*, 981-984 (May 1969).

2. L. Leibowitz, L. W. Mishler, and M. G. Chasanov, *Enthalpy of Solid Uranium Dioxide from 2500°K to Its Melting Point*, J. Nucl. Materials *29*, 356-358 (1969).

3. R. A. Hein and P. N. Flagella, *Enthalpy Measurements of UO_2 and Tungsten to 3260°K*, GEMP-578 (1968).

4. M. Tetenbaum and P. D. Hunt, *Total Pressure of Uranium-bearing Species over Oxygen-deficient Urania*, J. Nucl. Materials *34*, 86-91 (1970).

5. M. G. Chasanov and D. F. Fischer, *Out-of-pile Study of the Effects of Thermal Gradients on the Distribution of Plutonium in Fast Reactor Fuel Materials*, ANL-7703 (Jul 1970).

6. *Chemical Engineering Division Semiannual Report, July-December 1967*, ANL-7425 (May 1968).

7. *Chemical Engineering Division - Annual Report 1968*, ANL-7575.

Nuclear Safety Research and Development--LMFBR Safety

X. FAST REACTOR SAFETY TEST FACILITY STUDY*

(L. Baker, Jr.)

Overall scope. In this study, which is synonomous with Task 10-5.1, Analysis of Facility Requirements, in the LMFBR Program Plan,[1] in-depth analyses define and justify both the program and concept of key safety facilities required for the LMFBR Safety Program. The type and number of in-reactor experiments that should be performed in the LMFBR Safety Program are being determined by delineating potential LMFBR accidents, determining the key uncertainties in the resolution of the accident, and assessing the best methods to resolve the uncertainties through experimentation. Facility requirements for performing the recommended experimental program are being developed, as are priorities and scheduling of the experiments. The practicality of performing some or all of the experiments in existing or firmly planned facilities is being evaluated. Recommendations will be made to RDT on the optimum use of existing or firmly planned facilities, as well as on the need for new LMFBR facilities. Use will be made, wherever applicable, of RDT standards, and ASTM, ASME, USASI and other codes, specifications, and standard practices. Also, attention will be given to delineating any specific areas where new standards and codes might require development.

Programmatic Definition and Justification

(L. Baker, Jr. and D. R. MacFarlane)

Scope. This study is: (1) determining the type and number of in-reactor experiments that should be performed in the LMFBR safety program, (2) determining appropriate priorities for the required experiments, (3) determining the optimum time schedule for conducting the experiments,

*For references for this chapter, see p. 319.

and (4) documenting adequately all these determinations. Included is the development of adequate justification for the recommended experiments, their priorities, and their schedule. This is accomplished by delineating potential LMFBR accidents. The work includes: identification of potential accidents, description of accident sequences, development of approaches to accommodate the potential accidents, and the identification of key uncertainties and unknowns for each accident. Priorities are assigned to the accidents in terms of their importance to design and licensing and to the uncertainties in terms of their influence on the resolution of the accidents. The recommended program of experiments and experiment priorities is being derived from an assessment of the optimum means to resolve specific uncertainties through in-pile experimentation.

Summary. The project report, Vol. 1: Program,[2] was completed and distributed for review and comment. Comments were received and the report was revised accordingly. Accident delineation was begun in order to define the recommended experiments in greater detail and to define priorities and schedules. Potential accidents were categorized. Accident sequences, approaches, and uncertainties were developed. From this, a detailed experimental program, including priorities and schedules, is being prepared.

Preliminary draft of report "Vol. 1: Program," to RDT, DRL, PRO, and industry for review and comment. The initial efforts to define the in-pile experiments likely to be required in the LMFBR safety program culminated in a draft project report, Vol. 1: Program,[2] whose preparation covered all areas of LMFBR safety. For the report, a comprehensive survey was made of the analytical problems and data needs in each major technical area pertinent to LMFBR safety, including: sodium boiling,

fuel-element failure propagation, molten-fuel-coolant interaction, motion of molten fuel, severe excursions, testing of core protective systems and consequence-limiting systems, postburst phenomena, and instrumentation. The out-of-pile program and the in-pile program required to supply the data needs in each area were discussed. Conclusions and recommendations for each technical area were presented, and a preliminary in-pile safety test program was presented. Volume 1 was sent for review and comment to industry, other national laboratories, RDT, and DRL.

Comments on Vol. 1 draft; revision of draft to take account of comments. Comments were received from each organization to which the document was sent. Volume 1 was revised to take account of the specific comments of the reviewers. The draft was shortened and the number of appendices reduced. The coverage of fission-product dispersion was expanded. Specific information supplied in the comments was added to the chapter on instrumentation. Comments stressing the need for core-destruct tests were not accommodated in the revision, but further evaluation of the question will be made in the appropriate phase of the study.

Delineation of LMFBR accidents to identify potential accidents, accident sequences, approaches, and uncertainties. Attempts to develop a comprehensive basis for experiment priorities and schedules led to the conclusion that they must be based on a delineation of LMFBR accidents. To begin the delineation, the potential sources of LMFBR accidents were listed, and the likely effects of these initiating events were considered in detail. These effects were grouped to form a concise list of general accident categories. Then general accidents were reviewed in specific terms, first for FFTF, then for a representative demonstration plant, and finally for a representative 1000-MWe target plant. There were three steps to this review: (1) development of the most likely sequence of

events during the accident, including identification of each point in the sequence where accident detection and protective-system action could be achieved, (2) development of a favored approach to accommodate each potential accident, and (3) identification of key uncertainties. Calculations using the ANL SAS1A code were performed to substantiate considerations of accident sequences for FFTF and for a representative 1000-MWe target plant.

Single-assembly accident. Five general accident categories were identified from the survey of potential accident sources. These are shown under the first entry in Table XVIII. There were several potential sources of partial assembly blockage and fuel-pin failure with gas release that could not be prevented with certainty. Therefore, these accidents were considered to be Priority 1. A loading error within a single-pin or a full-assembly blockage was considered preventable but with some uncertainty, so these accidents were considered Priority 2. A loading error for an entire assembly was considered to be preventable by design or administrative practice, so this accident was considered Priority 3.

The accident sequences and key uncertainties for single-assembly accidents are outlined in Fig. 99. The approach (the principal element of approach to every accident considered in the study is the prevention of the source of the accident by design or quality-assurance measures) to each accident was developed with a view to demonstrating that an accident will not progress toward more serious consequences either because of the physical phenomena involved or because of detection and remedial action. For example, for the partial-assembly-blockage accident, studies of the behavior of a small blockage are expected to show that a broken spacer wire, one swollen fuel pin, or a small piece of debris will not lead to local

TABLE XVIII. Summary of General Accident Categories

Type of accident	Importance
Single-assembly accidents	
Partial assembly blockage	1
Fuel-pin failure: gas release	1
Loading error: single pin or pellet in otherwise normal assembly	2
Full fuel-assembly blockage	2
Loading error: full assembly in wrong location	3
Whole-core loss-of-flow accidents	
Gas-bubble accident	1
Pump-coastdown accident with scram	1
Hypothetical pump-coastdown accident (no scram)	1*
Pipe-rupture accident with scram	1†
Hypothetical pipe-rupture accident (no scram)	1*
Whole-core power-excursion accidents	
Reactivity insertion with scram	1†
Hypothetical reactivity-insertion accident (no scram)	1*
Hypothetical reloading accident	3*
Related safety issues	
Severe excursion	1*
Containment and energy release	1*
Postaccident heat removal	1*
Sodium fires and aerosol behavior	1‡

*Importance based on need to test adequacy of containments and associated consequence-limiting safety systems.

†Importance based on need to test adequacy of plant protective systems.

‡Category not related to in-pile testing.

boiling and fuel-pin failure. However, if a local blockage large enough to cause local boiling should develop, it should be shown that the local boiling is stable, i.e., that the boiling will not lead to a general flow stoppage throughout the assembly. If this can be shown, then the probable

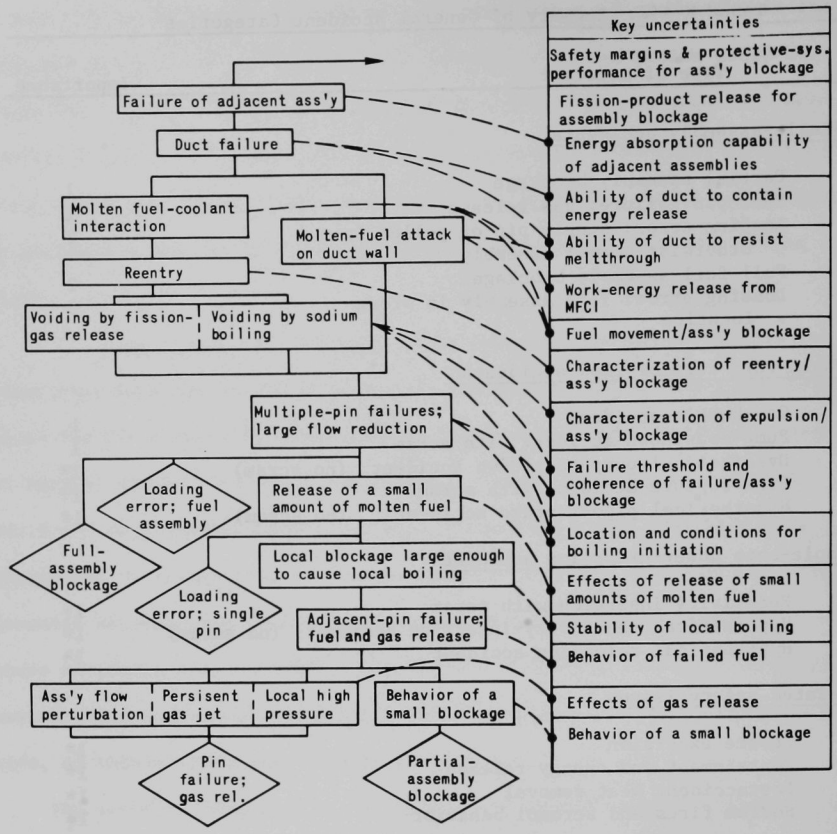

Fig. 99. Accident Sequences and Key Uncertainties for Single-assembly Accidents.

consequence of such a blockage is localized fuel failure and melting with the ultimate release of a small amount of molten fuel. It remains to be shown that the localized release of a small amount of molten fuel will not result in a rapid propagation of the blockage, but instead in either no propagation or a slow row-by-row propagation. Calculations have shown that there is at least 0.7 sec available, following a severe blockage, before boiling could begin as shown in Fig. 100. After boiling initiation and dry-out of any residual sodium film, it requires 3-5 sec for significant fuel

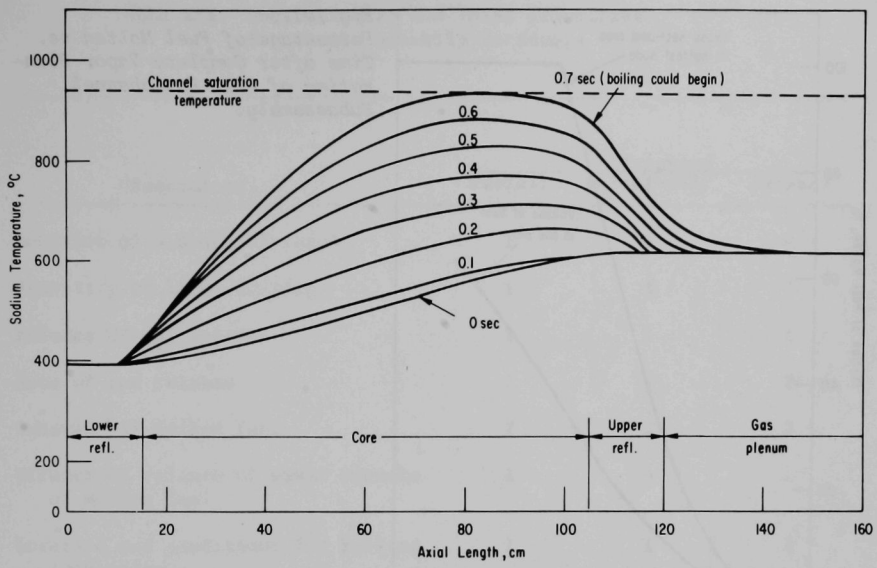

Fig. 100. Axial Coolant Temperature Profiles in FFTF Hot-channel Subassembly after Sudden Reduction to 10% Flow.

melting to occur (Fig. 101). Thus, if it can be shown that propagation can occur only in a sequential fashion, then it can be established that there is considerable time available for detection and reactor shutdown. A delayed-neutron detector, assembly thermocouples (or flowmeters), and pressure-pulse sensors offer means for detection.

If propagation of the local blockage continues, eventually boiling and a general expulsion of coolant from the assembly will occur. It should be shown that such an expulsion will result in a signal from outlet thermocouples, flowmeters, or pressure-pulse sensors. It must be shown that violent reentry, which could result in a damaging molten fuel-coolant interaction, cannot occur. Also, it must be shown that the quantity and motion of molten fuel is insufficient to result in meltthrough of the assembly duct wall. In general, it should be shown that any conceivable means of

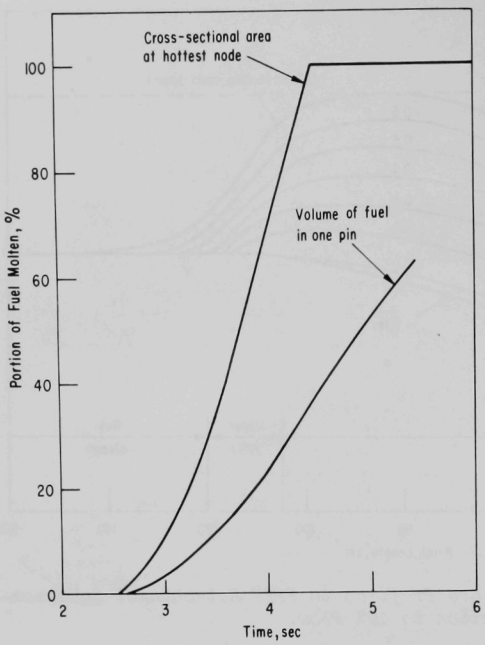

Fig 101.
Percentage of Fuel Molten vs. Time after Complete Vapor Blanketing of FFTF Hot-channel Subassembly.

propagation of failure to adjacent assemblies would result in time and opportunity for many additional signals to cause a safe shutdown of the reactor.

The uncertainties, listed in Fig. 99, were derived from the approach developed for the single-assembly accidents. An overall priority for each uncertainty was derived from the importance of the pertinent accidents and the importance of the uncertainty to the approach to the accidents. Then each uncertainty was examined to determine the best general approach to achieve resolution. Each uncertainty was given two additional priorities based on the potential for resolution by out-of-pile and in-pile experimentation. The uncertainties and their priorities are listed in Table XIX. In some cases, in-pile work is the only means to achieve resolution, in others out-of-pile work is the only means, and in still others both are

TABLE XIX. Uncertainties and Their Priorities for Single-assembly Accidents

Uncertainty	Priority		
	Overall	Out-of-pile	In-pile
Behavior of a small blockage	1	1	-
Stability of local boiling	1	1	2
Effects of gas release	1	1	1
Rate of gas release	2	-	2
Behavior of failed fuel	2	2	2
Effects of release of small amounts of molten fuel	1	-	1
Location and conditions for boiling initiation	1	1	2
Failure threshold and coherence of failure of elements for assy. blockage	2	-	2
Characterization of expulsion and reentry for assembly blockage	1	1	1
Fuel movement for assembly blockage	2	-	2
Work-energy release from molten fuel-coolant interaction	1	1	1
Ability of duct to resist meltthrough	1	-	1
Ability of duct to contain energy release	1	1	2
Energy-absorption capability of adjacent assemblies	1	1	-
Fission-product release for assembly blockage	3	3	3
Safety margins and protective-system performance for assembly blockage	1	-	1

needed, as indicated in Table XIX. The in-pile program of experiments to be developed will be based on the in-pile priorities listed in Table XIX.

Whole-core loss-of-flow accidents. Five general accident categories were derived from the survey of potential accident sources as shown in Table XVIII. It was concluded that a gas bubble entering the core of a pump coastdown (with scram) could not be prevented with certainty (Priority 1). However, a severe pipe rupture was considered important only as a test of the adequacy of plant-protective systems. A pump coastdown or pipe rupture without scram is extremely unlikely, but is considered to be important on the basis of the need to test the adequacy of containment systems.

The accident sequences and key uncertainties are outlined in Fig. 102. The approach to the gas-bubble accident is to show that the maximum possible quantity of external gas will not result in either failing fuel elements because of reduced heat transfer or in inserting excessive reactivity. To do this it is necessary to demonstrate that external gas bubbles are broken-up and distributed at the core inlet. Then the effects of entrained gas on heat transfer from the fuel elements and the failure thresholds for loss-of-flow conditions must be established.

The pump-coastdown accident with scram was considered primarily in terms of the means for detection. Calculations indicated that there was little difference in behavior between FFTF and the target plant. The calculated peak cladding temperature for FFTF was only 725°C (Fig. 103), using the conservative assumptions that reactor scram was initiated when the outlet coolant temperature reached 650°C (1202°F) and that there was a 0.60-sec delay in scram initiation. The fuel temperature during the flow transient did not increase at all.

The hypothetical pump-coastdown accident (without scram) differs significantly between FFTF and the target plant because of the difference in

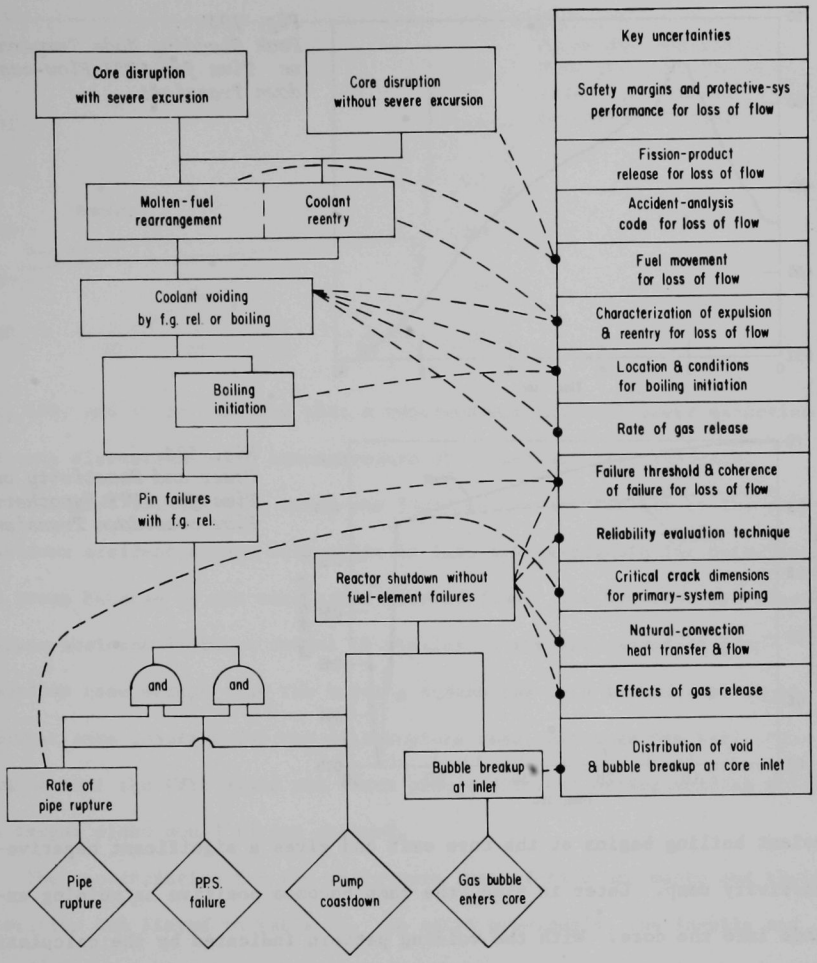

Fig. 102. Accident Sequences and Key Uncertainties for Whole-core Loss-of-flow Accidents.

sodium void coefficients. The results of a calculation for FFTF are shown in Fig. 104. After about 3.5 sec from the time of pump failure, highly irradiated fuel elements will probably begin to fail. This failure will be accompanied by fission-gas release and some reactivity effects, but these were not accounted for in the calculations. At approximatley 4.6 sec,

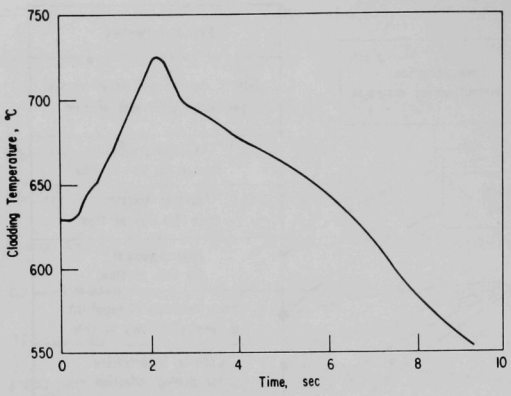

Fig. 103.
Peak Cladding Node Temperature vs Time for FFTF Flow-coastdown Transient.

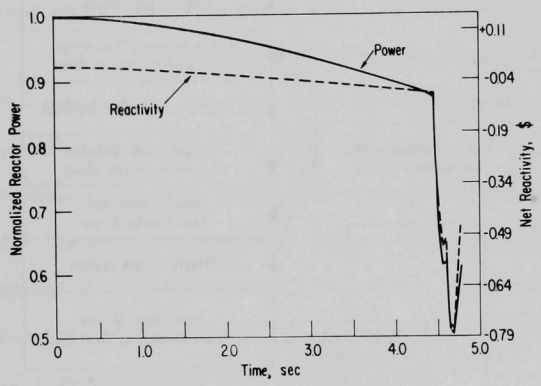

Fig. 104.
Power and Reactivity vs Time for FFTF Hypothetical Flow-coastdown Transient.

coolant boiling begins at the core exit and gives a significant negative-reactivity ramp. Later in time, the ramp becomes positive as voiding extends into the core. With the voiding pattern indicated by the calculations, it is unlikely that the positive-reactivity ramp would bring the reactor near prompt critical. Therefore, for FFTF, the sodium will void the core without resulting in a super-prompt-critical power excursion. The subsequent behavior of the voided core (molten fuel motion) will determine whether an excursion can occur or not. The calculations for the target plant are similar up to the point of voiding initiation. However, as voiding begins, the initial negative ramp turns around quickly, as shown in

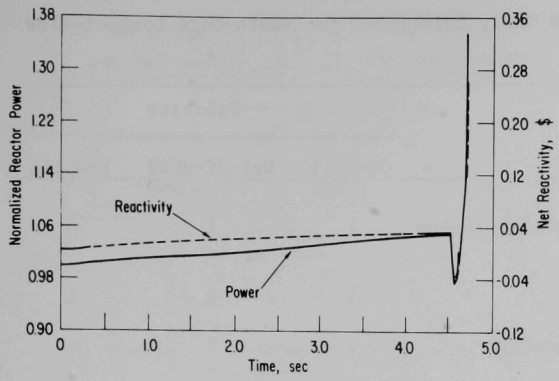

Fig. 105. Power and Reactivity vs Time for 1000-MWe Target-plant Hypothetical Flow-coastdown Transient.

Fig. 105, and it is expected that a super-prompt-critical power excursion and core disruption would occur because of void-reactivity feedback.

The pipe rupture with scram was found to be very similar to the pump-coastdown accident except that there is less time available for detection and scram because of the more rapid loss of flow. The hypothetical pipe-rupture accident (without scram) is similar to the corresponding pump-coastdown case except that the voiding across the core is expected to be somewhat more coherent for the pipe-rupture case, although the basic conclusion that the FFTF would not reach prompt critical during voiding while the target plant would is not changed.

The uncertainties for the whole-core loss-of-flow accidents and their priorities are listed in Table XX. As noted previously, the in-pile and out-of-pile priorities are based on the potential for resolution by in-pile and out-of-pile experimentation, respectively, and the in-pile program of experiments will be based on the in-pile priorities.

Whole-core power-excursion accidents. Three general accident categories were derived from the survey of potential accident sources shown in Table XVIII. It was expected that the quantity of reactivity and the potential insertion rate from all sources could be limited to acceptably

TABLE XX. Uncertainties and Their Priorities for Whole-core Loss-of-flow Accidents

Uncertainty	Priority		
	Overall	Out-of-pile	In-pile
Distribution of void and bubble breakup at core inlet	1	1	-
Effects of gas release	1	1	1
Natural-convection heat transfer and flow	2	2	-
Critical crack dimensions for primary-system piping	1	1	-
Reliability-evaluation technique	2	-	-
Failure threshold and coherence of failure of elements for loss of flow	1	-	2
Rate of gas release	2	-	2
Location and conditions for boiling initiation	1	1	2
Characterization of expulsion and reentry for loss of flow	1	1	1
Fuel movement for loss of flow	1	-	1
Accident-analysis code for loss of flow	1	-	-
Fission-product release for loss of flow	2	2	2
Safety margins and protective-system performance for loss of flow	1	-	1

low values by design. However, some reactivity-insertion accident must be considered in order to test the adequacy of the plant-protection system. Also, a reactivity insertion with failure to scram and a reloading accident must be considered in order to test the adequacy of containment systems.

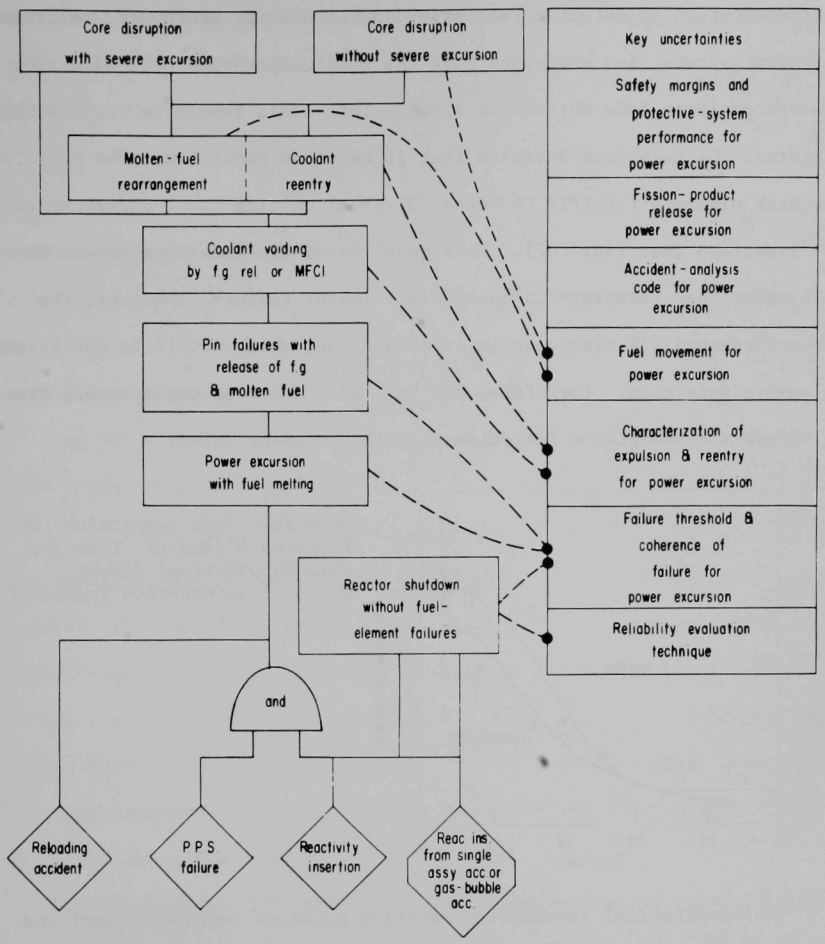

Fig. 106. Accident Sequences and Key Uncertainties for Whole-core Power-excursion Accidents.

The accident sequences and key uncertainties for power excursion accidents are outlined in Fig. 106.

The approach to the reactivity accident with scram is to prevent the occurrence of an inadvertent reactivity insertion and to make rapid or extensive insertions extremely unlikely by design. Also needed are

instrumentation to detect a reactivity increase or an overpower, reliable shutdown systems, and assurance that the fuel temperature reached during power transients does not exceed a value that would result in fuel-element failures. Calculations indicate that it requires about 1 sec for fuel in the peak elements for FFTF to reach 20% areal melting for a $1/sec reactivity insertion (see Fig. 107). This quantity of areal melting should be well under that necessary to cause fuel-element failure. However, the reactor reached 25% overpower in about 0.2 sec, which should be sufficient to assure detection. Therefore, for this case there is considerable time to effect a scram before fuel-element failures might occur.

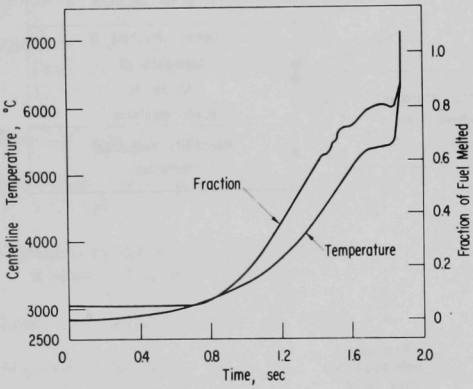

Fig. 107.
Peak Fuel Node Temperature and Fraction Melted vs Time for FFTF Hypothetical $1/sec Reactivity-insertion Transient.

The hypothetical reactivity-insertion accident (without scram) and the reloading accident differ from the pump-coastdown accident in that, for the reactivity accidents, fuel overheating rather than coolant overheating is the principal initial effect. Calculations for FFTF indicate that for a $1/sec reactivity insertion, the cross section of the peak fuel element is 75% melted at the earliest time coolant boiling could begin (1.66 sec after the start of reactivity insertion). For a $5/sec reactivity-insertion rate, the peak fuel temperature is calculated to

reach 5000°K at 0.43 sec when the coolant centerline temperature is only 720°C (1328°F). Because of this, it is expected that coolant voiding probably would occur as a result of fuel-pin failure and fission-gas release or molten-fuel release rather than by coolant overheating and boiling in intact channels. Accordingly, the principal approach is to establish reasonable upper limits to the rate of reactivity insertion caused by voiding by fission-gas release and molten fuel-coolant interaction. Reentry as well as molten-fuel motion also might have an important influence on the reactivity balance after voiding initiation.

The uncertainties for the whole-core power-excursion accidents and their priorities are listed in Table XXI.

Related safety issues. Four categories are listed in Table XVIII that are important only because of the need to test the adequacy of containments and associated consequence-limiting safety systems. These are: severe excursions, containment and energy release, postaccident heat removal, and sodium fires and aerosol behavior that follow from considerations of hypothetical whole-core accidents. The uncertainties that were derived from considerations of the likely sequence of events and the resulting priorities are listed in Table XXII.

Future program. The results of the accident-delineation study and the recommended in-pile program will be reported in "Volume II: Accident Delineation and Recommended Program of Experiments."[3] The revision of Volume I[2] will be completed and forwarded along with Volume II to industry, other AEC laboratories, RDT, and ACRS for review and comment. The comments on the draft reports will be used along with a continuing review of LMFBR accidents to develop a final program for inclusion in the drafts of the integrated reports of the study.

TABLE XXI. Uncertainties and Their Priorities for Related Safety Issues

Uncertainty	Priority		
	Overall	Out-of-pile	In-pile
Excursion energy release	1	-	1
Equation of state	2	2	-
Work-energy release from molten fuel-coolant interaction	1	1	1
Vessel and internal structures strain and rupture analysis	1	1	-
Reactor-vessel cover response	1	1	-
Sodium escape past reactor-vessel cover	1	1	-
Behavior of molten core material in sodium	1	1	1
Criticality sizes of core design	2	-	-
Interaction of molten core debris with structural material	1	1	1

TABLE XXII. Uncertainties and Their Priorities for Whole-core Power-excursion Accidents

Uncertainty	Priority		
	Overall	Out-of-pile	In-pile
Reliability-evaluation technique	2	-	-
Failure threshold and coherence of failure of elements for power excursion	1	-	1
Characterization of expulsion and reentry for power excursion	1	2	1
Fuel movement for power excursion	1	-	1
Accident-analysis code for power excursion	1	-	-
Fission-product release for power excursion	2	2	2
Safety margins and protective-system performance for power excursion	1	-	1

Facility Definition and Utilization

(L. Baker, Jr., R. O. Brittan)

Scope. This study is: (1) defining and substantiating the facility capabilities needed to carry out the recommended program, (2) determining the capabilities of existing or firmly planned facilities, such as TREAT, SEFOR, PBF, and ETR, (3) providing recommendations on the use of existing facilities (including modifications), (4) providing recommendations on the need for any new facilities, (5) developing the general nature and capability requirements of such facilities, and (6) documenting adequately all the above. Included is the development of adequate justification for the capabilities found necessary, the recommended facility modifications and facility usage, and recommendations concerning possible need for new facilities. The study will demonstrate: (1) the technical feasibility of various options for carrying out the program, (2) the technical advantages and disadvantages of the various options, (3) the comparative approximate costs and achievable time schedules of the different options, and (4) the rationale for rejection of the options not recommended.

Summary. A series of studies was completed to assess the capabilities of existing and firmly planned facilities. Test reactors (including TREAT, SEFOR, PBF, GETR), other water reactors, FFTF, and EBR-II have been evaluated in terms of accommodations, energetic capabilities, operating limitations, and availability. Studies to determine design considerations for in-pile test loops are in progress.

Evaluation of capability of existing and firmly planned facilities, including reasonable modifications. A brief outline of the capabilities and limitations of TREAT, SEFOR, PBF, and ETR are presented here.

TREAT description. The Transient Reactor Test Facility (TREAT) is an air-cooled homogeneous graphite-moderated and -reflected transient-test reactor using 93.1%-enriched U_3O_8 fuel, with the $C/^{235}U$ atom ratio equal to 10,000. It has been operational at the National Reactor Testing Station in Idaho since 1959. TREAT was designed for use as a neutron source for transient experiments requiring a large integrated thermal-neutron flux in a single burst with the flux distributed over a large sample volume. The reactor core consists of 4-in.-square zircaloy-clad urania-graphite elements. The maximum loading is a 19 x 19 square array of elements with 32 control rods. The largest core used contains ∿300 elements with 16 control rods. One or more central elements can be removed to form the test space. The active core height is 4 ft.

TREAT accommodations. TREAT has the provision for installation of a through-loop, and out-of-pile components for a large counterflow loop are installed. Two versions of a packaged loop, Mark I and Mark II, have been designed and operated with up to seven experimental LMFBR fuel elements. The packaged loops are presently not capable of holding full-length FFTF fuel elements. However, modifications are planned that would allow this.

TREAT can be loaded so that there is a horizontal viewing slot through the core that is almost 2-ft high by 3.5-in. wide. The slot can be used with the fast-neutron hodoscope, which provides means to record motion of experimental fuel in opaque capsules or loops.

TREAT has operated with up to 200 gm of plutonium in the test vehicle. Limited facilities are available for assembling and disassembling experiments and for examination of experiments.

TREAT energetic capabilities. TREAT has a highly thermalized air-cooled core with steady operation at 100 kW possible indefinitely.

Four modes of transient operation are possible: self-limiting transients, clipped transients, flat-top transients, and transient bursts followed by low-power operation for a limited time.

Self-limiting transients can be initiated to provide an adiabatic energy density that will raise the hot-spot core fuel-element temperature to 600°C. The total reactor energy release during the transient depends on the size of the core used and on the max/ave fission density. In addition to the hot-spot temperature limit, there is a limit imposed on the total available excess reactivity that can be employed in a transient. This latter restriction might be relaxed when operation is possible with the new programmed control system that has been installed. The present maximum allowable self-limited transient is realized with a reactor period of about 20 msec. Clipped transients are initiated in the same way as self-limited transients, however, they are terminated by control-rod insertion and the relatively slow power decay in self-limited transients is eliminated.

Energy deposition in test fuel elements is affected strongly by flux-depression effects. Detailed physics calculations or preliminary in-pile calibrations are necessary to relate the energy density in test fuel to that in the driver core. Calculations on the fission densities have been made for a single experimental pin and for clusters ranging from 7 to 37 pins. Results, confirmed by experiments, for a single fully enriched pin indicate a ratio of energy density at pin centerline to the core maximum of 75. The adiabatic energy density required to heat core fuel from 50 to 600°C has been determined to be 315 cal/cm^3. Therefore, the maximum energy density obtainable in one UO_2 pin of 85% theoretical density is about 75 x 315 or 23,600 cal/cm^3, which is approximately 7.6

times the energy required to heat UO_2 of 85% theoretical density from 25°C to the melting point and fully melt it.

The flux depression for a single 13%-enriched UO_2 pin results in a ratio of maximum-to-average radial power density of about 1.20. In a cluster of seven fully enriched pins, the maximum power density in the outer row of pins is about 6.5 times that at the centerline of the center pin. Hence, to attain a reasonably flat radial power-density distribution in clusters, the low-energy neutrons are filtered out and/or graded enrichments are used. Calculations with a boral filter show that the maximum ratio of radial-to-centerline power in the test cluster ranged from 1.23 for 7 pins to 1.41 for 37 pins. The corresponding ratio of centerline-sample-to-maximum-core energy density ranged from 22 to 14.8, so the center pin in a fully enriched 37-pin cluster could receive a maximum energy deposition only 1.5 times the energy required to fully melt UO_2 of 85% theoretical density. Therefore, experiments using 37 pins with a flux filter are marginal with respect to energy-generation capability using a neutron filter alone. If adequate flattening by graded enrichment is attempted, the energy-density ratio, 14.8, would be further reduced, and the margin could disappear.

One way to extend the capability of TREAT is to develop a fast-neutron converter region that would absorb the low-energy flux and create a fast-flux environment. Preliminary calculations have indicated that an energy-density ratio of 44 can be achieved with a maximum radial-to-centerline power-density ratio of 1.01 for clusters ranging from 7 to 37 pins. Thus, for practical purposes, flux-depression effects can be eliminated and each pin can receive an energy deposition of about 4.4 times that needed to melt UO_2.

In the flat-top mode of operation, initial reactivity is added, and the power is allowed to reach the self-limited maximum. Then, additional controlled reactivity is added to just balance the reactivity loss due to heating. This can be continued until the maximum allowable energy density in core fuel is deposited, or until all of the allowable available reactivity is added. Currently, the latter consideration is limiting and allows only a fraction of the former restriction to be realized.

To operate a pin with 0.23-in.-diameter oxide fuel (GE 1000-MWe reference) at 14 kW/ft corresponds to an average pin power density of 1713 W/cm^3 or 409 cal/cm^3-sec. The length of time over which this energy deposition can be sustained depends on the maximum core-to-sample-centerline power-density ratio. For the fully enriched 7-pin cluster with center-pin power density of 409 cal/cm^3-sec and the 600°C operating limit, this time is about 17 sec with the boral shield and 31 sec with the converter, as compared to 45 sec for the unshielded cluster.

TREAT operating limitations and availability. TREAT is available for full-time use in the LMFBR Safety Program although the design and installation of a fast-neutron converter would require about two years. Development of a test vehicle to utilize fully the enhanced capability of TREAT with a converter region would require a comparable lead time.

SEFOR description. The Southwest Experimental Fast Oxide Reactor is owned by the Southwest Atomic Energy Associated and operated by the General Electric Co. At present, the reactor is involved in a 3-yr program that includes transient experiments with two different cores. The primary purpose of the current SEFOR program is the systematic measurement and demonstration of the Doppler coefficient. However, a study is underway[4] to evaluate the capabilities of SEFOR as a fast-reactor test facility. The

study is focused on the use of SEFOR for safety-oriented fuel experiments. Consideration is being given to both transient overpower testing and loss-of-flow testing at steady power.

SEFOR is a 20-MWt sodium-cooled reactor that is fueled with mixed oxide containing 18.7% PuO_2. The 0.97-in.-OD 316-stainless-steel-clad fuel elements are clustered six per subassembly with a triangular pitch of 1.047 in. The active core of ∿100 subassemblies is 33.8-in. high.

SEFOR accommodations. Space is available for in-core testing in the off-center hexagonal fuel channels, which are 3.03-in. across flats and 106-in. long. Axial space above and below the core is very limited and there is no provision for a through-loop. Out-of-core handling and shielding limitations are such that a packaged loop appears to be limited to a total length of ∿15 ft and a diameter of 10 in. The capability of the reactor coolant to remove heat from experimental loops is limited by the low pressure drop (5 psi across the driver core) and by the amount of space above the core in which to install a heat-exchanger section.

SEFOR energetic capabilities. SEFOR has a core composition, neutron spectrum, and operating fuel temperatures similar to those of a large ceramic-fueled fast breeder reactor and is capable of operating at a steady core power of 20 MWt. It also has a transient operating capability with excursions from very low power or from operating power. A special reactivity insertion device makes it possible to attain a net reactivity >$1. However, it is not intended, during the transient, to damage the driver fuel, which has steady-state peak temperatures close to the melting point.

At a constant power of 20 MWt, the energy generation in an LMFBR test fuel element having the same composition as the driver fuel (1/4 in. dia.,

18.7% PuO_2) is about 1.2 kW/ft. It is possible to increase this to about 5.9 kW/ft by enriching the uranium in the test fuel to 93%. Because of the fast spectrum, there is a negligible flux depression and, therefore, a nearly uniform energy density can be maintained in clusters of experimental pins as well as in a single pin.

There are plans that would increase the steady-state capability of SEFOR from 20 to 50 MW. This would increase the energy-generation rate for fully enriched fuel elements to almost 15 kW/ft. However, a completely new core and a new intermediate heat exchanger would be required. A method that might be used to increase the capability at 20 MW would be to alter the pin size and enrichment of the inner core, increase the cooling rate, and use some moderator in the test region. The cost and time required for such a modification is far less than that for an overall core power increase; however, this would introduce flux-depression effects similar to those characteristic of thermal test reactors. The optimum tradeoff among the fission density, number of experimental elements, and flux depression introduced by moderator addition is unknown at present.

Another consideration is the potential for reactivity feedback to the driver core from an experiment in which fuel could melt and redistribute. This factor mitigates against conducting safety experiments with very large clusters of experimental fuel elements. SEFOR is capable of operating at an increased power for a short time, although no estimates of time at power are available.

The capability for rapid transient operation can be evaluated in terms of the calculated energy release for the driver core and the ratio of energy generation in test fuel to that in the driver fuel. A reactivity addition of $2 at a rate of $2/sec is representative of anticipated

SEFOR transient operation. Such a transient was calculated to release about 1480 cal/cm^3 to the peak driver fuel element. The corresponding maximum energy deposition in fully enriched test fuel would be about 7300 cal/cm^3, or about 2.5 times the energy required to fully melt oxide fuel. Clearly, if means can be found to increase further the ratio of energy density in the test section to that in the driver core for purposes of steady-state operation, transient energy capability will be increased correspondingly.

SEFOR operating limitations and availability. SEFOR will not be available for safety testing until the current physics program has been completed. After that, there appear to be no operating limitations that would preclude the performance of LMFBR safety experiments. However, possible limitations on the size of potential experiments were noted above. Also, the capability to generate peak design power in clusters of LMFBR fuel pins remains to be established.

PBF description. The PBF is a water-cooled and -moderated transient test facility designed to operate continuously at 20 MW. It is under construction at the National Reactor Testing Station in Idaho and is expected to be operational in about a year. The reactor core is in an open pool, and the test space is formed at the center by an octagonal aluminum filler piece with an 8.250-in. hole. The reactor is designed primarily for water-reactor safety tests with clusters of as many as 68 PWR fuel elements in a pressurized loop within the central test hole. The driver core contains about 2400 fuel elements of 0.75-in. diameter. The cladding is 304L stainless steel and the fuel is a urania zirconia, calcia ceramic that has a large heat capacity. The fuel is insulated from the cladding by a 48-mil zirconia sleeve. The active core height is 3 ft.

PBF accommodations. PBF has the provision for installation of a through-loop, including the necessary piping tunnels and controlled-atmosphere equipment cubicle. However, use of a packaged sodium loop for LMFBR experiments reduces the hazard associated with loading and unloading a stationary sodium loop over a water reactor. Vertical clearance for such a packaged loop is adequate. However, there are four transient-rod shrouds located about 12 in. radially out from the test hole. The water coolant has an adequate heat-removal capability for ultimate heat rejection from experiments by way of suitable heat exchangers. The use of plutonium-bearing experimental fuel is expected to be acceptable, although a doubly contained loop would probably be required. Shipping and handling of test vehicles is facilitated by the location of the reactor at NRTS and by the proximity of examination facilities.

PBF energetic capabilities. The core design has been optimized with respect to flux hardening and core cooling to the point that any improvement in either one will decrease the overall energy-generation capability. Four modes of operation are possible: self-limiting transients, shaped bursts, constant-power operation, and transient bursts followed by steady-state low-power operation.

Self-limiting transients can be initiated to release up to 1450 MW-sec. This energy release is such that the driver-fuel peak temperature reaches 2350°C, which is 100°C below the melting point of the ternary fuel mixture. The maximum allowable self-limited power transient has a minimum reactor period of about 1.3 msec. Shaped bursts are obtained by controlling the withdrawal rate and sequence of four transient rods. The rods are computer controlled. Overall energy release for shaped bursts is also limited by the peak driver-fuel temperature.

Energy deposition in test fuel elements is affected strongly by flux-depression effects. Thus, while there is a very large energy capability for a single LMFBR fuel element, flux shielding by successive rings of elements results in strong variation of energy deposition among pins of a fuel-element cluster. A convenient expression of energy-deposition capability is the figure-of-merit (FOM), which is the ratio of average energy deposition in test fuel to the peak in the driver fuel. For transient energy deposition starting from initial cold conditions, about 200 cal/gm can be safely absorbed by the driver fuel. Clearly, the quantity is less if the transient is initiated from an operating condition. The FOM for a single LMFBR test pin (¼ in. dia., 25% enriched) is about 16, but it is only about 1.5 for the center pin of a cluster of 37 LMFBR pins. In the latter case, only about 300 cal/gm can be deposited in an experimental fuel element, which is insufficient to completely melt oxide fuel. An improvement can be achieved using graded enrichment. An FOM of 2.5, or about 500 cal/gm, is potentially available if the enrichment is graded from 8 to 25%. There are two problems with enrichment grading: (1) flux depressions within each pin remain, and (2) if the experiment involves fuel melting and molten fuel motion, the location and degree of heat generation becomes very uncertain. A thermal-neutron filter can mitigate the flux-depression problems to a considerable degree. A cadmium filter combined with a nonhydrogenous moderator located within the test hole can reduce the radial flux depression to about 6%; however, there is a net loss in total flux available to the experiment. It is estimated that an FOM of 1.5 would be available using an enrichment of 25% and that the FOM could be increased considerably if test fuel having a greater enrichment were employed. More detailed calculations are needed to determine if sufficient energy could be supplied to a 37-pin experiment, but

it is likely that 19-pin LMFBR experiments could be powered adequately in the self-limiting and shaped-burst modes of operation using thermal-neutron filters. Preliminary considerations concerning the design of a fast-neutron converter region for PBF were unfavorable. The existing optimization of the spectrum and the cooling supplied to the core mitigates against the successful design of an economical and effective converter region.

Constant-power operation at greater than 20 MW can be maintained for limited times. The factors that control the time are the heat capacity of the fuel and the characteristics of the cooling system, which is designed for steady-state removal of 20 MW. Preliminary calculations indicate that 40 MW can be maintained for about 15 min, 50 MW for 80 sec, 60 MW for 40 sec, and 150 MW for 10 sec. At the basic power of 20 MW, the steady-state heat generation in an LMFBR fuel element (¼ in. dia., 25% enriched) is less than 2 kW/ft using a thermal-neutron filter. This can be increased somewhat by greater enrichment, but probably to less than 5 kW/ft. Therefore, operation at typical LMFBR peak powers of about 15 kW/ft is limited to about a minute. However, there is the potential for simulating full-power operation for a short time followed by reduction to decay power levels for a long time. Also, it might be possible to operate at a steady-state power higher than those indicated when the outdoor temperature is low.

PBF operating limitations and availability. There appear to be no operating limitations that would preclude the performance of LMFBR safety experiments in the PBF. Limitations concerning the quantity of excess reactivity that can be used to sustain short-term overpower operation might reduce the time-at-power capability to less than that noted above. The PBF will not be in operation for about a year. Although it

is expected that tests in the water-reactor safety program will have first priority, the PBF probably will be available for LMFBR tests if the tests do not involve modifications that would hinder the progress of the water-reactor safety program.

ETR description. The Engineering Test Reactor is owned by the AEC and operated by Idaho Nuclear Corp. at the National Reactor Testing Station. The reactor has been used for research and isotope production since 1958. ETR is a 175-MWt water-cooled and -moderated test reactor that has no transient overpower capability. There are about 50 fuel assemblies, each 3.04-in. square, composed of uranium-aluminum-alloy plates. The uranium is fully enriched. The active core height is 36 in.

ETR accommodations. ETR has nine high-flux test holes suitable for loop installation. The holes vary in size from 3 to 9 in. square. Since all work in servicing a loop installed in the ETR must be performed from the top head, the design and operation of a sodium through-loop poses formidable problems. A more suitable approach is a packaged sodium loop of the type being designed in the Fuel Element Failure Propagation program. Vertical clearance for a large loop is adequate and the reactor coolant has an adequate heat-removal capability for heat rejection from the experiment. Also, Pratt & Whitney designed a sodium loop for the ETR, so some of the potential safety problems associated with sodium-loop operation have been resolved.

ETR energetic capabilities. ETR has a thermal-neutron flux of about 4×10^{14} n/cm^2-sec and a fast-neutron flux greater than 2×10^{14} n/cm^2-sec. Two methods are available to overcome flux-depression effects in clusters of experimental fuel elements: enrichment grading and thermal-neutron filters. Calculations supported by tests in the

Argonne Thermal Source Reactor indicate that either enrichment grading or a combination of grading combined with the use of a filter can be used to equalize average fission density among the three rows of elements in a 19-element cluster. In one design, a 0.64-cm-thick boron filter combined with enrichments graded from 53 to 70% resulted in the uniform generation of 2000 W/cm^3 (16.3 kW/ft) in each of 19 LMFBR elements of ¼-in. diameter. Therefore, it can be concluded that there is adequate energy capability to simulate full-power LMFBR operating conditions. There is associated with such capability a variation in flux density across individual pins that probably can be limited to less than 20%.

ETR operating limitations and availability. There appear to be no operating limitations that would preclude the performance of LMFBR safety experiments in the ETR if scheduling arrangements with other users can be worked out.

Future program. The initial emphasis will be on determining the required test conditions and schedules for the tests recommended under programmatic definition and justification. Also, the evaluation of the capability of existing and firmly planned facilities, including reasonable modifications, will be completed. Then recommendations for their use will be prepared. Then detailed consideration will be given to the facility capabilities required to perform experiments that cannot be carried out in existing or modified facilities. Recommendations on the need for new facilities will be developed on the basis of these considerations. An integrated report of the study will be distributed for comment; a final report will be prepared.

References

1. *Liquid Metal Fast Breeder Reactor (LMFBR) Program Plan, Vol. 10, Safety*, WASH-1110 (Aug 1968).

2. C. N. Kelber et al., ANL, private communication (Jun 1969).

3. L. Baker et al., ANL, private communication (Aug 1970).

4. L. F. Fidrych and J. O. Arterburn, *SEFOR Construction, Operation: Preclude to LMFBR Development,* Nuclear News, *13*(3), 53-57 (Mar 1970).

5. C. N. Kelber, *A Bootstrap Concept of a Safety Test Facility,* Nuclear Applications and Technology *9*(6), 780-785 (Dec 1970).

6. C. N. Kelber and A. M. Judd, "A Research Program for LMFBR Safety," *Symposium on Dynamics of Nuclear Systems, ANS Topical Meeting,* (Mar 23-25, 1970), University of Arizona Press (in press).

Nuclear Safety Research and Development--LMFBR Safety

XI. FUEL-COOLANT INTERACTIONS*

(R. O. Ivins and R. W. Wright)

In-pile Tests

(J. J. Barghusen, R. W. Wright, C. E. Miller, J. F. Boland, and R. W. Mouring)

Pressure and work energy (S series). A series of TREAT meltdown experiments, which simulate reactivity-accident conditions, are being conducted using stainless-steel-clad UO_2 fuel rods contained in a sodium-filled piston autoclave. These experiments are designed to provide information on the pressures and mechanical energies that result from the interaction of molten fuel and coolant under such conditions. For the analysis of the simulated reactivity accident, data are obtained on pressure-time histories, the momentum transfer to a movable piston, the magnitude of failure threshold energy, and the coolant temperatures.

Description of piston autoclave. The piston autoclave used in the experiments is a double-containment assembly. The outer autoclave serves as an insulating jacket and a secondary containment vessel in the event the primary container is ruptured. The inner autoclave holds the fuel-rod cluster and sodium coolant (Fig. 108).

The autoclave contains a pressure transducer and rupture diaphragm (rated at 6000 psi) at the bottom. Above this is the fuel-rod cluster consisting of five fuel rods and four dummy rods (containing helium at 15 psia) arranged as in Fig. 109. The dummy rods were constructed from single sections of Type-304 stainless-steel tubing 12-in. long, with 0.29-in. OD and a wall thickness of 12 mils. Each fuel rod consisted of two separate sections joined by a dowel-pin fitting, an upper or blanket

*For references for this chapter, see p. 371.

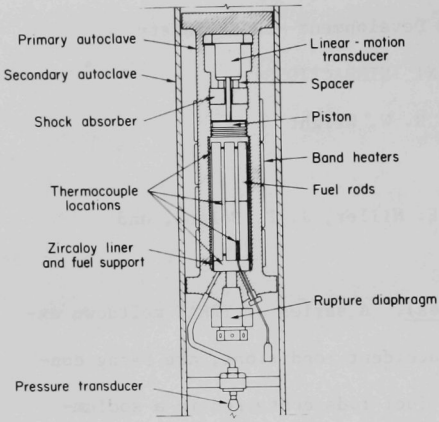

Fig. 108.
Piston Autoclave for High-energy Meltdown Experiments and Measurement of Transient Pressure and Sodium Expulsion. ANL Neg. No. 113-2610, Rev. 1.

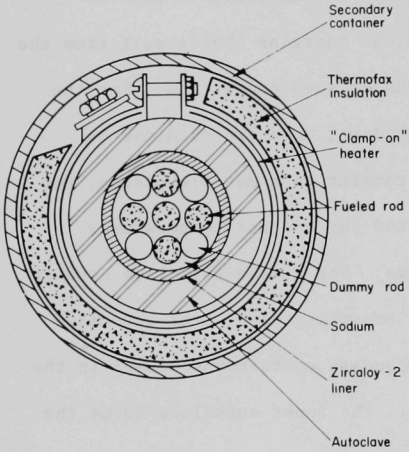

Fig. 109.
Top View of 9-rod Fuel Cluster for Fuel-meltdown Studies in Sodium.

section 6 1/8-in. long, and a 5 7/8-in.-long fueled section containing sintered pellets of 10%-enriched UO_2. Each fuel rod contained 41 gm of UO_2. The cluster is positioned between two support grids and contained within a Zircaloy-2 sleeve and the entire unit is submerged in sodium. Immediately above the fuel-rod cluster is a piston, made of tungsten-30% molybdenum alloy, which is attached to a connecting rod passing through a shock absorber to a differential-transformer linear-motion transducer. The shock absorber

is designed to absorb the major portion of the kinetic energy imparted to the piston during normal experiments and to sieze the connecting rod, thus preventing piston rebound. Four tungsten-5% rhenium-tungsten-26% rhenium thermocouples are located in the sodium, among the fuel rods, at distances from 3 to 12 in. above the bottom of the autoclave.

The complete inner autoclave, including external band heaters to heat the sodium to ∿200°C, is placed in the secondary autoclave. The inner autoclave is spring-loaded against its bottom support inside the secondary autoclave to permit 3/8-in. travel before it contacts a shock absorber mounted between the upper heads of the two autoclaves. This free travel space was provided to allow for thermal expansion.

Summary of experimental results. Four meltdown experiments have been performed in the piston autoclave. A calibration test (S1) was performed to determine the factor relating reactor integrated power was fission-energy input into the fuel. The first set of three experiments (S2, S3, and S4) was directed principally toward determining the effect of increasing fission energy on the consequences of fuel failure: fission-energy levels of 340, 460, and 720 cal/gm UO_2, respectively. The most recent experiment, S5, was made to examine whether fuel-coolant interaction will produce large pressures and work energies in the absence of bond gas. Principal results of the four experiments are presented in Table XXIII.

Test S2 used the piston autoclave and consisted of three transients of progressively higher energy (312, 481, and 495 MW-sec, corresponding to average fission energies of 214, 330, and 340 cal/gm UO_2). After each transient, a neutron radiograph was taken of the autoclave assembly to determine the condition of the fuel. The central fuel rod failed during the third transient.

TABLE XXIII. Experimental Conditions and Results from Piston-autoclave Tests S2, S3, S4, and S5

	S2 (He bonded)	S3 (He bonded)	S4 (He bonded)	S5 (Evacuated)
Reactor characteristics				
Peak power,* MW	2310	2664	6650	3357
Period, msec	62	53	34	45.6
Integrated power,* MW-sec	495	669	1050	740
Reactivity, %	2.1	2.4	3.3	2.7
Fuel and autoclave properties				
Internal pressure of fuel and dummy rods, torr	780	780	780	5×10^{-5}
Mass of UO_2 fuel, gm	205	205	205	205
Uranium enrichment, % ^{235}U	10	10	10	10
Mass of sodium in autoclave, gm	198	201	200	199
Mass of piston, gm	260	260	260	263
Sodium temperature at start of test, °C	190	165	165	170
Results				
Total fission energy, cal/gm UO_2	340	460	720	509
Amplitude of largest pressure pulse, psi	180	540	1800	2940
Impulse from largest pulse,† dyne-sec	0.25×10^5	0.68×10^5	1.84×10^5	3.3×10^5
Sum of impulse from all pulses,† dyne-sec	0.33×10^5	2.39×10^5	10.4×10^5	24.2×10^5
Fission energy at first pressure pulse, cal/gm UO_2	234	440	480	430
Calculated fractional conversion of nuclear to mechanical energy	‡	2.1×10^{-5}	2.5×10^{-4}	1.9×10^{-3}
Period during which major pressure pulses occur, msec	8	18	12	285

*Values for Tests S5 and S4 are corrected to provide consistency with the calibration factor and TREAT fuel loading for Test S3.

†Impulses calculated from pressure-response data based on application of the impulse to the area of the piston (0.601 in.^{2}).

‡ Only central pin failed by tear in cladding.

Figure 110 shows the motion, pressure, and reactor power recorded during a portion of the third transient. An apparent pin failure about 30 msec after the power peak is indicated by the first pressure pulse (80 psi). The energy input at this time was only 234 cal/gm, and the energy input at the time of the second pressure pulse (180 psi) was 280 cal/gm. The first pressure pulse occurred before fuel melting should have occurred, so it is postulated that this pulse resulted from escape of pressurized helium from a weak point in the cladding and the second pressure pulse was caused by contact of sodium and fuel.

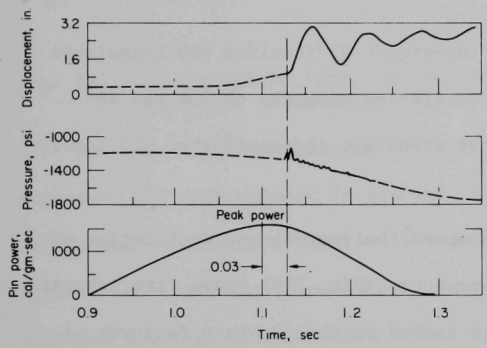

Fig. 110. Motion, Pressure, and Reactor Power during Third Transient of Test S2.

The first pressure pulse coincided with an increase in velocity of the piston from 8 to 86 cm/sec, while the second pulse caused the velocity of the piston to increase to 193 cm/sec. At the second pressure pulse, the change in momentum of the piston and the effective accelerated sodium mass was 3.7×10^4 dyne-sec. This is to be compared with the measured impulse of the second pressure pulse of 2.51×10^4 dyne-sec.

The center rod of the cluster failed during the third transient, allowing 24.3 gm, or 59.5% of the UO_2 in that rod to escape. Figure 111 shows the split in the cladding located at the top of the fueled section

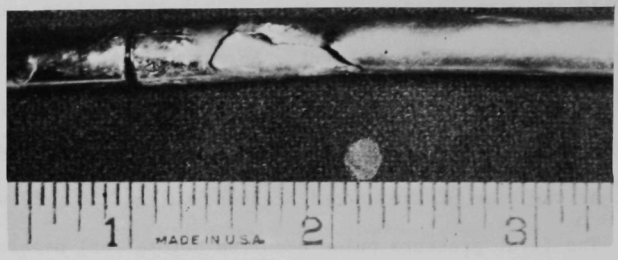

Fig. 111. Portion of Ruptured Fuel Rod Showing Failure. ANL Neg. No. 113-1449.

of the rod. No sign of cladding, melting, or expansion of the rod was observed.

Test S3. Meltdown Experiment S3 involved two transients of 344 and 669 MW-sec, equivalent to fission energies of 236 and 460 cal/gm UO_2, respectively. The first transient indicated that all instruments responded properly.

The 460 cal/gm UO_2 transient caused the rupture and destruction of all five fuel rods. The pressure response (Fig. 112) shows five separate pressure pulses, which perhaps were caused by the separate failures of the five fuel rods. The first two pressure pulses, I_1 and I_2, occurred almost simultaneously near the end of the transient (at 645 MW-sec, 444 cal/gm UO_2); the first pressure spike also coincided with a rapid acceleration of the piston from a velocity of 6 to 302 cm/sec. The third pressure pulse (I_3), the largest, had an amplitude of 540 psi and a pulse width of 2.7 msec, and caused the piston velocity to increase from 302 to 472 cm/sec. The final two pressure pulses (I_4 and I_5) occurred after the piston was locked in its final position; Pulse I_5, which occurred considerably later than the previous pulses, was essentially identical to Pulse I_4. As in Test S2, the pressure-response data could be correlated with the change in momentum of the piston.

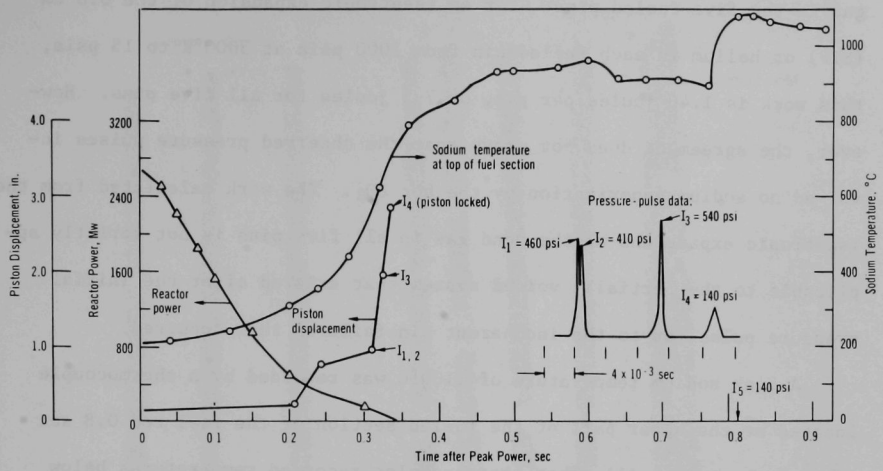

Fig. 112. Linear Motion, Pressure Response, and Sodium Temperature for Test S3. ANL Neg. No. 113-2352.

The sum of the impulses of the five pressure pulses was 2.39 x 10^5 dyne-sec. If this impulse is assumed to act on the free piston mass of 260 gm and an effective expelled sodium mass of 88 gm, then the fractional conversion of nuclear to mechanical energy for the test is 2.1 x 10^{-5}. For inertial loading, the effective sodium is taken to be all the sodium in the autoclave except for that in the chamber below the fuel-pin bundle and that in the bottom quarter of the fueled section of the bundle. In calculating the effective inertia of this sodium, the effective length of sodium in each cross section is weighed inversely as the area of that cross section relative to the piston area. The effective sodium mass to be added to the piston mass for estimating the conversion of nuclear to mechanical energy is 88 gm. The calculated kinetic energy of the piston and the effective mass of accelerated sodium is 8.2 joules.

The calculated kinetic energy of 8.2 joules is approximately equal to the work potentially available from the expansion of the high-pressure bond

gas in the five fueled pins. For an isentropic expansion of the 0.8 cm^3 (STP) of helium in each fueled pin from 1000 psia at 3000°K to 15 psia, this work is 1.46 joules per pin, or 7.3 joules for all five pins. However, the agreement does not prove that the observed pressure pulses involved no sodium vaporization by the hot UO_2. The work calculated from the isentropic expansions of the bond gas in all five pins is not strictly applicable to the partially voided system that existed after the initial pressure pulse, or to the incoherent pin failures that occurred.

A peak sodium temperature of 1100°C was recorded by a thermocouple located at the upper part of the fueled section of the fuel rod 0.8 sec after peak power. All other thermocouples recorded temperatures below 500°C.

The residue from Test S3, as shown in Fig. 113, indicated that the five fuel rods were completely destroyed during the transient. Only small (∿0.5-in. long) cylindrical sections of fused UO_2 remained (see Fig. 114); these sections were hollow (3/16 in. ID) and had an outside diameter of 0.265 in. This behavior might be explained in the following manner: the UO_2 pellets apparently expanded by virtue of partial melting and, upon contact with the cladding (cladding ID was 0.260 in.), the cladding melted, and the outer portion of the UO_2 solidified. The hollow core was the result of molten oxide flowing from the solid oxide annulus.

All dummy rods suffered cladding failure in the form of melted sections at the lower portions of the rods, as shown in Figs. 113 and 115. A section of one fuel rod was welded to the dummy rod (Fig. 115). Most likely, the mechanism of failure of the dummy rods was by contact with molten UO_2 expelled from the fuel rods.

Test S4. Experiment S4 involved a reactor transient of 1050 MW-sec, resulting in a fission energy release in the test fuel of

Fig. 113. Residue of Fuel and Dummy Rods from Test S3. ANL-ID Neg. No. 103-7535, Rev. 2.

Fig. 114. UO_2 Residue from Test S3 in Form of Hollow Cylinders. ANL-ID Neg. No. 103-7534A.

720 cal/gm UO_2. The value of peak reactor power was 6650 MW, and the reactor period was 34 msec. The fuel loading and configuration for this experiment were identical to those used for Experiments S3 and S2.

The high-energy transient caused the rupture and destruction of all five fuel rods. The pressure-response record (Fig. 116) shows five large discrete pressure pulses, and several minor pulses of amplitudes less than 550 psi. The first two pulses (I_1 and I_2) occurred about 30 msec after peak power. The integrated reactor power at the instant of the first pulse was about 705 MW-sec, equivalent to a fission-energy

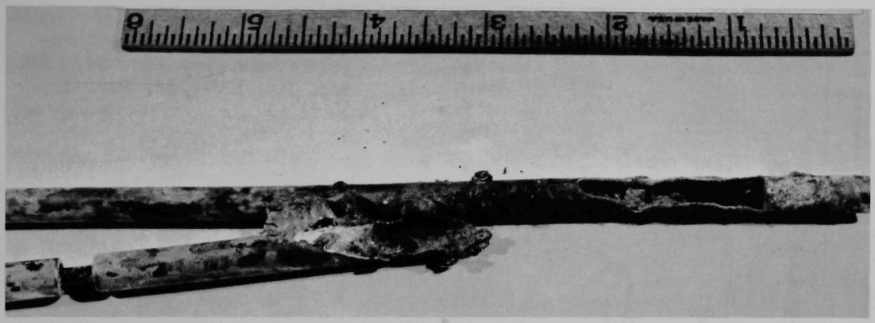

Fig. 115. Section of Fuel Rod Welded to Dummy Rod by Melting of the Cladding. ANL Neg. No. 113-1804A.

release in the test fuel of about 480 cal/gm UO_2. These pulses were followed by a large pulse composed of two peaks less than 0.3 msec apart. The first peak of the double pulse occurred 34.4 msec after peak power and had an amplitude of 1060 psi; the second peak had an amplitude of ∿1800 psi. Impulse I_5, 1280 psi, occurred 42 msec after peak power. The final pulse (I_6) was significantly delayed, occurring about 2.4 sec after peak power. This pulse might be the result of flashing of superheated liquid sodium. At the instant of the pulse, the temperature of the sodium decreased from ∿1700 to ∿1000°C. Flashing of sodium at 1700°C would generate a pressure pulse of ∿900 psi.

The output of the linear-motion transducer is reproduced in Fig. 116. As in the case of Experiment S3, acceleration of the piston occurred simultaneously with the generation of the pressure pulses. The maximum piston velocity was 807 cm/sec (Interval D in Fig. 116), which occurred coincidentally to the 1800-psi pressure pulse (Impulse I_4). The impulsive deceleration of the piston from 807 to 400 cm/sec for the final 2 cm of piston travel was probably caused by contact of the piston or the connecting rod with a burr.

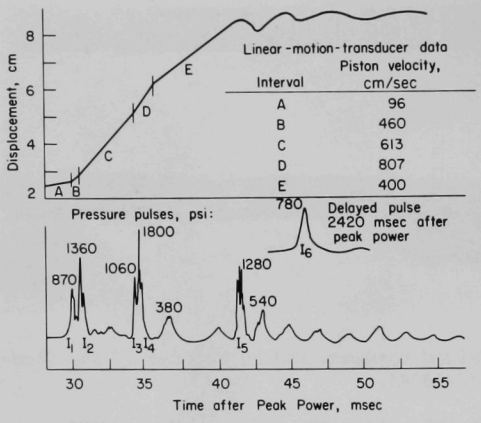

Fig. 116. Linear-motion and Pressure-pulse Data from Test S4. ANL Neg. No. 113-3137, Rev. 1.

Temperatures greater than 3000°C were recorded by the two thermocouples in the upper portion of the sodium cavity, at the 11-in. and 17-in. levels. A peak temperature of 3400°C was recorded by the 11-in. thermocouple 0.6 sec after peak power. The 17-in. thermocouple recorded event temperatures greater than 3600°C about 0.1 sec after peak power. These temperatures would result in melting of the tantalum sheath, beryllia insulation, and the W-Re thermocouple itself. Therefore, these very high readings cannot be considered meaningful.

The sum of all impulses for Test S4 was 10.4×10^5 dyne-sec. If it is assumed that this impulse acts to accelerate the piston and an effective sodium mass of 88 gm, then the fractional conversion of nuclear to mechanical energy is 2.5×10^{-4}, a factor of ten greater than in Test S3. The calculated kinetic energy for Test S4 is 154 joules. This is 21 times greater than the 7.3 joules potentially available in an isentropic expansion of the helium bond gas in the five fueled pins.

Test S5. The objective of Test S5 was to determine whether fuel-coolant interactions will produce large pressures and work energies in the absence of bond gas. It had been hypothesized that gas-

blanketing of the molten fuel by the bond gas in Tests S3 and S4 prevented extensive fuel-coolant interactions and that this accounts for the low pressures and mechanical energies that occurred in these tests. Test S5 was performed with fuel pins and dummy pins that had been sealed in vacuum. Although there was no bond gas in the evacuated fuel pins, the UO_2 pellets were of 93% theoretical density. The vacancies in the UO_2 matrix contained gas that would not be removed by the evacuation procedure, but which would be released upon fuel melting. Therefore, Test S5 is not completely free of the effects of gas upon fuel-coolant interactions and cladding failure. To provide a valid basis for comparison of the effect of bond gas, Test S5 was performed under conditions otherwise nearly identical to those employed in Test S3.

The fuel specimens and configuration used in Test S5 were identical to those used in Tests S2, S3, and S4, except that the fuel rods, dummy rods, and "blanket" sections were evacuated to 5×10^{-5} torr prior to welding the end caps. In all previous tests, the fuel rods, dummy rods, and blanket sections contained helium at 15 psia (780 torr).

The test was performed at 740 MW-sec (509 cal/gm UO_2), slightly higher than the energy for Test S3. A total of 16 pressure pulses of amplitudes greater than 50 psi were observed on the output of the pressure transducer. The appropriate sections of the pressure-response data are shown in Fig. 117, with the pulses identified sequentially by letters a through p. The initial pulse (69 psi) occurred 100 msec after peak power at a fission-energy input of 430 cal/gm UO_2. This pulse occurred coincidently with the acceleration of the 263-gm piston to a velocity of 206 gm/sec. The piston became seated before the second pulse occurred. The change in momentum of the piston and the effective mass (88 gm) of

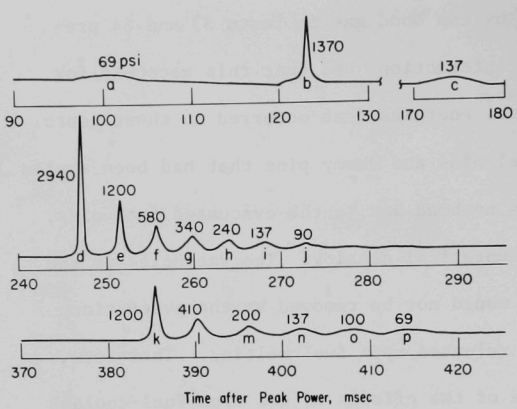

Fig. 117. Pressure-response Output from Test S5 with Evacuated Fuel Pins. ANL Neg. No. 900-435.

the expelled sodium (72,000 dyne-sec) agrees reasonably well with the measured value of the first impulse (85,000 dyne-sec). The fission-energy input to the fuel at the instants of Pulses b and c were 451 and 483 cal/gm UO_2. The transient was completed prior to Pulse d.

The apparent damped oscillations following Pulses d and k in Fig. 117 are not yet understood. These oscillations occurred after the piston had been seated at its maximum travel. Somewhat similar but smaller-amplitude pressure oscillations were observed in Test S4. The 4-msec period of the oscillations is an order of magnitude too large for acoustic oscillations in the vapor cavity within the autoclave at full piston travel. No spring-mass oscillations of the system in this period range have yet been identified.

The largest pulse (Pulse d) had an amplitude of 2940 psi and an impulse of 3.3×10^5 dyne-sec. The impulses calculated from the pressure-response data were based on the application of the pulse to the area of the piston (0.601 in.^{2}). The largest pulse observed in Test S3 had an amplitude of 540 psi and an impulse of 0.68×10^5 dyne-sec; the sum of impulses from all five pressure pulses in Test S3 was 2.39×10^5 dyne-sec. The total impulse from the pulses in Test S5 (24.2×10^5 dyne-sec) is

ten times that observed in Test S3. If this impulse is assumed to act on a free piston mass of 263 gm as well as the effective expelled sodium mass of 88 gm, then the fractional conversion of nuclear to mechanical energy for Test S5 is 1.9×10^{-3}. This fraction was 2.1×10^{-5} in Test S3. In Test S4, performed with helium-bonded fuel at a total fission-energy input of 720 cal/gm UO_2, the fractional conversion was 2.5×10^{-4}. If the damped oscillations observed in Test S5 are considered extraneous, so that only the initiating pulse in each train acts to accelerate the load, then the total impulse in the test is reduced to 11.3 dyne-sec, and the fractional converstion of nuclear to mechanical energy is reduced by a factor of 4.6 to 4.2×10^{-4}.

As shown in Table XXIII, removing the bond gas in Test S5 increased the time interval over which pin failure occurred by an order of magnitude to 285 msec from 18 msec in the comparison run, S3. This long time before failure must be due partly to the fact that the total energy input to the fuel in the S5 transient was apparently just sufficient to fail all the fuel. The initial pin failure associated with the first pressure pulse at 430 cal/gm may be anomalous. The pulse is very broad and has a peak pressure of only 69 psi, but Pulse c at 483 cal/gm is similar in shape and of low magnitude. In any case, the difference between Tests S3 and S5 indicates that pressurization of the cladding by bond gas produces greater coherence of pin failure than would occur without bond gas. It should be noted that gas within the UO_2 matrix that would be released upon UO_2 melting would be expected to produce some gas pressurization of the cladding even in Test S5.

A maximum event temperature of 1875°C was observed 0.45 sec after peak power by the thermocouple located in the vicinity of the fueled section of the fuel array. As in the case of Test S4, the upper thermocouple indicated event temperatures greater than 3000°C.

A portion of the residue from Test S5 is shown in Fig. 118. It is apparent that the extent of oxide fuel breakup and dispersion and the damage to the dummy pins was much greater than in Test S3.

Comparison of the results of Test S5 (evacuated fuel pins) with Test S3 (helium-bonded pins) at an equal energy level shows that the presence of the bond gas strongly decreased the extent of interaction between the molten fuel and coolant. The peak pressure was reduced from the S5 value of 2940 psi to 540 psi, and the calculated conversion of thermal to mechanical energy was reduced by a factor of

Fig. 118. Residue from Test S5 with Evacuated Fuel Pins. ANL-ID Neg. No. 103-7643.

100 to 2 x 10^{-5}. (These latter values can be compared with the thermodynamic upper limit of about 0.1 for this conversion ratio as given by Hicks and Menzies). The S5 residue was highly fragmented while the S3 residue was not, in accord with these results. These observations are consistent with the hypothesis that the bond gas forms an insulating layer between the molten fuel and the coolant that prevents extensive interaction between them.

Pressurization of the cladding by bond-gas heating decreased by an order of magnitude the time period over which pin failure occurred, even though the initial pin failure occurred at essentially the same energy in both cases.

Discussion of work energy. One of the principal objectives of the in-pile experiments is to obtain data that can be used to provide a reasonable estimate of the work-energy produced by fuel-coolant interaction following a reactivity-insertion-type accident. In our estimates of work-energy, we have conservatively assumed that the sum of all impulses performed work by imparting kinetic energy to the piston and an effective expelled mass of sodium. Thus the mechanical energy produced by virtue of fuel-coolant interaction is ½ $(\text{Impulse})^2/\text{Mass}$.

From these values, we can obtain an estimate of the fractional conversion of nuclear energy (total fission-energy input into the fuel) to mechanical energy. For the three tests (S2 excluded) in which data were obtained, the conversion factors ranged from 2.1 x 10^{-5} to 1.9 x 10^{-3}. The largest value represents the test with evacuated fuel and suggests that the bond gas in certain situations inhibits contact of molten fuel and sodium and thus the conversion of thermal energy to mechanical energy.

These conversion values for the molten fuel-coolant interactions observed in these simulated power-excursion tests are too low to give destructive energies. Other modes of contact of molten fuel and coolant, such as impact of coolant upon molten oxide following coolant reentry might be more energetic. This contact method is being investigated in in-pile experiments and is described in the following section.

Impact of sodium on molten UO_2 (I series). A series of in-pile experiments has been started to measure the pressures and mechanical energies resulting from the impact of a sodium column on a pool of molten UO_2 in vacuum. The experiment simulates a worst-case reentry impact of sodium on molten fuel. It also is clearly defined simple system suitable for direct comparison with analytical models. The experiment is conceptually similar to the TRW water-molten aluminum shock-tube experiment[1] that was performed to investigate the fragmentation and pressure generation in the SPERT-1D destructive test.[2] This experiment is performed in-pile so that the UO_2 can be melted by a TREAT transient.

The experimental apparatus for these experiments (Fig. 119) basically consists of four parts: a high-pressure primary autoclave constructed of stainless steel, a high-strength steel liner, a graphite crucible for accommodating the molten UO_2, and a chamber for the column of sodium. The sodium is supported in the chamber on a stainless-steel diaphragm 2-mils thick. About 540 gm of sodium, forming a column 22-in. deep, will be contained in the chamber. The chamber is wrapped with heating wire to provide a sodium temperature of about 200°C.

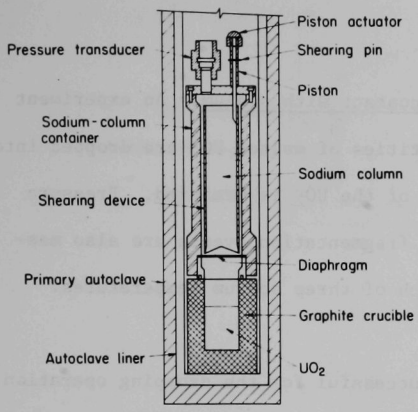

Fig. 119.
In-pile Autoclave for Tests of Sodium Impacting on Molten UO_2. Not to scale. ANL Neg. No. 113-3138, Rev. 1.

The principle of operation is to melt the oxide in the crucible by means of a TREAT reactor transient, and at a predetermined time initiate a device to shear the diaphragm, thereby releasing the sodium column onto the molten UO_2. The magnitude of the impulse generated by the impact of the sodium with the molten oxide is obtained by the pressure transducer mounted at the top of the sodium chamber.

The diaphragm shear device consists of a sharp-edged membrane cutter attached to a steel rod. The device is initiated by firing an explosive-actuated piston motor that applies a 20-lb load over 3/8-in. travel.

The autoclave assembly has been constructed, and a calibration test in the autoclave has been performed at the TREAT Facility. Of major concern is specifying a neutron transient that will produce, at a predetermined time, a pool of molten UO_2 so that, when the explosive device is initiated, the sodium contacts molten oxide. Arrangements for the first impact tests are underway.

Laboratory Experiments

(D. R. Armstrong and D. H. Cho)

Fragmentation of molten UO_2 upon contact with sodium. An experiment has been performed in which small quantities of molten UO_2 are dropped into a pot of sodium, and the fragmentation of the UO_2 is measured. Pressure pulses in the pot that result from the fragmentation events are also measured. Two tests have been made at each of three sodium temperatures: 200, 400, and 600°C.

The device that has proved most successful for the dropping operation is shown in Fig. 120. The apparatus consists of a tungsten crucible (contains the UO_2) mounted on a motorized shaft, and an induction coil operated from a 1000-kW generator. When the UO_2 becomes molten (∿2850°C), the motor attached to the shaft is activated and the crucible moves down from the induction coil and then rotates, allowing the molten UO_2 to fall into a pool of sodium positioned below the crucible.

During each test, continuous measurements were made of the pressure in the sodium container, the force exerted on the sodium container, and the overpressure in the gas space above the sodium. The entire sequence of events following the dropping was photographed with high-speed motion-picture film at 1000 frames/sec. After the test, data were obtained on the UO_2 particle-size distribution and the spatial distribution of sodium within the glovebox.

The experimental conditions and results for the tests are summarized in Tables XXIV and XXV. In each test, there were several separate violent ejections of sodium mixed with UO_2 particles from the sodium container. The quantity of UO_2 involved in each ejection was estimated from the size of UO_2 drops falling into the sodium on the film.

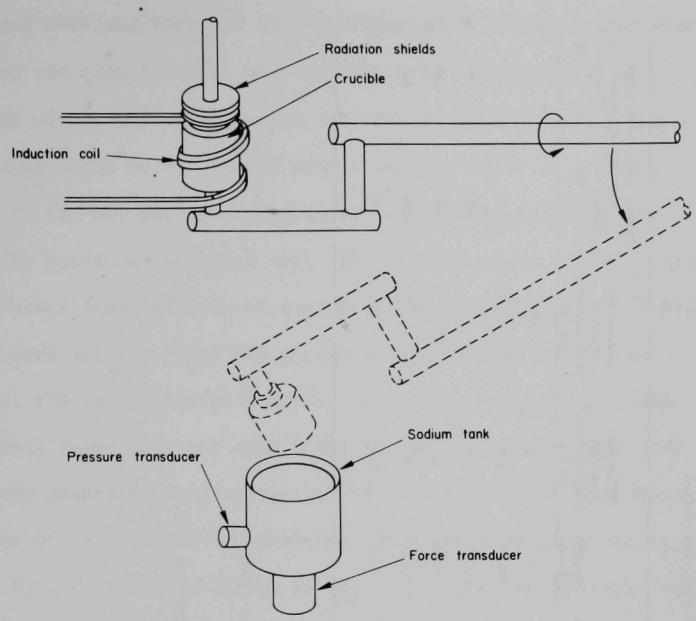

Fig. 120. Apparatus for Pouring Inductively Melted UO_2 into Liquid Sodium.

TABLE XXIV. Experimental Conditions for Dropping of UO_2 into Sodium

Run No.	Sodium Temperature, °C	Quantity of Sodium, gm	UO_2 Temperature, °C	Quantity of UO_2 Dropped, gm
1	200	290	2940	8.8
2	200	280	2900	7.4
3	390	280	2900	10.2
4	395	280	2900	16.5
5	600	252	2900	23.6
6	600	250	2900	7.5

The number of ejections in each test was also determined from the film. The total quantity of UO_2 dropped was determined by difference in the weight of the tungsten crucible. The total mass of sodium ejected was determined in a similar way.

TABLE XXV. Results of Experiments on Dropping Molten UO_2 into Sodium

Run no.	Quantity of UO_2 involved in each violent ejection,[a] gm	Number of violent ejections	Quantity of UO_2 ejected from tank gm	Quantity of sodium ejected from tank, gm	Peak pressure psi	Impulse lb-sec	Mechanical energy (calculated),[b] joules	Mechanical energy (calculated),[c] joules	Particle-size distribution of UO_2 residue: Total particles, μ	Particle-size distribution of UO_2 residue: Ejected particles, μ
1	4	4	<0.1	<10	d	e	---	0.07	f	f
2	g	g	1.2	51	350	0.15[e]	0.8	0.4	195	510
3	1	1	<0.1	2.6	200	0.10	0.3	---	370	---
4	13	2	3.8	86	655	0.38	5	0.78	355	225
5	10	2	7.9	124	h	0.42	8	i	195	240
6	7	3	<0.1	j	h	0.10	0.4	i	300	---

a. Estimated by analyses of film.

b. Calculated from impulse data and the total mass of sodium and ejected UO_2.

c. Calculated from distribution pattern of ejected sodium assuming hermispheric ejection.

d. Instrument records did not correlate with film.

e. Force transducer not used in Runs 1 and 2. Value in Run 2 estimated from pressure data.

f. No analysis performed on residues from Run 1.

g. No film record obtained in Run 2.

h. Pressure transducer did not operate in 600°C sodium.

i. Film showed most of ejected sodium impacted on the radiation shield.

j. Film showed most of ejected sodium fell back into tank.

It was observed that, of the two experiments at each temperature level, one was significantly more energetic in that substantial quantities of UO_2 and sodium were ejected from the sodium container. This is also noted by the values of the impulse and peak pressures. Analyses of the UO_2 particles indicated that fragmentation of the ejected UO_2 particles occurred while the particles were in the liquid state, whereas fragmentation of the particles remaining in the sodium tank occurred largely while the particles were in the solid state. Therefore, the particle-size distribution of the ejected particles more closely represents the size distribution at the time when pressure pulses were generated causing the violent ejection. The size distributions of the ejected UO_2 particles from the more energetic runs (Runs 2, 4, and 5) are presented in Fig. 121. The particle-size data show that the median diameter of the ejected particles decreases markedly as the temperature of the sodium is increased from 200 to 400°C, but that further increase in temperature to 600°C does not result in a significant change in particle size.

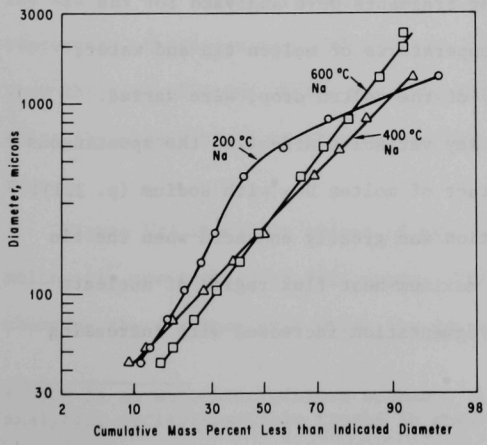

Fig. 121. Size Distribution of UO_2 Particles Resulting from Interaction of Molten UO_2 with Sodium.

The pressure and impulse data (Table XXV) show an increase in magnitude with an increase in sodium temperature. To provide an indication of the mechanical energy equivalent to the impulses, two estimates of the mechanical energies involved in the molten UO_2-sodium interaction are presented in Table XXV. For one estimate, it was assumed that the impulse accelerated the entire mass of sodium, and therefore the value of energy was $\frac{1}{2}(I)^2/m$, where m is the mass of sodium and I is the impulse. The second estimate of mechanical energy was based on the observed distribution pattern of ejected sodium and UO_2, assuming hemispheric expulsion about the sodium tank. Both estimates show an increase in mechanical-energy conversion with an increase in sodium temperature.

The next series of runs will examine the forces and pressures produced upon contact of molten stainless steel with sodium at the same three temperatures.

Fragmentation experiments with materials having different thermal properties. A small amount of molten tin was quenched in subcooled water and the resulting fragments were analyzed for the extent of fragmentation. The temperatures of molten tin and water, as well as the entrance velocity of the molten drop, were varied. The purpose was to identify the key variables affecting the spontaneous fragmentation observed upon contact of molten UO_2 with sodium (p. 321). The results show that fragmentation was greatly enhanced when the tin temperature corresponded to the maximum-heat-flux region of nucleate boiling. Also, the extent of fragmentation increased with increasing subcooling of the water.

Experimental procedure and data analysis. A 0.3-gm sample of tin was melted in a 3/8-in.-diameter stainless-steel crucible heated by electric resistance coils. A 1/4-in. hole at the bottom of the crucible was fitted with a ball valve. The valve was lifted to let the molten sample fall into a pool of laboratory-distilled water. The quenched sample was collected in a regular filter paper.

The method of determining the extent of fragmentation involved several steps: (1) prepare a 35-mm photograph of the fragmentation residue, (2) analyze the photograph by the CHLOE apparatus,* (3) generate the projected area of each particle from the CHLOE output on a CDC-3600 high-speed computer, and (4) compute the particle-size distribution from the projected area of individual particles. Also derived are such quantities as the total projected area per unit mass, the total number of particles, and various average diameters.

Results and discussion. Figures 122 and 123 summarize the results obtained with molten tin quenched in water. The extent of fragmentation (expressed in terms of total projected area per gram of tin) is plotted against the initial temperature of molten tin. Each data point represents an average value of at least five identical runs. Solid curves show the general trend of the results; the broken lines indicate the region where the extent of fragmentation was the greatest in a given series of runs.

Figure 122 shows the effect of the entrance velocity at which the molten tin was quenced in 22°C water. The entrance velocity was varied by changing the distance over which the drops fell. Generally, the extent of

*CHLOE is an automatic picture scanner, originally designed at Argonne for analyzing nuclear-particle tracks in spark-chamber photographs.

fragmentation increased with increasing entrance velocity or Weber number. The Weber number, N_{We},* represents the dimensionless ratio of inertial to surface forces. The inertial force is the dynamic pressure that water exerts on the impinging drop of molten tin. Figure 122 also shows that, for a given entrance velocity, the extent of fragmentation differed with initial tin temperature. Fragmentation was enhanced at tin temperatures

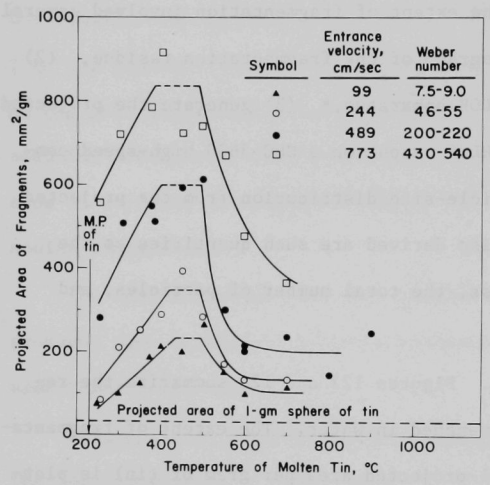

Fig. 122.
Effect of Entrance Velocity on Fragmentation of Molten Tin Quenched in 22°C Water. ANL Neg. No.900-71, Rev. 1.

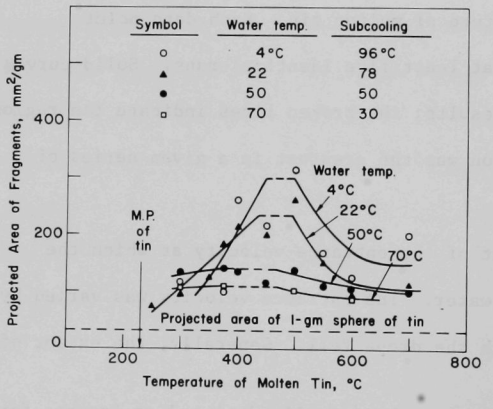

Fig. 123.
Effect of Water Subcooling on Fragmentation of Molten Tin Quenched in Water. Entrance velocity was 99 cm/sec and Weber number was 7.5-9.0. ANL Neg. No. 900-72, Rev. 1.

*$N_{We} = \rho D V^2/\sigma$, where ρ is density of water, D is diameter of tin drop, V is entrance velocity, and σ is surface tension of the molten tin.

between 400 and 500°C. This behavior was the same at each level of entrance velocity. The temperature range 400 to 500°C, at which greatest fragmentation occurred, appears to correspond to the maximum-heat-flux region of nucleate boiling in water.

Figure 123 shows the effect of water subcooling on fragmentation of tin. The entrance velocity was kept constant at 99 cm/sec, but the water temperature was varied. The Weber number, which ranged from 7.5 to 9.0, was below the critical value (13 to 22), so the dynamic pressure was not large enough to cause hydrodynamic breakup of the tin drop. Nevertheless, fragmentation was observed for a certain range of tin temperatures, with the extent of fragmentation increasing with an increase in subcooling of the water. When the temperature of the water was 70°C (30°C subcooling), little fragmentation occurred at any tin temperature. As the degree of subcooling was increased, enhancement of fragmentation apparently occurred at higher tin temperatures. Similar effects of subcooling on the maximum heat flux and wall superheat have been observed during quenching of a heated solid sphere.[3]

The results of these experiments on the fragmentation of molten tin in water indicate that the extent of fragmentation is affected by the entrance velocity as well as by the temperatures of the molten tin and water. The effect of the entrance velocity can be considered purely dynamic. Increasing the entrance velocity increases the dynamic pressure exerted on the drop of molten tin, which is the hydrodynamic driving force for fragmentation. Although detailed mechanisms of the temperature effect are not clear, Figs. 122 and 123 suggest a relationship between the temperature effect and the boiling characteristics of subcooled water.

A limited analysis of the particle-size distribution of the fragments was made. Figures 124 and 125 show a typical example. In Fig. 124 the cumulative percent of the number of particles (open circles) or the projected area of particles (solid circles) is plotted against the particle diameter on log-normal probability graph paper. The particle diameter here means the diameter of a circle having the same area as the projected area of the particle ("projected-area diameter"). Figure 125 is a frequency distribution plot of the same data based on the number of particles.

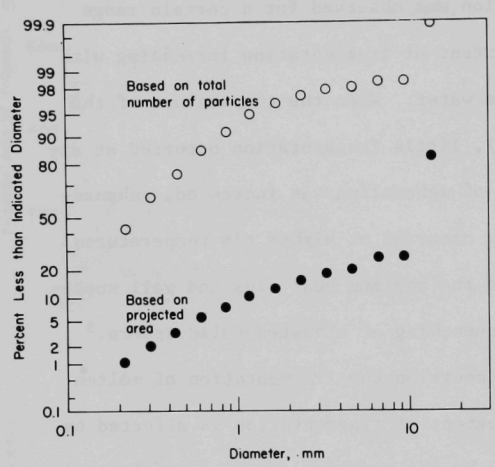

Fig. 124. Particle-size Distribution of Tin Fragmented in Water. Metal temperature was 385°C, water temperature was 22°C, entrance velocity was 244 cm/sec, atmosphere was air, total number of particles was 860, and projected area was 431.0 mm²/gm.

Both Figs. 124 and 125 show that the particle-size distribution is bimodal in nature. The double distribution is indicated by the break in the curves of Fig. 124. One part of the distribution consists of a large number of small particles, the median diameter being about 0.21 mm. The other part represents a small number of large but thin pieces of the fragments whose median diameter is about 6.7 mm. It appears that the first part of the double distribution follows a log-normal distribution.

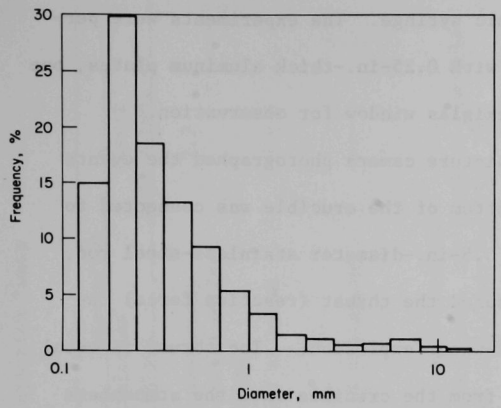

Fig. 125. Percent Frequency vs Log Diameter for Tin Fragmented in Water. Test conditions were the same as in Fig. 124.

Simulation experiments of coolant entrapment in molten fuel.

Laboratory experiments were performed to examine the hypothesis that the entrapment or inclusion of coolant in molten fuel might result in fragmentation and mixing of the fuel and coolant and an explosion. The experimental procedure consisted of injecting a small amount of room-temperature water into various molten materials. The results of initial survey studies are summarized here. It appears that explosions occurred when the entrapped water was suddenly dispersed in the molten material.

Experimental procedure and measurements. A 50-ml sample of molten material (metal or salt) was prepared in a 1- or 1.5-in.-ID stainless-steel crucible heated inductively. Also employed was a 1.25-in.-ID graphite crucible heated in a resistance furnace. Water (1 to 5 ml) at room temperature was injected into the molten mass through an 18-gage stainless-steel hypodermic needle. The water was injected above as well as under the surface of the molten mass. The injection was made either manually or mechanically. The mechanical injection employed a spring-loaded rod triggered by a solenoid, which

pushed the plunger of a hypodermic syringe. The experiments were performed in an enclosure shielded with 0.25-in.-thick aluminum plates, one of which had a 0.5-in.-thick plexiglas window for observation.

A Hycam high-speed motion-picture camera photographed the events following the injection. The bottom of the crucible was connected to a Kistler force transducer by a 0.5-in.-diameter stainless-steel rod, 8-in. long. The transducer measured the thrust (reaction force) resulting from the molten material-water explosion. The thrust is equal to the rate of momentum outflow from the crucible into the atmosphere that occurs during an explosion.

Results and discussion. Table XXVI summarizes the observations made. Each observation was rated as violent, mild, or none, depending on its explosive nature. It is emphasized that the explosion rating was not only qualitative but very subjective.

Calculations indicate that the impact force of the water jet used was of the order of 0.1 lb. Also, up to 5 ml of water was injected into a stainless-steel crucible (same one as used for the experiments) filled with water. The resulting forces were not greater than 0.6 lb. Thus, the observed thrusts exceeding about 1 lb should be attributed to some type of molten material-water interactions: bubbling, splashing, or explosions.

Figure 126 shows five selected frames from the motion picture taken in the experiment with molten tin at 600°C. The explosion was sufficiently violent to shatter the upper half of the graphite crucible.

A high-speed photographic test was conducted with molten sodium chloride in a transparent quartz tube to observe the course of the vapor-explosion phenomena. This test enabled detailed observation

TABLE XXVI. Molten Material-Water Explosions in Water-injection Tests

Molten material		Water	Observation		
Material (and amount, gm)	Initial temperature, °C	Amount and methods of injection	No. of tests	Explosion rating	Thrust peak value, lb
Aluminum (100)	1000	1-2 ml mechanically injected ∿0.5 in. above the surface	2	No explosion; aluminum surface bulged	2.2
Aluminum (100)	740-800	1 ml manually injected ∿1/8 in. both above and under the surface	4	Same as above	---
Tin (200)	300	1 ml manually injected ∿1/8 in. under the surface	1	Mild explosion	---
Tin (100-200)	500-600	Same as above	5	Violent explosions (in one case, the graphite crucible was shattered; see Fig. 19)	---
			2	Mild explosions	---
			2	None	---
Tin (300)	600 & 800	3 ml mechanically injected ∿0.5 in. above the surface; also 2 ml manually injected under the surface	3	No explosion surface bulging; some splashing of tin	---
Tin (380)	600 & 800	5 ml manually injected both above and under the surface	2	No explosion	4 pulses ranging from 3 to 6 lb (at 800°C)

TABLE XXVI. (Contd.)

Molten material		Water	Observation		
Material (and amount, gm)	Initial temperature, °C	Amount and methods of injection	No. of tests	Explosion rating	Thrust peak value, lb
Silver (400)	1100 & 1200	3 ml mechanically injected ∿0.5 in. above the surface	2	No explosion; violent boiling on the surface; some splashing of silver	2.5
	1100	5 ml manually injected under the surface	1		3.6
Zinc (370)	600 & 800	3 ml mechanically injected	2	No explosion	
Wood's metal (4 parts Bi, 1 Sn, 2 Pb, 1 Cd) (500)	220	3 ml mechanically injected ∿0.5 in. above the surface	1	No explosion; 20% of Wood's metal splashed out	Two peaks 5.6 & 4.5
	400	Same	1		2.5
	600	Same	1	No explosion; black oxide film on the surface virtually prevented intimate contact between water and the molten material	
Brass (yellow; 63% Cu, 37% Zn) (50)	1000	3 ml mechanically injected above the surface	1	No explosion; 30% of brass splashed out	Several pulses 3, 4, 3.7
	1100	Same	1	Mild explosion accompanied by a noise; 40% of brass blown out	One major peak (14 lb) followed by two minor ones (both 2.8 lb)
Potassium iodide (100)	800	1 ml manually injected ∿1/8 in. both above and under the surface	1	Violent explosion	---
			2	Mild explosions	---

TABLF XXVI. (Contd.)

Molten material		Water	Observation		
Material (and amount, gm)	Initial temperature, °C	Amount and methods of injection	No. of tests	Explosion rating	Thrust peak value, lb
Silver chloride 100)	600	2 ml manually injected ∿1/8 in. above the surface	1	Violent explosion	---
Sodium chloride (80)	1000	5 ml (in two increments) manually injected above the surface (first injection was 3 ml; second injection was 2 ml 2-3 sec after first)	1	Both first and second injections resulted in violent explosions accompanied by a loud noise; more than half of NaCl was blown out	Two peaks on first injection: first peak had max. 44 lb composed of damped oscillation pulses; second peak was 24 lb. On second injection, max. was 50 lb composed of damped oscillation pulses
Sodium chloride (100)	900	3 ml mechanically injected ∿3/4 in. above the surface	1	Violent explosion; the container (a quartz tube) was completely disintegrated and propelled away; see Fig. 20	
Sodium chloride	1000	3 ml mechanically injected ∿0.5 in. above the surface	1	Violent explosion 80% of NaCl blown out	4 peaks: 11 lb, max. 122 lb composed of 4 positive pulses, 22 lb, and 6 lb

TABLE XXVI. (Contd.)

Molten material		Water	Observation		
Material (and amount, gm)	Initial temperature, °C	Amount and methods of injection	No. of tests	Explosion rating	Thrust peak value, lb
Sodium chloride (65)	1000	1 ml mechanically injected ∿0.5 in. above the surface	1	Violent explosion; 70% of NaCl blown out	4 peaks: max. 205 lb composed of 7 positive and negative pulses, 22 lb, 8 lb, and 12 lb
Sodium carbonate (110)	1000	3 ml mechanically injected ∿0.5 in. above the surface 5 ml (in three increments) manually injected under the surface	1	No explosion; violent boiling on the surface; some splashing of sodium carbonate	1-2 lb ∿1 lb

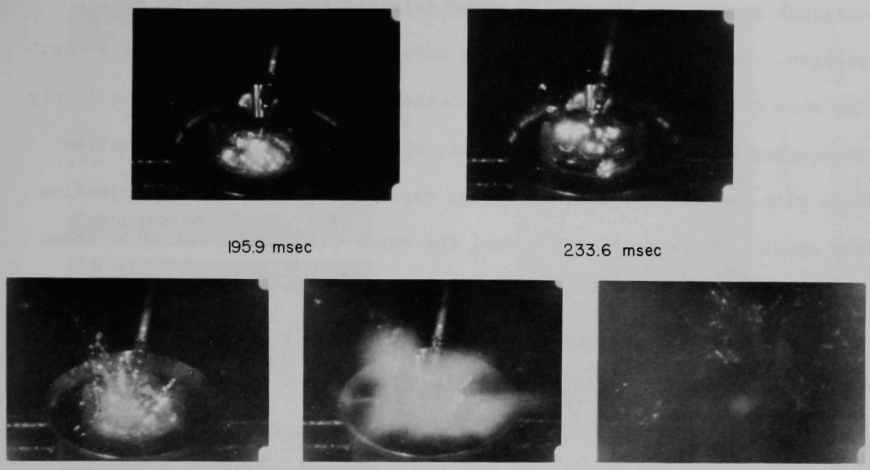

Fig. 126. Events after 1 ml of Room-temperature Water was Injected Just under Surface of 600°C Molten Tin at Various Times from Start of Injection. Immediately after injection (195.9 msec), tin surface bulged, probably because of sudden generation of steam; surface continued to bulge (233.6 msec) until certain size was reached, whereupon (303.7 msec) sudden explosion occurred (304.2 msec, which is only 0.5 msec later); at 337.5 msec can be seen pieces of shattered crucible flying in a cloud of mixed steam and tin particles. ANL Neg. No. 113-1355, Rev. 2.

of the behavior of the injected water in the molten material until the explosion occurred.

A 100-gm sample of sodium chloride was melted by torch heating in a rectangular quartz tube (1-1/4 in. by 1-9/16 in. and 1/16 in. wall). When the molten sodium chloride reached about 900°C, 3 cm^3 of water at room temperature was mechanically injected into the melt, and a Hycam high-speed motion-picture camera photographed the subsequent events.

Water injection resulted in a violent explosion, a loud noise, and the quartz tube was completely disintegrated and displaced from the

original location. Figure 127 shows selected frames from the motion picture. Before the explosion, the sequence of significant events was: (a) when the water was injected into the molten mass, it was immediately surrounded by a cloud of water vapor, which spread through the molten mass with small, sporadic, burstlike expansions, (b) when the injection was completed after about 0.1 sec, the vapor cloud had penetrated about two-thirds of the molten mass (it is possible that the water as liquid was dispersed as fine droplets within the vapor cloud), (c) the molten mass became relatively transparent, as though most of the vapor cloud had disappeared (probably most of the injected water reached near the bottom of the tube), (d) a new vapor cloud was formed near the bottom of the tube, and (e) the cloud became dispersed throughout the molten mass. No appreciable expansion of the system was observed during this interval, except for slight bulging of the upper surface. It appeared that the vaporization and expansion of the injected water was arrested. No significant changes were observed until the explosion occurred. During the interval of about 0.19 sec between 252.4 msec and the start of the explosion sequence at 446.0 msec, only sporadic burstlike expansions and small-scale turbulences were observed. The explosion started at about 0.45 sec after the start of the injection and reached its final stage about 0.6 msec later.

When there was no explosion, the injected water was quickly driven out of the molten material rather than mixed with it. This was evidenced by close examination of the solidified material remaining in the crucible. On the other hand, when there was an explosion, the injected water was dispersed into fine droplets in the molten material. Moreover, the droplets remained in an apparently stable state during

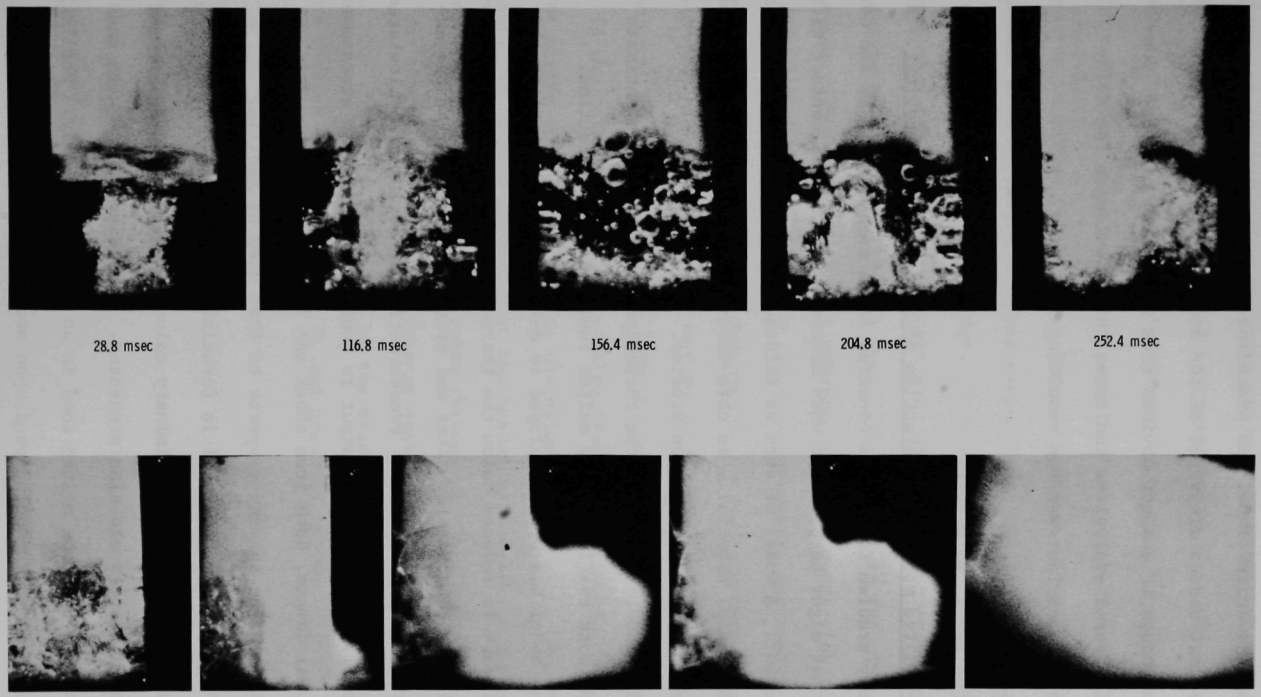

Fig. 127. Events after 3 ml of Room-temperature Water were Injected into Molten Sodium Chloride at 900°C (at various times from start of injection). ANL Neg. No. 113-2353.

a period of the order of 0.1 sec preceding the explosion ("delay period"). It appears that sudden dispersal of the droplets triggered the explosion, although it was not obvious from the motion picture. Comparison of several explosions indicates that the longer the delay period the more violent was the resulting explosion.

Model Development

(D. H. Cho and R. W. Wright)

Rate-limited model of interaction of molten fuel and coolant. A major safety problem for LMFBRs concerns large pressure pulses and work energies that might be produced when molten fuel comes in contact with the sodium coolant. A model of such an interaction between molten fuel and coolant is needed, especially in core-disassembly-accident analyses or in fuel-element failure propagation studies.

Earlier models have used the thermodynamic approach to estimate the maximum work available from molten fuel-coolant interaction.[4,5] The present model has been developed to determine to what extent the mechanical work is reduced below the thermodynamic limit by the inclusion of finite heat-transfer rates and system constraints for the expansion of the heated coolant. Pressure-time histories are calculated in this model. This form of output is needed for realistic assessment of structural damage, both from shock and from slug motion. This approach is similar in many respects to that used by Padilla.[6]

In this section, the model is formulated, incorporating various limiting rate processes. Preliminary calculations of pressure generation and voiding histories are also presented. The calculations were made considering a 35-cm-long molten zone in an FFTF subassembly. Realistic calculations with the model depend upon understanding the individual

rate processes. Major uncertainties lie in the complicated processes of molten fuel-coolant mixing and fragmentation, and in the processes of heat transfer. However, these unknown rates have been incorporated into the model as input parameters, and parametric studies of pressure generation in molten fuel-coolant interactions can be performed for reasonable assumed ranges of these parameters.

Formulation of the model. Consider a volume of molten fuel-coolant mixture formed in a certain zone of the reactor core. As the coolant is heated rapidly by the fuel, the pressure in the mixing zone increases. The mixing zone then expands against a constraint given by the surroundings. The course of pressure generation and coolant expansion is determined by the interaction between two competing processes: the heating of the coolant by the fuel (which produces pressures) and the expansion of the heated coolant (which reduces pressures).

If the volume change of the molten fuel is neglected, the expansion of the mixing zone is due only to the volume change of the heated coolant. It is also assumed that the heated coolant is in a state of uniform thermodynamic equilibrium throughout the mixing zone and that the mixing zone does not exchange heat or mass with the surroundings. The change in the volume of the heated coolant, V, is related to the changes in the enthalpy, H, and pressure, p, by

$$\frac{dH}{dt} = \frac{dQ}{dt} + \frac{Vdp}{dt} \tag{1}$$

(first law of thermodynamics)

and

$$H = H(p,V) \tag{2}$$

(equation of state)

where all quantities refer to unit mass of the heated coolant; dQ/dt represents the overall heating rate of the heated coolant. The form of dQ/dt depends on the processes of fragmentation and mixing as well as on the heat-transfer mechanisms.

Consideration of the constraint of the surroundings provides a dynamic relationship between p and V.

$$P = f\left(V, \frac{dV}{dt}, \frac{d^2V}{dt^2}\right) \tag{3}$$

(equation of constraint)

Equations 1-3 can be solved for H, p, and V with appropriate forms of dQ/dt. The forms of Eqs. 2 and 3 to be used are discussed below.

The actual form of the equation of state for computational use depends on available experimental data and correlations. For a pure liquid or vapor phase, it is convenient to use a p-V-T rather than p-V-H relationship. In this case, Eq. 1 is rewritten as

$$c_p \frac{dT}{dt} = \frac{dQ}{dt} + T V\alpha_p \frac{dp}{dt} \tag{4}$$

where the thermodynamic relation, $dH = c_p dT + [V - T\left(\frac{\partial V}{\partial T}\right)_p] dp$, has been used, and α_p is the thermal expansion coefficient,

$$\alpha_p \equiv \frac{1}{V}\left(\frac{\partial V}{\partial T}\right)_p$$

Eq. 2 is replaced with

$$V = V(p, T) \tag{5}$$

or

$$\frac{dV}{dt} = -\beta_T V \frac{dp}{dt} + \alpha_p V \frac{dT}{dt} \tag{6}$$

where β_T is the isothermal compressibility,

$$\beta_T \equiv -\frac{1}{V}\left(\frac{\partial V}{\partial p}\right)_T$$

For an ideal gas $\alpha_p = \frac{1}{T}$ and $\beta_T = \frac{1}{p}$. For a real gas, a useful form of the equation of state is

$$pV = ZRT \tag{7}$$

where Z is the compressibility factor.

For a two-phase mixture, Eq. 1 may be used as it stands. For the equation of state, it appears convenient to use the following forms of empirical correlations.

$$p = p(T) \tag{8}$$

(vapor pressure equation)

$$H = xH_v + (1 - x) H_\ell$$

or

$$\frac{dH}{dt} = x \frac{dHv}{dt} + (1 - x) \frac{dH_\ell}{dt} + \Delta H_{\ell v} \frac{dx}{dt} \tag{9}$$

with

$$H_v = H_v(T) \text{ (enthalpy of saturated vapor)} \tag{10a}$$

$$H_\ell = H_\ell(T) \text{ (enthalpy of saturated liquid)} \tag{10b}$$

where x is the weight fraction of vapor and $\Delta H_{\ell v} = H_v - H_\ell$

and

$$V = xV_v + (1 - x)V_\ell$$

$$\frac{dV}{dt} = x \frac{dV_v}{dt} + (1 - x) \frac{dV_\ell}{dt} + \Delta V_{\ell v} \frac{dx}{dt} \tag{11}$$

with

$$V_v = V_v(T) \text{ (volume of saturated vapor)} \tag{12a}$$

$$V_\ell = V_\ell(T) \text{ (volume of saturated liquid)} \tag{12b}$$

where $\Delta V_{\ell v} = V_v - V_\ell$.

Generally, the constraining effects of the surroundings must take into account the unheated coolant, intact fuel pins, and other structural materials. Here we assume the surroundings to be the unheated coolant, and consider two methods of formulating the constraint.

Compressible liquid; acoustic formulation. The expansion of the heated volume produces compression (acoustic) waves in the surrounding unheated coolant. Nonlinear propagation velocity and convective motion are negligible under conditions of interest. Reflected waves are not considered in the equation given here. Hence this acoustic formulation is valid only for the period of time up to $2L/c_o$, where L is the distance to a reflecting surface and c_o is the speed of sound of the unheated coolant.

The acoustic formulation is accurate during the initial shock phase of the molten fuel-coolant interactions. It can be extended to longer times by taking into account reflected waves and center-of-mass motion.

Incompressible liquid; inertial formulation. The surrounding unheated coolant is assumed to be incompressible. The expansion of the heated volume is resisted by the inertia of the surrounding coolant. Viscous forces are neglected. This formulation is accurate when the time is large compared with $2L/c_o$ and the liquid velocity is small compared with that of sound. The inertial formulation is a good approximation during the later two-phase expansion stage of the interaction.

For both formulations, one-dimensional or three-dimensional symmetric constraints may be considered. Figure 128 summarizes pertinent dynamic relations for volume change of the heated coolant, each of which represents a special case of Eq. 3.

Preliminary calculations. Preliminary calculations have been made that consider a molten fuel-coolant interaction that might occur following sodium reentry into a 35-cm-long molten zone at the core midplane of an FFTF subassembly. The calculations represent a first step toward examining the effects of various limiting rate processes.

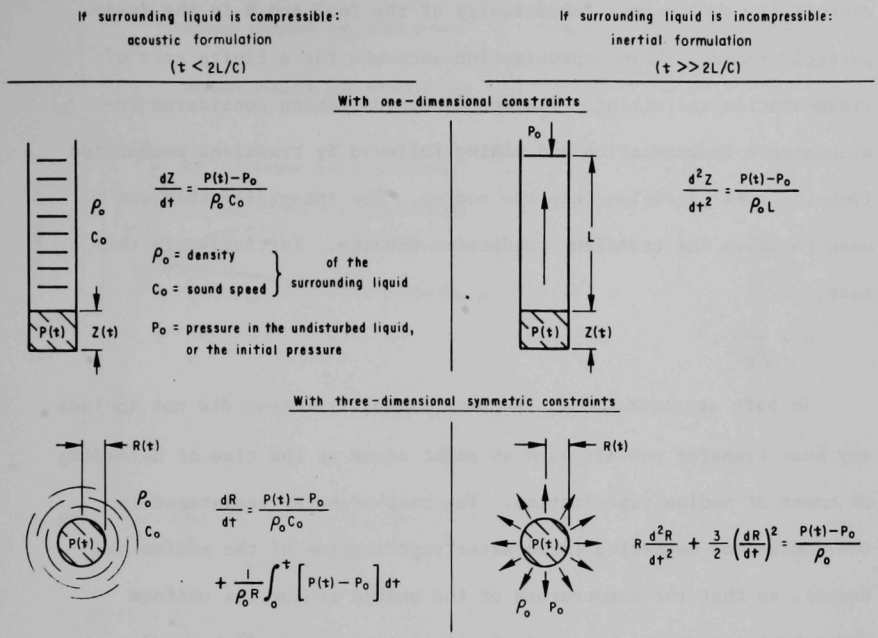

Fig. 128. Dynamic Relations of Volume Change of the Heat Coolant with Constraints by the Surrounding Liquid.

Two different approximations were used for the heating of sodium in the fuel-coolant mixing zone. The first approximation considered quasi-steady-state heat transfer with the heat flux given by

$$q = hA(T_f - T_{Na}),$$

where h is the effective heat-transfer coefficient, A is the heat-transfer surface area, and T_f and T_{Na} are the average fuel and sodium temperatures. The heat-transfer coefficient was given in the approximation by

$$h = \frac{k_f}{R},$$

where k_f is the thermal conductivity of the fuel and R is the fuel-particle radius. This approximation accounts for a finite rate of fragmentation and mixing. The second approximation considered instantaneous fragmentation and mixing followed by transient conduction from the fuel particles into the sodium. The integral method was used to solve the transient conduction problem. Initially, in this case,

$$q \propto \frac{1}{\sqrt{t}} .$$

In both approximations, the heat-transfer process did not include any heat transfer cut-off such as might occur at the time of unloading or onset of sodium vaporization. The heat-transfer resistance in the sodium was neglected (even after vaporization of the sodium had begun), so that the temperature of the heated sodium was uniform throughout the mixing zone and single state point could be used to represent the heated sodium.

The calculations assumed a uniform dispersion of fuel particles of radius 117μ in the liquid sodium, and used a fuel-to-sodium mass ratio of 8.3. The initial temperatures used for the sodium and fuel were 1100 and 2900°K, respectively.

Figure 129 is a p-V plot* of the results obtained when a one-dimensional acoustic constraint of infinite extent was assumed, both upward and downward. Table XXVII summarizes the parameters and initial conditions used and the peak pressures calculated. The equation of constraint used is

---

*The critical pressure shown in Fig. 129 is somewhat lower than Dillon *et al.'s* value (350 atm) (ANL-7025, p.42), because the calculations used the sodium vapor pressure equation of Stone *et al.* (ANL-7323, p. 18) up to the critical point.

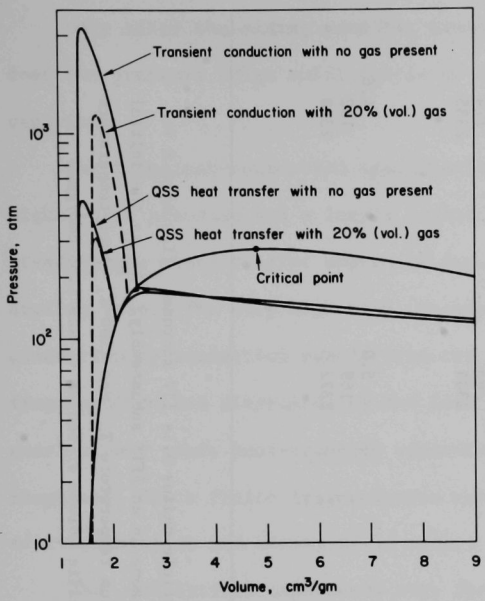

Fig. 129.
Effect of Heating Rates on Pressure Generation; Acoustic Constraints.

$$P(t) - P_o = \rho_o c_o \frac{dZ}{dt},$$

where P(t) is the pressure in the mixing zone, P_o is the initial pressure throughout, ρ_o and c_o are the density and sonic velocity of the unheated sodium in the loading column, and Z(t) is the position of the interface between the mixing zone and the loading column.

Figure 129 shows that the peak pressures occur during the liquid-phase heating and expansion. The high initial heat flux into the sodium produces a large pressure with rapid thermal expansion of the liquid sodium in the mixing zone. The initial rate of pressure rise is determined by the sodium thermal pressure coefficient and the initial rate of temperature increase of the liquid sodium in the mixing zone. (The thermal pressure coefficient is the quotient of the thermal-expansion coefficient, α_p, and the isothermal compressibility, β_T.) Therefore, the peak pressures might differ considerably, depending on the equation of state for sodium used.

TABLE XXVII. Calculational Results for Acoustic Constraint*

Conditions	Heat-transfer assumptions: Quasi-steady state, $V_{go} = 0$	Quasi-steady state, $V_{go} = 20\%$ of V_o	Transient conduction, $V_{go} = 0$	Transient conduction, $V_{go} = 20\%$ of V_o
Peak pressure in the liquid region:				
Time, msec	0.35	1.79	0.056	0.231
Pressure, atm	472	312	3286	1221
Sodium temp., °K	1306	1792	1751	1995
Vaporization starts:				
Time, msec	5.28	5.25	2.84	239
Pressure, atm	127	127	163	174
Sodium temp., °K	2193	2195	2304	2335
Peak pressure in the two-phase region:				
Time, msec	14.9	14.8	5.0	4.6
Pressure, atm	169	169	169	182
Sodium temp., °K	2321	2321	2322	2358

*Ratio of masses of fuel and sodium W is 8.3; fuel-particle radius R is 117 microns; flow area S is 0.077 cm^2/gm of Na, which corresponds to a 35-cm-long molten zone in an FFTF subassembly. V_{go} is the initial volume of noncondensable bond gas. Initial conditions: sodium temperature T_{Na} was 1100°K, fuel temperature T_{fuel} was 2900°K, sodium pressure P_o was 1 atm, and the specific volume of sodium V_o was 1.35 cm^3/gm.

Only after the mixing zone has expanded for several milliseconds does the pressure relax sufficiently to allow the heated sodium to vaporize.

The transient-conduction approximation gives an order of magnitude higher peak pressure and a larger amount of work than does the quasi-steady-state heat-transfer approximation, because of its higher initial heating rate. The very high peak pressures for the transient-conduction approximation result from the assumption of instantaneous fragmentation and dispersion of the fuel in the sodium. Use of the quasi-steady-state heat-transfer approximation accounts, in a very rough way, for a finite fragmentation and mixing time. A low rate of fragmentation and mixing would reduce the peak pressures considerably.

The calculations considered only the thermal resistance in the fuel particles. Additional thermal resistance in the mixing zone, such as vapor blanketing or other fuel-sodium contact resistances, would reduce the heat flux into the sodium and, therefore, the resulting pressure.

The broken curves in Fig. 129 indicate the compliance of a non-condensable gas present in the fuel-coolant mixing zone; the case of no noncondensable gas present is indicated by solid curves. The initial volume of the noncondensable gas was 20% of that of the liquid sodium. The presence of the noncondensable gas reduced the peak pressure and also delayed its time of occurrence. For the quasi-steady-state heat-transfer approximation, the peak pressure was reduced from 472 atm to 312 atm, and the time at which the peak pressure occurred changed from 0.35 msec to 1.79 msec. For the transient-conduction approximation, the peak pressure was reduced from 3286 atm

to 1221 atm, and the corresponding time changed from 0.056 msec to 0.231 msec.

Figure 130 shows voiding histories resulting from molten fuel-sodium interactions in a 35-cm-long molten zone of an FFTF subassembly. It is assumed that the coolant columns above and below the fuel-coolant mixing zone are incompressible and do not exchange heat or mass with the mixing zone. The heated coolant in the mixing zone expands against the inertia of the unheated coolant columns (one-dimensional inertial constraint). A macroscopic momentum balance gives the equations of motion of the constaining coolant columns,

$$\frac{dU_2}{dt} = -g + \frac{P - P_{ex}}{(Z_{ex} - Z_2)} - \tfrac{1}{2}U_2^2 \frac{f}{R_h} ,$$

and

$$\frac{dU_1}{dt} = g + \frac{P - P_{in}}{\rho Z_1} - \tfrac{1}{2}U_1^2 \frac{f}{R_h} ,$$

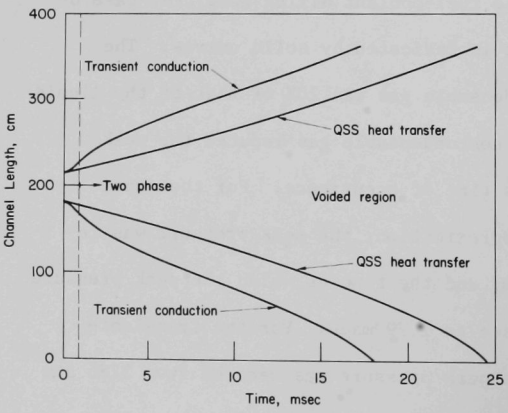

Fig. 130. Voiding Histories in an FFTF Subassembly.

where P_{ex} is the exit plenum pressure, P_{in} is the inlet plenum pressure, P is the pressure in the fuel-coolant mixing zone, ρ is the density of the unheated coolant, Z_{ex} is the position of the exit plenum (measured from the inlet plenum), Z_2 is the position of the interface between the mixing zone and the upper coolant column, Z_1 is the position of the interface between the mixing zone and the lower coolant column, U_2 is the ejection velocity of the upper coolant column, U_1 is the ejection velocity of the lower coolant column, g is the acceleration due to gravity, f is the friction factor, and R_h is the hydraulic radius of the coolant channel. The calculations used the following parameters based on FFTF conditions: P_{ex} = 1.456 atm, P_{in} = 7.485 atm, Z_{ex} = 420 cm, $Z_2(t = 0)$ = 215 cm, $Z_1(t = 0)$ = 180 cm, f/R_h = 0.0542 atm^{-1} (estimated). Other initial conditions were identical to those used for Fig. 129. Figure 130 gives the voiding histories for both approximations of quasi-steady-state heat transfer and transient conduction. The lower channel becomes completely voided in 25 msec for the quasi-steady-state heat-transfer approximation, and in 18 msec for the transient-conduction approximation.

Fuel failure analysis. An analysis has been made of cladding failure in a hypothetical accident involving a sudden complete loss of coolant capabilities. The failure mechanism considered here was the rupture of the cladding due to a combination of increased internal gas pressure and decreased ultimate strength of cladding, as a result of elevated temperatures.

In this analysis, a single FFTF-type fuel rod (unirradiated stainless-steel-clad UO_2-20% PuO_2, helium bonded), cooled by sodium and operating at steady-state power, was subjected to a loss of coolant and the time to cladding failure threshold was determined. Two cases of operating conditions were considered: (1) fuel power density of 304 cal/sec-cm^3 and

sodium coolant at 400°C, and (2) power density of 696 cal/sec-cm^3 and sodium coolant at 645°C. It was assumed that the fuel rod would continue to operate at the same power level after the accident, and that there was no heat loss from the rod. Radial temperature profiles across the fuel, gas gap, and cladding, in addition to gas pressure within the cladding, were calculated at various time increments after the loss of coolant.

Figure 131 gives the cladding yield strength and the internal gas pressure required for the cladding failure threshold as a function of the cladding temperature. Also plotted in Fig. 24 are the changes in the internal gas pressure for the two cases considered (corresponding times after loss of coolant are indicated). The failure threshold is reached when the internal gas pressure curve crosses the pressure curve corresponding to the cladding yield strength.

For Case 1, the threshold was reached 2.2 sec after loss of coolant by virtue of loss of strength of cladding. The cladding temperature at this time was 1330°C; the yield strength of stainless steel at that temperature was not sufficient to sustain the internal gas pressure without permanent deformation. During the interval between loss of coolant and threshold of failure, the fuel centerline temperature increased only slightly from 1690 to 1850°C. In Case 2, the failure threshold was attained ∿0.36 sec after loss of coolant by the same mechanism as in Case 1. The cladding temperature at this time was 1150°C.

These calculations show that the principal cause of fresh fuel failure is elevated cladding temperatures and the concomitant loss of cladding strength. The internal gas pressure at the threshold of failure was not much different from its steady-state value.

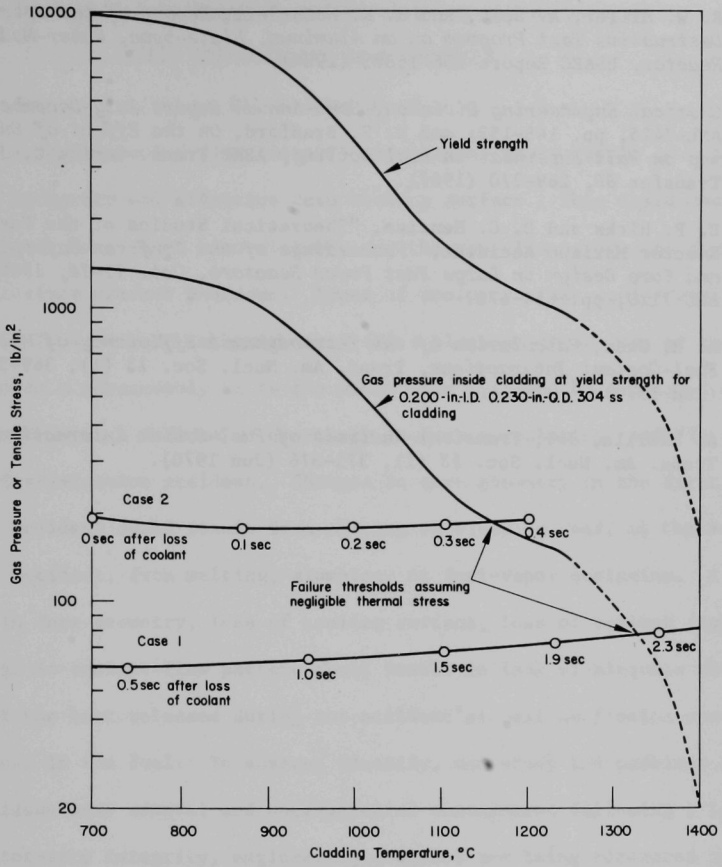

Fig. 131. Yield Strength of 304ss and Gas Pressure in Active Section of Fuel Pin. At steady state, for Case 1: 304 cal/sec-cm^3, 400°C Na temp; for Case 2: 696 cal/sec-cm^3, 645°C Na temp. Note: For Case 1, the inclusion of thermal stress would locate the threshold of failure at a cladding average temperature of 1030°C, a gas pressure of 66 lb/in.^{2}, and a total tensile stress (at the outer wall of cladding) of 2760 lb/in.^{2}, 1.24 sec after complete loss of coolant.

References

1. R. W. Wright et al., "Dispersal and Pressure Generation by Water-Impact upon Molten Aluminum," in *Kinetic Studies of Heterogeneous Water Reactors, Annual Summary Report 1965*, USAEC Report STL-372-30, pp. 62-74 (Dec 30, 1965).

2. R. W. Miller, A. Sola, and R. K. McCardell, *Report of the Spert 1 Destructive Test Program on an Aluminum, Plate-type, Water-Moderated Reactor*, USAEC Report IDO-16883 (1964).

3. *Chemical Engineering Division, Semi-Annual Report July-December 1967*, ANL-7425, pp. 148-152; and W. S. Bradford, *On the Effect of Subcooling on Wall Superheat in Pool Boiling*, ASME Trans. Series C, J. Heat Transfer *89*, 269-270 (1967).

4. E. P. Hicks and D. C. Menzies, "Theoretical Studies of the Fast Reactor Maximum Accident," *Proceedings of the Conf. on Safety, Fuels, and Core Design in Large Fast Power Reactors, Oct. 11-14, 1965*, ANL-7120, pp. 654-670.

5. A. M. Judd, *Calculation of the Thermodynamic Efficiency of Molten-Fuel-Coolant Interactions*, Trans. Am. Nucl. Soc. *13* (1), 369-370 (Jun 1970).

6. A. Padilla, Jr., *Transient Analysis of Fuel-Sodium Interaction*, Trans. Am. Nucl. Soc. *13* (1), 375-376 (Jun 1970).

Nuclear Safety Research and Development--LMFBR Safety

XII. POSTACCIDENT HEAT REMOVAL*

(J. C. Hesson)

In a sodium-cooled fast reactor, an accident could result in a loss of core integrity and effective core cooling surface. This could cause a problem of decay-heat removal from, and the containment of, the core material after reactor shutdown. Types of accidents that could result in such a loss of core integrity are: (1) a blockage of or loss of coolant flow to a subassembly or to the whole core followed by a delayed or partial scram or a failure of emergency coolant circulation, and (2) a reactivity-excursion accident. Changes in core geometry in the first type of accident could result from melting or slumping, and, in the second type of accident, from melting, slumping, or fuel-vapor explosion. A change in core geometry, loss of cooling surface, loss of coolant flow, or change in coolant-flow pattern could result in lack of adequate removal of the heat released during the accident as well as fission-product decay heat in the fuel. To assess, identify, and study the problems of postaccident heat removal and core-material containment following a loss of reactor-core integrity, engineering analyses are being conducted and interactions of fuel and structural materials are being studied. For this work, the parameters and needs of the FFTF are used as a reference design.

In the event of an accident that causes a loss of core integrity or a loss of core-cooling capability, the reactor would be shut down (nuclear); however, heating from the fission-product decay in the fuel would continue to heat the core fuel material. This continued decay heat along with heat generated during the accident would need to be

*For references for this chapter, see p. 387.

removed to maintain control of the core or core debris. The conditions of the core after shutdown, resulting from an accident, that would require special heat-removal consideration would depend on the severity of the accident. The condition of the core could range from a blocked subassembly to a dissembled and molten core. In addition, coolant flow to the core might be more or less impaired.

In the case of a blocked subassembly, particularly with impaired coolant flow to the remainder of the core, the decay heating, under certain conditions, would cause melting of the fuel in the subassembly. This blockage and melting might propagate to adjacent subassemblies and eventually involve melting of a large portion of the core. Accidents of a nature more severe than a blocked subassembly could cause extensive and continued melting of the core and formation of a molten mass due to decay heating.

Extensive melting of the core would cause: (a) a release of gaseous and volatile fission products, (b) formation of a molten mass due to incorporation of structural materials such as cladding, subassembly cans, and supports, (c) redistribution of core residue due to melting, flotation, and boiling, (d) a possible reassembly criticality accident, (e) interactions, possibly violent, between the molten mass and sodium coolant, and (f) interactions with and meltthrough of structural supports such as lower grid plates and containment vessels, which could result in a loss of fission-product containment.

The basic problem becomes one of analyzing the probable normal course of events following accidents of various severities with respect to postaccident heating and to investigate means for removal of decay heat and containment of the damaged core, core debris, or molten mass that would result.

For a milder accident involving a small portion of the core, such as a blocked subassembly, an analysis is needed to determine under what circumstances the blockage would propagate, and studies must be made of means to remove decay heat and to prevent such propagation to avoid further core involvement.

For a severe accident that leads to melting of a significant fraction of the core, analyses must be made of circumstances under which critical reassembly would occur and the conditions under which the molten core debris could penetrate the reactor vessel. Studies must be made of ways and means to remove heat, contain the core debris, and prevent or retard penetration of the reactor vessel.

In the event of penetration of the reactor vessel, the core debris must be retained within the secondary containment vessel. This requires analyses and studies of the containment of the molten mass within the secondary containment.

Engineering Analyses

Engineering analyses are being conducted to examine postaccident heat removal and core-material containment following a loss of reactor core integrity. The engineering analyses consist of studying and assessing the work needed to identify and define the problems, the experimental information needed, and methods of obtaining it. The analyses include: (1) assessment of the conditions of the core after assumed accidents, (2) studies of fission-product decay-heat source magnitudes and distribution in solid, molten, and volatile phases by element as a function of time, and (3) the possible criticality of collapsed and molten core geometries. The analytical work includes heat-transfer and heat-removal studies, together with studies of thermally stable sizes and geometries of pieces, piles,

and pools of heat-generating fuel materials in sodium coolant and in contact with structural materials, as well as decay-heat removal from a blocked subassembly. It also includes developing models of interaction between molten-fuel debris and structural materials and of meltthrough or penetration of bottom supports.

For the study, initial core-geometry changes are assumed for accidents of various severities: (1) the core assembly essentially intact, but coolant circulation to the core impaired, (2) partial or complete blockage of one subassembly with coolant flow to the remainder of the core either intact or impaired, (3) several subassemblies blocked with coolant flow to the remainder of the core either intact or impaired, (4) the core partially or largely collapsed with some displacement and melting, and (5) the core disassembly and partially or largely molten, with the following three associated conditions (a) core debris on grid plate as either a loose pile of pieces or as a molten mass, (b) the core debris in the reactor-vessel head as either a loose pile of pieces or as a molten mass, or (c) the core debris on concrete or structural material in the secondary containment below the reactor-vessel head.

In considering the problems of cooling and retaining core debris, it is assumed that reactor and guard vessels retain a pool of sodium that covers the core debris and that this sodium is provided with sufficient cooling to avoid its loss by evaporation. The problems of retaining and cooling gaseous and vaporous fission products are not being studied at this time.

The above assumed postaccident core geometries lead to fuel in configurations as follows: (1) individual pieces of fuel material in sodium, (2) porous piles of fuel material in sodium, (3) fuel in a blocked

subassembly as either a porous bed of pieces or as a molten mass, and (4) pools of molten fuel debris on the lower grid plate, on the pressure-vessel lower head, and on concrete or sacrificial material of construction in the secondary containment vessel.

Analyses are being made of the behavior of fuel debris in these configurations, as well as of the problems of cooling and containment.

The preliminary analyses that were made will be described briefly.

Thermal conduction from and stability of individual fuel-debris pieces in sodium. Analyses of the thermal conduction from fuel pieces in sodium have been made.[1] When individual fuel pieces, with decay-heat generation, are in liquid sodium, the heat-transfer coefficient from the surface to the sodium is large compared to the thermal conductivity of the fuel, and the surface remains near the temperature of the sodium, or at about 900°C in the case of boiling sodium. Thick pieces would overheat and erupt into smaller and more stable pieces due to interior boiling. Figure 132 shows the calculated stable sizes for slabs, cylinders, and spheres as a function of decay heat.

Natural convection from porous piles of fuel debris in sodium. If a porous pile of pieces of fuel debris exists under liquid sodium, the fission-product decay heat in the fuel debris will cause a thermal-convection circulation of the sodium up through the porous pile, if the sodium has free access to the bottom of the pile. The driving force for this circulation is the pressure due to differences in densities between the sodium in the pool and the heated sodium in the porous pile. The resistance to the circulation is the flow friction loss through the porous pile. The circulating sodium removes heat from the pile and, for a pile sufficiently small, will keep the pile from overheating and melting. An equation for maximum depth of the pile was developed.[2]

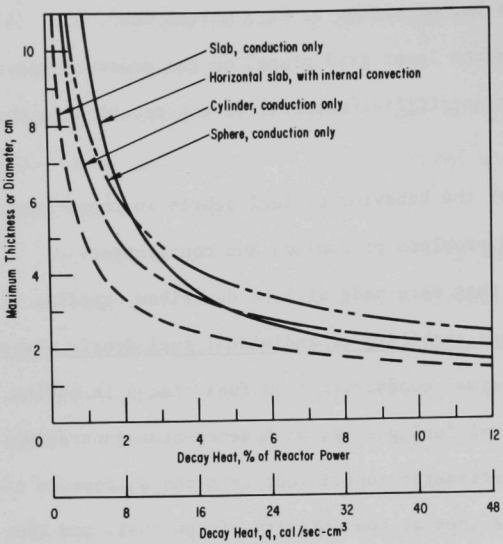

Fig. 132. Calculated Maximum Thickness or Diameter of a Slab, Cylinder, or Sphere for No Fuel Boiling, where T_s = 900°C, T_b = 3179°C, and k = 0.005 cal/sec-cm-°C. ANL Neg. No. 900-610.

A simplified version of the equation for depth of the pile for sodium at its boiling point of 900°C (at 1.18 atm) is

$$L = \frac{480}{q} \left(\frac{\varepsilon}{1-\varepsilon}\right)^{1.621} (\phi D)^{0.621}, \text{ cm}$$

and for pool sodium, at 300°C, which just reaches its boiling point (900°C) as it leaves the top of the pile,

$$L = \frac{1080}{q} \left(\frac{\varepsilon}{1-\varepsilon}\right)^{1.621} (\phi D)^{0.621}, \text{ cm}$$

where q is decay heat in cal/sec-cm^2, ε is pile porosity, ϕ is particle shape factor (1 for spheres), and D is particle effective diameter in cm.

Change in effective thermal conductivity due to nonfuel material in the debris. Calculations have been made of heat removal from slabs of solid fuel containing steel, assuming additive conductivity relationship (fuel and steel in laminae parallel to direction of heat conduction) and additive resistivity relationship (fuel and steel in laminae perpendicular to direction of heat flow). In the case of an additive-resistivity relationship, the heat-removal rate is reduced by the steel. However, in

the case of an additive-conductivity relationship, heat removal can be improved and the maximum improvement occurs at a volume fraction of fuel dependent on the ratio of steel-fuel conductivities.

For a steel-fuel conductivity ratio of 10, the maximum improvement in the heat-removal factor of 1.66 occurs at 0.55 volume fraction of fuel. For the same conditions for an additive-resistivity relationship, the heat-removal factor is 0.97. Because in an actual mixture the conditions would be somewhere between the additive-resistivity and -conductivity cases, the presence of steel in solid fuel would affect the heat removal only moderately.

Heat conduction from porous beds of fuel pieces in sodium. In a previous section (p. 377), natural heat convection from a porous pile of fuel pieces in sodium with free entry of sodium at the bottom of the pile was discussed. The question arises as to how well a flat porous bed of fuel pieces on a solid support without free access of sodium liquid at the bottom would be cooled by conduction only. Equations are available[3] for estimating the conductivity of material with void volumes; however, in this case, the conductivity of the bed was assumed to be half additive resistivity and half additive conductivity in nature. Calculations indicated that a bed having 35% porosity in sodium at 300°C could contain about twice as much fuel as a solid bed for equal heat removal at temperatures below the boiling temperature of sodium. However, the bed would be limited to a few centimeters thickness. In thicker beds, sodium boiling would occur and the bed might dry out and overheat. Boiling of the sodium would set up some circulation in the bed, depending on particle size and porosity, and some dispersal of fine bed particles into the sodium might occur, resulting possibly in a thicker bed that would not dry out.

Heating in a blocked subassembly. Heating in a blocked subassembly due to fission-product decay has been investigated. For an accident-damaged subassembly, a number of fuel-structural configurations would be possible. The fuel might be present as a porous bed of fragments that would be cooled by forced sodium coolant flow or by natural convection, as discussed on p. 377, or the subassembly might be partially blocked so that the sodium flow through the subassembly is insufficient for adequate cooling. In this latter case, the decay heat would need to be transferred to adjacent subassemblies, particularly in the event that sodium were prevented from entering the top of the blocked subassembly due to "vapor locking" or solid blockage. In this case, the heat flux to adjacent subassemblies might be great enough to cause meltthrough, particularly early in an accident when the decay heat is great and at places where fuel vapor, formed in the blocked subassembly, condensed on the subassembly walls. Figure 133 shows the estimated heat flux as a function of decay heat.

Heat transfer from pools of fuel debris. When the penetration of a barrier, such as concrete or steel, by a pool of molten fuel debris is analyzed, the rate of heat transfer from the molten pool to the barrier material is important because this heat transfer heats and melts the barrier material. Preliminary models were developed[5] to describe the heat transfer from the melt or pool to the bottom melting interface for both boiling and nonboiling conditions of the pool. The models are based on inversion layers at the bottom of the pool, and convection above the inversion layer due to rising vapor in boiling pools or temperature gradients in nonboiling pools.

The heat flux from the melt to the bottom of a pool is

$$Q_b = \sqrt{2k(T - T_m)q}, \text{ cal/sec-cm}^2$$

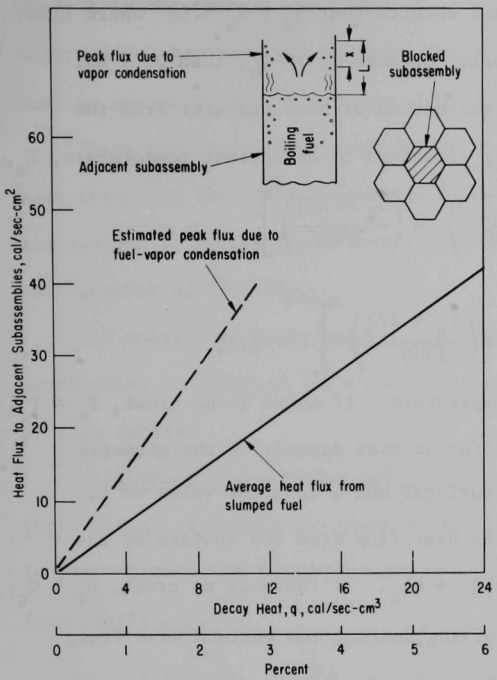

Fig. 133.
Heat Transfer from Blocked Subassembly to Adjacent Subassemblies (for 4.335-in. subassembly). The approximate burnout-flux region for heat transfer to boiling sodium is 38-75 cal/sec-cm².

where k is the thermal conductivity of the molten fuel in cal/sec-cm-°C, q is the specific-decay-heat-generation rate in cal/sec-cm^3, and T_m is the bottom (barrier melting) temperature in °C. In the case of a boiling pool, T is the boiling temperature T_b of the pool.

In the case of a nonboiling pool, T is the inversion-layer upper temperature, T_i, in °C.

$$T_i = T_s + \frac{1}{2}\left(\frac{Q_t}{0.068}\right)^{3/4} \left(\frac{\mu^2}{\rho^2 g\beta k^3}\right)^{1/4}$$

where T_s is the surface temperature of the molten pool in °C, μ is the viscosity in poise, ρ is density in gm/cm^3, β is the coefficient of thermal expansion in °K^{-1}, g is the acceleration due to gravity (980 cm/sec^2), and Q_t is the heat flux from the surface of the pool in

cal/sec-cm^2. T_s determines Q_t and we note that $Q_t + Q_b = Lq$, where L is the total depth of the liquid pool. Because $Q_t >> Q_b$, then $Q_t \simeq Lq$.

The value of T_s depends on the method of heat transfer from the surface of the pool. If it is by radiation to an ambient temperature, T_a,

$$Q_r = 1.37E \left[\left(\frac{T_r + 273}{1000} \right)^4 - \left(\frac{T_a + 273}{1000} \right)^4 \right]$$

and

$$T_r = 10^3 \left[\frac{Q_r}{1.37E} + \left(\frac{T_a + 273}{1000} \right)^4 \right]^{1/4} - 273,$$

where T_r is the crust surface temperature. If there is no crust, $T_s = T_r$.

The term E is an emissivity factor that depends on the geometry and emissivity ε. For parallel surfaces and a constant value of ε, $E = \varepsilon/(2 - \varepsilon)$. The term Q_r is the heat flux from the surface of the crust of thickness L_c; Q_r equals $Q_t + qL_c$. If there is no crust, $Q_r = Q_t$.

If heat is transferred to boiling sodium, the maximum heat flux, $h\Delta T$, is approximately 38-75 cal/sec-cm^2. For values of Q_r greater than this, a vapor blanket would form and heat transfer would be by radiation. For lesser values of Q_r, T_r would be approximately 900°C (just above the boiling temperature of sodium).

If the calculated value of T_r is greater than T_b, the pool is boiling at the surface and $T_s = T_r = T_b$. If T_r is greater than T_m (the melting temperature, °C) but less than T_b, $T_s = T_r$. If the calculated T_r is less than T_m, a crust forms on the pool and $T_s = T_m$.

The relationship between Q_r, Q_t, T_r, and T_m for a crust is

$$Q_r = \sqrt{2k(T_m - T_r)\, q + Q_t^2}$$

and

$$L_c = \frac{Q_r - Q_t}{q} = \frac{2k(T_m - T_r)}{Q_r + Q_t},$$

where k is the thermal conductivity of the crust. A trial-and-error solution is required, but for thin crusts (which might usually occur) one can assume $Q_r = Q_t$ for calculating T_r and L_c.

These models for heat transfer depend largely on the assumptions made regarding the thermal convection in the pool. Simulation experiments are planned to verify these assumptions for convective heat transfer in heat-generating liquids.

The models are being used to make preliminary computations of the penetration of concrete (silica-type aggregate) and depleted-UO_2 barriers by core debris.

Meltthrough of uncooled thin semisupported steel plates by molten fuel debris. A simplified equation was developed for the time required to heat an uncooled thin steel plate to its failure temperature by molten fuel debris. It is

$$t = \frac{2\rho C_p}{\sqrt{2k}} \left\{ (T_b - T_o)^{1/2} - (T_b - T_f)^{1/2} \right\} \frac{L}{\sqrt{q}} \text{ , sec}$$

where C_p is plate specific heat in cal/gm-°C, ρ is density of the plate in gm/cm^3, T_o is the plate initial temperature in °C, T_f is the plate failure temperature in °C, L is the thickness of the plate in cm, k is the fuel thermal conductivity in cal/sec-cm-°C, T_b is the fuel temperature in °C, and q is the fuel decay heating in cal/sec-cm^3.

Penetration by molten fuel debris of sacrificial barrier material such as concrete or depleted UO_2. Preliminary analyses were made of the penetration of concrete (silica aggregate) and depleted-UO_2 sacrificial barrier material.[6] In these analyses, it was assumed that the barrier material and fuel debris were completely miscible, that the decay-heat sources were uniformly dispersed in the molten pool, and that heat was

removed from the top of the pool by radiation. The equations for heat transfer from the pool to barrier (p. 380) were used. Cases where 100% and 50% of the decay heat remained in the molten mass were assumed. Figures 134 and 135 show the penetration results of these analyses for a reference reactor design.

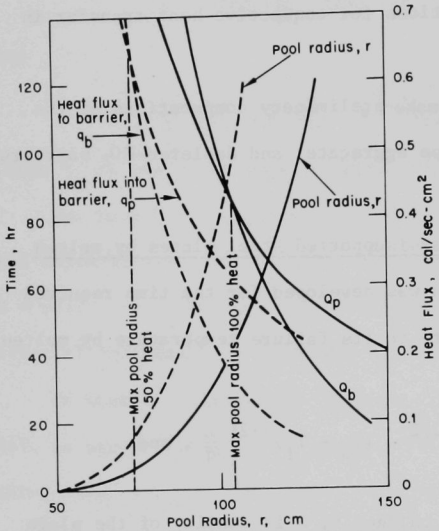

Fig. 134.
Pool Radius for Depleted-UO_2 Barrier. ————100% of decay heat; ------50% of decay heat.

Meltthrough of metal plates or trays in sodium. In the case of fuel debris resting on support members under sodium, the problem of meltthrough of the support member arises, particularly where the depth of the fuel is substantial or the cooling of the support by sodium is hindered, for example, by sodium vapor. The fuel might consist of a solid layer, resting on the support, with perhaps a higher molten central layer. If the heat flux from the fuel to the support exceeds the heat flux from the support to sodium, the support will overheat and fail. This heat flux can be determined from the equations given on pp. 380-382.

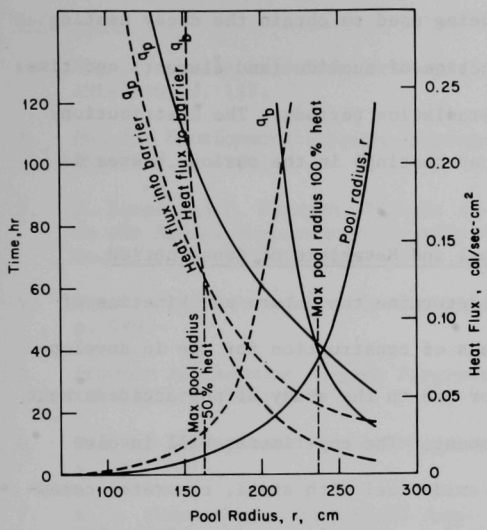

Fig. 135. Pool Radius for Concrete Barrier. ————100% of decay heat; -------50% of decay heat.

for boiling and nonboiling pools. If the metal is in contact with liquid sodium lying above it, a potential heat flux of about 38 to 75 cal/sec-cm^3 could be expected (boiling burnout flux). For flowing sodium, the flux would be higher. However, if the sodium is beneath the plate, lower heat fluxes would be obtained. Experiments are being planned to determine burnout heat fluxes to boiling liquids below heated plates.

Fission-product-decay heating. In the postaccident heat-removal studies, the fission-product-decay sources as a function of time and distribution in the vapor, liquid, and solid phases of the core debris are needed. The decay heating and its distribution can be estimated from information on the decay heating as a function of time and fission-product element together with estimates of the fission-product-element distribution in the vapor, liquid, and solid phases.

The computer code RIBD[7] is being used to obtain the decay heating (beta, gamma, and total) as a function of nuclide (and element) and time for PuO_2-UO_2 fuels for several irradiation periods. The distributions of the elements (and hence of decay heating) in the various phases is being estimated.

Experiments on Interactions of Fuel and Materials of Construction

Experiments were started to determine the nature and kinetics of interactions of fuel with materials of construction for use in developing information and parameters for use in the study of postaccident heat removal and core-material containment. The experiments will involve interactions of solid and molten oxide fuel with steel, concrete, ceramics, and possibly other materials of construction to determine melt-through or solution rates, behavior of molten, solid, and unmelted phases with respect to flotation of less-dense components, unusual or energetic reactions and other phenomena, as well as misicibility of molten phases and the characteristics of molten and resolidified phases.

Small-scale experiments of interactions of solid UO_2 with molten concrete were started. In these experiments, concrete is melted in an induction-heated graphite crucible in the presence of solid UO_2. Changes in melting temperatures due to interactions and posttest examination of the penetration and dissolution of the UO_2 are made.

Future program. Plans include continuing these experiments and the construction of a plasma-torch-heated furnace for melting UO_2 in contact with structural materials (static temperature gradient effects) and for melting UO_2 to pour onto structural materials (dynamic effects). Experiments to investigate heat transfer from UO_2 particle beds under sodium are planned.

References

1. *Reactor Development Program Progress Report November 1969*, ANL-7640, p. 137.

2. *Reactor Development Program Progress Report January 1970*, ANL-7661, p. 134.

3. H. Kampf and G. Karsten, *Effects of Different Types of Void Volumes on the Radial Temperature Distribution of Fuel Pins*, Nucl. Appl. Tech., *9*(3), 288-300 (Sept 1970).

4. *Reactor Development Program Progress Report June 1970*, ANL-7705, p. 189.

5. *Reactor Development Program Progress Report April-May 1970*, ANL-7688, p. 244.

6. *Reactor Development Program Progress Report July 1970*, ANL-7726, p. 162.

7. R. O. Gumprecht, *Mathematical Basis of Computer Code RIBD*, DUN-4136 (June 17, 1968).

XIII. 1000-MWe SAFETY STUDY CONTRACT MANAGEMENT, TECHNICAL REVIEW, AND EVALUATION*

(L. W. Fromm)

Overall scope. Studies of 1000-MWe LMFBR plant designs by industrial subcontractors are planned, reviewed, guided, and evaluated. Argonne maintains close technical and administrative liaison with the subcontractors performing the studies and with the AEC. In this program, Argonne: (1) prepares scope of work and ground rules so the studies will produce information needed to achieve program goals, (2) ensures that all subcontractor studies are performed in accord with the work scopes, ground rules, schedules, and contract funding, (3) assists the subcontractors in obtaining the latest related information being developed elsewhere, (4) ensures that the studies are realistic, that appropriate methods of analysis are used, that decisions are based on adequate depth of study, and that no study is distorted by unjustified assumptions, (5) provides AEC with evaluations of study results where appropriate, and (6) recommends further profitable study areas.

Argonne technical specialists meet with each subcontractor periodically, review his technical notes and informal monthly and quarterly reports, and furnish reviews and guidance. As formal phase and topical reports are received, the specialists evaluate them in those aspects having an important effect on the guidance of the national LMFBR program, and report the results to AEC. Fiscal and schedule

*For references for this chapter, see p. 394.

control are maintained through subcontractor's monthly and quarterly administrative reports.*

Management and Technical Review of Subcontractors' Studies

(L. W. Fromm)

Scope. Management and technical review of subcontractors' studies encompasses all activities connected with the initial establishment of study programs by the subcontractors, and with the day-to-day technical monitoring of the subcontractors' work, exclusive of in-depth evaluation of formal reports. The management and review work centers on the following types of activity: (1) preparation of work scopes and negotiation of scopes with subcontractors and AEC to ensure compatibility with AEC objectives and available funding, (2) review and approval of subcontractors' work plans, (3) technical review of subcontractors' informal documents (monthly and quarterly progress letters, and technical notes), and review of results presented at periodic review meetings (these reviews are based largely on judgment factors, with only minimal rudimentary check calculations where necessary for support), (4) provision of guidance to subcontractors, as appropriate, based on technical reviews, and (5) preparation of recommendations to AEC as to further profitable study areas.

Summary. Contract management and technical-review activities were continued with respect to the Babcock & Wilcox safety study initiated in FY1969. Negotiations on scopes of work and subcontracts for various safety studies supplementing the earlier 1000-MWe Follow-on Studies (see p. 443) were completed with General Electric,

---

*Budget stringencies after the report period resulted in termination of all 1000-MWe Safety Analysis Study Subcontracts (see p. 395) and of this related program.

Westinghouse, and Atomics International. Contract management and technical-review activities were initiated as the subcontractors began their studies.

Preparation and negotiation of technical scopes of work with subcontractors. Subcontract negotiations begun with General Electric and Westinghouse were concluded. The Westinghouse subcontract covers a combined Plant Safety Analysis, Dynamics, and Loop-type Primary System study. In the case of General Electric, the earlier scope of work was revised to emphasize the probabilistic-safety-analysis study, and to include minimal effort in upgrading the GE pool-type primary system and in dynamics and control analysis to provide a firm basis for the safety study. A scope of work was developed jointly with Atomics International for a study of emergency reactivity shutdown systems applicable to 1000-MWe LMFBRs, and a subcontract was negotiated.

Management and review of Babcock & Wilcox 1000-MWe LMFBR Accident Analysis and Safety System Design Study. Contract management and technical review activities were continued on the Babcock & Wilcox 1000-MWe LMFBR Accident Analysis and Safety System (A^2S^2) Design Study initiated in FY1969. The B&W work plan for the study was received and reviewed, and modifications were made to the plan by B&W in response to ANL comments. A B&W technical note describing the analytical methods to be used in the study was reviewed and comments were forwarded to the subcontractor for guidance. The B&W TART transient-analysis code for reactors was made operational at ANL for checking the B&W calculations. In response to an ANL inquiry, B&W proposed an adjunct study to determine the effects that large radiation-induced metal swelling in the reactor core and related structures might have on the analytical models

and parameter ranges being used in the base A^2S^2 study. A scope of work was developed and a subcontract supplement was executed calling for completion of the work by the end of FY1970. The adjunct study considered two models of radiation-induced steel swelling; B&W selected the Westinghouse-PNL correlation for cold-worked stainless steel as one model, and ANL furnished data based on the latest version of the Harkness-Li correlation to be used as the second model. Toward the end of the fiscal year, five additional technical notes on various aspects of B&W Phase-II work were received and reviewed. Monthly review meetings were held with the subcontractor, including two special meetings at which B&W presented its results to the utility participants partially supporting the study.

Management and review of Westinghouse 1000-MWe Loop-type LMFBR Safety, Dynamics, and Primary-system Study. Contract management and technical-review activities were initiated upon completion of subcontract negotiations with Westinghouse for a combined Plant Safety Analysis, Dynamics, and Loop-type Primary-system Study. Semiquarterly review meetings were initiated and drafts of the Westinghouse work plan for the combined study were reviewed. A preliminary partial draft of a technical note describing the oxide core designed by Westinghouse (at its own expense) to serve as the basis for the combined study (in substitution for the Follow-on Study reference carbide core) was received and review was initiated.

Management and review of General Electric 1000-MWe LMFBR Probabilistic Plant Safety Analysis Study. Contract management and technical-review activities were initiated upon completion of subcontract negotiations with General Electric for a probabilistic plant safety analysis study.

Management and review of Atomics International 1000-MWe LMFBR Emergency Shutdown System Study. Contract management and technical-review activities were initiated upon completion of subcontract negotiations with Atomics International for an emergency-shutdown-system study.

Future program. Management and technical review of the work of four subcontractors on studies initiated in FY1970 will be continued. Guidance will be provided to the subcontractors where important to the further conduct of the study, and will be reported to AEC in informal documents, along with brief comments on the work status and subcontractors' performance. No work on scope preparation and negotiation is expected in FY1971.*

Technical Evaluation of Subcontractors' Formal Study Reports

(L. W. Fromm)

Scope. Subcontractors' studies are generally divided into three or four phases, each of which represents a segment of the work program that can logically be reported as a technical unit. At the conclusion of each phase, the subcontractor is required to submit a formal phase report (called "task reports" in the earlier 1000-MWe Follow-on Studies), suitable for open publication. In some cases, the phase reports are augmented by formal topical reports covering particular technical areas. Argonne technical specialists review all subcontractors' phase and topical reports to determine whether evaluation is appropriate with respect to the guidance of the national LMFBR development program. If warranted, evaluations are carried out and are directed toward aspects of importance to the national program. The

---

*See footnote on p. 389.

comments and opinions comprising these evaluations are based on judgment and experience, supported as necessary by check calculations. Evaluations performed during the course of each study are reported to AEC informally as they are completed. At the conclusion of each study, a final evaluation report is compiled if appropriate.

Summary. Evaluations of the safety aspects of the Task-II, -III, -IV, and -V reports by the 1000-MWe LMFBR Follow-on study subcontractors were completed (see p. 460). The results were incorporated into the four-volume draft final evaluation report issued to AEC and the LMFBR Program Office. The Phase-I report on the Babcock & Wilcox Accident Analysis and Safety System (A^2S^2) Design Study was reviewed to determine need for detailed evaluation.

Evaluation of safety aspects of 1000-MWe LMFBR Follow-on Studies; preparation of draft final evaluation report. Evaluations of the safety aspects of the 1000-MWe Follow-on Study Task-II, -III, -IV and -V reports by Atomics International, Babcock & Wilcox, Combustion Engineering, General Electric, and Westinghouse were completed. The results of the evaluations were incorporated into a four-volume draft ANL final evaluation report that was issued to AEC and to the LMFBR Program Office. The draft summary volume was also issued to the subcontractors for their comments. For reasons indicated on p. 448, further work on the Follow-on Study evaluations was terminated at this point. Some broad observations of the 1000-MWe Follow-on Study evaluation, including safety, are given on pp. 448-460.

Evaluation of phase reports on Babcock & Wilcox 1000-MWe LMFBR Accident Analysis and Safety System Design Study. The Phase-I report, "Fault Trees and Malfunction Catalog," BAW-1344, of the Babcock & Wilcox 1000-MWe LMFBR Accident Analysis and Safety System (A^2S^2)

Design Study was reviewed to identify any aspects of the report having importance to the national LMFBR program and that, therefore, warranted detailed evaluation. It was decided that no detailed evaluation was appropriate at that time.

Future program. The Phase-I report of the Atomics International Emergency Shutdown System Study, and the Phase-II report on the Babcock & Wilcox Accident Analysis and Safety System Design Study will be reviewed to determine whether evaluation is appropriate with respect to the guidance of the national LMFBR development program. If warranted, the evaluations will be initiated, and will be directed toward aspects of importance to the national program, but in lesser depth than those pertaining to the earlier 1000-MWe Follow-on Studies. No phase reports are expected from Westinghouse and General Electric during FY1971.*

References

See p. 460.

*See footnote on p. 389.

Nuclear Safety--LMFBR Safety

XIV. 1000-MWe SAFETY STUDY SUBCONTRACTS*

(L. W. Fromm)

Overall scope. Four industrial subcontractors are performing definitive safety studies based upon their reference plant concepts developed in the 1000-MWe LMFBR Follow-on Study program (see Reference on p. 460). Limited further engineering and dynamics analysis work on primary-coolant system designs is being conducted as needed, to provide firm bases for the safety studies, and analytical methods are being developed, also to a limited extent, in areas where no suitable methods now exist. Detailed accident analyses are being carried out, and designs of safety systems are being prepared and evaluated.**

This activity covers only subcontractors' efforts; ANL contract management, technical review, and evaluation efforts are described on pp. 388-394.

The studies performed in this program are related to the LMFBR demonstration-plant program in that dialog on LMFBR safety problems will be established between manufacturers and regulatory bodies that will be helpful in licensing the demonstration plants. Also, these studies will identify and help to solve safety problems whose solutions are also required for the design of the demonstration plants. The results of this program will provide guidance and direction to the Commission's overall LMFBR research and development program, and in that sense will influence all future LMFBR research and development, design, construction, and applications-study programs of the AEC.

---

*For references for this chapter, see p. 403.

**Budget stringencies after the report period resulted in termination of this entire study program.

The Babcock & Wilcox Co. Subcontract

(I. Charak)

Scope. The Babcock & Wilcox Co. is performing a 1000-MWe LMFBR Accident Analysis and Safety System (A^2S^2) Design Study, based on the B&W reference plant concept developed under the 1000-MWe LMFBR Follow-on Study. Malfunctions and safety problems are being surveyed, using the fault-tree technique, and potential accidents are being analyzed. Sensitivity studies are being performed to determine effects of varying input constants and assumptions. In an adjunct study, the effect of radiation-induced metal swelling, now recognized as a major problem in large LMFBRs, on the models and parameter ranges used in the accident analyses is being assessed. The design basis accidents for the concept are being selected and the rationale for the selection is being given. Functional requirements for safety systems are being defined, systems are being selected, conceptual designs for the systems are being developed, and system design descriptions (SDDs) are being written. Research and development requirements are being delineated.

Summary. The A^2S^2 Design Study commenced the last month of FY1969, so essentially all accomplishments were in FY1970. The work consisted primarily of a survey of malfunctions and safety problems (Phase I) and preliminary selection of candidate safety systems. For the purposes of this study, the safety systems are categorized as emergency decay-heat-removal systems, reactor protective features, primary-containment safety features, and secondary-containment support systems. The adjunct study on metal swelling was completed.

Program Definition Phase: Preparation of Work Plan. The work plan for the A^2S^2 Design Study (BAW-1339) was prepared by B&W and, after

changes were made at the request of the Laboratory, the work plans for Phases I and II were approved.

Phase I: Malfunction and Safety Problem Survey. Phase I was completed and resulted in the preparation of the Phase-I report.[1] This report presents the results of the survey in the form of a malfunction catalog and fault-tree displays.

Adjunct study to determine effect of metal swelling on models and parametric ranges used in accident analysis. B&W completed the adjunct study, which was initiated to determine the effects of radiation-induced steel swelling on the A^2S^2 Design Study. A technical note was prepared summarizing the work performed and a separate proposal presented B&W recommendations for future work in the A^2S^2 Design Study.

Phase II: Accident Analysis and Selection of Safety Systems. B&W completed studies of accident-initiating conditions due to flow abnormalities and reactivity-insertion transients, including sensitivity studies thereon, and technical notes were prepared on each subject. In addition, the review and identification of candidate safety systems were completed. A technical note was prepared for each of the four categories of safety systems. Accident analyses and sensitivity studies were begun.

Phase IV: Research and Development Delineation. During the course of Phase-II work, new and revised research and development needs were identified and compiled for inclusion in the Phase-II Report.

Future program. The results of the adjunct study on metal swelling will be assessed as to their effect on the A^2S^2 study, and the work plan and, if necessary, the work scope, will be revised accordingly. Phase-II work will continue with accident analyses and sensitivity studies, design-basis-accident selection, determination of safety-system

functional requirements, safety-system selection, and the writing of the Phase-II report. Phase-III work on conceptual design of the safety systems will begin. Research and development needs will be reported as they are identified.*

Westinghouse Electric Corp. Subcontract

(J. P. Burelbach)

Scope. The Westinghouse Electric Corp. is performing a 1000-MWe LMFBR Plant Safety Analysis Study, based on the Westinghouse reference plant concept developed in the 1000-MWe LMFBR Follow-on Study, but modified to utilize a mixed-oxide rather than a mixed-carbide core. The core redesign was performed by Westinghouse at Westinghouse expense, and includes features that allow for radiation-induced metal swelling in the core. Malfunctions and faults are being catalogued, and plant responses are being analyzed quantitatively. Engineering work on the loop-type primary-coolant system is resulting in an upgraded system design and an assessment of concept limitations. Dynamics analyses include system modeling, control and safety system analysis, and consequent upgrading of control-system design. Accidents are being analyzed, their radiological consequences determined, and design basis accidents selected. Safety-system functional requirements are being established, reference systems are being selected, and system design descriptions (SDDs) are being prepared. General design criteria developed in the Follow-on Study are being upgraded. A document analogous to a preliminary system design description is being prepared and discussed with AEC regulatory groups. Research and development requirements are being delineated.

---

*See footnote on p. 395.

Summary. While awaiting AEC authorization of the study and negotiation of a subcontract, the subcontractor at his own expense developed a design for an oxide core for his 1000-MWe LMFBR Follow-on Study reference plant, in substitution for the carbide core specified therein. After completion of subcontract negotiations, a work plan for the entire study program was prepared and submitted to ANL, and Phase-I work was begun.

Reference-design modification for oxide core. A design for an oxide core was prepared by the subcontractor at his own expense to replace the carbide core in his 1000-MWe LMFBR Follow-on Study reference plant concept and to serve as a basis for the study program. Preparation of a technical note was initiated, describing the oxide core in its neutronic, thermal-hydraulic, and mechanical aspects, and showing plant modifications necessary to accommodate the revised core design.

Program Definition Phase: Preparation of Work Plan. A work plan was prepared describing Phase-I work for the combined study program comprehensively and for later phases in a more general manner. The plans for the later phases will be updated in detail before the start of work on those phases of the program.

Phase I: Preparation for Accident Analysis and Safety System Development, and Related Work in Concurrent Dynamics and Loop Studies. Phase-I work was initiated in limited areas pending approval of the work plan.

Future program. Phase-I work begun near the end of FY1970 will continue. Potential malfunctions and faults will be catalogued, fault-tree displays will be constructed, initiating conditions for reactor

accidents will be defined, and plant responses will be analyzed. Block diagrams illustrating safety-system concepts to be examined will be prepared. Computer programs for safety-system simulation and accident analysis will be obtained. Inherent plant dynamic behavior will be determined. Mathematical models for components will be improved; an overall code will be developed. Reference features of the primary-coolant system will be evaluated and upgraded as necessary to provide a firm basis for safety analysis. New R&D needs will be identified.*

General Electric Co. Subcontract

(I. Charak)

Scope. General Electric Co. is performing a 1000-MWe LMFBR Probabilistic Safety Analysis Study, based on the GE reference plant concept developed under the 1000-MWe LMFBR Follow-on Study, with the core design modified to accommodate the radiation-induced metal swelling now recognized as likely in large fast reactors. Methods for probabilistic analysis are being obtained, adapted, and developed where necessary. Reliability data are being compiled. Malfunctions and faults are being catalogued in the form of fault trees, and the fault trees are being analyzed quantitatively. Accident-frequency criteria are being developed; probabilities of occurrence of various accidents are being established and their acceptabilities are being judged against these criteria. Engineering work on the pool-type primary system, and certain dynamics analyses, are being carried out to the extent necessary to provide a firm basis for the safety study. Safety-system functional requirements are being established, and the reference-

---

*See footnote on p. 395.

system designs are being upgraded. AEC General Design Criteria are being assessed as to their applicability to the contractor's upgraded reference design. Research and development requirements are being delineated.

Program Definition Phase: Preparation of Work Plan. After completion of subcontract negotiations, the preparation of a comprehensive work plan for the entire study was begun.

Future program. The work plan will be completed. Phase-I work will begin. Accident frequency criteria will be established. Potential malfunctions and faults will be catalogued and fault trees will be constructed. Codes for probabilistic analysis and reliability data will be obtained, and the fault trees will be quantitatively analyzed. Initiating conditions for reactor accidents will be defined. Work will be started on assessing the feasibility of safety systems and iterating the designs to identify necessary changes. Primary-coolant-system dynamic analyses will be performed, and reference features will be evaluated and modified as necessary to provide a firm basis for safety analysis. New R&D needs will be identified.*

Atomics International Subcontract

(J. P. Burelbach)

Scope. Atomics International is performing a 1000-MWe LMFBR Emergency Shutdown system Study, based on the AI reference plant concept developed in the 1000-MWe LMFBR Follow-on Study, but also applicable to other LMFBR power-plant designs. The AI reference-plant core design will be modified to accommodate the radiation-induced metal swelling now recognized as likely in large fast reactors, if such

---

*See footnote on p. 395.

modification is deemed important to the emergency-shutdown-system study. Initially, the subcontractor is updating the safety analyses prepared as part of the Follow-on Study to reflect the effects on the design basis accident (DBA) of the modifications made to accommodate metal swelling. A fault-tree analysis of the primary (control and safety rod) shutdown system is being performed, and the need for an emergency shutdown system is being evaluated. Functional requirements for such a system are being developed, potential design approaches are being identified and evaluated, and the most promising approaches are being selected. Conceptual designs for these approaches are being developed and system design descriptions (SDDs) are being written. A fault-tree analysis is being made of the emergency shutdown system as applied to the subcontractor's modified reference plant, and the effects of the system on the DBA for the plant are being determined. Research and development requirements are being delineated.

Program Definition Phase: Preparation of Work Plan. After completion of subcontract negotiations, the preparation of a comprehensive work plan for the entire study was begun.

Future program. The work plan for the study will be completed. Phase-I work will be carried out and reported. The primary shutdown system of the modified reference plant will be analyzed by fault-tree techniques, and the need for an emergency shutdown system will be evaluated. Phase-II work, including development of functional requirements and identification and evaluation of design approaches, will be started.*

---

*See footnote on p. 395.

Reference

1. The Babcock & Wilcox Co., *1000-MWe LMFBR Accident Analysis and Safety System Design Study - Phase I Report - Fault Trees and Malfunction Catalog*, BAW-1344 (Dec 1969).

XV. REACTOR SYSTEM AND CONTAINMENT STRUCTURAL DYNAMIC RESPONSE*

(S. H. Fistedis)

The fast-reactor program is geared to the ultimate development of safe and economic fast-reactor power plants. Although these plants are designed for continuous safe operation, additional safety provisions are made to safeguard public health and safety. This program on fast-reactor containment provides this additional safeguard over and above reactor control. Containment is provided to confine the effects of hypothetical reactor accidents.

Some of the safety issues that are being resolved in the containment program are: (1) accurate assessment of the energy-absorption capability of the primary system, (2) accurate prediction of the response of the reactor-vessel cover and cover-holddown mechanism to work-energy releases, (3) calculation of the amount of sodium that can escape past the cover during an energy release, and (4) prediction of secondary-containment response to temperatures and pressures resulting from fires due to sodium spillage past the cover.

To gage the effects of the excursion on the primary-system components, a two-dimensional hydrodynamic code and a two-dimensional inelastic code were developed. The hydrodynamic code ignores shear stresses and the material strength and is applied to high-energy excursions. The inelastic code includes shear strength and is more suitable for medium-energy excursions. Emphasis had been placed on the completion of the hydrodynamic code. Development of the inelastic code will benefit from experience obtained on the hydrodynamic code.

---

*For references for this chapter, see p. 425.

The preliminary version of the two-dimensional computer code for the numerical calculation of hydrodynamic response of primary containment to a high-energy excursion has been completed. Outstanding features of the code are that it (a) contains equations of state of reactor materials (the present version of the code contains the equations of state of core, breeding blankets, plenum, sodium, steel, and argon), (b) gives the energy partition at all times, (c) gives the motion of the medium at all times, (d) determines whether or not and when the reactor vessel breaks, (e) gives the pressure loading on the plug and determines when the plug jumps, and (f) provides input to the plug-jump problem.

The code output is on printed sheets that give the displacements, velocities, pressures, internal energies, densities, and strains at every time step for all spatial points. The output of displacements and pressures can also be given pictorially, showing the movements and deformations or magnitudes of pressure of all spatial points at any instant of time. It is believed that this code will give the reactor designer information with which to adjust the geometry of the layout and the strength of structural components to achieve a balanced design or a design that will dissipate the excursion energy with least hazard to the primary containment.

The reactor configuration selected for testing the code, as well as the initial layout of the Lagrangian grids, is shown for time zero in Fig. 136; axial symmetry permits only half the cross section to be shown. The core is assumed to have oxide fuels contained in stainless-steel pins supported in stainless-steel grid plates (not included in the analysis) and to be cooled by liquid sodium. The sodium is covered by argon gas and is held in a steel pot within a concrete primary containment that has a rotatable shield plug in the platform at the top of the primary cavity.

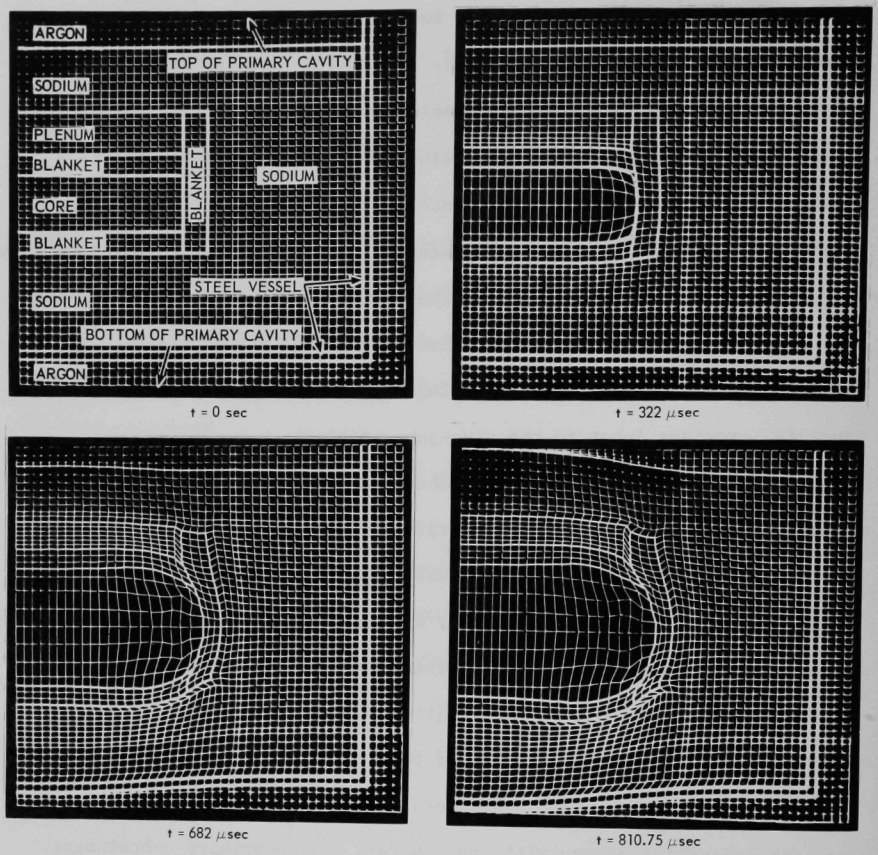

Fig. 136. Deformations of Lagrangian Grids at Various Times after Start of a Power Excursion in a "Pancake" Core Configuration. ANL Neg. No. 113-2382 Revision 1.

For the excursion model, it is assumed that at the start of the power excursion the core is molten, and the sodium has already been vaporized and expelled from the core region. However, the blankets are assumed to be intact. The energy is released so rapidly in the excursion that the molten oxide fuel is assumed to be vaporized and superheated to high temperature and pressure. Therefore, at the end of the power excursion, the core consists of only high-pressure oxide vapor.

Figure 136 shows the time sequence of deformations of the Lagrangian grids. Figure 137 shows the pressure profiles along the vertical centerline at various times. Figure 138 shows the pressure profiles along the horizontal axis of the core at various times. The computation was terminated at t = 811.28 μsec because at that time the force acting on the plug exceeded the strength of the plug-holddown device.

To determine the maximum pressure and force that can be produced in the excursion, the computation was resumed by assuming that the plug could be rigidly secured to the platform. Figure 139 shows the variation of pressure at a typical mesh zone underneath the plug from t = 811.28 to t = 1350 μsec; note that the pressure is of an oscillating nature and has several peaks. The maximum peak pressure is about 33.3 kbar at 892 μsec. Once the pressure reaches a peak, the direction of the fluid is reversed. When the returning fluid collides with the oncoming fluid, the direction of the fluid changes again. The total force acting on the rotating plug is shown in Fig. 140. The maximum magnitude of the force is $\sim 6.44 \times 10^{14}$ dynes. In this case, the plug-holddown device should be designed to resist the <u>impulse</u> resulting from such a force.

To extend the hydrodynamic analysis to the domain where the tensile strength of the vessel material might become important, the computer code has been revised to include the effects of the membrane strength of the vessel material in the analysis. The mechanical properties of a solid material at high pressures can be described by using a compressible-fluid model. Thus, during shock compression, the momentum equation developed for fluids also can be used for solids. However, as the material recovers from the shock loading, or the material is under tension, the tensile strength becomes important, particularly for a cylindrical shell where

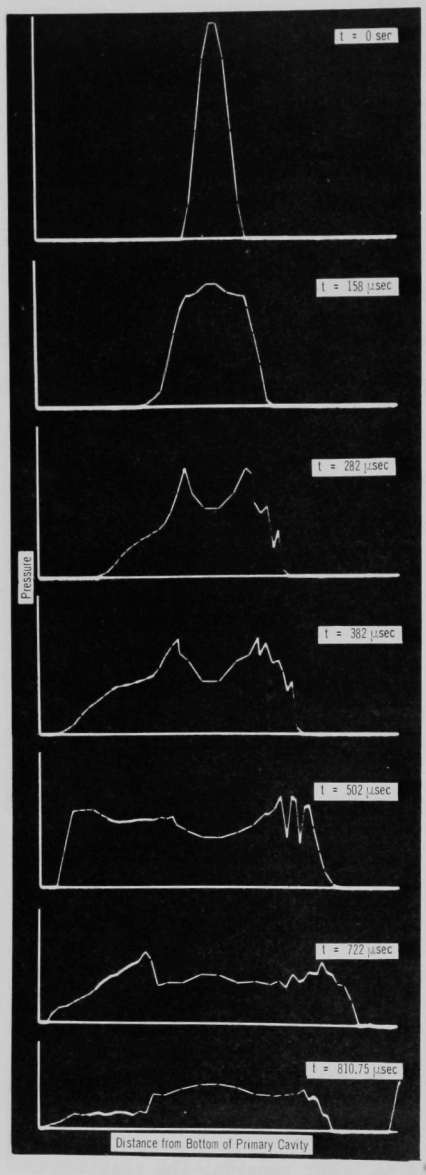

Fig. 137. Pressure Profiles along Vertical Centerline of Core at Various Times. ANL Neg. No. 900-691.

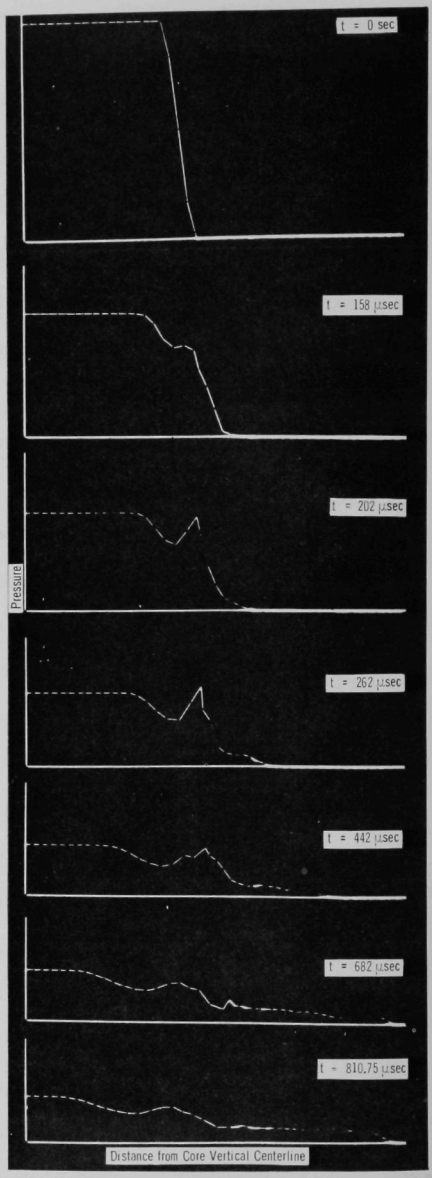

Fig. 138. Pressure Profiles along Horizontal Axis of Core at Various Times. ANL Neg. No. 900-691.

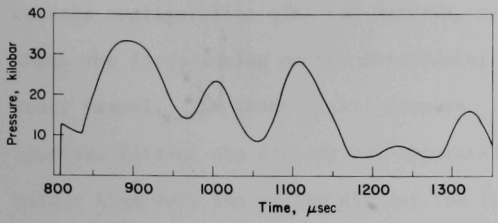

Fig. 139.
Variation of Pressure at a Typical Mesh Zone underneath the Plug. ANL Neg. No. 113-1947, Rev. 1.

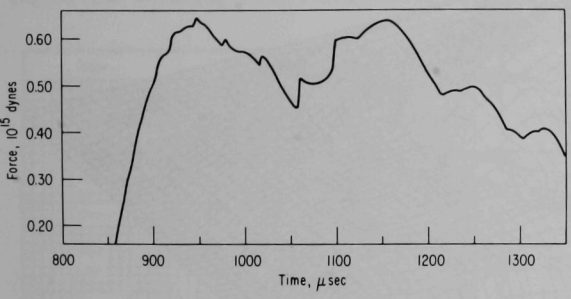

Fig. 140.
Total Force Acting on the Rotating Plug as a Function of Time. ANL Neg. No. 900-791.

the radial movement of the shell produces membrane forces, and where the tensile strength of the material is the key mechanism for stopping the motion of the shell.

The revised code has been completed and is being documented. It is now available through the Argonne Code Center under the name REXCO-H.

A PLOT-3D Fortran subroutine has been developed to draw three dimensional surfaces. It improves the visualization of the complicated functions such as pressure, displacement, and velocity from tabulated data on the computer digital printout. The PLOT-3D output subroutine can be displayed either by the IBM-2280 Film Recorder or the Calcomp-780 Plotter. PLOT-3D draws a three-dimensional surface from an array of points (x, y, z), where x and y are the spatial coordinates of a point, and z is the value of the function to be displayed at that point. The surface can be drawn after arbitrary rotations. Figure 141 shows the surface of the pressure at time 810.75 μsec as drawn by PLOT-3D with a Calcomp-780

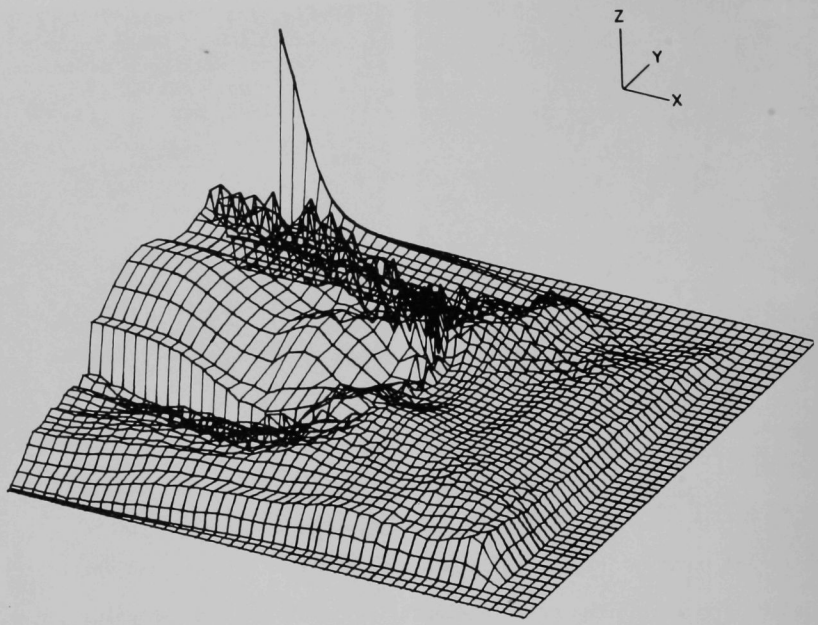

Fig. 141. Pressures (z) at Points on x-y Plot as Drawn by PLOT-3D Fortran Subroutine. Reactor radial axis is x; axial axis is y. ANL Neg. No. 900-590.

plotter for the sample problem shown in Fig. 136. The surface has been rotated first 60° around the z axis and then 30° around the y axis.

System Geometries and Excursion Magnitudes and Durations

(Y. W. Chang and J. Gvildys)

The REXCO-H code developed for containment analysis can be used for studies of system geometry. The reactor designer can use the code to study the failure sequence of various components and its effects on loads imposed on other system components, or to vary a single parameter so that its independent effect can be studied.

For example, to study how rupture of a reactor vessel affects loads imposed on the shield plug, the reactor designer could consider using a

reactor configuration with two vessels, as shown in Fig. 142. Figure 143 shows the force acting on the shield plug for systems with or without the inner vessel. The inner vessel directs the kinetic energy of the coolant upwards, lifting the coolant and compressing the inner gas blanket much harder than does the system without the inner vessel. Thus the force acting on the rotating shield plug could be reduced considerably if the inner

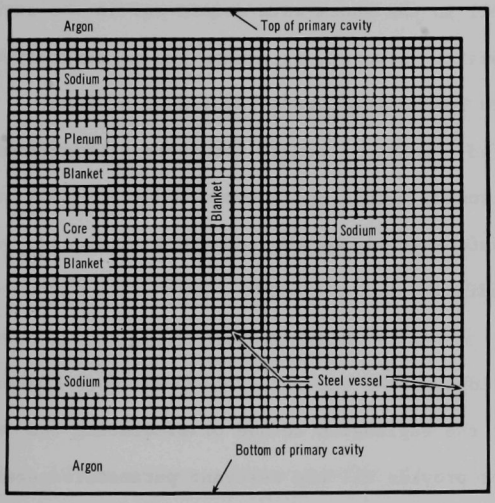

Fig. 142.
Reactor Configuration with Two Vessels Is Typical of Arrangement for Which REXCO-H Code Can Be Used to Study Sequence of Failures and Effects of Loads Imposed on System Components. Inner vessel in this example has 390-cm diameter and 7.5-cm-thick wall. ANL Neg. No. 900-591.

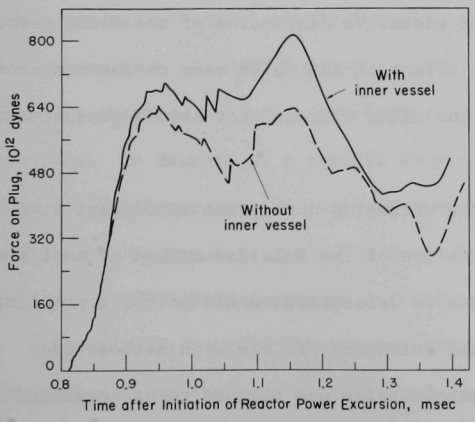

Fig. 143.
How Presence or Absence of Inner Vessel That Ruptures During Excursion Affects Total Force Imposed on Shield Plug. ANL Neg. No. 113-3150, Rev. 1.

vessel were designed to rupture at the beginning of the excursion. By varying the numerous parameters involved in the codes, the designer can study their effects on the overall safety of the design.

Automatic Rezoning of Code to Extend Excursion Treatment into Sodium-momentum Domain

(Y. W. Chang and J. Gvildys)

The REXCO-H Code works well in the shock-wave domain and in the early part of the liquid-momentum domain. However, as meshes become severely distorted, the computer results become inaccurate. Rezoning of the Lagrangian meshes was considered a possible remedy for these difficulties. It was decided to develop a rezoning method and a computer code so that the rezoning can be accomplished automatically by the computer. Various rezoning methods are being studied.

Code Transformation

(A. H. Marchertas and J. Gvildys)

Experience has shown that the Lagrangian method of simulating the fast-reactor excursion does not provide all the relevant parameters necessary for complete containment design. The Lagrangian solution must be terminated prematurely because of excessive distortion of the fluid mesh. At the point of termination, the effect of the shock wave on the containment can be determined, but not the other effects that become predominant later.

To follow the progress of the excursion during the subsequent time period, consideration was given to use of the Eulerian method of analysis. With the Eulerian approach, excessive deformation would not be a problem, as in the case with the Lagrangian solution. To use both methods most effectively, the study of a given excursion was planned to be conducted

by using the Lagrangian method for the initial stages, up to the time of excessive deformation; after the point of termination, the solution would continue by means of the Eulerian method. This approach would effectively utilize the advantages of both methods. However, transformation of the Lagrangian variables into those of the Eulerian would be needed, and this preferably should be done automatically. Such a systematic transformation could only be accomplished by knowing in advance the specific Eulerian method to be used.

In search of available Eulerian methods, the one called PIC[1] (particle-in-cell) was found to enjoy considerable success in solving numerous practical problems of compressible fluids. In addition, it appeared as if this approach could be adapted to the containment problem without too much difficulty. Thus, the task of accepting the output of the available hydrodynamic Lagrangian-coordinate REXCO-H code[2] at the instant of termination and converting this information into such form as would be needed for the input of the Eulerian-coordinate solution was the first step of the effort. Consequently, the computer program called TRANSF was written to accomplish this operation. This program in effect provided a means for superposition of the Eulerian mesh over the Lagrangian mesh in such a way that meaningful properties of the individual Eulerian grids could be obtained. In this way initial data for the Eulerian solution was provided. An example of a typical output of REXCO-H is shown in Fig. 144. Figure 145 illustrates the corresponding output of the TRANSF code which would serve as input to the Eulerian method of solution. The TRANSF code, written in FORTRAN-IV language, has been completed and is operational.

The second step was the construction of an Eulerian-coordinate code for following on the time scale the progression of the excursion. A

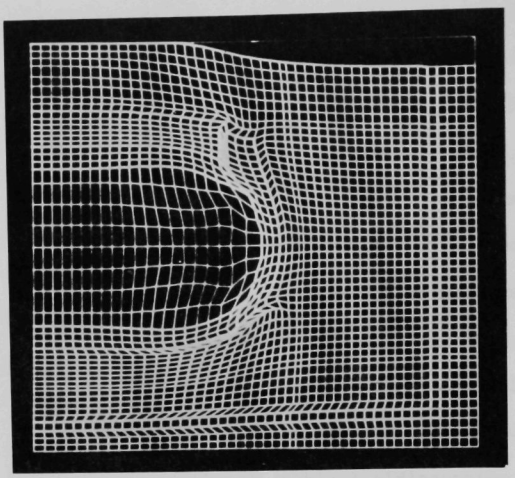

Fig. 144.
Example of Deformed Lagrangian Grid for Containment Study.

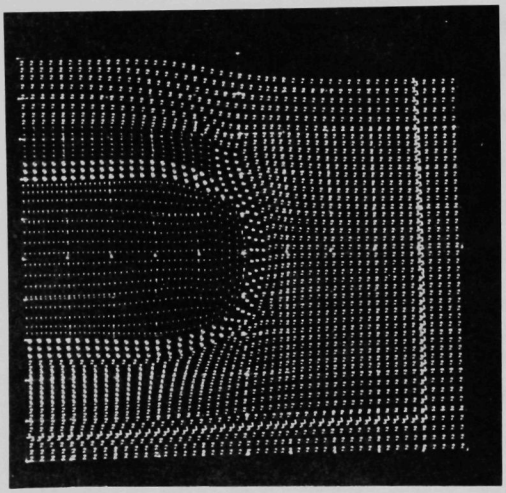

Fig. 145.
Eulerian Particle Distribution Corresponding to Deformed Lagrangian Grid Shown in Fig. 144.

preliminary version of the Eulerian code incorporating the PIC method has been written and is being "debugged." The name REXCO-P has been given to this code to refer to its parent REXCO-H, the code in Lagrangian coordinates. The original PIC computer code could not be obtained, so we wrote our own program, referring mainly to the description and flow diagrams

available.[1] Although certain outlines of the PIC procedure were followed quite conscientiously, others were not. Adaptations of the outlined procedures were also controlled by convenience and previously established methods or specific requirements of the overall containment problem.

The present version of the REXCO-P code incorporates only hydrodynamical properties of materials. Identical equations of state are used as those in the most elementary version of the Lagrangian code. The simplest assumptions possible are made at this first attempt so as to provide best conditions for success. This version of the REXCO-P code will be thoroughly examined before any improvements (and hence, complications) are added to it.

At this time, progress in debugging operations of the Eulerian code can be described by the following characterizations: Symmetry of all calculations with respect to a symmetrical core has been established. Qualitatively, the Eulerian solution with time is a reasonable one, i.e., progression of disturbances and their configurations appear similar to those of the Lagrangian solution.

To test the performance of the Eulerian code, comparison with the existing Lagrangian code has been planned. This will involve quantitative comparisons of an identical problem using both methods. Although progress in this area is well advanced, no meaningful results have been compiled as yet.

Comparison of Codes with Existing Experiments

(J. E. Ash and R. T. Julke)

Safety considerations in the design and development of reactor structures depend on knowledge of the loadings and strains imposed throughout the system by an accidental rapid energy release. In the past, assessment

of the structural integrity of the reactor and containment vessel has been based on data obtained from model experiments. The general approach in these experiments has been to simulate the nuclear-energy release by a chemical explosion and the sodium coolant by water, all contained within a structurally simplified configuration. Such experiments are difficult to perform, the scaling rules are open to question, and the data are limited to a relatively few measurements of wall loadings and gross motions, or simply consist of visual evidence of structural failures. To provide the kind of detailed information necessary to achieve optionally safe designs, it is apparent that experimental data must be supplemented by engineering computations. Such computations can be provided by reliable computer codes capable of numerically predicting the loadings and strains resulting from any feasible excursion. In addition to permitting conveniently the continuous variation of parameters required for optionally safe design, the computation can reveal greater insight into the complex processes involved in the shock propagation, pressure waves, and material velocities throughout a detailed system. However, the question that must be faced in the application of a computer code is its reliability, which can be established only through comparison with available data from simulated model experiments and existing real excursions.

The data that we have collected to date consist mainly of reported results of model experiments performed by the U.K. Atomic Energy Authority over a period of years at the Atomic Weapons Research Establishment. The experiments are sufficiently basic to contribute to an evaluation of the fundamental physical assumptions underlying our computer code, and also, to a limited extent, the data might be useful to check the equations of state employed in the code. The data are measurements of the wall and

roof loadings (on a strong tank partially filled with water) produced by the detonation of a small charge of high explosive. A series of experiments were run for 1/25- and 1/16-scale models of prototype fast-reactor single-tank systems. The models were instrumented with piezoelectric pressure gages and strain-gage load cells and the resulting records are available for comparison with computer-code predictions. Although the models are simplified representations of an actual reactor, they are still complex in the sense that a variety of materials (graphite, lead and bronze shot, and various crushable materials) were employed to simulate the density distribution of the breeder, reflectors, and core support structure. The selection of the correct equation of state for each of these materials will complicate the application of the computer code to the experiment. Further reservations in the verification of the computer code must take into account the lack of cylindrical symmetry in the models and the lack of detailed internal measurements.

Some limited experimental data are available for tests conducted jointly by the U.K. and the French CEA in sodium rather than water. Although the data for the sodium tests appear to be insufficient for a direct comparison with computer-code results, they might be useful in establishing a basis of comparison with water of the effects of the sodium equation of state.

Available U.S. test data appear to be insufficient to establish the validity of code predictions. In the early 1960s, the Ballistic Research Laboratory of the Naval Ordinance Laboratory and Stanford Research Institute were engaged in research to determine the effects of simulated nuclear excursions. The work of BRL was directed chiefly toward determining the response of steel containment models to internal loadings produced explosively. The SRI experiments were aimed at determining vessel response

and concrete-fragment sizes and velocities for loadings produced by explosive mixtures in water. The response of water-filled vessels was examined at BRL to both slow-burning propellant loading and fast explosive detonations. Plug-jump experiments in both water and sodium were performed for 1/30- and 1/15-scale models of the Fermi LMFBR using pentolites scaled for an equivalent excursion energy release of 1000 lb of TNT.

Although no large-scale experimental data are available, analyses and interpretations have been made for the SL-1 accident at Idaho Falls.[3] A model study of that accident was conducted in Britain.[4] Although the British model data are for a greatly reduced scale of 1/30, it might be profitable to compare both the model test results and the prototype SL-1 accident with the computer-code predictions. Such an analysis might prove of value for mutual verification of the code predictions and to assess the reliability of scale-model tests. In the British scale-model test of SL-1, the excursion was simulated by the activation of a metal resistance tape electrically energized by a condenser bank to achieve an improved simulation of the long duration (several millisec) of the power pulse.

A difficulty in the use of a high-explosive charge to simulate the nuclear excursion is the much higher pressure gradient and consequent extremely rapid initial deformations that occur. It is much more difficult for the computer code to follow the model experiment than the actual slower nuclear excursion. Consequently, numerical stability and rezoning requirements impose a much more severe test on the code than is necessary for verification of code applications to actual excursions. It might be found that further experimental data are required to establish reliable code predictions. In particular, special tests might be required to reveal

intermediate and internal features of the processes and to provide more detailed and accurate equations of state, especially for multicomponent-material mixtures. At present, it appears that the primary objective of existing tests has been to determine the end effects of excursions for specific reactor configurations. As such, the model configurations have been too complex and internal measurements are lacking. It also appears that existing tests are predominantly designed to model the mechanical energy explosively released by fuel vaporization. Less than 10% of the total accident energy is released in this highly transient (fraction of millisec) event, and it is conceivable that large volumes of sodium vapor can be built up at a slower rate to produce damaging pressures. Hence, while the code predictions might be verified for the description of the highly transient phenomena simulated by the existing model experiments, there will remain the question of the validity of the code predictions for the slower-excursion phenomena. The slower phenomena might include significant heat transfer, change-of-phase processes, bubble dynamics, and sodium-droplet dispersion and ignition.

The first experimental data to be studied for comparison with the code prediction is the simple case of a bare 2-ounce charge of RDX-TNT 60/40 immersed in water (see Fig. 3 of Ref. 5). The recorded pressure trace at Position 3 was measured in this British experiment with a quartz-crystal pressure transducer (Type M020). The pressure recorded at Gage 3 can be compared (in Fig. 4 of Ref.5) with our code prediction. Successive positions of the decaying pressure wave computed by our code as the wave travels toward the gage are shown. Distortion of the cells at the ends of the cylindrical explosive charge becomes excessive 35 μsec after detonation, diminishing the allowable time interval between numerical iterations to an impractically small value. At this point, a rezoning of the

computational grid is required. The rezoning for this particular study was accomplished by detailed hand computations, which are tedious and time consuming, but have the merit of revealing graphically the influence of grid-size selection, numerical-stability criteria, and the effects of grid distortion. A supplementary rezoning computer code is being completed to facilitate the study of further experiments.

Heat Transfer in Postburst Accident Analysis

(T. J. Marciniak)

If an accident occurs in a fast reactor that does not have specifically defined initiating conditions but in which reactivity was inserted, the accident itself causes all sodium to be boiled out of the core, causing further reactivity addition if a positive void coefficient exists. The excursion then continues until the nuclear portion of the accident is terminated by core disassembly, but very little core material has actually moved outside the original core boundaries. At this point in time, the core boundary is moving at some velocity and the state of the core is such that the pressure and temperature are high and the core has been vaporized.

Continuing from this time, a shock wave propagates toward the reactor vessel and plug that will cause subsequent deformation and, possibly, rupture of the reactor vessel, as well as dislodging the plug. The time elapsed since the termination of the nuclear portion of the accident might be about a few milliseconds, depending on the magnitude of the excursion and the geometry of the system.

That part of the accident occurring after the nuclear excursion has terminated is considered to be the "postburst" phase and is essentially the third phase of the accident--the first being the initiation of the accident, and the second being the core disassembly and nuclear-burst

termination. The postburst phase takes into consideration the effect of the shock waves on the primary containment (reactor vessel) and subsequent pressurization of the system and long-term effect of sodium momentum.

Of prime importance during this phase of the analysis is the determination of the amount of energy available for doing destructive work in the system. The energy release in a nuclear burst that causes vaporization of the core might be about 3500 Mw-sec. If all of this energy were converted to work, the containment necessary would be economically prohibitive. However, in the actual case, not all of this energy would be available. Some fraction, hopefully large, will be absorbed in heating up the sodium, blanket, and internal structure of the reactor and will not be available to do destructive work. The ameliorating effects of the latent heats of vaporization and fusion of the coolant and structure would be helpful in reducing the destructive component.

Analysis of an Accident

(Y. W. Chang)

The analysis of a complete nuclear accident involves the coupled analysis of each individual phase based on a hopefully realistic model of that particular phase. Each of the models is the basis of a code, as in the following sequence.

Phase	Codes
1. Initial stages of accident through core voiding and some melting or slumping.	SAS1A, FORE-II, AIROS
2. High reactivity input rates due to core slumping, leading to a high-energy release and core disassembly.	VENUS, MARS (any code based on some modified Bethe-Tait model)

3. Postburst phase, including shock propagation and energy partition. REXCO-H and REXCO-I

Coupled together, the above codes in their present form can provide a reasonable analysis of a nuclear excursion through the propagation of the shock wave and sodium momentum.

Heat-transfer effects are included in the Phase-I type codes, such as SAS1A, FORE-II, etc., and they might include rather sophisticated models of coolant boiling and ejection. However, the "hydrodynamic" codes, such as VENUS and REXCO-H, do not include heat-transfer effects because the times over which their analysis is valid are very short, and thus this effect can be neglected. However, continuing the analysis for longer times will necessitate including heat-transfer effects into REXCO-H, especially if some estimate of the energy available to do destructive work is to be made.

The Heat-transfer Problem

(T. J. Marciniak)

At the beginning of the time domain in which we are interested, that is, the postburst phase, we know the state of the reactor core and its surroundings. In the case we are presently studying, the core is gaseous UO_2 with a maximum centerline temperature of $\sim 7000°K$. At the corners there is a small region where the fuel is molten. We also know that the core is expanding with a fairly high velocity of the boundary. (A somewhat simpler set of initial conditions have the boundary stationary at time $t = 0$, but the pressure gradient across the boundary will accelerate it.) This velocity is the cause of the shock wave that propagates from the core to the vessel wall. The reflections of this shock wave from the vessel wall and core cause a very complicated pressure-time history during the time they are present and dissipating.

From the above considerations one can delineate two separate heat-transfer problems in a postburst accident. They are: (1) shock-wave dissipation due to heat conduction effects, and (2) heat transfer between the hot core and its relatively cool surroundings.

The first of these effects is rather easily taken care of as an extra term in the energy equation of the hydrodynamic equations in the form[2]

$$dE = -pdv + \frac{k}{\rho}\nabla^2 T dt$$

where in the axisymmetric case

$$\frac{k}{\rho}\nabla^2 T = \frac{k}{\rho}\left(\frac{\partial^2 T}{\partial r^2} + \frac{1}{r}\frac{\partial T}{\partial r} + \frac{\partial^2 T}{\partial z^2}\right) .$$

The conduction term has been programmed for use with the REXCO-H code and is compatible with it. The differencing scheme provides for an explicit solution of the energy transfer due to temperature gradients. The addition of the heat-conduction term will aid in the stability of the differencing scheme, and at the same time will provide a first step in the consideration of the more important heat transfer occurring at the boundary between the gaseous core and the cool surroundings.

The second heat-transfer effect has already been mentioned, i.e., the energy-partition problem, and, more explicitly, the problem of heat transfer at the boundary between the hot gaseous core and the relatively cool surroundings. The problem of heat transfer in this zone is complex and no experimental data exist at this time on the problem of heat transfer between gaseous UO_2 and liquid sodium.

Due to the state of the core (gaseous and high temperature), one would expect rapid heat transfer toward the boundary due to radiation.

At the boundary itself, the problem is complicated by heat and mass transfer as the gaseous UO_2 is condensed to liquid and solidified while, at the same time, sodium is being vaporized and superheated. Mixing and subsequent heat-transfer rates in this area are not known. However, some work has been done on the heat transfer of liquid UO_2 to sodium, although this work is still preliminary and no data involving heat-transfer rates per se have been obtained. Some data involving particle size is known; from this one might be able to obtain some estimate of heat-transfer rates.

Analysis of the Heat-transfer Problem

(T. J. Marciniak)

As far as energy transfer due to conduction is concerned, the problem is well in hand because this term is included in the energy equation of REXCO-H. The main problem now exists at the boundaries between the core and sodium and vaporized sodium and liquid sodium.

Initially, one should be able to assume some sort of temperature-difference-dependent heat-transfer rate across the boundary of the form $\dot{q} = hA\Delta T$, which would be flexible enough to be able to incorporate such data, if and when it becomes available. One could also assume, as a first approximation, that the sodium and fuel will not mix. This last assumption is necessary because the Lagrangian coordinate system currently being used will not permit mixing of materials. The degree of error in this assumption is not known.

Once one has an estimate of the energy transfer across the boundary, he then can go back to the equation of state of the materials involved and calculate a new pressure gradient for the next time-step calculation. The vaporization and superheating of the coolant will cause large pressures to be developed and will provide the driving force for the sodium-

momentum stage of the accident. By taking into account the heat transfer more realistic evaluations of the amount of energy available for doing work might be made (as compared to the conservative Hicks-Menzies approach[6]).

References

1. A. A. Amsden, *The Particle-in-Cell Method for the Calculation of the Dynamics of Compressible Fluids*, LA-3466 (Feb 1966).

2. Y. W. Chang, J. Gvildys, and S. H. Fistedis, *Two-Dimensional Hydrodynamic Analysis for Primary Containment*, ANL-7498 (Nov 1969).

3. A. Smaardyk, *Hazard Summary Report on the Argonne Low Power Reactor (ALPR)*, ANL-5744 (Oct 1957).

4. G. R. Warren and T. W. Rice, *An Assessment of Reactor Safety Modeling Techniques Based on the Accident to the SL-1 Boiling Water Reactor* Nucl. Struct. Eng. (2), 490-493 (Nov-Dec 1965).

5. N. J. Rees (UKAEA), *A Model Investigation of Explosive Containment in Single Tank Fast Reactors*, in ANL-7120, 692-719 (Oct 1965).

6. E. P. Hicks and D. C. Menzies, *Theoretical Studies on the Fast Reactor Maximum Accident*, ANL-7120, 654-670 (Oct 1965).

Nuclear Safety Research and Development--

Effluent Control--Environmental Studies

XVI. THERMAL-PLUME DISPERSION STUDIES*

(B. M. Hoglund)

Scope. Three basic activities aim toward the goal of ensuring that effective methodologies are available to predict the plume temperature patterns at a power-plant outfall with accuracy suitable for interpreting local influences on the aquatic biota: (1) publication and updating of state-of-the-art reports on analytical modeling of thermal plumes, physical scale modeling of thermal plumes, and field studies of thermal discharges at actual power plant sites on the Great Lakes, (2) development of analytical techniques for predicting the dispersion characteristics of a thermal plume in a large lake and critical evaluation of existing prediction methods, and (3) design and analysis of field experiments to measure temperature and lake-current patterns in the vicinity of power-plant outfalls.

Numerical Modeling

(S. M. Prastein, T. H. Hughes, and A. Szewczyk)

The approach was to search for a general methodology that would be an improvement over the existing semiempirical methods. This approach necessitated finding the solution of the fundamental three-dimensional conservation equations. Because three-dimensional numerical calculations with realistic boundary and initial conditions would require extensive development, it was decided to experiment with the numerical techniques on a two-dimensional x-y model that could be compared with scale-model studies and available field data.

---

*For references for this chapter, see p. 436.

The x-y problem treated the flow of a two-dimensional jet in a crossflow current. The basic nondimensional equations in the vorticity-stream-function formulation are:

$$\frac{\partial\omega}{\partial t} + \frac{\partial}{\partial x}(u\omega) + \frac{\partial}{\partial y}(v\omega) = \frac{1}{R_e}\left\{\frac{\partial^2\omega}{\partial x^2} + \frac{\partial^2\omega}{\partial y^2}\right\},$$

$$\frac{\partial^2\psi}{\partial x^2} + \frac{\partial^2\psi}{\partial y^2} = -\omega \quad , \; u = \frac{\partial\psi}{\partial y} \quad , \; v = \frac{\partial\psi}{\partial z}$$

and

$$\frac{\partial\theta}{\partial t} + \frac{\partial}{\partial x}(u\theta) + \frac{\partial}{\partial y}(v\theta) = \frac{1}{R_e P_R}\left\{\frac{\partial^2\theta}{\partial x^2} + \frac{\partial^2\theta}{\partial y^2}\right\}$$

where R_e is the Reynolds number and P_R is the Prandtl number, the viscosity and diffusion coefficients appearing in these nondimensional numbers have been assumed to be constant, θ is the excess temperature above ambient, and the remainder of the symbols have the usual meanings.

The finite-difference solution integrated these unsteady equations from an approximate initial solution to an asymptotic steady-state solution. In all cases, the initial solutions assumed the vorticity to be zero, with ψ and θ being solutions to Laplace's equation with suitable boundary conditions. To obtain results quickly, an explicit finite-difference method using a variable space step was chosen. The nonlinear terms were approximated by directional differences and the diffusion-term approximation was the usual centered difference. This method was conditionally stable with a rather severe restriction on the time step.

The programming for the first problem (a symmetric two-dimensional jet without cross-flow) was completed and steady-state solutions were obtained. The problem used a laminar viscosity and was intended to be

used for comparing numerical results with well-established theory and laboratory experiments. It quickly was found that a strongly graded variable mesh size would be needed, so this was incorporated into the program. Subroutines that produce film displays of streamlines, constant-temperature contours, and velocity profiles were written and debugged. The program for a jet with crossflow was completed but testing has not been finished. Considerable experimentation concerning the proper boundary conditions at the jet inflow have been carried out; it has been found that specifying $v - 0$ and the value of ψ at the jet wall boundaries is satisfactory. This permits a definite jet core to persist out from the outfall.

The calculation of the initial solution was satisfactory and some experimentation was carried out in an attempt to choose an initial solution closer to the final steady-state solution. The calculation of the stream function, vorticity, and velocities appeared to give reasonable answers, but difficulty was experienced in solving the temperature equation. This difficulty was solved by a modification of the differencing method used for the nonlinear terms. This is not well understood and needs further study.

As stated before, a simple explicit method was used to solve the vorticity and temperature transport equations. The stability condition on this method has resulted in excessively long calculation times, so it is deemed necessary to try an unconditionally stable implicit method or to solve the steady-state equations directly, to improve the computational speed greatly.

It is felt that the two-dimensional numerical approach can be developed to yield useful results. However, it is imperative that good field data and laboratory experiments be available to guide the selection

of problems to be studied and to validate the results. Work in this area has been temporarily curtailed until such data are available.

Three-dimensional calculations, using the full Navier-Stokes equations, appear not to be feasible to provide practical results at this time. If one has the computing power of Los Alamos or Livermore, then it is possible, at this time, to solve idealized three-dimensional unsteady problems in cubes or other regular regions with simple boundary conditions (e.g., frictionless lids). The possibility of solving three-dimensional plume problems with irregular boundaries, inflow and outflow boundaries, turbulence, density stratification, etc., within the next few years is remote.

State-of-the-Art Reports

(J. V. Tokar and D. Miller)

Physical scale modeling. The state-of-the-art report on physical scale modeling of thermal-plume dispersion, developed for ANL at the St. Anthony Falls Hydraulic Laboratory, has been completed.[1] The report discusses principles of thermal-plume modeling, fundamental laboratory studies, case studies of hydraulic models (a comparison of field data and data from the scale models) and concludes with a discussion of the status of hydraulic modeling of thermal plumes. Highlights of the conclusions are abstracted here.

To completely model a given plume, it is ideally necessary to model three regions--the near field, the joining region, and the far field. These may be differentiated by the physical phenomena that they do not hold in common. In the near field (close to the outlet), entrainment of ambient fluid is very important. In the joining region, entrainment is still important, but buoyancy, surface cooling, and convection are also important.

In the far field, surface cooling, dispersion, and convection are most significant.

In most situations, these regions cannot all be combined in one physical model because the vertical scale of the model needs to be large enough to allow room for differentiating stratified layers to prevent surface tension forces from controlling the dynamics of flow, and to assure turbulent Reynolds numbers. Then, if the horizontal scale were the same as the vertical scale, the model surface area would be so large as to make the model unwieldy and would prevent placing it under a roof where the environment could be controlled. When parts of a plume are modeled separately, it is very important to place the proper boundary conditions on the separate models. Unfortunately, this is not always easy from a practical point of view. Table XXVIII summarizes some of the modeling problems.

A review of the case studies and a summary of the general utility of hydraulic models indicates that hydraulic modeling of thermal plumes is not merely an application of a set of scale ratios, but requires judgment as to the phenomena to be modeled. Comparisons between model and prototype are most likely to be qualitatively than quantitatively correct at the present state-of-the-art. The basic physical phenomena associated with thermal plumes are not apparently understood, but not enough well-controlled model studies have been conducted to make possible the tabulation of numerical coefficients for use in the applicable equations and the extension of the coefficients to full-scale problems.

To improve this situation: (1) more comparisons between field data and model-study results need to be made (such comparisons should be given high priority) and (2) a program of fundamental studies needs to be carried out to determine the importance and influence of each of the dimensionless numbers on the flow pattern in each region of the plume.

TABLE XXVIII. Hydraulic Modeling of Thermal Plumes

Model	Most important physical phenomena	Important parameters*	Remarks
Near field (outlet region)	Entrainment	Geometry; densimetric Froude no.; local Richardson nos.; boundary conditions at end of model.	Can be modeled with any two miscible fluids of different density. Undistorted scale required.
Joining region	Entrainment, buoyancy, surface cooling, convection	Boundary conditions at upstream and downstream ends of model; rate of surface cooling; local Richardson nos.; preexisting stratification; preexisting currents; wind.	May be combined with near-field model to eliminate problem of upstream boundary condition; this complicates the near-field model.
Far field	Surface cooling, convection, dispersion	Boundary conditions at upstream and downstream ends of model; rate of surface cooling; densimetric Froude no.; preexisting currents; wind.	Distorted model usually required. Latter part of joining region may be placed in far-field model, but, combination with near field is impracticable.

*It is assumed that suitably large Reynolds numbers are obtained in each case.

Experimental field work. A survey of the utilities bordering the Great Lakes revealed that very little information is now available with respect to plume temperature data to support or verify existing predictive correlations. One of the serious problems plaguing the plume field work is the lack of permanently and strategically placed continuous recording instrumentation to provide adequate current and temperature data. The usual procedure of obtaining measurements from a boat traversing the plume for a period of several hours can lead to considerable error if the plume is not steady. The Waukegan, Illinois, plume, for instance, was observed to fluctuate considerably during a 1-hr period.

Most of the field work is accomplished in several favorable days, usually at the planned convenience of the investigators. There appears to be no systematic effort on the Great Lakes to choose "representative data days." Also, very few coordinated efforts have been undertaken on the Great Lakes to coordinate infrared measurement overflights with three-dimensional measurements of water temperature, currents, and meteorology.

A list of power plants (fossil and nuclear) sited along the shores of the Great Lakes has been compiled.[2] Work is continuing on the compilation of information on those power plants that are planning, are doing, or have completed thermal-plume transport studies, be they analytical, laboratory scale model, or field studies.

Analytical modeling. The ultimate objective in thermal-plume modeling is to obtain spatial and temporal temperature and velocity distributions within the affected receiving water that can be used to make biological and ecological predictions. The bodies of water receiving the discharge can be categorized by their unique characteristics, i.e., lakes, rivers, estuaries, etc. Each of these receiving environments presents special design requirements and simplifications.

The classical analytical approach to such problems involves solving the basic equations of continuity, momentum, and energy with the appropriate boundary conditions and transport coefficients. Mass, momentum, and heat transport within any large body of water can be assumed to be governed by turbulent mechanisms, so the needed transport coefficients are not simple properties of the water alone, as they would be in laminar flows, but depend on the geometrical and environmental characteristics of the flow.

The functional relationship of the transport coefficients to these geometrical and environmental characteristics is complex and not yet well defined. To provide solutions to turbulent problems, recourse is generally made to "turbulent equations of state"[3] that relate the turbulent coefficients to local or global mean flow properties. Analytical solution of complex turbulent flows by necessity becomes a "trial and error" process in which simplifications are made to the governing equations, boundary conditions, and transport coefficients in order to obtain solutions.

Observations of plume behavior show it to meander, with parts of the plume occasionally detaching and dissipating by themselves. Over a significant portion of the plume, a sharp lateral boundary exists, particularly at the upstream edge in the presence of a current. The meandering implies a need for stochastic analytic models such as that of Gifford[4] or that a deterministic model be a suitably averaged presentation. One hypothesis that allows for a sharp boundary in the presence of entrainment and mixing is that of a gravity-driver "head" flow;[5] other models assuming "Gaussian like" temperature distributions cannot account for these phenomena although they have given satisfactory predictions of long time changes.

It is sufficient to state that the available models are by necessity heavily semiempirical in nature, relying on assumed similarity conditions,

such as Gaussian or other distributions (of momentum, mass, and heat), spread coefficients, entrainment coefficients, on eddy diffusivities of heat, mass, and momentum.

There does not appear to be a suitable analytical model of the jet regime that will provide *a priori* predictions of "typical" Great Lakes outfall designs. The jet regime is of interest because it is the highest-temperature portion of the plume. Many of the available analytical models for the far field region were developed for rivers or estuaries, with their unidirectional or strongly periodic currents. Application of these models to a lake is questionable. No models are available that consider the wind effects on the plumes in the far-field region. Simple analytical far-field models, such as the Edinger and Polk model,[6] in the absence of *a priori* information about the ambient current and ambient diffusivity, have little predictive value.

Further development of the numerical modeling of thermal plumes should be considered when data suitable for checking the models become available. Numerical techniques have the potential capacity to account for nonlinear features and complex boundary conditions that often have to be ignored for purely analytical approaches.[7] Recent advances in the theory of turbulence and computation of effects[8] encourage application to modeling of plumes.

Mass-and Energy-Balance of the Great Lakes

(J. V. Asbury)

Lake-wide physical effects of thermal discharges on Lake Michigan, particularly as these effects relate to the mass/energy balance, have been investigated and reported.[9] This study was specifically concerned with the heat-assimilative capacity of Lake Michigan relative to present and

projected man-made thermal loads. The methods developed for the Lake Michigan study were also used to estimate the heat-assimilative capacities of the other Great Lakes.

It was concluded that the lake-wide effects of man-made thermal discharges into Lake Michigan are presently negligible and will continue to be so for the rest of this century. Man-made thermal discharges can be compared with the Lake Michigan energy budget. A one-gigawatt advective input, averaged over the lake, is equivalent to 0.13 Btu/ft^2-day; the naturally occurring average rate of increase of lake heat content during the March-August warming season is 1100 Btu/ft^2-day.

The average annual increase in water surface temperature for the whole lake has been determined to be 1.4 $\pm$ 0.4 x 10^{-3}°F/gigawatt of thermal discharge; the associated annual average increase in evaporative water loss if 9 $\pm$ 2 ft^3/sec-gigawatt of thermal discharge. The existing and projected effects of power-plant thermal inputs on the mass-and-energy balance of the five Great Lakes are summarized in Table XXIX.

TABLE XXIX. Effects of Utility Discharges on the Great Lakes--Present and Projected

Lake	Year	Utility Discharges, Gw	$\bar{q}$, Btu(ft^2-day)	$\overline{\Delta T_s}$, °F	Q_e, ft^3/sec
Superior	1970	0.72	0.066	0.0008	6
	2000	4.8	0.44	0.0053	34
Michigan	1970	7.0	0.91	0.0098	63
	2000	90.	12.	0.126	810
Huron	1970	1.25	0.16	0.0017	11
	2000	54.	6.8	0.076	460
Erie	1970	7.0	2.1	0.022	63
	2000	95.	29.	0.29	850
Ontario	1970	5.2	2.0	0.022	44
	2000	70.	27.	0.29	600
Whole Basin	1970				187
	2000				2750

References

1. E. Silberman and H. Stefan, *Physical (Hydraulic) Modeling of Heat Dispersion in Large Lakes*, ANL/ES-2 (Aug 1970).

2. J. V. Tokar, *Thermal Plumes in Lakes: Compilations of Field Experience*, ANL/ES-3 (in press).

3. W. C. Reynolds, "A Morphology of the Prediction Methods," *Proc. Conf. Computation of Turbulent Boundary Layers - 1968 AFOSR-IFP-Stanford Vol. I Methods, Predictions, Evaluation and Flow Structure*, S. J. Kline et al., eds., pp. 1-15, Stanford, Calif., Thermoscience Div., Stanford Univ. (1969).

4. F. Gifford, Jr., "Statistical Properties of a Fluctuating Plume Dispersion Model," *Advances in Geophysics, Vol. 6, Atmospheric Diffusion and Air Pollution* (F. N. Frenkiel and P. A. Sheppard, Eds.) Academic Press, New York, 117-137 (1959).

5. M. P. Tulin and J. Schwartz, *Hydrodynamic Aspects of Waste Discharge*, AIAA 3rd Fluid and Plasma Dynamics Conf., Los Angeles, Calif., June 29-July 1, 1970, AIAA Paper 70-755 (1970).

6. J. E. Edinger and E. M. Polk, Jr., *Initial Mixing of Thermal Discharges into a Uniform Current*, Report No. 1, Dept. of Environmental and Water Resources Engineering, Vanderbilt University (1959).

7. A. A. Amsden and F. H. Harlow, *The SMAC Method: A Numerical Technique for Calculating Incompressible Fluid Flows*, LA-4370 (Feb 1970).

8. P. I. Nakayama, *Turbulence Transport Equations and Their Numerical Solution*, AIAA 8th Aerospace Sciences Meeting, New York, N. Y., Jan 19-21, 1970, AIAA Paper No. 70-3 (1970).

9. J. G. Asbury, *Effects of Thermal Discharges on the Mass Energy Balance of Lake Michigan*, ANL/ES-1 (Dec 18, 1970).

Component Development--LMFBR--Instrument and Control

XVII. PLANT DYNAMICS AND CONTROL ANALYSIS*

(W. C. Lipinski and L. J. Habegger)

Scope. The control systems that are proposed for the LMFBR plant designs in conjunction with the 1000-MWe LMFBR plant design studies are being studied. The proposed control systems will be analyzed to assess adequacy to meet the overall control and performance goals of the large LMFBRs. In particular, the program will: (a) identify current and potential LMFBR control problems, (b) identify systems where further control system optimization would improve the economic and operational aspects of the LMFBRs, and (c) identify development required in the area of LMFBR reactor and plant control.

Summary. The 1000-MWe LMFBR designs were reviewed and the work scopes of the follow-on dynamics simulation studies were formulated. Information on individual-component dynamics was compiled and a simplified plant model was simulated on a hybrid computer.

Review and Monitoring of 1000-MWe LMFBR Follow-on Studies

Review of the 1000-MWe LMFBR follow-on contracts and work scopes was completed, as was examination of the proposed schedule so as to ensure coordination that will meet the needs of the LMFBR program.

Compilation of Information on Component Dynamics

A compilation was made of information on the dynamic behavior of plant components and of information on instrumentation performance and component dynamics generated by the various test programs. Evaluation of the adequacy of the analytical models (by use of test data) was initiated.

Development and Simulation of Complete-plant Model

A simplified complete-plant model for a 1000-MWe LMFBR was developed and is being programmed on the existing ANL hybrid computer. The program

*For references for this chapter, see p. 442.

will be used in simulation of mild LMFBR transients that would be grouped as resulting from normal or upset conditions according to ASME classifications, with provision for future extension to more severe transients resulting from emergency or faulted conditions. General descriptions of the major plant-component models being simulated are given below.

Reactor. For the mild transients to be considered, the single-node or point-model description of neutron kinetics with six delayed-neutron groups is adequate. The dynamics of the coolant and fuel temperature in the core are assumed to be represented adequately by a single-channel model using two axial nodes. Average temperatures in the radial direction in the channel are used, and changes in cladding and structural-material energy storage are ignored. The dynamics of the temperature of the coolant that passes through the reflector, blanket, and bypass channels are modeled by an additional representative channel with a single axial node. Feedback reactivity of the core is a linear function of the temperatures in each axial node. Single-node models are also used in describing mixing and transport lags in both the inlet and outlet plenums.

Intermediate heat exchanger (IHX). The dynamics of the secondary and primary sodium temperatures in the IHX are also based on the dynamics of a single representative channel. Two nodes in the channel will be used, and the changes in the structural heat storage are not to be included.

Reheater. The model of the component for reheating the steam before it enters the intermediate- and low-pressure turbines is similar to that of the IHX.

Steam generator. A once-through steam generator, which includes the vaporizer and superheater in a single unit, has been selected as the steam source for the turbines. Simulation of this component will comprise a major effort, since it is potentially the most sensitive to instabilities

and is difficult to model. The difficulty is due to the change of phase in the tube side and the change of heat-transfer coefficients that correspond to the transition to different flow regimes. Recent publications have demonstrated the advantages of using continuous-space-discrete-time (CSDT) simulations for counterflow heat exchangers.[1-3] However, this approach complicates the total-plant simulation, because a discrete-space-continuous-time (DSCT) approach is used in simulation of the remaining plant components. A compromise approach that appears to have merit is to use a DSCT simulation with parameters based on spatial temperature profiles computed using the continuous-space model. The parameters in the continuous-time simulation would be updated at appropriate intervals based on new computations of spatial temperature profiles. The quasi-linearization procedure for solving nonlinear multipoint boundary-value problems may be of use in obtaining the spatial temperature profiles.[4-5]

A simplified model of the steam generator was developed for use in an overall-plant simulation prior to completion of an advanced model that includes all salient features. The model selected is based on regions, which correspond to regions with major differences in heat-transfer coefficients between the tube wall and secondary fluid (H_2O), are the one-phase water region, boiling region with 0-25% quality, boiling region with 25-100% quality, and superheat steam region.

Coolant pipelines. Included in the simplified plant model are pure time delays for the coolant temperatures introduced by transport lags through the piping connecting the major plant components. These time delays are simulated digitally on the hybrid computer. For the variable flow velocities to be used in the simulation, the time delay becomes a variable that depends on the flow velocity history.

Turbine, generator, condenser, and feedwater heaters. These components will not be modeled in detail in the initial plant simulation, but will be included in the advanced plant simulation to provide a complete closed loop.

Control systems. The overall plant simulation will include the following control actuators: a control rod for reactor power control, a primary pump for reactor-coolant flow control, an intermediate pump for control of intermediate coolant flow, a feedwater pump, feedwater pump turbine, and control valves for control of feedwater flow, an intermediate-coolant bypass valve to control intermediate-coolant flow to the steam generator, a reheater control valve to control intermediate-coolant flow to the reheater, and a main steam-throttle valve and steam-bypass valve to control steam flow from the steam generator to the high-pressure turbine. Various modes of operation for the above systems and their associated controllers will be considered to determine overall control-system performance and to identify and resolve problems.

Multiple loops. The advanced simulation will include two IHX and steam-generation loops to determine their interaction during transients. A single loop is used in the initial simulation.

Future Program

The 1000-MWe LMFBR follow-on studies will continue to be monitored for changes and new information. Models and simulation information on plant components will continue to be compiled. The model of the plant that has been simulated on a hybrid computer will be used to analyze the overall control-system performance, and control problems will be identified and resolved. An improved model simulation for an entire LMFBR will be started.

Turbine, generator, condenser, and feedwater heaters. These components will not be included in the initial plant simulation, but will be included in the advanced plant simulation to provide a complete closed loop.

Control systems. The overall plant simulation will include the following control actuators: a control rod for reactor power control, a primary pump for reactor-coolant flow control, an intermediate pump for control of intermediate coolant flow, a feedwater pump, feedwater pump turbine, and control valves for control of feedwater flow, an intermediate-coolant bypass valve to control intermediate-coolant flow to the steam generator, a reheater control valve to control intermediate-coolant flow to the reheater, and a main steam-throttle valve and steam-bypass valve to control steam flow from the steam generator to the high-pressure turbine. Various modes of operation for the above systems and their associated controllers will be considered to determine overall control-system performance and to identify and resolve problems.

Multiple loops. The advanced simulation will include two IHX and steam-generation loops to determine their interaction during transients. A single loop is used in the initial simulation.

Future Program

The 1000-MWe LMFBR follow-on studies will continue to be monitored for changes and new information. Models and simulation information on plant components will continue to be compiled. The model of the plant that has been simulated on a hybrid computer will be used to analyze the overall control-system performance, and control problems will be identified and resolved. An improved model simulation for an entire LMFBR will be started.

References

1. J. F. L. M. Brukx and J. H. Tessier, "Serial Solution of Nonlinear Partial Differential Equations of a Counterflow Heat Exchanger Using S/360-CSMP," *Proc. 1970 Summer Computer Simulation Council*, pp. 360-371 (Jun 1970).

2. L. N. Carling, *Hybrid Computer Solution of Heat Exchanger Partial Differential Equations*, Annales de l'Association international pour le Calcul Analogique *1*(6) 6-18 (Jan 1968).

3. C. Chamboredon, M. Hery, and B. Marion, *Study of the Control of a Fast-Reactor Nuclear Power Plant on a Hybrid Computer*, ANL-TRANS-771. Translated from Proc. 5th Inter. Analogue Computation Meetings, pp. 1065-1970 (1967).

4. R. Bellman and R. Kalaba, *Quasilinearization and Nonlinear Boundary-Value Problems*, American Elsevier Publ. Co., Inc., N. Y. (1965).

5. L. Habegger and C. Hsu, *The Use of Quasilinearization for the Solution of Nonlinear Space-Dependent Reactor Equations*, Trans. Amer. Nucl. Soc. *12*(2) 830-831 (Nov 1969).

Systems and Plant Development--LMFBR--Plant and Design

XVIII. 1000-MWe PLANT STUDY CONTRACT MANAGEMENT, TECHNICAL REVIEW, AND EVALUATION*

(L. W. Fromm)

Overall scope. The 1000-MWe LMFBR Follow-on Studies, performed in FY1967 through 1969, were a group of parallel in-depth investigations by industrial subcontractors. In those investigations the subcontractors prepared company-favored conceptual designs of LMFBR power plants that they expected to be commercially competitive in the 1980s. Trade-off and parametric studies were performed to make design selections, and research and development programs to provide information vital to the successful detailed design, construction, and operation of the plants were delineated. The definition of research and development programs was the principal objective of these studies.

The studies were carried out under the management of Argonne National Laboratory. In this work, Argonne: (1) prepared scopes of work and ground rules so the studies would produce information needed to achieve program goals, (2) ensured that all subcontractor studies were performed in accord with the work scopes, ground rules, schedules, and contract funding, (3) assisted the subcontractors in obtaining the latest related information being developed elsewhere, (4) ensured that the studies were realistic, that appropriate methods of analysis were used, that decisions were based on adequate depth of study, and that no study was distorted by unjustified assumptions, (5) provided AEC with evaluations of study results, and (6) recommended further profitable study areas.

Argonne technical specialists met with each subcontractor periodically, reviewed his technical notes and informal monthly and quarterly

*For references for this chapter, see p. 460.

reports, and furnished reviews and guidance. As formal phase and topical reports were received, the specialists evaluated them and reported the results to AEC. Fiscal and schedule control was maintained by reviewing subcontractors' monthly and quarterly administrative reports.

Since the Follow-on Studies by the subcontractors were completed at the end of FY1969, Argonne's activities under this account in FY1970 were limited to (1) preparation and negotiation of scopes of work for further definitive studies to be performed by the subcontractors based upon their Follow-on study plant designs, and (2) technical evaluation of subcontractors' final reports on their Follow-on Studies.

This account describes the Argonne activities in all technical areas except nuclear safety (activities in that area are described on pp. 388-394).

Management and Technical Review of Subcontractor's Studies

(L. W. Fromm)

Scope. Management and technical review of subcontractors' studies during FY1970 encompassed all activities connected with the initial establishment of new study programs by the subcontractors, including preparation of work scopes and negotiation of scopes with subcontractors and AEC to ensure compatibility with AEC objectives and available funding.

Summary. Negotiations on subcontracts and scopes of work for various studies supplementing the earlier 1000-MWe Follow-on Studies were pursued with General Electric, Westinghouse, and Atomics International. With issuance of the AEC Program Assumptions for FY1971, some of this work was terminated, and the remainder was transferred to

the contract management and technical review of plant safety analysis studies (p. 388).

Preparation and negotiation of technical scopes of work with subcontractors. Subcontract negotiations were continued with General Electric for its combined pool-type primary system, plant safety analysis, and dynamics analysis and control study program, but were deferred for most of the year pending direct negotiations of patent and background information provisions between GE and AEC. Negotiation of a scope of work for a similar study program by Westinghouse Electric Corp., based on a loop-type primary system, was concluded, and subcontract negotiations were begun upon receipt of AEC authorization. A work scope for a refueling-system study was prepared and agreed to by Atomics International, and preliminary work was done on a scope for a plant-maintainability study. With the issuance of the AEC Program Assumptions for FY1971, it became apparent that the refueling-system and plant-maintainability studies would not be funded in FY1970, and work in connection with initiating these studies was dropped.

Future program. The Program Assumptions also indicated that the GE and Westinghouse studies would be funded in FY1971 and beyond under the Nuclear Safety Program. Therefore, activities under this program were transferred to the contract management and technical review of plant safety analysis studies (p. 388).

Technical Evaluation of Subcontractors' Formal Study Reports

(L. W. Fromm and K. A. Hub)

Scope. The subcontractors' 1000-MWe Follow-on Studies were divided into four phases, each of which represented a segment of the work program that logically could be reported as a technical unit. At the conclusion of each phase, the subcontractor submitted a formal task

report suitable for publication. In some cases, the task reports were augmented by formal topical reports covering particular technical areas. Argonne technical specialists comprehensively evaluated all subcontractors' task and topical reports. The comments and opinions comprising these evaluations were based on judgment and experience, supported as necessary by check calculations. Evaluations performed during the course of each study were reported to AEC informally as they were completed. At the conclusion of all subcontractors' studies, a final evaluation report was compiled.

Summary. Evaluations of the Task-II, -III, and -IV reports by the 1000-MWe LMFBR Follow-on Study subcontractors were completed, and a four-volume draft final evaluation report was issued to AEC and to the LMFBR Program Office. The draft summary volume was also issued to the subcontractors for their comments. The results of an ANL Plant Temperature Study were included in this evaluation report.

Evaluations of 1000-MWe LMFBR Follow-on Studies. [These evaluations, in all aspects except safety, were conducted in this program. The safety aspects were evaluated in the program 1000-MWe Safety Study Contract Management, Technical Review, and Evaluation (p. 388). However, for convenience, this section covers all aspects, including safety.]

Evaluations of the 1000-MWe Follow-on Study Task-II, -III, and -IV reports by Atomics International, Babcock & Wilcox, Combustion Engineering, General Electric, and Westinghouse were completed. The ANL Plant Temperature Study conducted as part of this evaluation work was concluded with the completion of independent analyses and overall screening and integration of the Follow-on Study data with other current information to arrive at best-judgment temperature-range recommendations.

The results of the evaluations and the temperature study were compiled in an ANL final evaluation report in four volumes: Volume I, a summary report providing a brief history, general results, and evaluations summary of the subcontractors' work; Volume II, a plant design report containing the plant descriptions and evaluations of the plants, trade-off studies, parametric studies, safety, and economics; Volume III, a report on the R&D programs proposed by the subcontractors; and Volume IV, a compilation of backup and contractual material, including tables of capital-cost estimates for each subcontractor, an evaluation of the capital-cost estimates by an independent architect-engineer consultant, descriptions of the subcontractors' reports, and summaries of work scopes, guidelines, etc. The draft reports were transmitted to AEC and the LMFBR Program Office for review. The draft summary volume (Volume I) of the evaluation report was also issued to the subcontractors for their comment.

The primary objective of the 1000-MWe LMFBR Follow-on Studies was the delineation by the subcontractors of the research and development programs they believed would be necessary in bringing large commercial LMFBR power plants to competitive fruition in the 1980s. Therefore, the evaluations of the subcontractors' final Follow-on Study reports were originally prepared by Argonne with a view toward providing the maximum amount of information, opinions, and comments on the studies to the organizations having the responsibility for planning and directing the national LMFBR research and development program, i.e., the AEC and the LMFBR Program Office. Thus, it was recognized that the evaluation reports would require a major revision to make them suitable for public release. It had been planned earlier to effect this revision after receipt of comments on the draft reports from AEC and the

subcontractors. However, it was decided to terminate further revision efforts and not to publish the evaluations--because the principal beneficiaries of the studies and evaluations, in respect to their primary objective of research-and-development program delineation, had already received the evaluation information, because all information developed by the subcontractors had already been published (see References, p. 460), and because of the press of higher-priority work demanding the attention of the staff that had been involved in the evaluations.

During the Follow-on Study, a very large amount of information was generated and documented. The following description provides broad observations on design trends, results, conclusions, and recommendations in the categories of Plant Design and Safety, Plant Temperature Study, Engineering Analysis, Economics, R&D, and Overall, as gleaned in the ANL evaluation.

Plant design and safety. The secondary objectives of the Follow-on Study, which were associated with plant design, were well met. Briefly, these were: to encourage originality, to better understand safety problems, to supply industry with LMFBR-system functional requirements, and to provide the AEC with plant information for the LMFBR Program Plan. Many different approaches were used in these studies, and their diversity should provide useful alternatives for industry and the AEC to weigh and compare.

By way of introduction, a brief review of the significant variations in the contractors' plants is worthwhile. Each contractor was responsible for design selection of the entire plant, except Combustion Engineering, whose scope of work was limited to the heat-generation portion of the nuclear steam-supply system.

For their reference primary-system configurations, Combustion Engineering, Atomics International, and Westinghouse use the loop-type system design. Babcock & Wilcox and General Electric use the pool-type system design.

Conventional containment structures are used by all contractors except General Electric. GE states that adequate safeguards could be incorporated in the design to ensure against any major accident. Based on this premise, the GE design has a confinement-type structure enclosing the reactor complex.

All contractors use reheat in their steam-cycle design, except Westinghouse, which uses a nonreheat cycle, based on the results of the Westinghouse trade-off study of reheat vs. nonreheat.

The Westinghouse design has a four-module core; all other contractors' designs have a single cylindrical core. For the fuel, Westinghouse and Combustion Engineering use carbides, and the other contractors use oxides. A hexagonal fuel-subassembly design is used by AI, B&W, and GE; CE uses a circular design, and W uses a square design.

The contractors' approaches varied in specifying design requirements relating to safety. ANL did not attempt to quantify safety items; for example, neither fuel-element damage, nor even damage thresholds, were calculated. During the course of the Follow-on work, safety criteria for LMFBRs were proposed, weaknesses in models and analysis became more extensively known, and the economic impact of safety restraints under certain assumptions was shown.

The design of the core and blanket for the LMFBR plant has some notable trends. The core heights are generally taller than in previous designs because compromises in core geometry might not materially

improve safety characteristics and/or because of greater reliance on instrumentation to avoid or minimize accidents. The fuel-element diameters for two of the three mixed-oxide-fueled reactors are significantly larger than the 0.250-in. diameter at which most mixed-oxide irradiation data are currently being obtained. All five reactors have been designed for vented-to-coolant fuel elements, although only four reactors will have vented-to-coolant fuel elements in the initial core loading. Optimum reactor outlet temperature depends partially on the assumed relationship between cladding temperature and fuel life. Although different fuel models were used to estimate thermal and mechanical performance for the four reactors with orificed cores, the range of outlet sodium temperatures was only 1098 to 1150°F.

Table XXX summarizes the main plant parameters for each of the contractors' designs.

Plant temperature study. Based on the results of the contractors' work and on ANL's independent investigations, ANL made a plant temperature study. The main objectives of this study were to determine the sodium outlet-temperature range for a nominal commercial plant and to recommend possible changes in the temperature ranges that currently form the bounds of the overall LMFBR program.

The guiding criterion for temperature selection is the cost of electrical energy, which defines the competitiveness of the LMFBR with other energy systems. This ability to compete is largely unknown; however, a reasonable assumption is that competition with other energy systems will be intense.

For the reactors using oxide fuel in the core, ANL studied the electrical-energy cost sensitivity vs. reactor outlet temperature. Figure

TABLE XXX. Summary of Plant Characteristics Reported

	Atomics International	Babcock & Wilcox	Combustion Engineering	General Electric	Westinghouse
OVERALL PLANT					
Reactor thermal power, MWt	2400	2450	2465	2416	2600
Gross electrical power, MWe	1040	1034	----	1038	1074
Net electrical power, MWe	1002	1009	1000	1008	1044
Plant efficiency, %	41.7	41.2	40.6	41.7	40.2
Net heat rate, Btu/kWh	8175	8281	----	8192	8500
Reactor outlet temperature, °F	1140	1100	1095	1150	1000
Reactor inlet temperature, °F	780	800	797	810	770
Primary-loop ΔT, °F	360	300	298	340	230
Secondary-Na hot-leg temperature, °F	1070	1000	----	1071	967
Secondary-Na cold-leg temperature, °F	670	700	----	646	658
Secondary-loop ΔT, °F	400	300	----	425	309
Steam conditions					
Superheat/reheat temperature, °F	1000/1000	950/950	900/900	950/950	900/ (no reheat)
Pressure, psig	2400	2400	2400	2400	2400
REACTOR					
Refueling cycle, yr	1	1.1	0.94	1	1
Fuel material	PuO_2-UO_2	PuO_2-UO_2	PuC-UC	PuO_2-UO_2	PuC-UC
Fuel-cladding material	316 SS	304 SS	316 SS	316 SS	316 SS
Reactor geometry	Cylindrical	Cylindrical	Cylindrical	Cylindrical	Modular
Heat-transfer-system geometry	Loop	Pool or primary tank	Pool or primary tank	Pool or primary tank	Loop
Reactor geometry					
Core height, in.	43.0	34.7	24.0	30.0	39.3
Core L/D	0.42	0.29	0.225	0.308	0.842
Axial-blanket height, in.: Upper	12	14	18	15	15
Lower	15	14	18	15	15
Rows of radial blankets	2	2	1	2	~2
Radial-blanket height, in.: Inner	56.5	42.7	36.0	60.0	69.3
Outer	43.0	42.7	----	60.0	69.3
Reactor subassemblies, Number					
Fuel	274	288	219	234	244
Control rods	15	25	22	31	60
Radial blankets: Inner	66	66	60	60	120
Outer	72	72	----	66	141
THERMAL HYDRAULICS					
Peak fuel-pin power, kW/ft (100% power)	16.0	15.7	43.5	16.3	39.2
Cladding-ID hot-spot temperature °F	1282	1300	1223	1300	1400
Fuel peak temperature					
At nameplate-power rating, °F	4500	3900	2575	4900	2622
At overpower, °F	----	4500	----	5100 (10% over)	2846 (12% over)
Maximum heat flux, 10^6 Btu/hr-ft^2	0.690	0.656	1.360	0.930	1.691
NUCLEAR (MIDEQUILIBRIUM) CHARACTERISTICS					
Core power fraction	0.917	0.938	0.83	0.876	0.954*
Axial-blanket power fraction	0.031	0.043	0.11	0.076	
Radial-blanket power fraction	0.052	0.019	0.06	0.048	0.046*
Core volume fractions					
Fuel	0.439	0.442	0.386	0.467	0.276
Sodium	0.326	0.381	0.400	0.351	0.590
Other	0.235	0.177	0.214	0.182	0.134
Breeding ratio	1.30	1.36	1.44	1.42	1.32
Average fuel burnup, MWd/MT	67,000	100,000	100,000	100,000	100,000
Doubling time, yr	13.0	10.4	7.99	7.75	9.9
HEAT TRANSFER					
Number of loops, pri./sec.	3/3	6/3	6/-	3/3	2/2
Total reactor flow, 10^6 lb/hr	75.6	92.4	94.0	80.6	128.5
Primary sodium pumps	3	6	----	3	2
Intermediate heat exchangers	3	6	----	3	2
Duty per IHX, 10^6 Btu/hr	2735	1396	----	2760	4437
Surface area per IHX, ft^2	29,900	10,509	----	25,800	49,770
Secondary sodium pumps	3	3	----	3	2
Steam-generator banks (total)	3	3	----	3	2
Surface area per bank, ft^2	45,200	71,220	----	53,240	56,000
Tube materials					
Superheater	321 SS	Croloy 2-1/4	----	316 SS	Incoloy 800
Evaporator	2-1/4 Cr - 1 Mo	Croloy 2-1/4	----	2-1/4 Cr - 1 Mo	Incoloy 800
Reheater	321 SS	Croloy 2-1/4	----	316 SS	none
TURBINE GENERATOR					
Type of machine	Tandem-compound 6 flow, 33.5 LSB	Tandem-compound 6 flow, 30.0 LSB	----	Tandem-compound 6 flow 33.5 LSB	Tandem-compound 4 flow, 44.0 LSB
Speed, rpm	3600	3600	----	3600	1800
Main steam flow, 10^6 lb/hr	6.85	7.35	----	7.265	9.813

*At beginning of life.

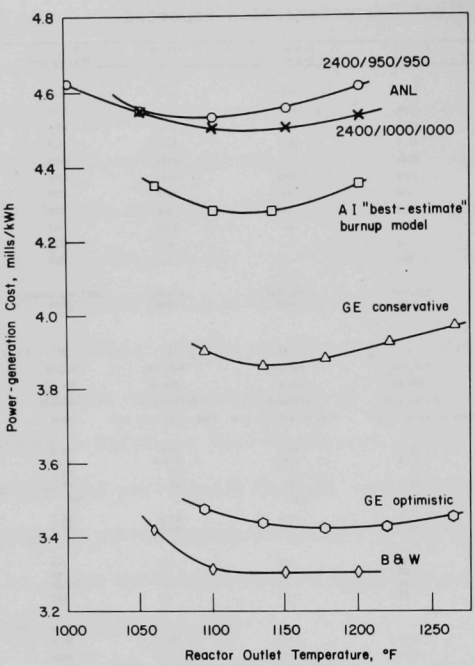

Fig. 146. Power-generation Cost vs Reactor Outlet Temperature.

146 shows the contractor and ANL results. The important observation is the small variation (0.05 mill/kWh) between power-generation costs with 1100°F outlet temperature and the optimum temperature. The scale of total costs, i.e., 3.3 to 4.6 mills/kWh, is not important, except that it shows apparent insensitivity of the variation to absolute cost magnitude. Plant reliability and unavailability factors were not included in the cost optimization because of the lack of data. However, based on conventional-plant experience, these factors could be significant in the selection of reactor outlet temperature.

The establishment of research-and-development temperature goals for various portions of the LMFBR plant can be considered on two bases: the selection of temperatures that assure a good probability of the LMFBR becoming competitive at the target date, and the justification of

a temperature higher than that required for competitiveness because the worth of a decrease in power costs is greater than the worth of the R&D cost. At this stage of development, the emphasis is naturally on the temperature required for competitiveness; however, many questions exist, for example, the impact of stainless-steel swelling on design-point selections.

Plant design temperatures are selected within a dynamic framework; that is, new information, either cost or experimental data, can alter old relationships and thus necessitate a new evaluation of selected design parameters.

The conclusions within the general study limitations are: (1) compared with higher temperatures, an 1100°F competitive-target temperature will inflict a penalty no greater than 1% of the total LMFBR electrical energy cost, (2) temperature rises of 300-350°F in the primary sodium appear reasonable from a cost standpoint, (3) secondary-system hot-leg temperatures are determined in part by materials selection for the superheater and reheater-superheater-evaporator configuration; all contractors except B&W used austenitic-type stainless steel rather than Croloy 2-1/4 for their superheaters and reheaters, (4) the major consideration in establishing plant temperature is the burnup and thermal performance of the fuel element at various temperatures; at present, the fuel burnup has the greatest uncertainty of all the factors considered; maximum cladding temperatures of ~1300°F were used by the contractors.

The investigations using temperature-dependent cost functions resulted in analytical optimum sodium outlet temperatures of 1125 to 1150°F. Although the relationships between outlet temperature and

forced-outage rate, and between outlet temperature and unavailability, are unknown, forced-outage rate and unavailability are expected to increase with increasing temperature. Based on this study, ANL recommended that a value of 1100°F be selected as the sodium outlet temperature goal for competitive LMFBR plants.

Engineering analysis. The mechanical, safety, neutronics, and economic aspects of nuclear plant engineering have a number of problem areas and analytical weaknesses.

A major design concern that strongly influences core design is the accommodation of stainless-steel swelling; this problem was not considered by any of the five contractors in the design of their cores, because its importance was not generally recognized during design. Another item that has a strong influence on core design is the fuel fabrication cost. The contractors used different models of the dependence of this cost on fuel-pin parameters such as diameter and length. Their design selections directly reflect these assumptions.

A core-design area that was not well covered by the Follow-on work was reactivity control. Further analytical work must be performed to provide suitable control-rod designs, to determine modes of control management during normal operation, and to find the overall effects of control rods on thermal-hydraulic and fuel-burnup performance.

Analysis methods varied considerably among the five contractors, reflecting the current state of active development. An important area of weakness was fuel-cycle analysis; however, ongoing activities will soon improve this situation considerably. Methods for predicting fuel lifetime in terms of MWd/MT varied among contractors. A large deficiency existed in this area of core design at the start of the

contracts; however, with the method development and fuel-modeling work under way, the analytical predictions should be greatly improved.

Before the Follow-on activity began, there was a general belief in the U.S. that a reasonable safety criterion would be to design a reactor with a nonpositive total coolant-voiding reactivity change. During the course of these studies, most of the designers took the position that satisfying this criterion severely compromised the LMFBR economics. The designs of Atomics International, Babcock and Wilcox, and General Electric were not modified in any way to reduce the positive-void effect. Westinghouse's reference design did satisfy a nominal void-effect criterion, but Westinghouse showed a strong preference (represented by an alternate reference design) for an unspoiled geometry. Combustion Engineering arrived at a system with a fairly small positive-void effect. Physics design is greatly simplified by removing this criterion; the criterion is arbitrary in any case, and does not in itself guarantee safety against release of contaminants.

The neutron cross-section data were in a state of important changes during the Follow-on Study. The original recommendation by ANL was that all contractors use the Category-I file of ENDF/B. This recommendation was relaxed when it became apparent that this file would not be available in time for general use (also, this file had not been fully tested for accuracy when it was released). As a result, the contractors used a variety of data files for their analyses. During the Task-II work, ANL recommended that the contractors recalculate their reference designs with the Revised Category-I file of ENDF/B for the purpose of normalization; in general this was done. The comparison calculations of the final reference designs that were made by ANL employed the Revised Category-I file, with the exception of the Pu^{239}

data. By the time this work was started, there was general agreement that the recent capture-to-fission-ratio measurement of Pu^{239} should be incorporated into the data file. Consequently, the ENDF/B file was modified to correspond to the ORNL-RPI measurements of this ratio.

With the exception of Westinghouse, the contractors favor the reheat steam cycle (CE did not study steam cycles). Westinghouse chose a nonreheat moisture-separation steam cycle. All contractors chose a 2400-psig turbine throttle pressure and throttle temperatures in the range of 900 to 1000°F.

Although most contractors favor the reheat steam cycle, the total cost-of-energy differential is not large. However, the trend toward reheat is reinforced by items such as the following: turbine size limitations are less severe for the 2000-MWe units projected for the future; a reheat cycle will produce less waste heat; and turbine-generator maintenance might be lower because of less moisture in the exhaust steam. On the negative side, none of the contractors adequately assessed the effects of the reheat cycle's greater complexity of equipment arrangement and its more complex control aspects. While the reheat cycle might be desirable for the future 2000-MWe plants, the nonreheat cycle has an advantage for the first demonstration plant because of simpler equipment and control. However, the experience with the reheat cycle will be lost if a nonreheat cycle is selected for the demonstration plant.

Economics. The capital-cost estimates, after ANL modification, averaged $185/kWe, with a deviation from the average of +3.8 and -4.9%. The small range of the estimates is not surprising because much of the plant cost is not unique to the concept. From an evaluation standpoint, the capital costs for all the concepts are approximately equal.

The total energy costs reported by the Follow-on Study contractors for their reference designs varied from 3.87 to 4.56 mills/kWh. The ANL modified total energy costs are based on a cursory evaluation and are not necessarily more accurate than the contractor's reported values; however, these total energy costs are on more consistent bases. The energy cost normalization did not include ANL changes in the contractors' reported neutronics or fuel-management schemes. The ANL-modified total energy costs varied from 4.6 to 5.0 mills/kWh.

The economic feasibility of the LMFBR concept depends strongly on the plant capital cost. The capital-cost estimates are highly uncertain because of the lack of system and safety definition. LMFBR capital-cost estimates are difficult to compare with LWR cost estimates because of differences in ground rules, design and safety requirements, cost escalation, etc. However, to provide a partial reference for LMFBR cost, a 1000-MWe LWR plant based on a revised estimate of WASH-1082* was costed according to LMFBR indirect-cost procedure. This comparison indicated that the LMFBR would cost $20/kWe more than the LWR. However, a cost comparison of different generating-plant concepts is not very meaningful for independently prepared estimates. Only by making side-by-side capital-cost-estimate comparisons can the cost of the LMFBR be assessed meaningfully.

The fuel fabrication costs vary widely among contractors. This variation is not surprising because of the many unknowns affecting the fabrication of LMFBR fuels. The cost of reprocessing LMFBR fuels is also highly uncertain.

---

*USAEC, "Current Status and Future Technical and Economic Potential of Light Water Reactors," WASH-1082, March 1968.

Research and development. Two of the four primary objectives of the Follow-on Study were to assess the relative value of performing the R&D in each area, and to estimate the probability of successful achievement in each of the R&D areas. These were not well met by each contractor. However, collectively there is enough information to allow a qualitative insight into the value of performing the R&D and the probability of success.

To a large extent, this study confirmed the general content of the existing LMFBR Program Plan; in addition, the Program Plan should receive much definitive guidance from the various contractors' reference-design descriptions. A continuing study of large LMFBR plants on the part of industry is recommended to augment the existing knowledge on safety aspects of the plant and on licensing requirements to further define target-plant conditions and to provide in-depth information such as the magnitude and duration of temperature transients that will be experienced throughout the plant. By further careful work, the R&D required will be better defined and R&D money and time will be saved.

A general comment on the programs of Safety R&D that have been proposed by the five contractors is that the specific R&D requirements should have been more thoroughly evaluated for the particular reference system and the R&D program should have been more coherently and logically planned so as to make optimum use of R&D results both from activities already in progress elsewhere and from the activities within the R&D program. A general criticism that cannot be leveled with equal force at all the contractors is that wherever feasible and useful there should be intimately interacting programs of analysis and experiment.

The physics research and development sections of the study reports generally called for many detailed integral experiments to aid the

designers of 1000-MWe plants. Some of the requests would severely strain the capabilities of existing facilities and might require large expenditures for special equipment. These requests should be carefully reviewed to find whether some of these physics experiments should be carried out in early demonstration plants.

The contractors were required to give a brief description of the base of current technology considered to be the starting point for the new R&D information needed. These descriptions were generally quite brief and lacked detail. The contractors are not in possession of enough detailed information about the EBR-II plant and probably the Fermi plant. ANL believes that the LMFBR state-of-technology must be assessed more thoroughly throughout the industry. This assessment would prevent duplication of effort by better defining the starting point for new R&D information needed.

The introduction date for commercial LMFBR plants appears to have slipped since the original LMFBR studies. At the present time, the ANL expectation of nonsubsidized power operation is between 1984 and 1990. In most cases, the earlier studies appeared to expect commercial operation sooner; however, one company did state the late 1980s. Interpretation of the Program Plan results in a circa-1985 commercial date. Competive expectations due to probable U_3O_8 price increases with large ore demands in the future, and the uranium-plutonium fuel system synergism with LWR and LMFBR plants, will be the two main factors in the industrial decisions to move ahead. The commercial target date should be intimately tied to the R&D schedule and the timeliness of efforts. System studies of LMFBR plants in utility electrical networks should be made to keep information on the competitive position and the target dates current.

Overall. The most important primary objective, identifying the R&D information needed for the industry-favored reference concept, was successfully accomplished. Although it was not possible for the contractors to perform in-depth work in all areas, we do not think that the objectives of the study were unduly compromised.

Future program. Work on the Follow-on program was completed. Extension of the work in the safety area is described on pp. 388-394.

References

1000-MWe LMFBR Follow-on Study Subcontractors' Reports:

Atomics International:

AI-AEC-12765 (revised) ANL 1000-MWe LMFBR (Liquid Metal Fast Breeder Reactor) Follow-on Study
- Vol. I and II - Task I Report (May 3, 1968)

AI-AEC-12791 1000-MWe Liquid Metal Fast Breeder Reactor Follow-on Study
- Vol. I, II, and III - Conceptual System Design Description

AI-AEC-12792 1000-MWe Liquid Metal Fast Breeder Reactor Follow-on Study - Conceptual Design Report
- Vol. I - Summary
- Vol. II - Engineering Studies
- Vol. III - Plant Safety Analysis
- Vol. IV - Description of Plant Design
- Vol. V - Methods

AI-AEC-12793 1000-MWe Liquid Metal Fast Breeder Reactor Follow-on Study - Research and Development Requirements

Babcock & Wilcox:

BAW-1316 1000-MWe LMFBR Follow-on Study
- Vol. 1 - Task I Report (Jun 1967)
- Vol. 2 - Task I Concept I System Description Report (Apr 1967)
- Vol. 3 - Task I Concept II System Description Report (Jun 1967)
- Vol. 4 - Task I Concept III System Description Report (Jul 1967)
- Vol. 5 - Task I Concept IV System Description Report (Aug 1967)

BAW-1328 1000-MWe LMFBR Follow-on Study - Tasks II and II Final Report
- Vol. 1 - Summary Description and Cost Estimate (Oct 1968)
- Vol. 2 - Conceptual System Design Descriptions
- Vol. 3 - Conceptual System Design Descriptions (Feb 1968)
- Vol. 4 - Trade-off Studies (Nov 1968)
- Vol. 5 - Parametric Studies (Jan 1969)

BAW-1330	1000-MWe LMFBR Follow-on Study - Control Studies Topical Report (Oct 1968)
BAW-1326	Sodium Parameter Study Code "NAPS" - Topical Report (Apr 1968)
BAW-1331	1000-MWe LMFBR Follow-on Study - Task IV Final Report - Research and Development Requirements
Combustion Engineering:	
CEND-322	1000-MWe Liquid Metal Fast Breeder Reactor Follow-on Study: Task I Report, "Preliminary Studies for a Reference Conceptual Design of a 1000-MWe LMFBR" (Dec 1967)
CEND-337	Tasks II and III Report. A Reference Conceptual Design of a 1000-MWe LMFBR
Vol. 1	- Conceptual System Design Descriptions (Jul 1968)
Vol. 2	- Static Design and Performance Analyses (May 1968)
Vol. 3	- Safety and Control Analyses (Sept 1968)
CEND-346	Task IV Report. A Research and Development Program Needed for the CE Reference Concept (Feb 1969)
General Electric:	
GEAP-5618	Comparison of Two Sodium-cooled 1000-MWe Fast Reactor Concepts - Task I Report of 1000-MWe LMFBR Follow-on Work (Jun 1968)
GEAP-5678	Conceptual Plant Design, System Descriptions, and Costs for 1000-MWe Sodium-cooled Fast Reactors - Task II Report of a 1000-MWe LMFBR (Dec 1968)
GEAP-5710	Methods, System Optimization, and Safety Studies for a 1000-MWe Sodium-cooled Fast Reactor - Tasks III and V Report (Feb 1969)
GEAP-5769	Research and Development Requirements for a 1000-MWe Sodium-cooled Fast Reactor - Task IV Report of 1000-MWe LMFBR Follow-on Work (Apr 1969)
Westinghouse:	
WARD-2000-33	1000-MWe Fast Breeder Reactor Follow-on Study. Task I Final Report (Jun 1968)
WARD-2000-20	Moisture Separation or Steam Reheat versus Sodium Reheat Plant Cycle Technical and Economic Evaluation (Apr 1968)
WARD-2000-22	Steam Generator Concept Selection (Jan 1968)
WARD-2000-23	Survey of State-of-the-art of Intermediate Heat Exchangers (Mar 1968)
WARD-2000-31	Evaluation of Vented-to-coolant Design for Sodium-bonded Carbide Fuel Rods (Feb 1968)
WARD-2000-84	1000-MWe LMFBR Follow-on Study. Task V Safety Studies (Dec 1968)
WARD-2000-90	1000-MWe LMFBR Follow-on Study. Task IV Final Report
WARD-2000-93	Comparisons of the Westinghouse 1000-MWe LMFBR Reference Design Calculations Using the Westinghouse 6602-M Data and the MC^2 Code with Neutron Cross-section Data from the NEDF/B File. Task III Topical Report

WARD-2000-96	Cost Optimization and Parametric Studies. Westinghouse 1000-MWe LMFBR. Task III Topical Report
WARD-2000-97	1000-MWe LMFBR Follow-on Study. Tasks II and III Westinghouse Conceptual Design Report

ARGONNE NATIONAL LAB WEST
3 4444 00010952 0

B